ELECTRICAL PROCESSES
AT
METALLIC CONTACTS
TO
SODIUM ION CONDUCTING GLASS

ALAN GORDON CAMPBELL

A Thesis Submitted for the degree of
Doctor of Philosophy

to

The University of Edinburgh

May 1987

To my Father

ABSTRACT

The most important aspect of the metal-glass interface in a solid-connected glass pH electrode is the stability of electric potential at the interface. The development of this potential is a function of the behaviour of charge carriers near the glass surface and of any electrode process which takes place.

The mechanism of conduction in the soda-lime-silica glass system, to which some pH-sensitive glass belongs, is reviewed briefly. Solid electrolytes in general, and the theory applying to contacts to them, are examined, with a view to their relevance to the problem of the glass-metal system. The importance of electrochemical effects in solid systems is emphasised. Chemical and electrochemical phenomena at glass surfaces and interfaces are also reviewed.

In order to investigate their applicability to sensors, contacts of aluminium, copper, silver, tungsten trioxide and sodium tungsten bronze were used in metal-glass-metal structures. These had the form of two- and three-electrode electrochemical cells, on which AC and galvanostatic measurements were made.

The complex admittance graphs obtained from the AC data are generally of the form of a circular arc whose centre is situated below the real axis, and which approaches the origin at the low-frequency end, indicating the absence of conduction across the interface under conditions of zero bias.

Nonblocking behaviour of all the contacts has been inferred from the galvanostatic data when the conditions of zero-bias are relaxed; after the passage of any amount of current, the potential tends to approach its starting point after the current has been switched off. Evidence of a kinetically-limited electrochemical reaction has been found in the case of evaporated aluminium contacts, and less strongly in the cases of silver and copper. Sodium tungsten bronze appears to achieve a steady potential difference when in contact with glass, and so seems the most likely candidate for application as a back electrode for a practical sensor.

Suggestions are made for further research to test the applicability of the results to sensors, and to extend the investigation of electrode processes at glass surfaces.

DECLARATION

This thesis has been written by myself and its content has not been submitted for any other degree or publication. The work described in it is my own except where specific reference has been made to other authors.

Alan G Campbell

ACKNOWLEDGEMENTS

I would like to thank Dr RG Kelly for supervising the project. Thanks also to Prof AE Owen, and to Dr Brian Birch and Dr A Cattell of Unilever Research, for many useful discussions, Dr PG Bruce at Heriot-Watt University for access to his equipment for the sodium electrode experiment, and to Dr A Firth for reading the proofs.

CONTENTS

CHAPTER 1

INTRODUCTION

1.1. Solid Electrodes on Glass and Chemical Sensors

The subject of this thesis is the origin and measurement of the potential difference between a metal electrode and the soda-lime-silica glass with which it is in contact.

The work was undertaken with a view to the possible application to the development of a solid state potentiometric pH sensor based on pH-sensitive glass. The conventional glass electrode consists of a glass bulb containing a solution of constant, known pH. This is immersed in the test solution and a potential difference is developed between the two sides of the glass membrane which is proportional to the pH difference between them. The source of this potential difference is an electrochemical reaction which maintains an equilibrium between the activities of negatively charged immobile sodium sites in the glass, and sodium and hydrogen ions in the glass and the solution [1]. The manufacture of this device involves blowing a glass bulb and attaching it to a stem. This is an expensive process and results in a device which is delicate, and inconvenient for many applications. A new sensor which could be mass produced using standard manufacturing techniques, and was small and robust, would be a very valuable step forward. Such a sensor would be an all-solid state device, which requires a solid connection to the glass in place of the reference solution. Solid electrodes have been produced for a wide variety of other membranes [2], and normally involve a reversible electrochemical reaction which fixes the potential between the electrode and the membrane.

Attempts to replace the reference solution in a pH sensor with a solid contact have resulted in devices with sensitivity equivalent to that of conventional ones, but with considerable variation of offset voltages and with a tendency to drift [3,4]. Since the actual sensing mechanism is the same in the solid-state case as in the conventional electrode, the drift is due to the instability of the potential difference between the solid

contact and the glass. The present work was undertaken to investigate directly the mechanism of potential development at interfaces between metal and glass with a view to finding a combination which can provide a stable contact.

1.2. The Glass-Metal Interface

The problem of the electrical properties of the interface between a metal and a soda-lime-silica glass is similar to that of any other electrode-electrolyte system. Conduction within the glass is by the motion of sodium ions rather than electrons. The potential difference between the glass and a current-carrying electrode depends on the disposition of of electrical charge in the vicinity of the interface. This in turn depends on the composition and structure of the electrolyte in this region, the nature of the interface itself, and the presence or otherwise of an electrochemical reaction involving species in the two media.

1.3. Electrical Properties of the Metal-glass Interface

Although there is a considerable amount of experimental data on the interaction of metal and glass of a wide range of types, very little has been concerned with the potential difference between the two. The chemical and physical effects of interdiffusion of metal ions into the glass from amalgams and metal salts, as well as from the metal itself, have all been studied, with or without an applied electric field (eg [5,6,7]).

Electrical measurements involving metal contacts to the glass are usually concerned with measurements of the bulk electrical response where electrode effects are treated as an interference to the true value of the quantity [8]. For these purposes, the electrode potential is often assumed to be constant or zero, or it is interpreted in terms of the impedance presented to a small-signal voltage stimulus.

The investigation of potentials at contacts to glass is really one of electrochemistry and so the present work is particularly concerned with the application of electrochemical techniques to solid electrolytes of which soda-lime-silica glass is one type. Chapter 2 deals with the basic conduction processes within the glass. Chapter 3 is a survey of the possible electrode processes in different solid state electrode systems. In Chapter 4, the ideas introduced in the previous two chapters are applied to the specific case of glass. The experimental techniques which were employed for the present work are described in Chapter 5, and the experimental results are presented and discussed in Chapter 6. Conclusions and some suggestions for further work are presented in Chapter 7.

REFERENCES

1. Eisenman G, in *Glass Electrodes for Hydrogen and Other Cations* (ed G Eisenman)p133-136, Dekker, New York (1967).
2. Nikolskii BP and Materova EA, Ion-Selective Electrode Review **7**, 3-39 (1985).
3. Portnoy HD, in *Glass Electrodes for Hydrogen and Other Cations* (ed G Eisenman)p159-266, Dekker, New York (1967).
4. Kelly RG, Phd thesis, University of Edinburgh (1979).
5. Dunken HH, in *Treatise on Materials Science and Technology*, **22**, (ed H Herman) p1-73, Academic Press, (1982).
6. Borom MP and Pask JA, Phys Chem Glasses **8**, 194-205 (1967).
7. Pescatore C and Machiels AJ, J Non-Cryst Solids **49**, 370-388 (1982).
8. Macedo PB, Moynihan, CT and Bose R, Phys Chem Glasses **13**, 171-179 (1972).

CHAPTER 2

CONDUCTION IN SILICATE GLASS

2.1. Introduction

In soda-lime-silicate glasses electrical conduction is by the movement of sodium ions [1]. This is true of most silicates, both crystalline and amorphous, in which sodium is present. Glass therefore behaves as a solid electrolyte and is capable of supporting a variety of electrode phenomena where it is in contact with an electronic conductor. Electronic conduction in the glass is usually undetectable because of the relatively high mobility of sodium. However, there are some other cations, such as lithium, silver, potassium and many others which, if they are present in silicate glasses, may have high enough mobilities to contribute significantly to the conductivity [2,3]. These may form part of the initial composition of the glass or be introduced from the surface whereupon they interdiffuse with sodium. This implies the presence of some electrochemical mechanism, for example ion-exchange from an aqueous solution, which forms the basis of the principle of operation of the glass electrode [4].

2.2. Structure

The electrical characteristics of glass arise from the way the sodium ions are incorporated into the atomic structure. Soda-lime-silicate glasses are materials whose structure is primarily determined by the "network forming" ions of silicon and oxygen [1]. The basic structural unit is composed of a Si atom tetrahedrally coordinated to four O atoms, and is similar to that of crystalline silicates. According to the continuous random network model [1], the Si-O-Si bond-angles vary sufficiently to allow adjacent units to be randomly oriented with respect to one another without any bonds being broken. The tetrahedral units link together in such a way as to accommodate the sodium and calcium ions, the "network modifiers", between them. The extra oxygen atoms associated with these cations have one bond to a silicon atom and the other negatively charged, with a cation in its vicinity. These are the "non-bridging oxygens" and in a perfect network there would be one for each Na^+ ion and two for each Ca^{2+}

ion.

2.3. Conductivity and Impedance Measurements

The conductivity of glass follows the Arrhenius law, so that its temperature dependence may be expressed as [2]:

$$\sigma = \sigma_o \exp\left(-\frac{E_d}{kT}\right) \qquad 2.1$$

where E_a is the activation energy and σ_o has a much weaker temperature dependence than the exponential term.

The electrolytic nature of conduction in glass causes problems in measurement of its electrical properties, since electrode phenomena at the contacts influence the voltage and current being measured. In order to separate the effects of electrodes from those of the bulk, alternating current is usually used to measure the conductivity. Figure 2.1 shows the in-phase and 90° out-of-phase (real and imaginary) parts of the admittance against frequency of a typical glass cell with metal contacts. The real part has a region where it is constant over a considerable range of frequency. The constant value is attributed to the bulk low-frequency conductance, since it scales with the dimensions of the cell and is not affected by the type of contacts used. It is from this value that the DC conductivity is often calculated.

2.4. Conduction Mechanisms

The temperature-dependence of the conductivity and high-frequency response may be interpreted in terms of a potential-well model which is illustrated in one-dimensional form in figure 2.2 [1]. The ion vibrates in the well at a frequency ν_o and requires an energy W_a to surmount the barrier and move to the next well. The probability per second, p, of an ion escaping is

$$p = \nu_o \exp\left(-\frac{W_a}{kT}\right) \qquad 2.2$$

When a field E is applied, the barrier is effectively lowered by an amount $(Ed/2)$, where d is the spacing of the ionic sites. The probability that the ion will move in the direction of the field is increased by a factor of $(expEd/2kT)$, which is approximately

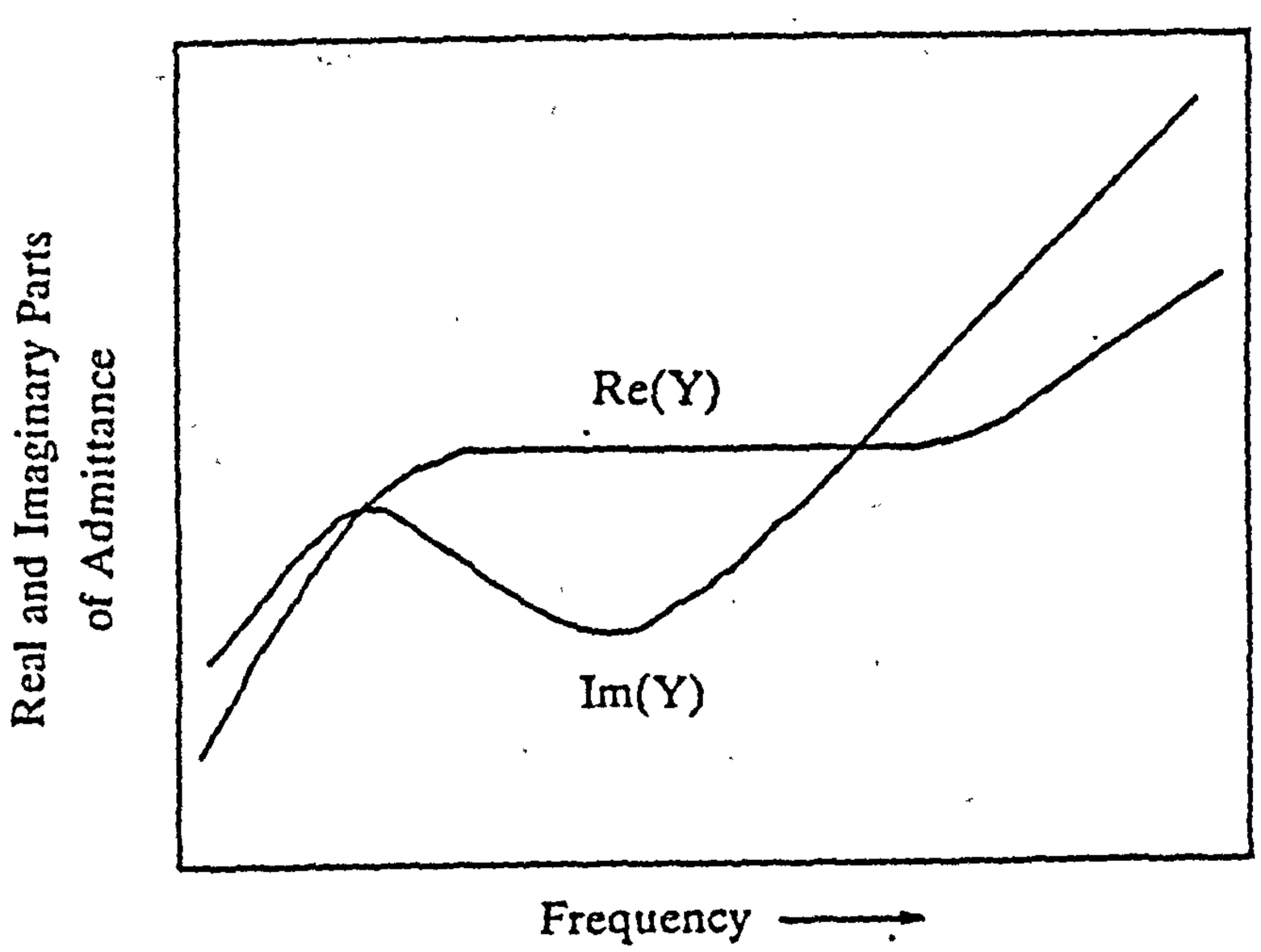

Fig 2.1 Real and imaginary parts of the AC response of glass with metal contacts.

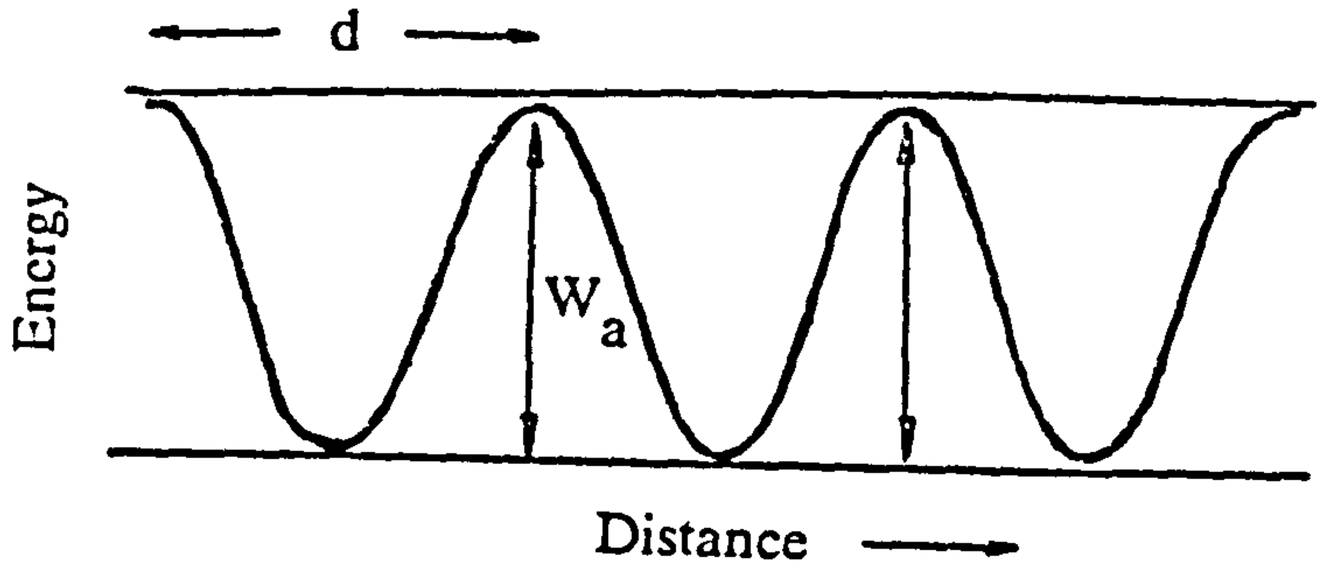

(a)

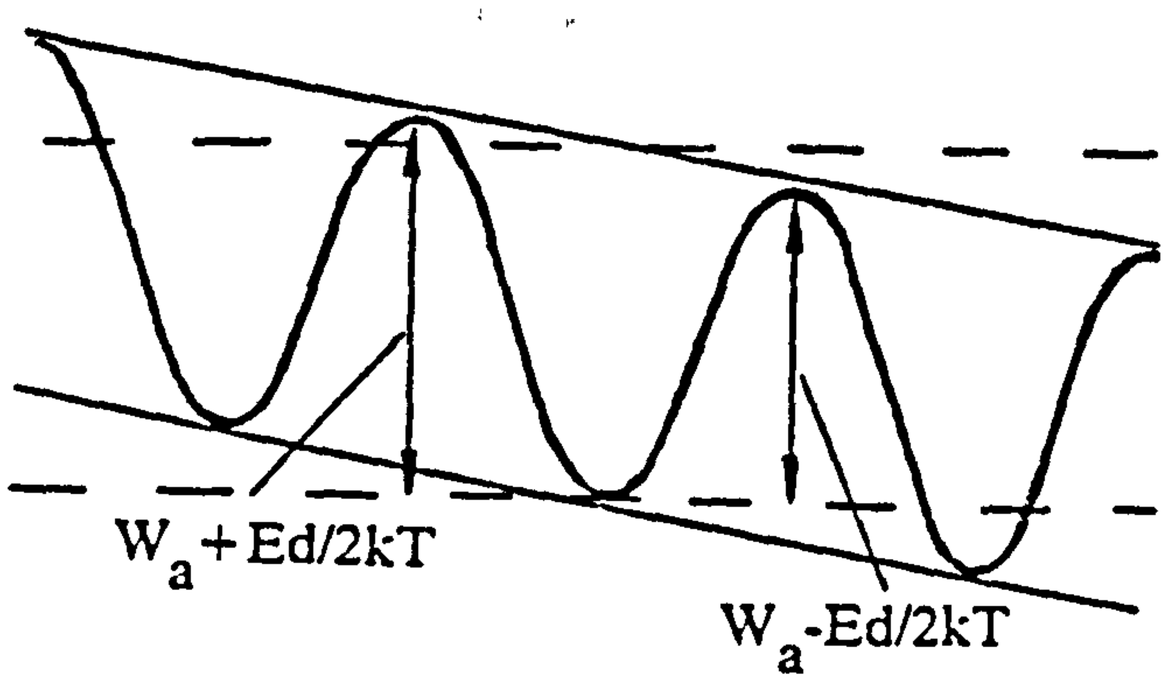

(b)

Fig 2.2 (a) Schematic diagram of simple potential well model of glass conductivity (after Owen [1]).

(b) As (a) but with applied field E.

equal to $(Ed/2kT)$ when $(Ed \ll 2kT)$. Similarly, the probability of a jump in the opposite direction is decreased by the factor $(-Ed/2kT)$. Hence the current density is given by:

$$j = epC_{Na}\ (Ed/kT) \qquad 2.3$$

where C_{Na} is the concentration of sodium ions and e is the charge on the ion.

The existence of identical potential wells implies that all the ions are in identical sites in the silica network. Experiments by Kraus and Darby in 1922 [5] using the displacement of sodium by silver ions from a silver metal contact showed that all the ions were potentially mobile since the sodium was completely replaced. However electrical measurements by Ravaine and Souquet [6], on glasses with different sodium concentrations, demonstrated that the conductivity does not scale linearly with the number of sodium ions present. Two possible explanations were offered for this. Either the depth of each well varies with sodium concentration, or the number of ions occupying wells shallow enough to allow movement is only a proportion of the total. The first explanation is equivalent to saying that the number of carriers is equal to the total sodium ion concentration, so that the variation in conductivity is accounted for by the variation in the mobility. It is unlikely because the environment of the sodium ion does not change significantly as the mole fraction of sodium is varied. The second explanation is supported by the fact that the relation between conductivity and ionic concentration is consistent with the existence of a dissociation equilibrium between mobile and bound Na^+ ions, if it is assumed that the mobility of dissociated ions is constant [1]. This is similar to the relation between concentration and conductivity of weak electrolytes in liquid solutions.

The validity of this model was investigated by Ravaine and Souquet [6] who measured the potentials developed across concentration cells of two different glasses. From these the activities of the sodium were calculated through the relation

$$V_{12} = \ln\left(\frac{a_1}{a_2}\right)$$

where V_{12} is the measured voltage and a_1 and a_2 are the activities in the two glasses. Although the relation between C_{Na} and a_{Na} was found not to be a simple function (it increases approximately exponentially with Na_2O mole fraction), the conductivity

turned out to be proportional to the square root of the activity. This relation between sodium activity and conductivity has the same form as that of weak electrolytes in aqueous solutions, which confirmed the existence of a dissociation equilibrium involving Na^+ and O^{2-} ions [7]. One practical implication of this model is that only dissociated Na^+ ions take part in the conduction process, and these form a small fraction of the total.

It is also possible to derive the conductivity properties from consideration of the microscopic processes involving the sodium ions. Anderson and Stuart [8] developed a model for the energy barrier which the ions have to overcome by assuming that it is made up of the coulombic interaction between two neighbouring ions, and the elastic strain in the surrounding network for the required passage to open up to allow an ionic jump to take place. Evidence that the model was a valid description of the environment of the sodium ion was its satisfactory prediction of the conduction activation energy and its variation with temperature. A similar calculation was also done for the mobility of other ions.

The Anderson and Stuart approach was one where all the ions were assumed equally mobile. An alternative view, first developed by Charles [9], and more in keeping with the limited dissociation of the weak-electrolyte theory, was based on Mott and Gurney's theory for the migration of activated defects in ionic crystals [10]. This involves the motion of two types of charged point defects. Schottky defects are cation and anion vacancies, which are assumed to occur in pairs so that charge neutrality is maintained. Frenkel defects are caused by ions from regular sites moving to interstitial sites. The number of each type is determined by the energy of formation which can be calculated from an electrostatic model for the crystal because of the well-characterised bonding arrangement which makes up the lattice.

The two different types of defect give rise to three different forms of transport [12]:

(i) By travelling between regular sites and vacancies (vacancy mechanism).

(ii) By exchange between interstitial and lattice sites (interstitial mechanism).

(iii) By displacement of an ion from a lattice site to an interstitial one accompanied by the opposite process allowing its original site to become reoccupied (interstitialcy mechanism).

For crystals, the energies associated with the formation of these defects can be calculated theoretically and so the likelihood of transport by each mechanism and even

the conductivity may be found.

Charles adapted this model for glass by assuming that sodium could take up several possible positions around a single non-bridging oxygen atom. If a second sodium takes up one of these positions on a site which is already occupied, the status of the second ion would correspond to an interstitial ion in a crystal. In order to calculate the conductivity from this model, he used Mott and Gurney's expression for the diffusion constant derived for Frenkel defects in binary ionic crystals (such as the alkali halides) [10]:

$$D = \gamma BC\, \nu a^2 \sqrt{\left(\frac{N'}{N}\right)} \exp\left(-\frac{Wo/2 + Uo}{kT}\right) \qquad 2.4$$

where γ is a parameter expressing the correlation of the change in vibrational frequency with direction of motion

ν is the vibrational frequency of an atom in a regular site

a is the lattice constant

N is the number of ions

N' is the number of ionic sites

and B and C are constants involving the compressibility of the crystal.

Unfortunately not all of these constants were available for glass. However the theoretical frequency dependence of the AC impedance and the dependence of the conductivity on hydrostatic pressure were derived, assuming the validity of the Nernst-Einstein relation between diffusion coefficient and mobility:

$$\frac{\mu}{D} = \frac{q}{kT} \qquad 2.5$$

The expressions obtained fitted experimental data.

Tracer-diffusion experiments have been used to assess the validity of the different defect models by Haven and Verkerk [11] and Lim and Day [12]. These allowed the determination of the correlation factor f, which is the adjustment to the Nernst-Einstein relation between mobility and diffusion coefficient:

$$\frac{\mu}{D} = \frac{fq}{kT} \qquad 2.6$$

Values of f between 0.4 and 0.5 were found. Haven and Verkerk found that their data could be interpreted as either a paired interstitial (interstitialcy) or a vacancy mechanism. Lim and Day, using a more refined experiment, found a temperature dependence of f which could not be explained by either mechanism on its own, and proposed that both were present in varying proportions, with the vacancy mechanism dominant above about 400°C in the glass they tested.

Following from the work of Charles [9], another defect mechanism has been proposed by Ingram [13], based on the possibility of the presence around a single non-bridging oxygen of two ions in "subinterstitial" sites. If this double occupation is energetically favourable over the occupation of one ordinary interstitial and one regular site, then transport then takes place by the hopping of one of these ions to an ordinary interstitial site, followed by the formation of another interstitial pair, with the remaining ion taking up a regular position. This model is more consistent with the weak-electrolyte theory because only the small fraction of ions forming the interstitial pairs are available for conduction.

2.5. Summary

The processes of conduction in silicate glasses containing sodium have been reviewed. The most important aspect is that under normal circumstances, all detectable conductivity may be attributed to the motion of positive ions, usually sodium. This is because electronic conduction is virtually absent, whereas sodium ions are relatively free to move between their sites in the network.

The dependence of conductivity on ionic concentration is formally similar to that of weak aqueous electrolytes [1]. Various models based on the microscopic environment of the sodium ion have been proposed for the mechanism of transport, using calculations of the energies of the ions at their sites. The analogy between the environment of the sodium ions and defects in ionic solids has been made use of, and a paired interstitialcy mechanism found to fit the observed behaviour best [14].

The most significant aspects of the transport mechanism, from the point of view of interfacial processes, are that there are a number of equivalent sites for each ion, allowing the possibility of accumulation, and that there is a range of bonding energies for the ions, so that at any time only a fraction of them may have sufficient energy to

make a transition and thus be effectively mobile.

REFERENCES

1. Owen AE, in *Progress in Ceramic Science* **2,** (ed JE Burke) p77-196, Pergamon, London (1963).
2. Carlson DE and Tracy CE, J App Phys **46,** 1575-1580 (1975).
3. Raleigh DO, Electroanal Chem **6,** (ed AH Bard) p87-186, Dekker, New York (1973).
4. Eisenman G, in *Glass Electrodes for Hydrogen and Other Cations,* (ed G Eisenman) p133-135, Dekker, New York (1967).
5. Kraus CA and Darby EH, J Amer Chem Soc **44,** 2783-97 (1922).
6. Ravaine D and Souquet JL, Phys Chem Glasses **18,** 27-31 (1977).
7. Ravaine and Souquet JL, Phys Chem Glasses **19,** 115-120 (1978).
8. Anderson OL and Stuart DA, J Amer Ceram Soc **37,** 573 (1954).
9. Charles RJ, J App Phys **32,** 1115-1126 (1961).
10. Mott NF and Gurney RW, *Electronic Processes in Ionic Crystals,* p 40-63, OUP, London (1948).
11. Haven Y and Verkerk B, Phys Chem Glasses **6,** 38-45 (1965).
12. Lim C and Day DE, J Amer Ceram Soc **60,** 198-203 (1977).
13. Ingram MD, J Amer Ceram Soc **63,** 244-53 (1980).

CHAPTER 3

ELECTRODE EFFECTS AT SOLID INTERFACES

3.1. Introduction

The previous chapter pointed out similarities between the conduction mechanisms of soda-lime-silica glass and those of some other ionic conductors. In considering the processes which might play a part in determining the potential between an electronic conductor and glass, the phenomena which are observed in other solid state electrode systems must be considered. This chapter is concerned with a variety of electrode phenomena in a number of different electrode-electrolyte systems.

Theoretical calculations of electrode potential are based on the solution of the equation of motion of charged particles, known as the Nernst-Planck electrodiffusion equation, with an appropriate set of boundary conditions. These boundary conditions have to represent the physical processes at the interface, which can take a wide variety of forms, ranging from simple charge blocking, where the electrode is simply a stopping point for the carriers, to rate-limited charge transfer. Geometrical effects, such as the roughness of the interface, may also be involved. The electrical response of the system is calculated in such a way as to be comparable with electrical experiments. In the case of small-signal effects, where the system is approximately linear, it is usual to calculate the frequency response of the system to an AC signal of small amplitude. This is usually presented as a complex admittance or impedance often in the form of the component values of an equivalent electrical circuit.

Approaches to these calculations may also be divided into two categories. A complete solution of the Nernst-Planck equation can only be found for a comparatively simple set of boundary conditions, which are sometimes difficult to justify on physical grounds. Another approach may be employed when one or more of the phenomena which govern the boundary conditions, such as reversible charge transfer, surface adsorption, surface roughness etc, completely dominate the response; in these

circumstances calculations can be based solely on the boundary conditions themselves.

3.2. The Nernst-Planck Equation

All noninteracting particles in a homogeneous medium move under the influence of self-diffusion, characterised by a diffusion constant D. If the particles carry an electric charge they also migrate in an electric field E, with a mobility μ. If the charged particles are moving between plane parallel boundaries such that charge densities and potentials vary in one direction only, then they obey the one-dimensional Nernst-Planck electrodiffusion equation [1]. For a single carrier type this has the form:

$$\frac{\partial C}{\partial t} = D\frac{\partial^2 C}{\partial x^2} + \mu\left(E\frac{\partial C}{\partial x} + \frac{\partial E}{\partial x}C\right) + G - R \qquad 3.1$$

where C is the carrier concentration
x is the distance from one of the boundaries
G is the rate of generation of the carriers
and R is the rate of recombination.

This is a nonlinear equation, since the field is a function of the excess charge concentration through Poisson's equation:

$$\frac{\partial E}{\partial x} = \frac{Fz}{4\pi\epsilon}(C - C_o) \qquad 3.2$$

where C_o is the equilibrium bulk concentration
ϵ is the permittivity of the medium
F is Faraday's constant
and z is the charge on the carrier.

The distribution of potential and ionic concentration, and their variation with time, can be found in principle by solving equations 3.1 and 3.2 together with the appropriate boundary and initial conditions. In the case of electrolyte systems, the boundaries are the electrodes, and the boundary conditions represent the electrode processes. The initial conditions are the values of all the dependent variables at t=0, and in electrolyte applications usually correspond to those of an equilibrium or steady state.

There is a wide variety of physical situations to which these equations apply within the field of electrolyte-electrode systems. Any attempt to obtain a solution which represents the behaviour of a real system should start with the establishment of a model which is justified on physical grounds [2] Then appropriate mathematical approximations may be made which allow a solution to be obtained [3].

3.3. Solving the Nernst-Planck Equation

Exact solutions are available only for comparatively simple idealised conditions [2]. One set of those is for the case of supported liquid electrolytes, and they form the basis of the techniques of electrochemistry, which is the subject of the next section. Another category, described in detail in section 3.5, is the small-signal perturbation of unsupported electrolytes when the system is at the point of zero charge, where the electrode potential is zero and the carrier concentrations are uniform throughout the electrolyte.

3.4. Electrochemical Techniques

3.4.1. Basic Assumptions

The purpose of electrochemical studies of liquid electrolytes is to investigate the reactions involving chemical species in the solution when an electric current is passed from an electrode into the solution. In order to do this, the equation of motion of the charged species is recast using a set of simplifying assumptions [4]:

(1) The species undergoing the reaction are not subject to an electric field, so that all of their movement is due to self-diffusion. This in turn implies that there is negligible ohmic voltage drop in the solution.

(2) All voltage is dropped across a small region called the "double layer" which has constant dimensions and is very thin compared with the size of the electrode.

(3) The electrode is smooth and its area is known precisely.

The first two conditions are satisfied by the inclusion in the solution of a relatively large concentration of charged species which do not undergo any electrochemical reaction in the voltage range used. This is called the "supporting electrolyte", and in practice it is often potassium chloride in aqueous solutions. When there is any shift in potential at the electrode, the resulting field in the solution causes migration of supporting ions. Since these are blocked at the electrode, the concentration of these ions

adjacent to the electrode, and hence the charge stored in the double layer, changes until the potential difference there is equal to the whole electrode potential, and the field within the solution becomes zero. Thus the only contribution of the supporting electrolyte to the electrical response of the system is a capacitive charging and discharging.

The third condition is often ensured by using a liquid electrode, usually a "dropping mercury electrode" which is perfectly smooth. In addition, since a fresh surface may be made for each measurement by dropping the mercury, the interface is free from impurities or leftover reaction products. When all of these assumptions have been taken into account, equation 3.1 is reduced to the one-dimensional self-diffusion equation:

$$\frac{\partial C}{\partial t} = D \frac{^2C}{\partial x^2} \qquad 3.3$$

and the boundary conditions need only specify the surface concentrations as functions of time.

3.4.2. The Double Layer

The theory of the electrochemical double layer is based on the consideration of the distribution of ions in the solution in conjunction with the requirements of electrostatics [5]. A potential difference is present at an electrode as a consequence of excess charge on it and in the electrolyte. Since the electrolyte is assumed to be semi-infinite, the net charge within it, Q_o, must exactly balance that on the electrode, Q_e, ie

$$Q_o + Q_e = 0 \qquad 3.4$$

The double layer consists of the electrode and that region of the electrolyte where the net charge density is nonzero. Its structure is very complicated since the distribution of all charged species has to be taken into account. The simplest view which is used to model the double layer divides the region into three: the electrode, the compact or Stern layer and the diffuse layer, as shown in figure 3.1 [5]. On a metallic electrode, Q_e resides on the surface. On the electrolyte side, the excess charge is distributed among the compact and diffuse layers. The compact layer is bounded by the electrode and the outer Helmholtz plane. The latter is the point of closest approach of solvated

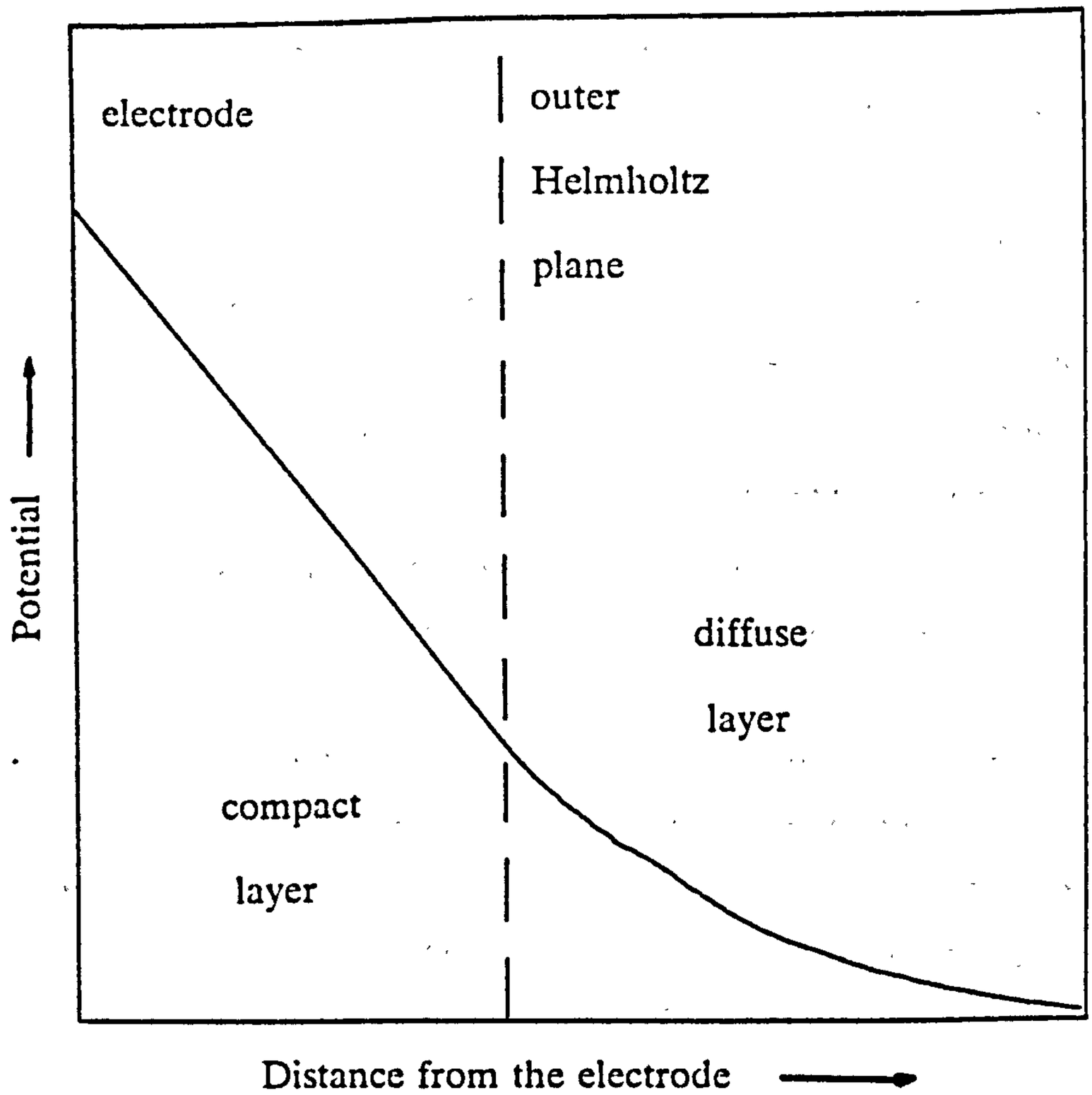

Fig 3.1 The electrochemical double layer (after [5]).

ions, and is determined by the thickness of the sheath of solvent molecules, so that electroactive ions can approach the electrode to the same distance as the supporting ions. ·This distance is only a few angstroms, so that the double layer has a very high capacitance, typically 0.1-1 Fm^{-2}. Because of the thermal motion of the ions, not all of the excess charge stays in the outer Helmholtz plane all the time, but distributes itself in a more extended layer into the electrolyte. This constitutes the diffuse layer, and its extent is dependent on the bulk ionic concentration. It can be up to about a hundred nanometres thick in very dilute solutions, but in the normal case of a large supporting electrolyte concentration it is within about one nanometre.

In addition to purely electrostatic effects, there is also the phenomenon of direct attachment of ions to the electrode, by chemical forces, known as contact adsorption [6]. In the absence of a charge transfer reaction, the effect of contact adsorption is to change the capacitance as the interfacial potential drop is changed. The rate at which this happens is only calculable via a more sophisticated model of the double layer, which takes into account the energy of the association of the ions and the electrode. In general, as the electrode is made positive with respect to the solution, the capacitance increases to a maximum and then decreases. A typical curve of this type is shown in figure 3.2. The initial increase is due to the increasing concentration of adsorbed ions. As their number increases, the repulsive forces between them become important and an increasing proportion of ions attracted to the interface only get as far as the outer parts of the double layer and so the overall capacitance decreases again.

The foregoing description of the double layer has assumed a state of equilibrium. What happens when charge passes through the system depends on the nature of the chemical species present. The two extreme cases are of ideally reversible and ideally polarisable electrodes. The charge distribution across the double layer in an ideally reversible system readjusts itself so as to maintain the potential at the level defined by the nature of the electrode reaction. The effects of mass transport on the ionic concentrations at the electrode are considered for a particular electrode reaction in section 3.4.3. If a voltage source is connected across an ideally polarisable electrode, the capacitance of the double layer charges up and this voltage is maintained even when the source is removed [4]. In practice such an electrode is very difficult to realise because of the spurious effects of impurity reactions, often involving dissolved oxygen or traces of metal ions.

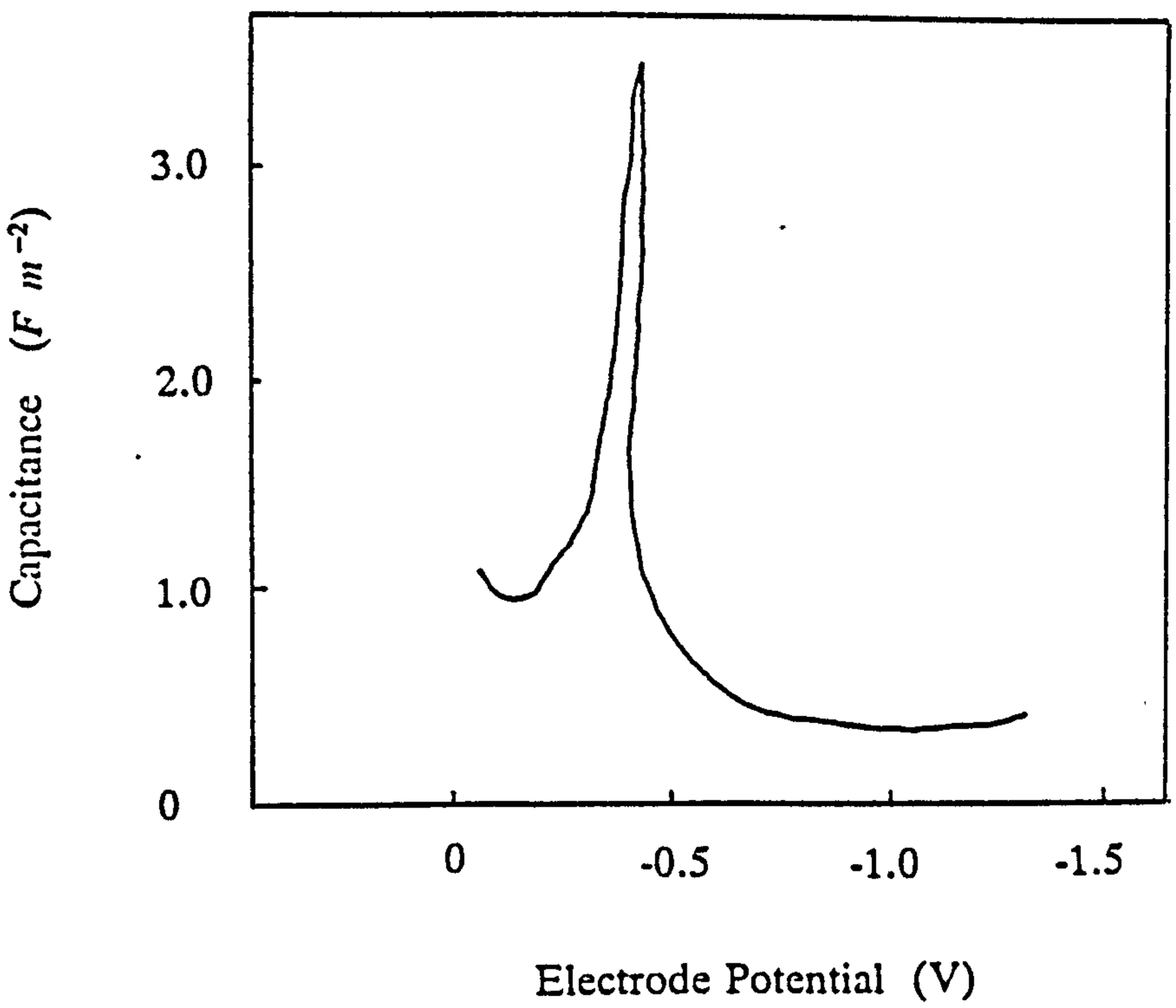

Fig 3.2 Variation of interface capacitance with potential in the presence of surface adsorption (after [6]).

3.4.3. Response to Applied Current

The response of an electrode-electrolyte system to an externally applied current is described by Macdonald [7], and the following is largely taken from that source. If there is an electroactive species O present in redox equilibrium with another soluble species R, via an electrochemical reaction at the electrode of the form

$$O + ze^- \rightleftharpoons R \ , \qquad 3.5$$

where z is the number of electrons supplied from the electrode, then at equilibrium, the potential difference is given by:

$$V = V^o + \frac{RT}{F}\ln\left(\frac{a_O}{a_R}\right) \qquad 3.6$$

where V^o is the potential at infinite dilution and a_O and a_R are the activities of O and R respectively. This expression contains the activities, which are related to the concentrations in solutions via the activity coefficients γ_O and γ_R. The activities may therefore be replaced in equation 3.6 by γ_O, C_O and $\gamma_R C_R$.

If the reaction is ideally reversible, then when a current flows, the potential will continue to be a function of the relative activities of the reactants, but the activities will change as the reaction proceeds. Within the electrolyte, a concentration gradient is set up so that the species being used up at the electrode diffuse towards it, and vice-versa [8]. The situation is illustrated in figure 3.3. The rate of change of potential may be calculated by solving the diffusion equation:

$$\frac{\partial C_O}{\partial t} = D_O\left(\frac{\partial^2 C_O}{\partial x^2}\right) \qquad 3.7$$

and

$$\frac{\partial C_R}{\partial t} = D_R\left(\frac{\partial^2 C_R}{\partial x^2}\right)$$

where D_O and D_R are the diffusion coefficients of the reagents, t is time and x is the distance from the electrode. Because a reversible reaction occurs sufficiently fast to

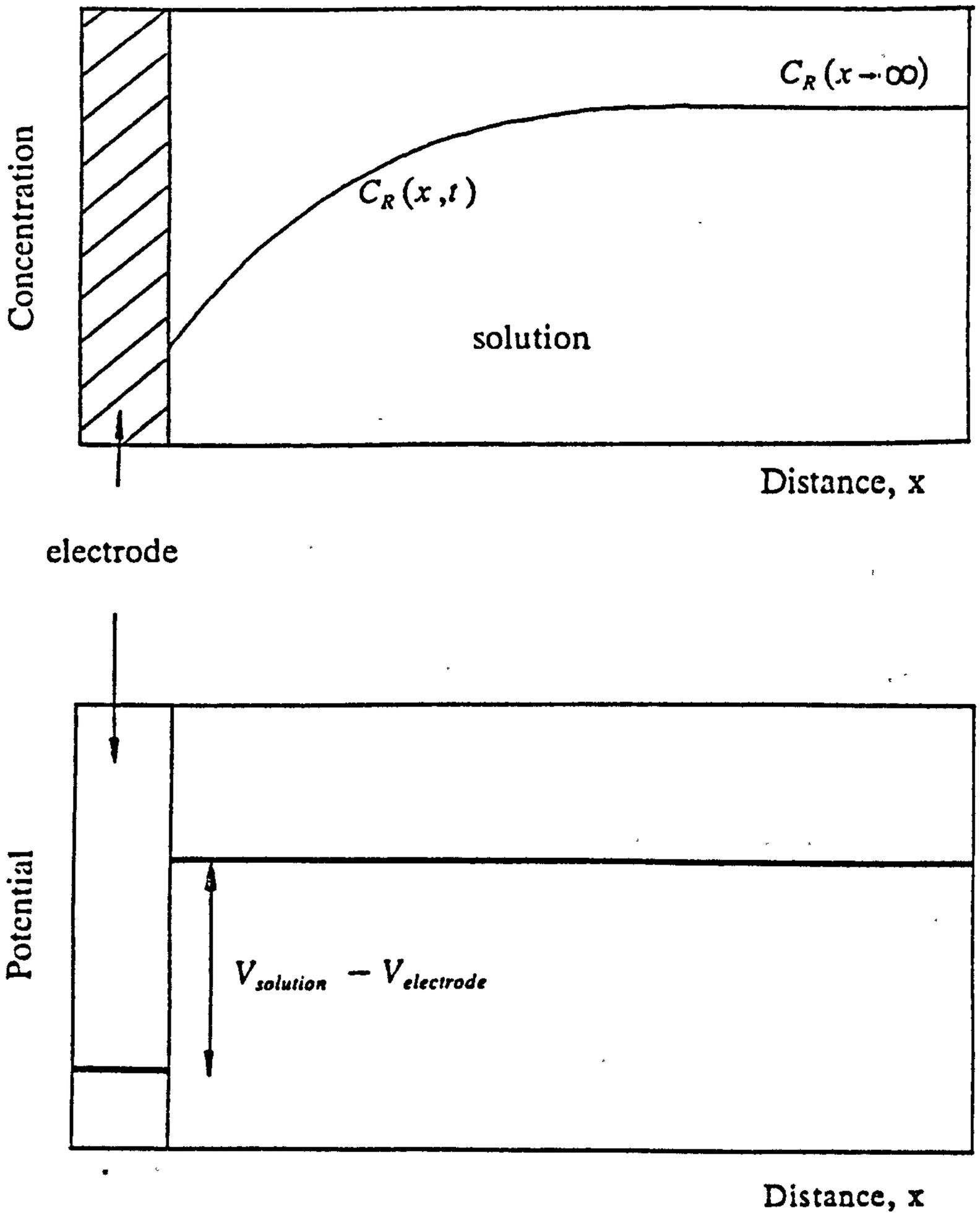

Fig 3.3 Distribution of potential and ionic concentration in an electrochemical cell (after Macdonald [8]).

maintain equilibrium at all times, the development of potential is a quasistatic process. This implies that the concentrations at the electrode are not affected by the current, and the rate of diffusion of products away from the electrode is equalled by the rate of diffusion of the reactants towards it. One of the boundary conditions for equations 3.7 may therefore be expressed as:

$$D_O \frac{\partial C_O}{\partial x} + D_R \frac{\partial C_R}{\partial x} = 0. \qquad 3.8$$

For the same reason, the rate of charge transfer is equal to the rate of diffusion of reactants, setting another boundary condition:

$$i(x=0) = zFAD_O \frac{\partial C_o}{\partial x} = zFAD_R \frac{\partial C_R}{\partial x}. \qquad 3.9$$

where A is the area of the electrode. The bulk concentrations remain unchanged at ${C_O}^b$ and ${C_R}^b$:

$$C_O \to {C_O}^b \text{ and } C_R \to {C_O}^b \text{ as } x \to 0. \qquad 3.10$$

The initial condition is

$$C_O = {C_O}^b \text{ and } C_R = {C_R}^b \qquad 3.11$$

for all x at $t=0$.

The method of Laplace transforms is usually applied to this system since equations 3.7 are linear. If i is constant then the solution is

$$C_O\ (x=0) = {C_O}^b - \frac{2it^{1/2}}{zFA{D_O}^{1/2}\pi^{1/2}} \qquad 3.12$$

and similarly for C_R. Clearly there is a time at which C_O becomes zero. This is called the transition time τ.

The potential may be calculated for all times up to τ via equation 3.12. For the situation where ${C_O}^b = 0$, equations 3.6 and 3.12 may be combined to give the potential at any time before τ:

$$V = V^o - \left(\frac{RT}{zF}\right)\ln\left(\frac{\gamma_R D_O{}^{1/2}}{\gamma_O D_R{}^{1/2}}\right) + \left(\frac{RT}{zF}\right)\ln[(\tau/t)^{1/2} - 1] \qquad 3.13$$

After τ, more current is flowing through the system than can be accommodated by the reaction, and the "extra" charge then charges up the double layer.

An electrochemical technique based on application of a constant current is known as chronopotentiometry, and the curve of figure 3.4 as a chronopotentiogram. The values of D_O, D_R, E_o, C_O and C_R can all be found through equation 3.13 by measuring τ. The relations between potential, concentration, diffusion coefficient and time have been worked out for a great variety of possible types of electrode reaction, of which the reversible reaction described above is the simplest.

Another very important case is when the potential between the electrode and the solution is dependent on the rate of the reaction as well as the equilibrium potential. This dependence is derived from the activated complex theory of chemical kinetics. For the case of a metal oxidising so that its ions pass into solution, it is described by Koryta et al [9] in terms of the potential energies of the products and reactants. This is represented diagrammatically in figure 3.5. Curves I and II are the potential energy wells of the metal ion in its solid and solvated states at equilibrium. The crossover point, Q_o, represents the maximum energy which the ion has to gain so that it can pass from one state to another. This is the transition state, or activated complex. The energy differences between point a_o and the minimum energies of the two wells, W_{10} and W_{20}, are the activation energies of the reactions taking the ion into and out of the solution respectively. The rates of these are therefore:

$$j_1 = k_1 \exp\left(\frac{-W_{1O}}{RT}\right) \qquad 3.14$$

and

$$j_2 = k_2 C_O \exp\left(\frac{-W_{2O}}{RT}\right) \qquad 3.15$$

where k_1 and k_2 are constants containing the ratios of the activity coefficients and the vibrational frequency, and C_O is the concentration of the metal ions in the solution. Ionic concentration does not appear explicitly in equations 3.14 and 3.15 because the

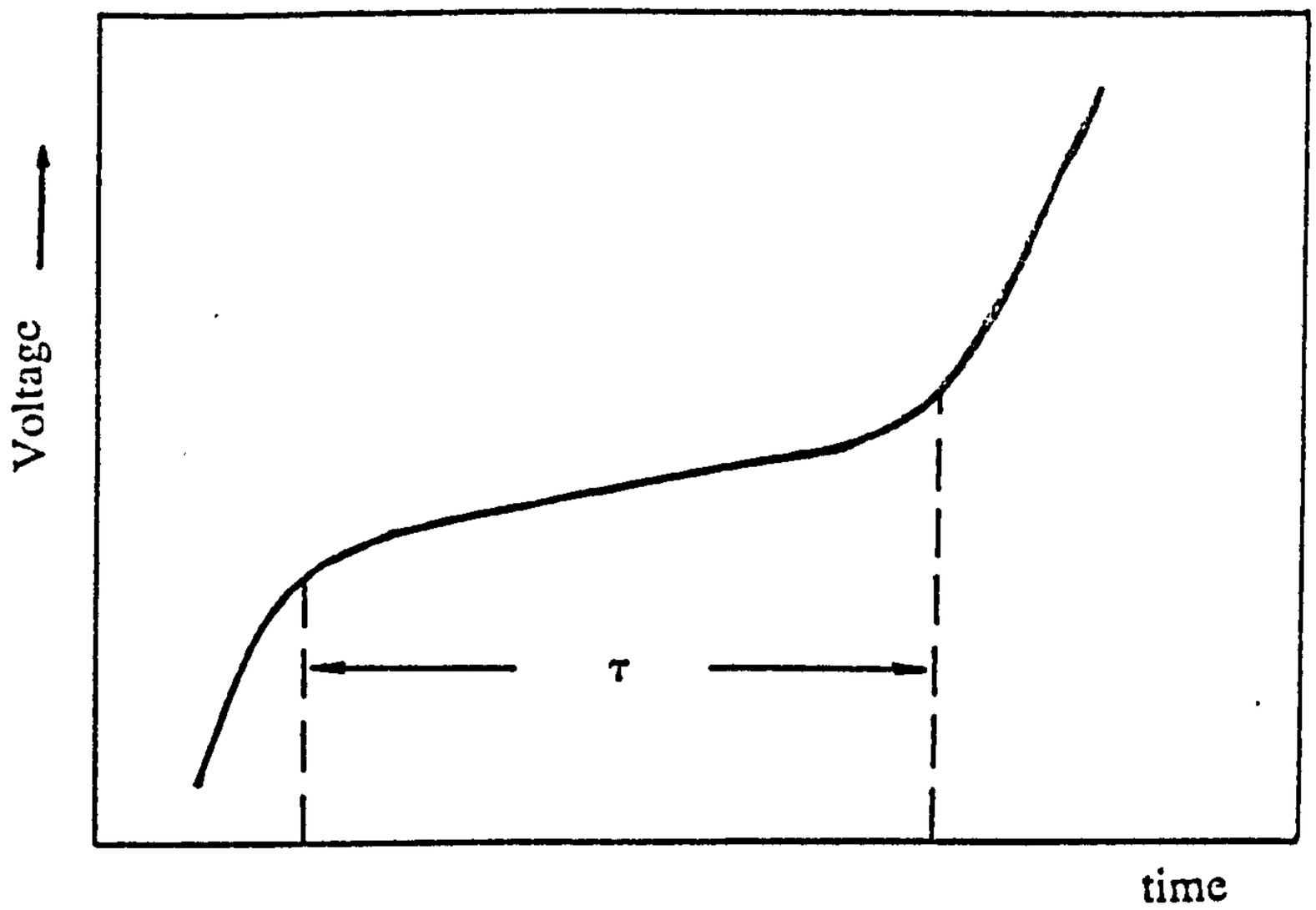

Fig 3.4 Chronopotentiogram for a reversible reaction (after Macdonald [7]).

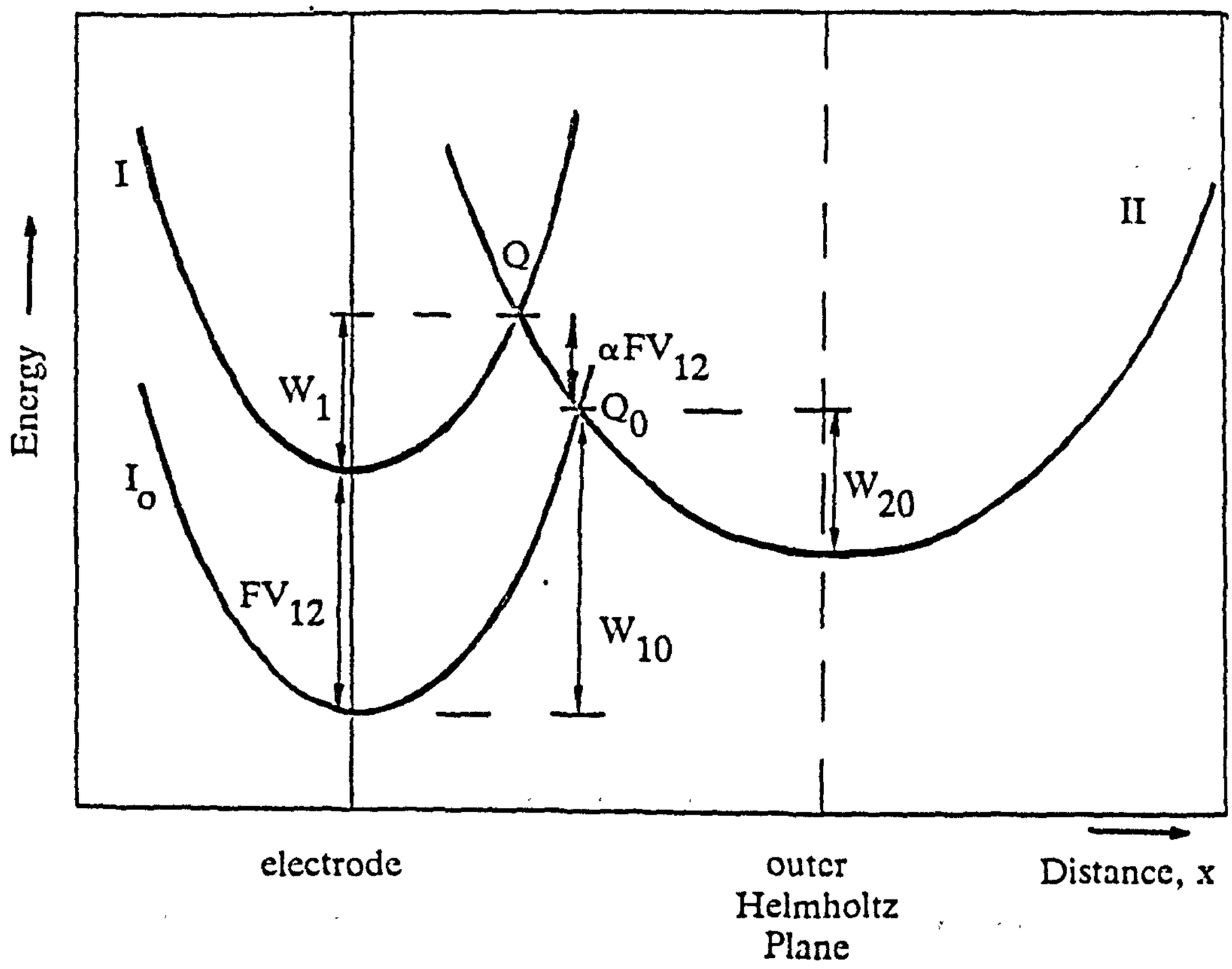

Fig 3.5 Potential energy diagram model for kinetics of electrochemical reaction (after Koryta [9]).

activity of the metal ions in the electrode is unity. When a potential is applied so that the system deviates from equilibrium, the energy difference between the potential wells changes by the amount V_{12}, which is the fraction of the total potential which is dropped between the electrode and the outer Helmholtz plane. The transition point Q does not move by the full amount V_{12}, as can be seen from the diagram, and the activation energies change to $W_{10} - (1-\alpha)V_{12}$ and $W_{20} - \alpha V_{12}$. The reaction rates change to

$$j_1 = k_1 \exp\left(\frac{-W_{10} + (1-\alpha)zFV_{12}}{RT}\right) \qquad 3.16$$

and

$$j_2 = k_2 C_o \exp\left(\frac{-W_{20} + \alpha zFV_{12}}{RT}\right). \qquad 3.17$$

The rate of charge transfer is equal to the difference between j_1 and j_2. The constants k_1 and k_2 may be related and replaced by a single constant by using the fact that when $j_1 = -j_2$, the electrode potential is equal to the equilibrium potential so that

$$k^o = k_2 \exp\left(\frac{-\alpha nFV^o}{RT}\right) = k_1 \exp\left(\frac{(1-\alpha)nFV^o}{RT}\right). \qquad 3.18$$

The current can then be expressed as

$$\frac{i}{RT} = k^o \left(C_o \exp\left(\frac{-\alpha nF\eta}{RT}\right) - \exp\left(\frac{(1-\alpha)nF\eta}{RT}\right)\right) \qquad 3.19$$

where η is equal to $(V - V^o)$, and is known as the overpotential. A more exact theoretical procedure, also given in reference 6, arrives at the same result but allows for a reaction between two species in solution, for which the second term has an extra factor C_R. This is the Butler-Volmer relation for electrode kinetics, and its form has been encountered in many experimental situations. If k is very small, so that no current flows until the overpotential is more than about a tenth of a volt, then one of the terms may be neglected. Sometimes the voltage range used is such that the

reaction only ever goes one way, in which case it is termed "irreversible", although in principle it may be still be thermodynamically reversible, since it may be in equilibrium with a very slow reverse reaction In either of these two cases, the relation between the current and the overpotential is exponential. When both the forward and reverse terms are significant, the reaction is called quasi-reversible.

The Butler-Volmer relation can be used as a boundary condition in equation 3.7, and the variation of potential and concentrations found as functions of time, as for the reversible case. When η is small, its development with time may be approximated by

$$\eta = i\,(At^{1/2} + BC_{dl} + X) \qquad 3.20$$

where C_{dl} is the double-layer capacitance and A and B are constants. If interface concentrations, transport of electroactive species, and charging of the double-layer are taken into account, the relation between total electrode potential is at least a very complicated expression, and sometimes an analytical solution is not possible at all [7]. For simple reactions, the most serious factor interfering with the interpretation of experimental results is usually the effect of double layer charging, which can be eliminated by increasing the current by the amount required to charge a capacitor of the same value as C_{dl}. More complicated situations have also been studied and it is possible to use the chronopotentiometric approach to extract kinetic data along with the equilibrium potential and diffusion constants from a very wide range of electrochemical reactions, including those involving other factors, such as coupled chemical reactions, plating out of reaction products etc.

However if the kinetic data alone is required, a simpler approach is to vary the current and plot it against the overpotential [9]. The result is called a Tafel plot, an example of which is given in figure 3.6. This simply shows the exponential relationship between voltage and current at overpotentials greater than about RT/F. The slopes of the lines on each side of the $\eta = 0$ ordinate give the values of α and $(1-\alpha)$.

The derivation of the Tafel relation assumes that the changing potential is due solely to drops between the electrode and the outer Helmholtz plane. This is only ever approximately true because of the concentration-dependence of the potential drop across the diffuse part of the double layer. Taking this into account alters the ideal Tafel plot in the vicinity of the point of zero charge, ie that state of the electrode-electrolyte system where the total charge stored in the double layer is zero. Further

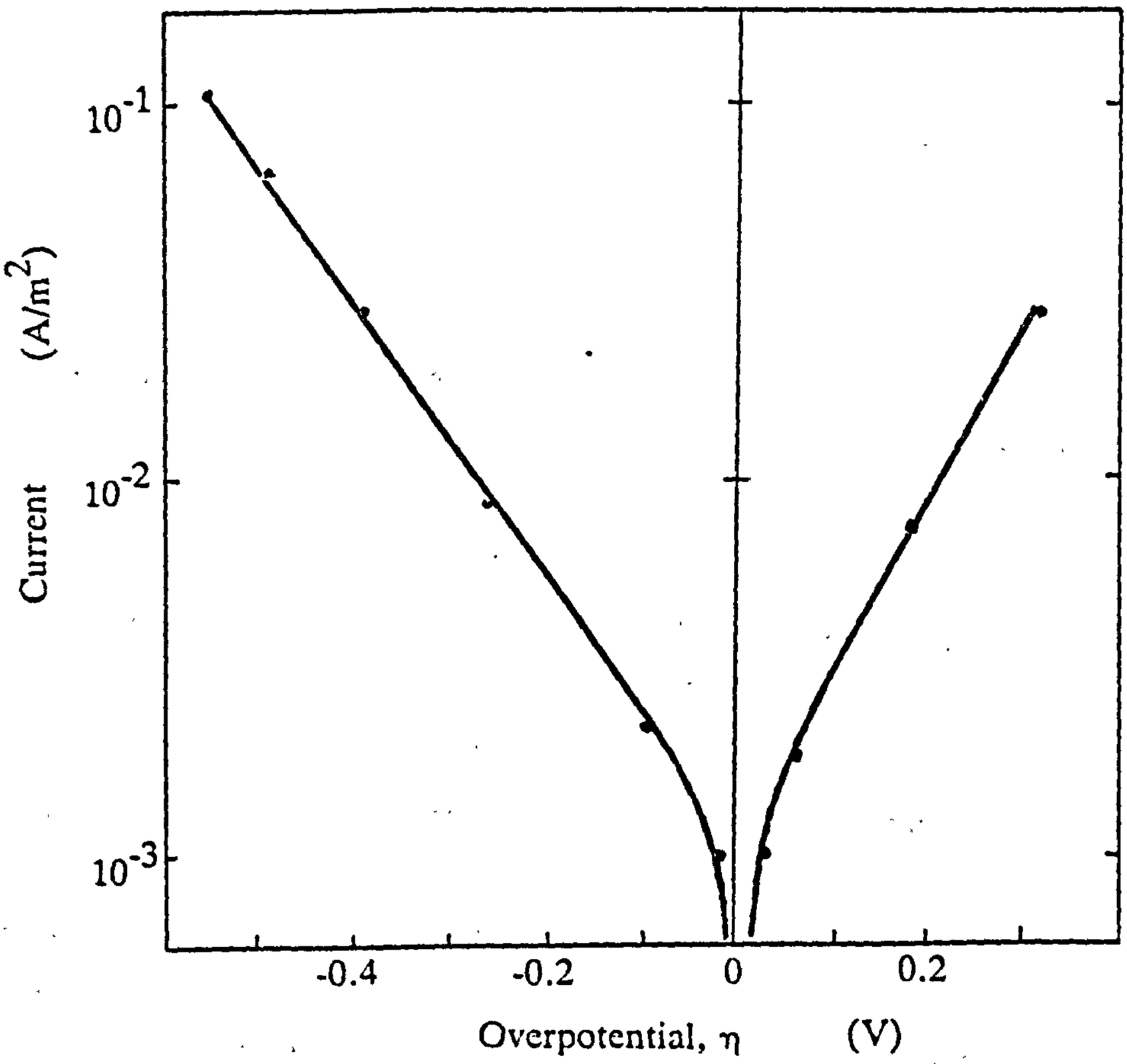

Fig 3.6 Tafel plot of a kinetically limited reaction (after Koryta [9]).

deviation from ideality is caused by the other double-layer effects referred to in the discussion of the double layer above. Calculations of the effects of these are specific to the particular model of the double layer applied to the situation.

3.5. Point of Zero Charge Analyses

3.5.1. Unsupported Electrolytes

Inside sodium silicate glass, Na^+ ions are the only charge carriers. This implies that any deviation from equilibrium concentration causes a change in the excess charge density and hence a change in the electric field, so that the migration term of the Nernst-Planck equation must be explicitly taken into account. An exception to this may be where foreign ions are introduced from the electrode for which the sodium may act as a kind of supporting electrolyte.

Even with smooth, plane parallel electrodes and a homogeneous electrolyte, the direct solution of the equation presents a very complicated problem except where the boundary conditions are sufficiently simple. The complexity of the calculation is very sensitive to the existence and nature of any charge-transfer reaction at the electrode and depends on whether a steady-state or fully time-dependent solution is required.

Many solutions of the Nernst-Planck equation have been based on the assumption that the steady state around which the perturbation is being made is the point of zero charge [2]. This is the state of the system where the excess charge near the electrode is zero, so that the double-layer is uncharged. The concentrations of all the carriers have the same values next to the electrodes as they have in the bulk, and the field is zero throughout the electrolyte. A wide variety of conditions can still apply even with this restriction, and solutions involving variable carrier number, type and mobility, as well as the presence of finite rates of generation and recombination, and discharge at the electrodes, have been produced [2].

3.5.2. Assumptions Required for Solution

Most solutions specify the important condition that the magnitude of the perturbation to the system is sufficiently small that the equations are linearisable, ie can be cast in a form where the field is decoupled from the carrier concentration. This is valid where the total applied voltage is less than about RT/F [10].

For higher applied voltages, the fully coupled nonlinear equation must be solved. This has been done [2] by assuming a step potential, but has only been solved numerically for a few special cases. Restrictions on the maximum carrier concentrations have also been considered [12].

3.5.3. Forms of Solution and Presentation

The above assumptions concerning the behaviour of the charges within the system allow the current in response to a small voltage signal to be calculated, and the result to be presented in the form of the electrical impedance or admittance of a circuit composed of linear elements.

For the small-signal cases, linearisation is achieved by imposing a harmonic driving potential [12]:

$$V = V_o e^{j\omega t} \qquad 3.21$$

and assuming a solution of the same form:

$$C = C_o(x) + C_1(x)e^{j\omega t} \qquad 3.22$$

This is the response to an AC applied voltage, and may be used to make comparisons with AC data for real systems. However, although the complete solution may be expressed in terms of the concentration dependence in space and time, it is not in a convenient form for electrical measurements, where the carrier concentrations are not measured directly. The relation between carrier density and field is therefore used to obtain an expression for the overall current and hence for the impedance presented by the system.

There are two ways of presenting the results of an AC analysis. Analytical expressions for the real and imaginary parts of the impedance or admittance may be given, which is equivalent to giving the component values of a series or parallel RC circuit which has the same characteristics of the system. Alternatively, a more sophisticated equivalent circuit consisting of linear elements, usually resistors and capacitors, is constructed which models the calculated response, with some of the circuit elements being frequency dependent. The second approach is usually much more convenient both for physical insight into the data and for comparison with experimental results

[13].

A basic function of the equivalent-circuit representation is the division of the system into bulk and interface regions. The interface region may be defined as that where the carrier concentration deviates significantly from the bulk level. Its depth is characterised by the Debye length L_D, which is the average distance an excess carrier must travel from the electrode to establish space-charge equilibrium. It is approximately the spacing required between two parallel plates to have the same capacitance as the space-charge region. This is described more fully in section 3.6.

Different equivalent circuits are appropriate to different systems. A particular example, possibly of some relevance in the present context, is charge transport in a solid polycrystalline electrolyte. According to Macdonald [2] this can be modelled by the series circuit of figure 3.7 (a), the three elements of which correspond to transport within the crystallites, between them, and at the electrodes. Figure 3.7 (b) shows the three contributions to the response of a liquid or single crystal and the ladder circuit which represents them.

Care must be taken in ascribing physical significance to the components of equivalent circuits, because by correct choice of values, the responses of all of these circuits can be identical at all frequencies. In fact there are an infinite number of equivalent circuits which can reproduce any given response. The usefulness of the method lies in the ease with which a circuit can be constructed for a given situation so that the processes responsible for the observed behaviour may be visualised. The validity of particular circuits may be assessed by varying the dimensions, temperature etc of specimens of the material.

3.5.4. Specific Solutions of the Nernst-Planck System

Macdonald [11], following on from and improving earlier work by Jaffe, and Chang and Jaffe [14], obtained analytical expressions for the potential and concentration distributions of a two-carrier system at the point of zero charge under sinusoidal AC stimulus by linearising the Nernst-Planck equation. His major assumptions were:

(a) The two carriers have equal mobilities and opposite charges.

(b) Carriers are generated and recombine bimolecularly, ie the concentrations of each are always equal.

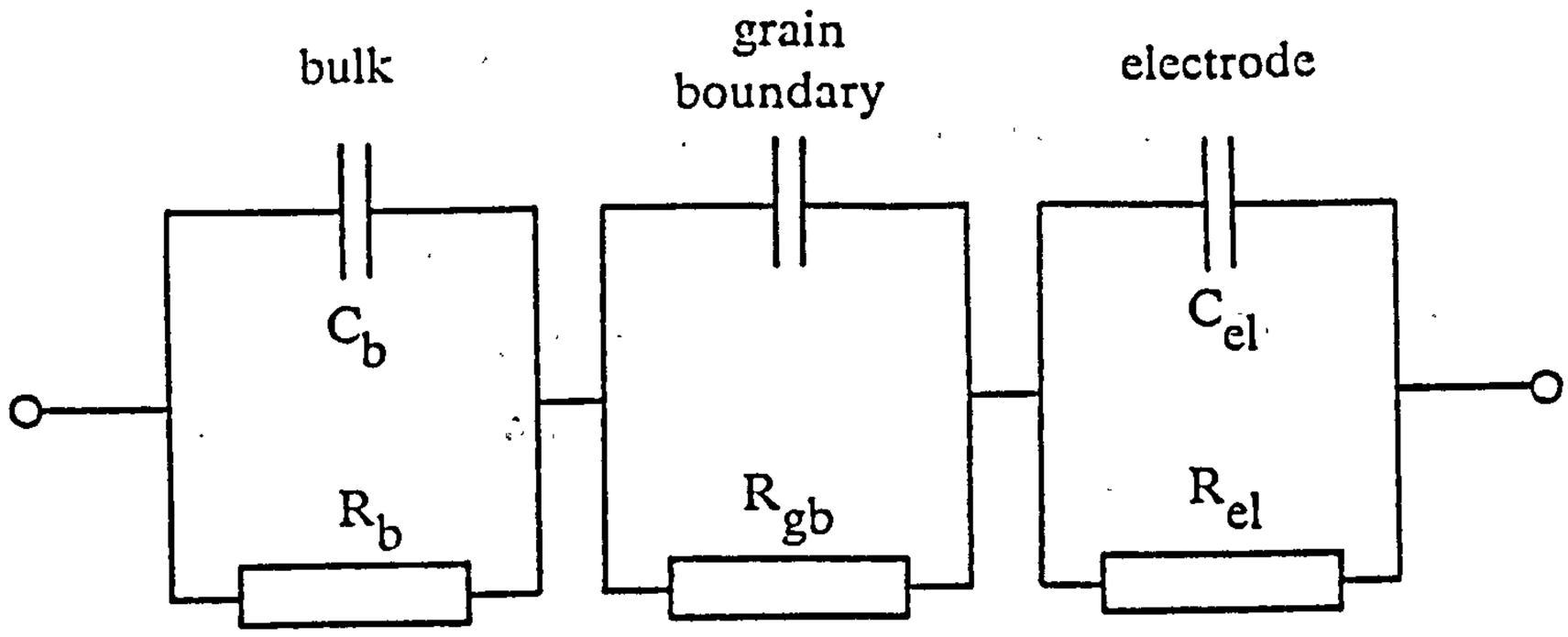

(a) Voigt circuit

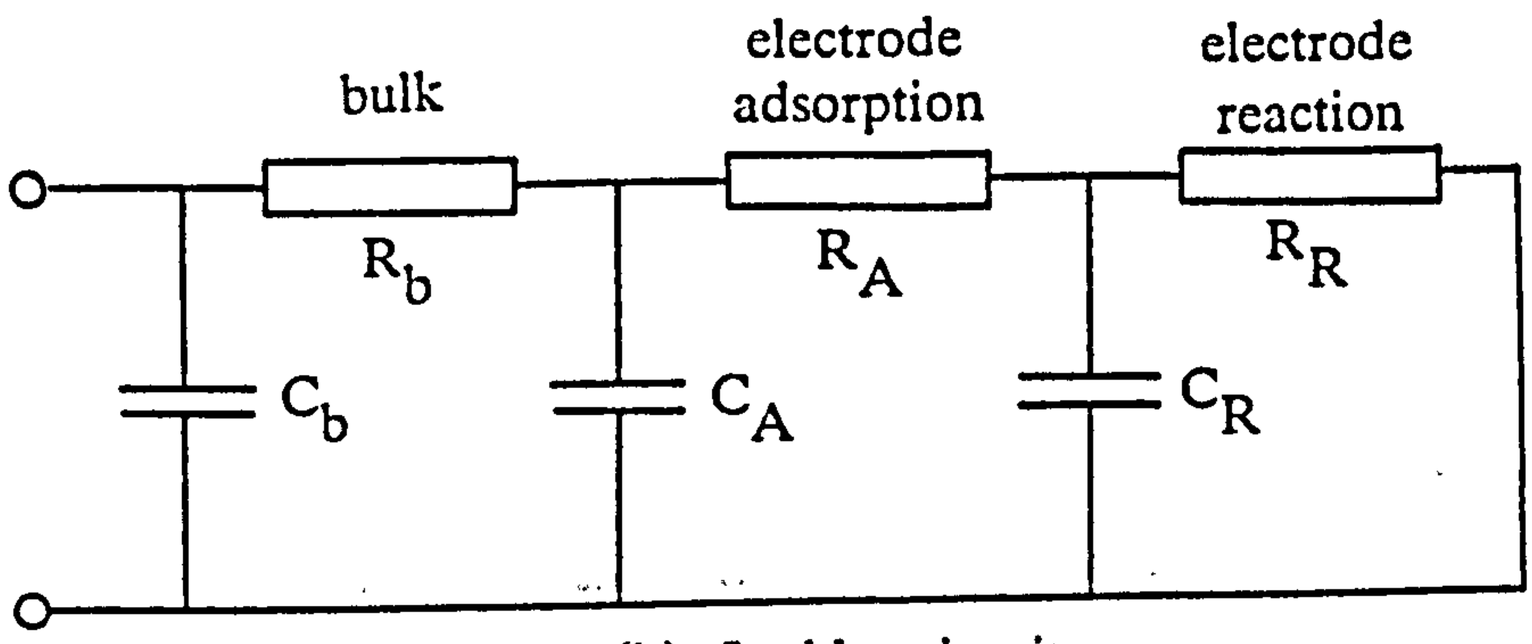

(b) Ladder circuit

Fig 3.7 Equivalent circuits representing solid electrolyte systems (after Macdonald [2]):
(a) Three-element series circuit for polycrystalline electrolyte.
(b) Ladder circuit for liquid or single crystal.

(c) Neither carrier is discharged at the electrodes.

(d) There is no restriction of the excess concentrations of carriers.

(e) The Nernst-Einstein relation between mobility and diffusivity holds exactly.

Even with these assumptions, introduced to allow mathematical tractability, the solutions consist of such complicated analytical expressions that immediate application of the resulting theory to electrolytes is not possible. However this solution established a procedure on which all further analyses involving similar conditions were based. The form of presentation of the results was designed to allow a convenient means of comparison with experimental data through their expression as a frequency-dependent admittance Y:

$$Y = j\omega C_g + G_p + j\omega C_p \qquad 3.23$$

where C_g is the geometrical capacitance of the electrodes, G_p and C_p are the parallel conductance and capacitance, and ω is angular frequency. However the full expressions for G_p and C_p involve complicated combinations of hyperbolic trigonometric functions, and in order to be interpreted in a qualitative manner, special cases have to be considered. The expressions for C_p and G_p when the mobilities are equal, also apply when the mobility of one carrier is zero.

In 1954, Macdonald and Brachman [15] published a solution for the steady state reached by a system after a voltage step has been applied. It is valid for voltages within the linear region, under similar conditions to the above, but in the absence of generation and recombination. In this case the potential and concentration distributions were calculated at all points between the electrodes. Although the results are not directly applicable to any physical systems, they have provided the basis for further studies.

Discharge of the carriers species at the electrodes was taken into account by Friauf in 1954 [10] who assumed equal equilibrium numbers of positive and negative carriers but allowed for different mobilities. His analysis was done with the purpose of modelling the AC response of the solid electrolyte silver bromide with silver and gold electrodes. The boundary condition used for the discharge was based on the assumption that the rate of charge transfer was proportional to the excess concentration of the ions:

$$I(x=0) = \left(\frac{eD_p}{L}\right) r_p \Delta C \qquad 3.24$$

where I is the current at the electrode

e is the charge

D_p is the diffusion coefficient

L is the electrode spacing

r_p is the discharge parameter

and ΔC is the excess concentration of positive carriers.

This representation of discharge had first been used by Chang and Jaffe [14] who applied it purely formally. The physical interpretation given for it by Friauf, is the presence of a symmetrical barrier of height W at the electrode. This gives r_p as:

$$r_p = aL\,\nu_o D_p^{-1} \exp\left(-\frac{W}{kT}\right) \qquad 3.25$$

where a is the interionic distance and ν_o is the vibrational frequency. No physical reason was given why such a barrier might be expected at these electrodes, nor was any example given of it having been observed in any other system.

Friauf solved the equation analytically, but in order to present his data in a form which was comparable to experimental data, he derived approximate expressions for parallel capacitance and conductance (C_p and G_p) which were valid for a restricted range of frequency. Numerical results were calculated using mobility values for silver bromide in which silver and bromine vacancies are the charge carriers. The values had been obtained from previous conductivity data. The electrode materials were chosen because silver was expected to form a reversible contact via the discharge of silver vacancies, while no such reaction was expected for gold which would then be completely blocking.

The form of the frequency response of both gold- and silver-contacted samples was the same as that calculated theoretically for discharging electrodes, but C_p for gold was a factor of ten less at all frequencies than that for silver, and was much greater in both cases than had been predicted.

Friauf claimed that the matching of the frequency response was sufficient evidence to conclude that the observed polarisation was due to the accumulation of

interstitial silver near the electrode, with Ag^+ ions undergoing a finite rate of discharge, and that the discrepancy in magnitude was due to an increase in effective surface area caused by the roughness of the interface.

Another attempt involving similar conditions by Macdonald in 1971 [16] introduced the same Chang-Jaffe boundary conditions to his existing two-carrier theory. His results, even when expressed as overall impedance, are extremely complex analytical expressions, of which only the zero-frequency limiting forms were given.

Further generalisation was introduced [3] by defining the system in terms of six parameters r_p, r_n, π_m, π_z, ξ and M in the equations and boundary conditions: r_p and r_n are the electrode discharge parameters for the positive and negative carriers as defined in equation 3.24; π_m and π_z are the ratios of the mobilities and of the valencies; $\xi = N^2_{\sigma/2zn} i$, where N_σ is the number of free carriers; and $M = (l/L_D)$ where l is the electrode separation. This allowed the investigation of a wide range of experimental conditions with a unified mathematical approach. The results are presented as C_l and R_l in the equivalent circuit of figure 3.8. The other components in this circuit are the geometrical capacitance, C_g, and constant resistances associated with bulk conduction, G_D, and interface-region conduction, G_E. The frequency dependence of C_l and R_l are very complicated expressions and the form of the response is given graphically only for a very restricted range of parameters in the limit of zero frequency. No attempt was made in the first instance to fit them to any experimental data which, involving as it does the variation of six parameters to fit frequency and temperature ranges, could be very difficult.

However a method was given for handling the results of the theory [13] based on the observation that the complex impedance plot is, in general, made up of three arcs, two circular and the other skewed. The skewed arc was of the same form as that found in liquid electrochemical systems when transport is diffusion-controlled, when it is known as a Warburg response [17]. Since there was no supporting electrolyte present in this case, the results seemed to indicate that the observation of Warburg-type response does not constitute sufficient evidence for diffusion control. Discharge of one of the carriers results, approximately, in the addition of a parallel resistance to these circuits, but with two different values of Warburg impedance in different frequency ranges, with $(Z_{W1}/Z_{W1}) = 2$. Macdonald applied his results to liquid electrolytes for the most part, but the general form of the results, which translate to a measured capacitance proportional to $\omega^{-3/2}$ at high frequency and $\omega^{-1/2}$ at low frequency, should also

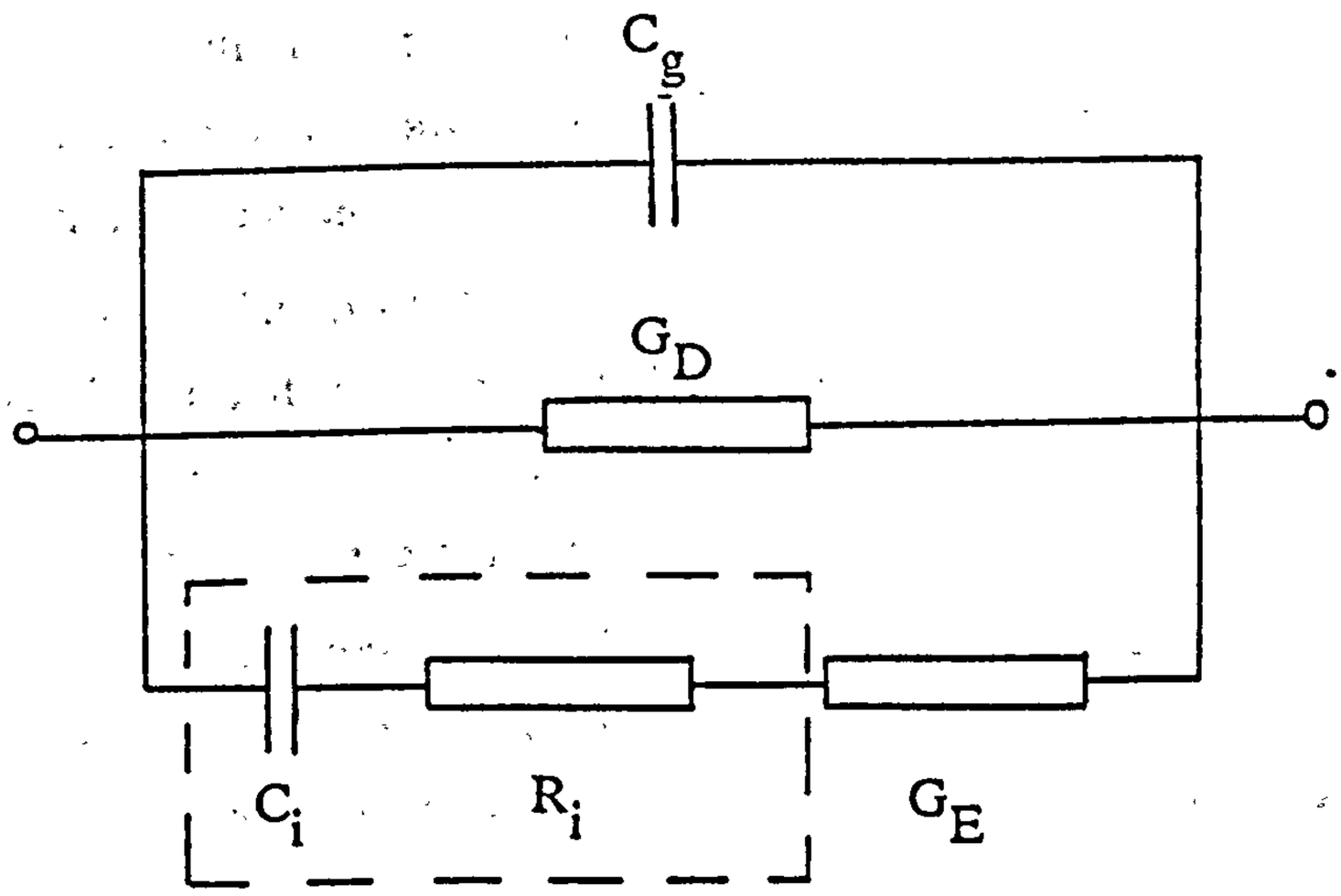

Fig 3.8 Equivalent circuit used by Macdonald to present theoretical frequency response of electrolyte-electrode system (after [2]).

be applicable to solid state electrode systems.

A further observation contained in reference 13, relevant to present considerations, is that the response of rough electrodes may be similar for both blocking and partially nonblocking situations.

In general, the variation of the response with different values of the six parameters of reference 3 still had to be calculated by computer using the exact formulae, but the presentation in the form of equivalent circuits and physical identification with physical processes was made considerably easier.

The same discharge boundary conditions were used by Beaumont and Jacobs [18] for a single-carrier system. Their results, reproduced in figure 3.9, were presented in the form of frequency-dependent capacitance and conductance. AC experiments were carried out on a crystal of strontium-doped potassium chloride with carbon and platinum electrodes. The charge carriers were assumed to be cation vacancies induced by the presence of strontium. The discharge parameter was adjusted so as to fit as closely as possible the straight lines of the theory to the curves obtained experimentally, as figure 3.9 shows. They also found that an AC amplitude of up to 45 V rms could be used without the measured C_p and G_p changing, which was very surprising in view of the expected breakdown of the linear approximation above 25 mV.

3.6. Solid-State Electrochemical Processes

The major drawback to applying the analyses of section 3.5 is not their complexity, but the inappropriateness of their initial assumptions. Even in the cases where results of measurements on real systems have been compared with the theory, the necessary condition of the point of zero charge has not been established. The actual condition determining the potential at the electrode depends on how the charge carriers react when they reach the electrode, ie on the discharge conditions. For example Friauf [10], in comparing experimental data with theory for the parent metal system $Ag : AgBr$ and an inert electrode system $Au : AgBr$, assumed that flat-band conditions would hold both at the equilibrium expected at the former and the charge blocking situation of the latter, a state of affairs which has been demonstrated as being very unlikely [19]. The factors governing the potential at a parent metal electrode have been discussed in detail by Raleigh [19]. A parent metal electrode is formally reversible, since the ions which are mobile in the electrolyte can take part in a redox equilibrium with the electrode. In this case, the potential across the interface will be

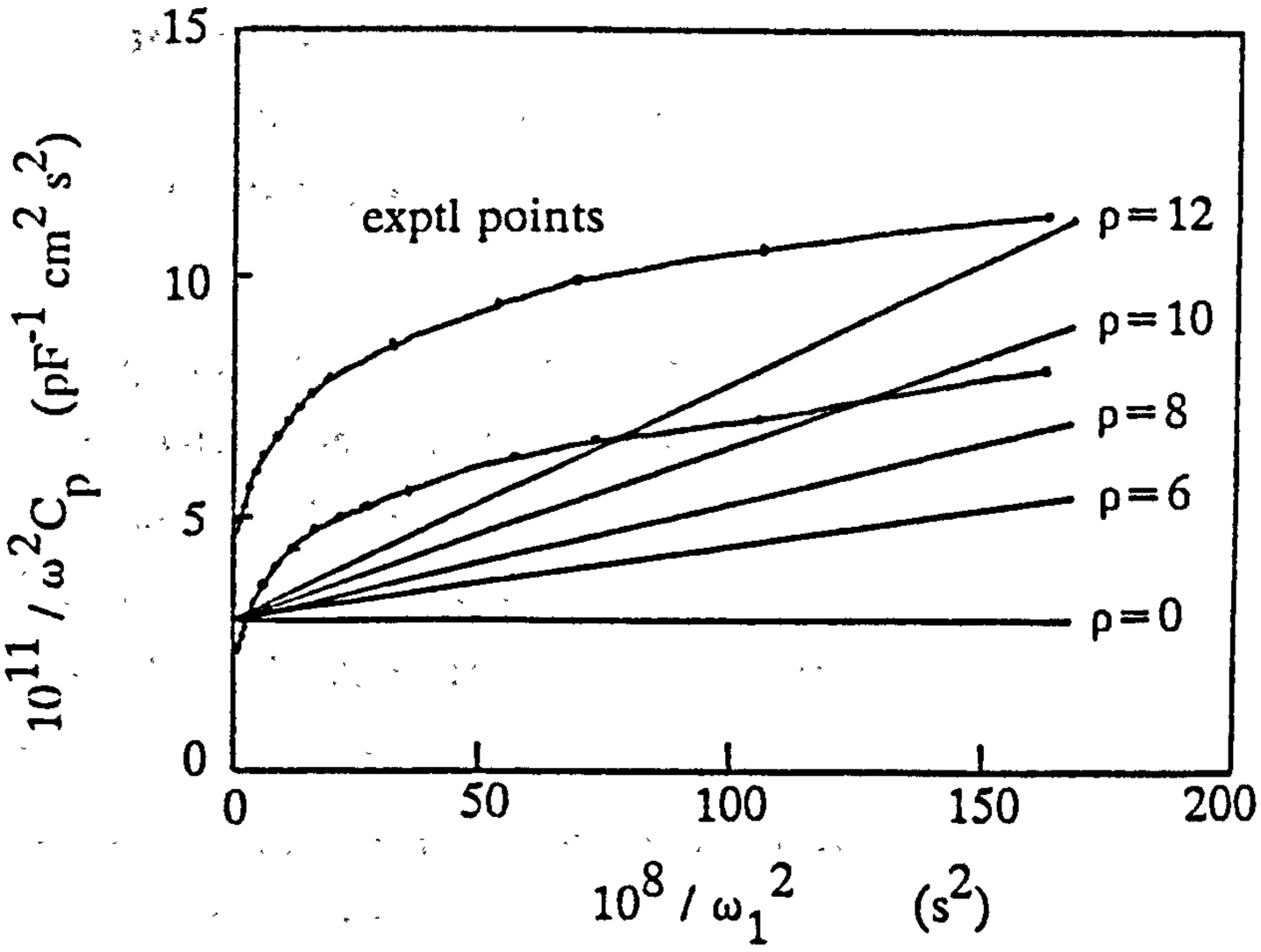

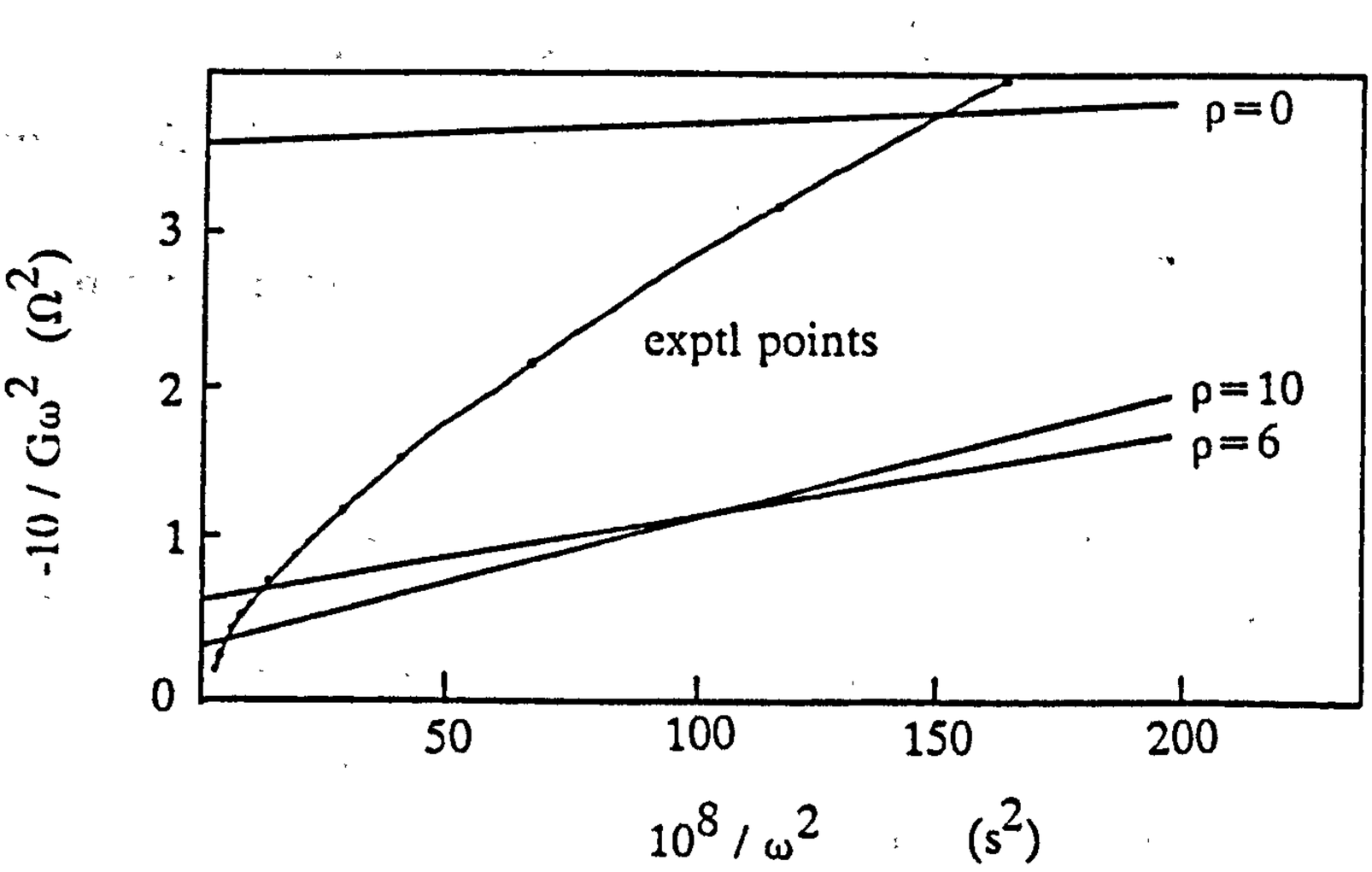

Fig 3.9 Theoretical and experimental frequency response obtained by Beaumont and Jacobs for strontium-doped potassium chloride crystal (after [18]).

determined by the equilibrium potential of the reaction, which is unlikely to be zero as required by the point of zero charge assumption. The potential at an electrode which is not formally reversible, such as the gold electrode at $AgBr$, is an accidental function of the effects of varying stoichiometry near the surface of the electrolyte and of impurity reactions at the interface, unless its potential is referred to an electrode which is reversible.

The Chang-Jaffe boundary conditions universally adopted to model the charge-transfer in the analyses described above were chosen because they allowed mathematical tractability, and not because they were the most physically justified. This point was made by Franceschetti and Macdonald [20] who admitted the desirability of using the more realistic Butler-Volmer model of the interfacial reaction but found that the mathematics become too complicated.

A completely different approach to the effects of interfacial charge-transfer is to start from the point of view of electrochemical equilibrium, in the same way as with liquid electrochemistry. This requires the identification of a reversible reaction which can be assumed, through purely chemical considerations, to have a well-defined equilibrium potential. A salt in contact with its parent metal is one example, as mentioned above. Another type is an electrode of the second kind, where contact to an electrolyte is made through a second electrolyte with a parent-metal contact. An example is the system $Ag : AgF : LaF_3$ [21] where the silver reacts reversibly with the AgF and F^- ions are passed between AgF and LaF_3.

The experimental investigation of electrochemical reactions at solid electrodes on solid electrolytes and the special considerations which are associated with them have also been reviewed by Raleigh [19]. He devoted most attention to the specific cases of contacts to single-crystal and polycrystalline $AgBr$ but his general ideas are applicable to other electrolytes. He used inert electrodes of platinum and graphite, which were assumed not to react with the electrolyte, with a parent metal (ie silver) electrode as a reference. The activities of the ions near the inert electrodes were thus determined solely by the potential with respect to the silver electrode. Since the activity a_M of M in a compound MX is, by definition, unity at an M electrode, then its activity on an inert electrode is given by:

$$a_M = \exp\left(\frac{qV}{kT}\right) \qquad 3.26$$

and the activity of X by

$$a_X = \exp\left(\frac{q(\epsilon_d - V)}{kT}\right) \qquad 3.27$$

where ϵ_d is a constant, called the decomposition potential of MX. Nonparent metals which may react with the electrolyte were not considered in detail, because a stable equilibrium is not expected at these.

An important consideration in Raleigh's analysis of the solid $AgBr$ system was the physical effects on the interfaces of the flow of current through a parent-metal electrode cell. Figure 3.10 is a schematic diagram of one of his cells before and after charge has passed. Even if the interfaces are initially perfectly smooth and in contact, the movement of silver from the anode into the electrolyte will leave behind it vacancies or gaps which may grow sufficiently to affect the distribution of field and potential at the interface. At the cathode, silver metal will accumulate, possibly disrupting the interface. This is one example of the general problem of buildup of electrode products at solid state electrodes. Such phenomena complicate the interpretation of the response to applied voltage and current, and their representation in a convenient mathematical form as boundary conditions for the Nernst-Planck equation is not normally possible.

The experimental cells used by Raleigh involved a reference electrode through which no current passed. This arrangement, analagous to that used in liquid electrochemistry, avoided the development of overpotential and the associated problem of deposition and depletion described above. It also allowed the potential being measured to be identified with the working electrode, which was of one of the "inert" materials, platinum and graphite.

Most of the measurements were made with the working electrode cathodic with respect to silver, but well above the breakdown potential. Outside these limits either silver metal was deposited or bromine gas evolved. On application of a small potential step within this range, the current rose immediately and decayed asymptotically to zero, but not with an exponential form as predicted from electrochemical theory for an ideally polarisable (blocking) electrode.

For quantitative evaluation of the results, the capacitance, as calculated from the total charge passed and the height of the voltage step, was plotted as a function of the starting potential. The results are reproduced in figure 3.11. The constant capacitance

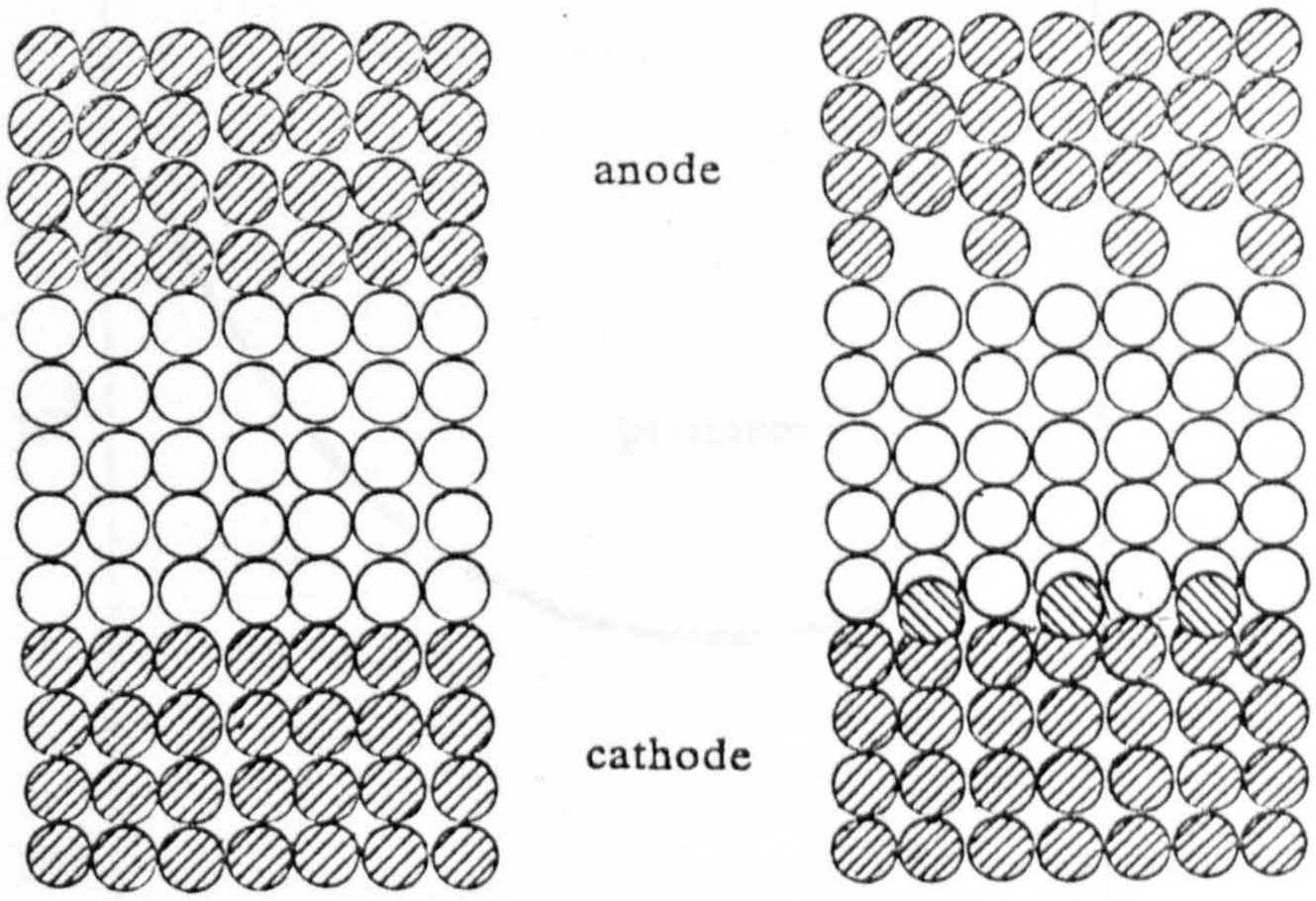

Fig 3.10 Schematic of atomic arrangement at parent metal/solid electrolyte interface (a) before and (b) after passage of current (after Raleigh [19]).

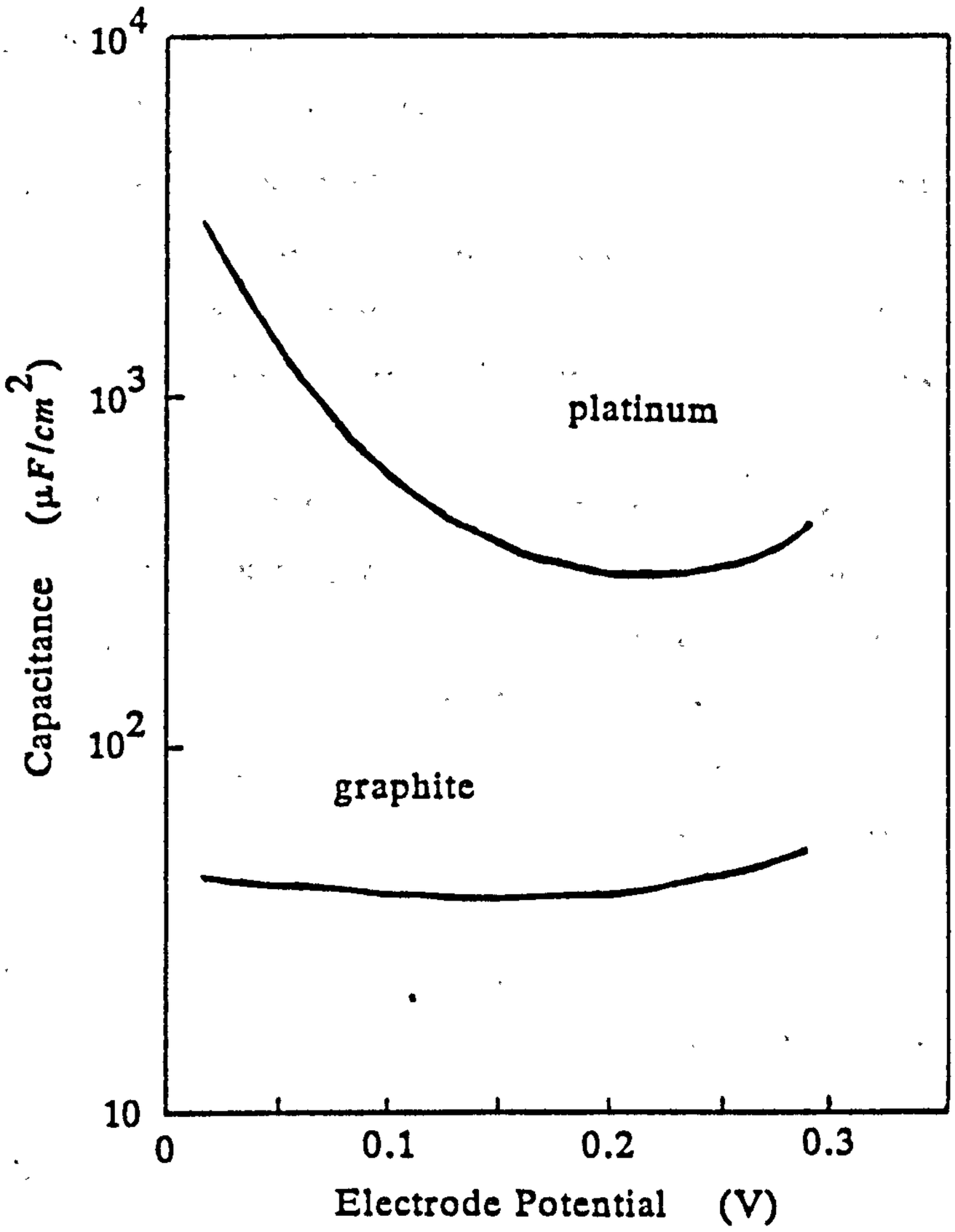

Fig 3.11 Voltage dependence of capacitance of graphite and platinum electrodes on solid AgBr. The voltage is referred to a silver electrode. (After Raleigh [19]).

of the graphite electrode suggests that the ions reach a point of closest approach but do not undergo any adsorption or reaction. This is directly analogous to double-layer charging at an ideally polarisable electrode in a liquid electrolyte. The increase of the capacitance of platinum electrodes as the silver potential is approached was held to be indicative of the buildup of a monolayer of silver.

Figure 3.12 shows the development of electrode potential under galvanostatic conditions. The curves confirm the view that a reaction takes place at the platinum electrode below the decomposition potential but not at the graphite one: the straight-line charging of the graphite electrode up to the silver potential demonstrates constant capacitance; and the curve of the platinum response indicates that charge-transfer is involved. In addition, the total charge which passes across the platinum electrode before the silver potential is reached is exactly the right amount to form a monolayer. The potential for the graphite electrode, on the other hand, rises to beyond the silver equilibrium voltage and reaches a peak after a further amount of charge equivalent to (1/1000) of a monolayer has passed. This behaviour was interpreted as being due to a nucleated discharge pattern with charge transfer taking place only at certain favourable points.

A more detailed analysis of the potentiostatic data allowed identification of secondary processes by plotting the total integrated charge, Q, against time, as in figure 3.13. Between 1 s and 1000 s, the capacitance is the same at all temperatures, indicating that the same discharge process is at work. For the lower-temperature measurements, a slow-charging process, probably associated with lower carrier mobility, appears, and at high temperature the total charge continues to increase, which was held to be evidence of a secondary faradaic process, identified as an impurity reaction.

The techniques used by Raleigh were of the type usually associated with the standard procedures of electrochemistry, but the system being investigated was far from the sort which conforms to the standard assumptions usually involved in interpreting the results of such measurements. Neither were the full theoretical descriptions of the interface of the kind used by Macdonald and others applied. Instead, an ad hoc set of assumptions appropriate for each situation was applied, based on a knowledge of the chemistry of the electrodes. That is, parent metal electrodes were assumed to be in equilibrium with the electrolyte giving rise to a well-defined voltage, and "inert" electrodes were assumed not to undergo any reaction with the electrolyte at all. The investigation as a whole illustrated how standard electrochemical measurements can be

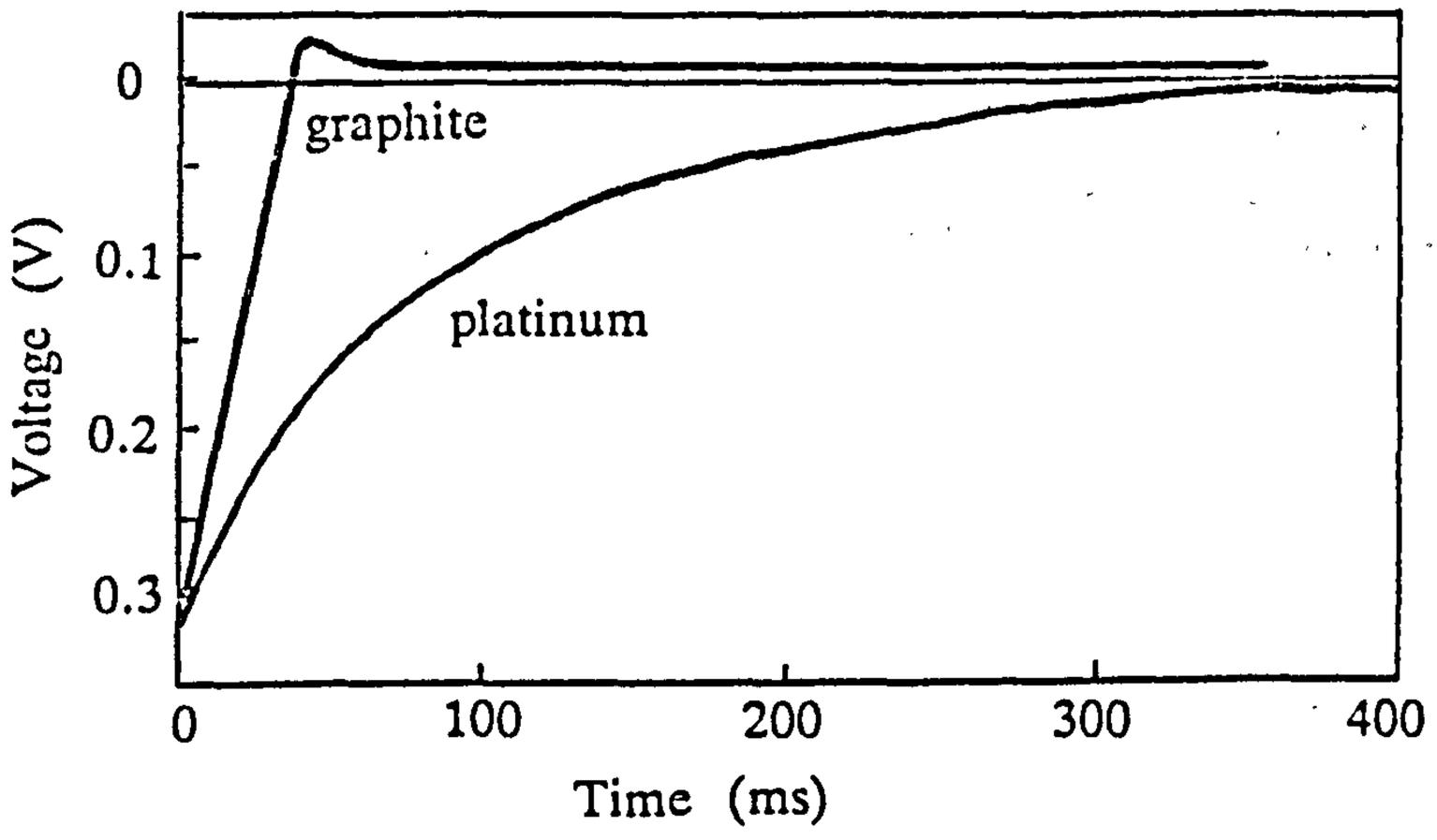

Fig 3.12 Galvanostatic voltage-time sweeps on graphite and platinum electrodes on solid AgBr (after Raleigh [19]).

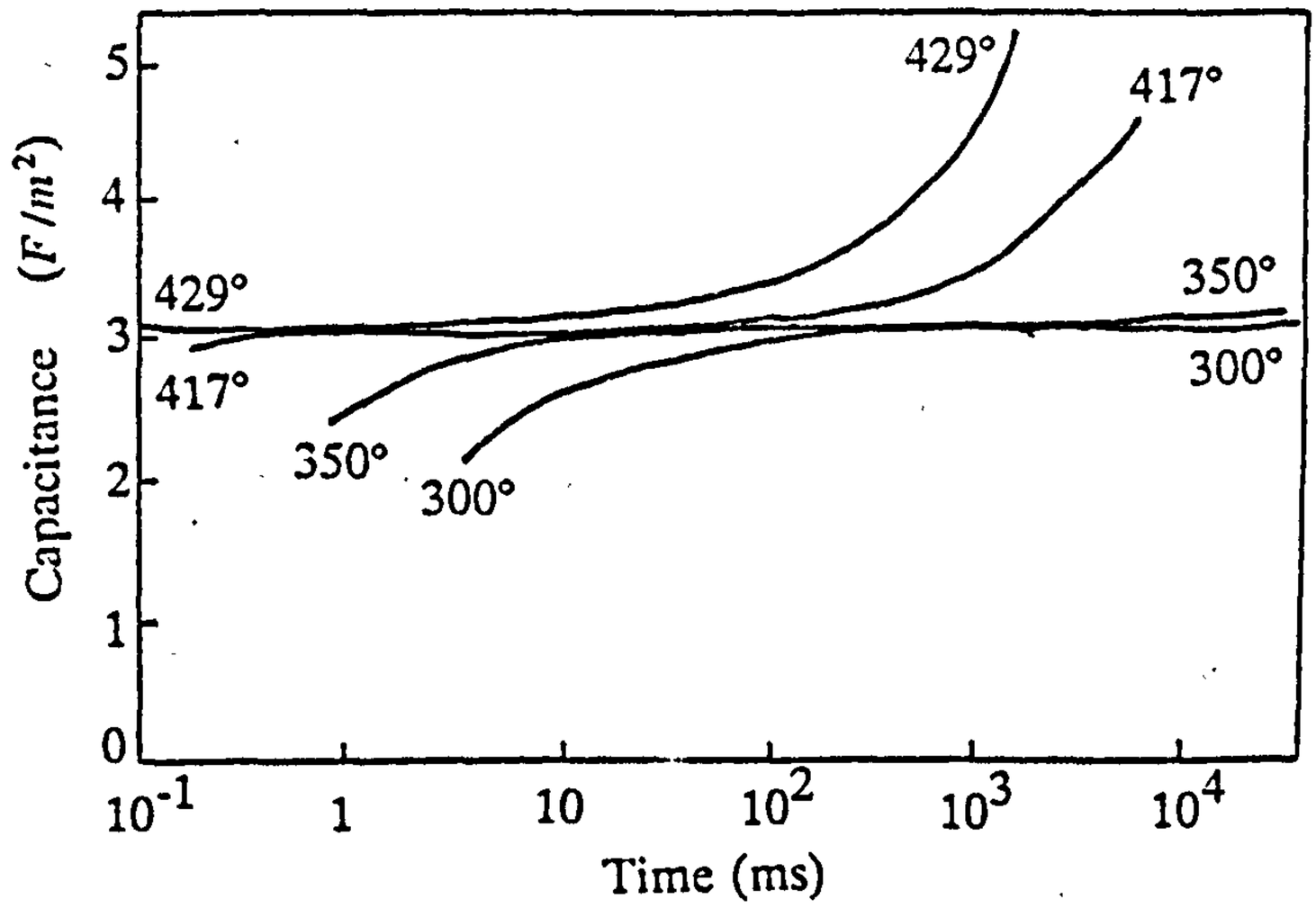

Fig 3.13 Effective capacitance of Pt:AgBr interface versus time at various temperatures (after Raleigh [19]).

usefully applied and interpreted even when the conditions for the standard voltage-current-time relations derived from the Nernst-Planck system do not apply.

The possibility of the existence of well-defined potentials at nonparent electrodes was proposed and investigated theoretically and experimentally by Lanyi and Hricovini [22]. They used single-crystal sodium chloride with platinum and graphite electrodes in symmetrical cells without a parent metal or other formally reversible electrode.

After a comparatively long polarisation of one hour at a constant applied voltage, the voltage source was disconnected and the new voltage measured. The immediate change was attributed to the overvoltage associated with the remaining current, and this voltage, when plotted against the current, followed the Butler-Volmer characteristic of a kinetically-limited electrode reaction.

The results of AC measurements made between electrodes biased to the same voltage were also presented in reference 21. For these, the arrangement shown in figure 3.14 (a) was used. The DC biasing voltages had been applied for the same times as for the overpotential measurements, so that the system could be treated as if it was in a quasi-steady state. This assumption was justified by the observation that the DC current was changing very slowly on the scale of the AC frequency used. The complex impedance plots obtained by Lanyi and Hricovini are reproduced in figure 3.14 (b). These have three arcs: a high-frequency bulk response, and two lower-frequency arcs which were identified with charge-transfer and adsorption or diffusion. The calculated capacitance associated with the mid-frequency arc was found to vary with the applied voltage. This variation was attributed to surface concentrations of the reactants.

From this data, it was concluded that the equilibrium potential at an inert electrode on NaCl is fixed by two redox reactions:

$$Na \rightleftharpoons Na^+ + e^- \qquad 3.28$$

and

$$2Cl^- \rightleftharpoons Cl_2 + 2e^- . \qquad 3.29$$

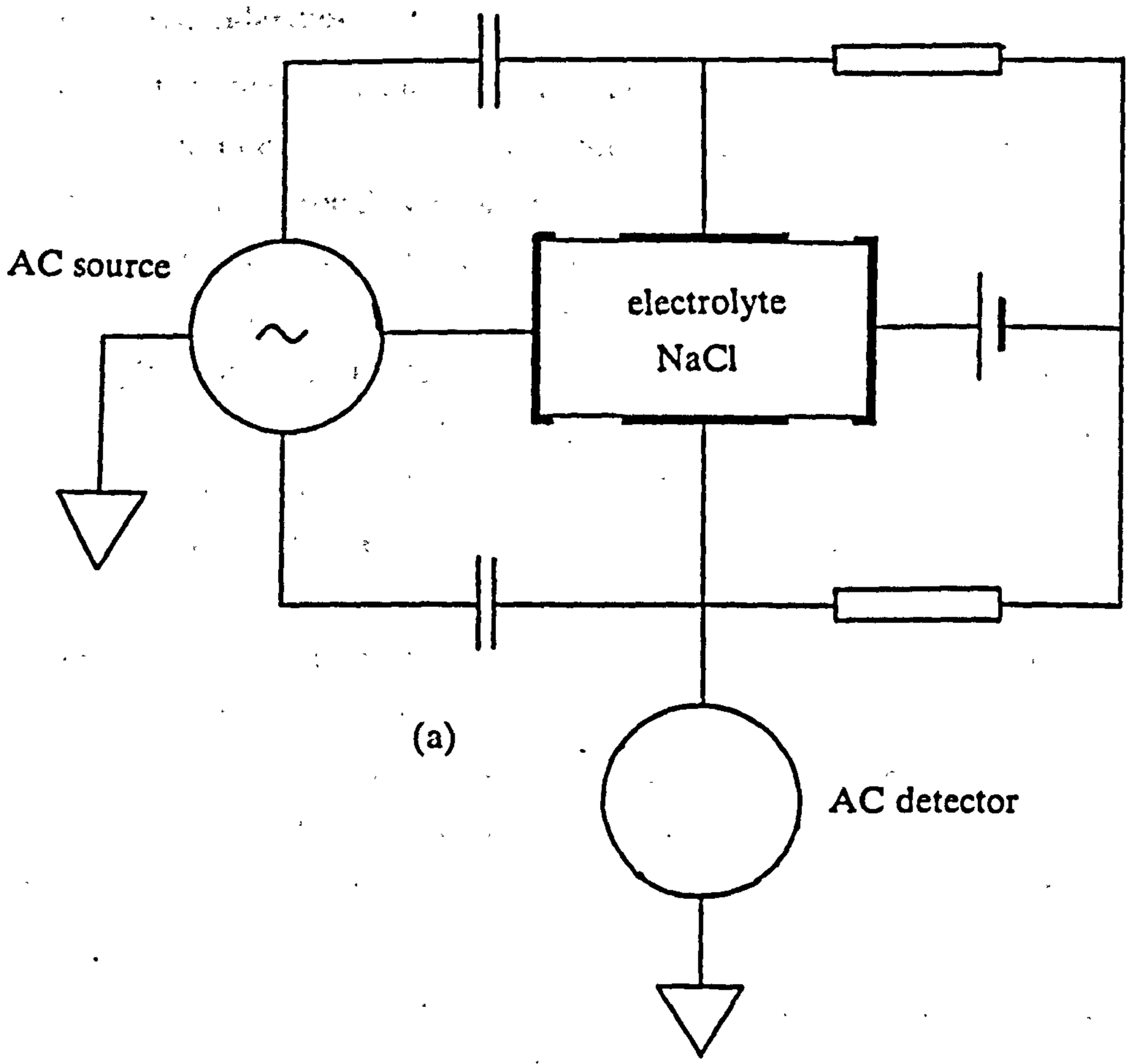

Fig 3.14 (a) Cell for AC measurements of ref 22.
(b) Idealised complex impedance of NaCl.

3.7. Surface Irregularities

In all of the analyses mentioned in sections 3.2-7 it has been assumed, sometimes implicitly, that all interfaces are flat with perfect contact over their entire area. In fact the existence of surface roughness, air gaps, interphase regions and stoichiometric deviations are always important considerations in solid-state contacts. These either have to be minimised by careful construction of test cells, or taken account of in the analysis. Raleigh's AgBr cells were made by electropolishing the metal electrodes and heating the interface briefly so that the electrolyte softened at the surface. In this way surface roughness effects were effectively eliminated. The effect of roughness on the frequency response was analysed by de Levie [23] assuming the electrode was indented by triangular grooves, and that the electrolyte was homogeneous and followed the shape of the surface shown in figure 3.15. He found that a transmission-line element was introduced into the impedance of the system, with a Bessel-function form which depended on the groove angle β. As with many other mathematical models, the results are far too complicated to compare routinely to experimental data. The situation was more applicable to liquid electrolytes because of the assumption of conformity of the surfaces.

Incomplete contact between the electrode and a solid electrolyte was analysed by Armstrong et al [24]. The model was devised for use with a blocking electrode at the point of zero charge and considered two impedances operating in parallel, one due to that fraction of the surface, α, which was in perfect contact with the electrode, and the other for the air-gap. This led to an overall capacitance which was proportional to ω^{-n} at high frequency. Such a relationship fits a great deal of experimental AC data for solid state electrodes.

The sensitivity of the electrode kinetics to the structure of the double layer in the case of liquid electrolytes indicated that a similar dependence should be expected for the solid state. The theoretical calculation of this would be even more difficult than for the frequency dependence as calculated by Friauf [10], Macdonald [2], Beaumont et al [18], and others. Observation of a near-ideal Tafel relation, as in the case of Lanyi and Hricovini, is consistent with the view that the structure of the double layer in their system is of the same form as that in liquid systems but it does not provide conclusive evidence.

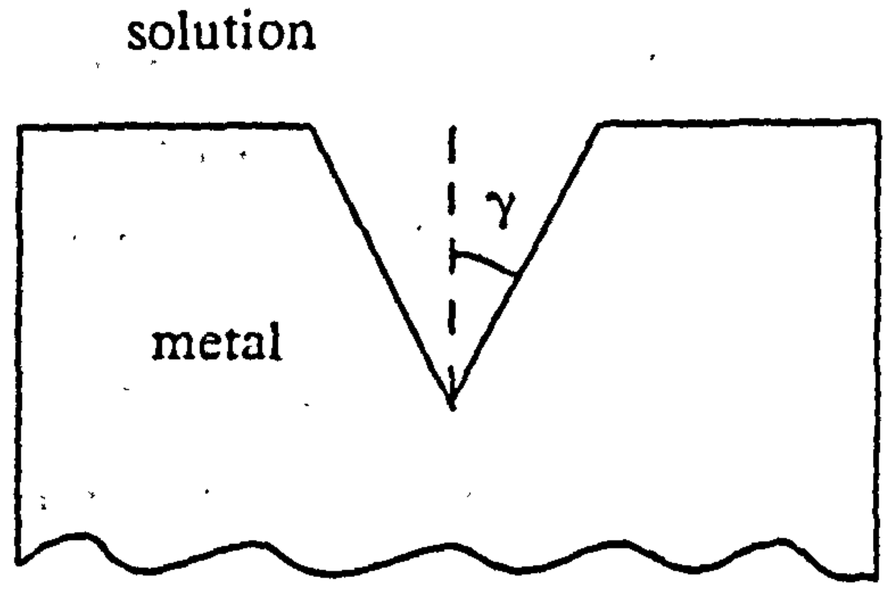

Fig 3.15 de Levie's model for surface roughness (after [23]).

3.8. Summary

The most significant aspect of all the experimental and theoretical work described here is the importance of ensuring that the assumptions on which a theoretical model is based are appropriate. The theoretical calculations based on systems at the point of zero charge, although worked out very thoroughly for a wide variety of situations, employ a set of boundary conditions which are very seldom applicable to real systems. When realistic physical phenomena are included in the investigation the results are often more directly applicable to experiments on real systems even if a full analysis is not possible. In such a case the experiment must be designed so that the effect under consideration shows up in the response. The study of kinetically limited effects at electrodes on AgBr by Lanyi et al [22] is typical of this approach, where the potentiometric technique was adapted to measure the current overvoltage.

Raleigh's [19] measurements on platinum and graphite electrodes on AgBr showed that electrochemical measurements on inert electrodes in unsupported electrolytes may be useful in cases where the potential can be referred to that of a reversible electrode [19,22].

Much of the discussion of electrode phenomena reduces to consideration of the structure of the double layer, since arguments over what constitute nonblocking, partially blocking or ideally blocking electrodes with chemisorption are frequently resolvable when the microscopic environment of the approaching ion is taken into account. Perhaps the most important experimental consideration is that of preparation of the interface so that the response is not due to spurious effects such as extraneous impurities and avoidable morphological irregularities.

REFERENCES

1. Cohen H and Cooley JW, Biophys J **5**, 146-163 (1965).
2. Macdonald JR, Annual Report of Electrical Insulation and Dielectric Phenomena, p 3-49, Nat Academic Press (1980).
3. Macdonald JR, J Chem Phys **58**, 4982-5001 (1973).
4. Koryta J, Dvorak J and Bohackova V, *Electrochemistry*, p 115-118, Methuen, London (1970).
5. ibid, p 210-214.
6. ibid, p 229-233.
7. Macdonald DD, *Transient techniques in electrochemistry*, p 119-130, Plenum, New York (1977).
8. ibid, p 2.
9. Koryta J, Dvorak J and Bohackova V, *Electrochemistry*, p 249-257, Methuen, London (1970).
10. Friauf RJ, J Chem Phys **22**, 1329-1228 (1954).
11. Macdonald JR, J Chem Phys, **75**, 3155-3157 (1981).
12. Jaffe G, Phys Rev **85**, 354-363 (1952).
13. Macdonald JR, J Chem Phys **61**, 3977-3796 (1974).
14. Chang HC and Jaffe G, J Chem Phys **20**, 1071-1077 (1952).
15. Macdonald JR and Brachman MK, J Chem Phys **22**, 1314-1316 (1954).
16. Macdonald JR, J Chem Phys **54**, 2026-2050 (1971).
17. Macdonald DD, *Transient techniques in electrochemistry*, p 267, Plenum, New York (1977).
18. Beaumont JH and Jacobs PWM, J Phys Chem Solids **28**, 657-667 (1967).
19. Raleigh DO, Electroanal Chem **6**, (ed AH Bard) p 87-186, Dekker, New York (1973).

20. Franceschetti DR and Macdonald JR, J Electroanal Chem **82,** 271-301 (1977).

21. Fjeldly TA and Nagy K, J Electroch Soc **127,** 1299-1303 (1980).

22. Lanyi S and Hricovini K, J Phys Chem Solids **44,** 905-912 (1983).

23. de Levie R, Electrochimica Acta **10,** 113-130 (1965).

24. Armstrong RD,J Electroanal Chem **52,** 413-422 (1974).

CHAPTER 4

GLASS SURFACES AND INTERFACES

4.1. Introduction

In this chapter, electrode effects specific to silicate glasses, and the way they are influenced by the surface properties of the glass are discussed. Some of the various solutions of the Nernst-Planck equation and some of the electrochemical ideas which were introduced in previous chapters have been applied to the system of metal contacts on glass. The theories and experimental results discussed in this chapter nearly all relate to glasses of sodium-calcium-silicate and sodium-silicate compositions.

4.2. Glass Surfaces

Electrode processes are sensitive to the conditions in the electrolyte next to the interface, whether the electrolyte be liquid or solid, crystalline or amorphous [1]. Many of the models devised to explain the electrode polarisation of glass assume that the distribution of sodium ions is uniform at all points between the electrodes [2-8]. However there are many factors which can make the structure and composition of the glass different near the surface from what it is in the bulk depending on its method of fabrication and how it has been treated.

The range of surface properties was described in a review by Dunken [9]. If a piece of glass is fractured in vacuum, there is little change in the environment of the component atoms near the surface, except of course for broken bonds. Exposure of a newly fractured surface to the atmosphere leads to attack by moisture which results in the breaking of some Si-O-Si bonds to form Si-OH groups on the surface. Further treatment, such as cleaning and polishing, can cause the development of surface layers containing components of the abrasive or cleaning agent and to leaching of the glass constituents.

At interfaces with aqueous solutions, the leaching of alkali ions and the associated breakdown of the glass network is a continuous process. Its significance as part of the mechanism of glass corrosion has led to its receiving considerable attention in investigations into the durability of glasses for long-term storage of nuclear waste [10,11]. Sophisticated models of the time-dependent transport and chemical processes have been set up and analysed. Since no account is taken of the overall electric potential in these analyses, there has been no application of their results to electrode phenomena, but the physical processes involved are in many ways similar. All of them involve transport of ions within the glass, and dissolution of the silica network.

The effect of reaction with aqueous solution on the electrical resistance of surface layers of pH-sensitive glass has been investigated by Wikby [12,13]. He found that the glass is attacked first by ion exchange involving H^+ from the solution and Na^+ from the glass. This is followed by gradual dissolution of the silica network itself, which is accompanied by the uptake of water into a surface layer on the glass. The electrical resistivity of this layer was sufficiently greater than that of the bulk of the glass that the resistance of the whole glass membrane was significantly increased.

The long-term effects of exposure to the atmosphere depend on the ambient conditions. The mechanism of attack depends on the pH of the adsorbed aqueous layer. If the solution is frequently changed, for example by washing, the top layer becomes depleted of sodium ions, and this layer is quite resistant to further attack. However, if the same solution remains, then the pH increases due to the buildup of leached sodium. This alkaline solution then attacks the silica network and accelerates corrosion.

The chemical activity of the hydrated glass surface has been cited as a possible source of charge-transfer at electrodes but the mechanism has not been elucidated or quantified [14]. However the mechanism of a similar electrochemical system, that of the glass electrode, has been the subject of considerable theoretical and experimental study [15]. Although there are different theories which account for the operation of the glass electrode, which vary in points of detail, there is a generally accepted view that the potential difference between the interior of the glass membrane, and the solution with which it is in contact, is the sum of two potentials. One is due to the equilibrium distribution of sodium and hydrogen ions between the glass surface and the solution. The other is a diffusion potential. The ion exchange is not relevant to the consideration of processes at solid electrodes, but the diffusion potential arises whenever a

cation with a mobility different to that of sodium interdiffuses from the surface, such as in the case of a metal electrode oxidising and its ions becoming mobile in the glass. The Nernst-Planck equation for an interdiffusing cation, M, is:

$$D_M \frac{\partial C_M}{\partial x} + D_{Na} \frac{\partial C_{Na}}{\partial x} = -E(\mu_M C_M + \mu_{Na} C_{Na}) \qquad 4.1$$

where D_M and D_{Na} are the diffusion coefficients, μ_M and μ_{Na} are the mobilities, and E is the electric field. Electroneutrality implies that:

$$C_M + C_{Na} = C_o \qquad 4.2$$

where C_o is the concentration of Na in the bulk. For fixed surface and bulk concentrations, the overall potential, V_D, was found by Doremus [16] assuming constant activity coefficients and the validity of the Nernst-Einstein relation, giving:

$$V_D = \frac{nRT}{F} \ln \frac{C_M(surface) + C_{Na}(surface)(\mu_{Na}/\mu_M)}{C_o(\mu_{Na}/\mu_M)} \qquad 4.3$$

where n is the ratio of M to Na activity coefficients assuming zero concentration of M^+ in the bulk. This relation holds no matter how the ion concentrations vary between the surface and the interior.

4.3. AC Measurements

When an AC potential is applied across a cell consisting of soda-lime-silica glass between metallic electrodes, the overall frequency response has the same form as other solid electrolytes, with the electrode polarisation showing up at low frequency. The representation of the results as real and imaginary parts of the admittance or impedance, and plots in the complex plane are therefore often used. However the same experimental technique is often used to study the dielectric properties of glass. Polarisation in this case is looked upon as a phenomenon of the bulk of the dielectric at all frequencies, and is presented as a complex dielectric constant, ϵ^*, such that [17]:

$$\epsilon^* = \epsilon' - j\epsilon'' = \epsilon' - j\left(\frac{\sigma}{\omega}\right) \qquad 4.4$$

where ϵ' and ϵ'' are the real and imaginary parts of the dielectric constant, σ is the DC conductivity and ω is the angular frequency. The definition of ϵ^* is

$$D^* = \epsilon^* E^* \qquad 4.5$$

where D^* is the electric displacement and E^* is the electric field. The parallel capacitance C_p is related to the dispersion by:

$$C_p = \epsilon' A / l \qquad 4.6$$

where A is the area of the electrodes in a symmetrical cell and l is the spacing between them.

In the case of electrode polarisation, the capacitance associated with charges accumulating and depleting near the electrodes is unlikely to be dependent on the electrode spacing. Since this capacitance is clearly responsible for the reactive part of the observed impedance at low frequency, the use of the ϵ^* representation, whose capacitive part explicitly contains l, seems inappropriate. However it is used when data for the bulk polarisation is also being considered.

Kim and Tomozawa [14] used the ϵ^* representation to investigate the electrode polarisation at gold and silver contacts deposited as pastes or by vacuum evaporation on soda-lime and binary sodium silicate glasses. Measurements were carried out in a vacuum at various temperatures between 100 and 300°C. Their results for gold electrodes, reproduced in figure 4.1, show that interface response is sensitive to the method of application of the electrodes, but that at the lowest frequencies ϵ' always varies as ω^{-2}.

These were compared with the results of the single-carrier space-charge theory of Beaumont and Jacobs [18], which incorporates the Chang-Jaffe discharge boundary conditions. Kim and Tomozawa used the theory to calculate the imaginary part of the dielectric constant:

$$\epsilon' = \frac{2\epsilon \dfrac{\sigma^2 L_D}{(\epsilon_o \epsilon \omega)^2 l}}{1 + (2+\rho)^2 \left(\dfrac{\sigma^2 L_D}{(\epsilon_o \epsilon \omega)^2 l} \right)} \qquad 4.7$$

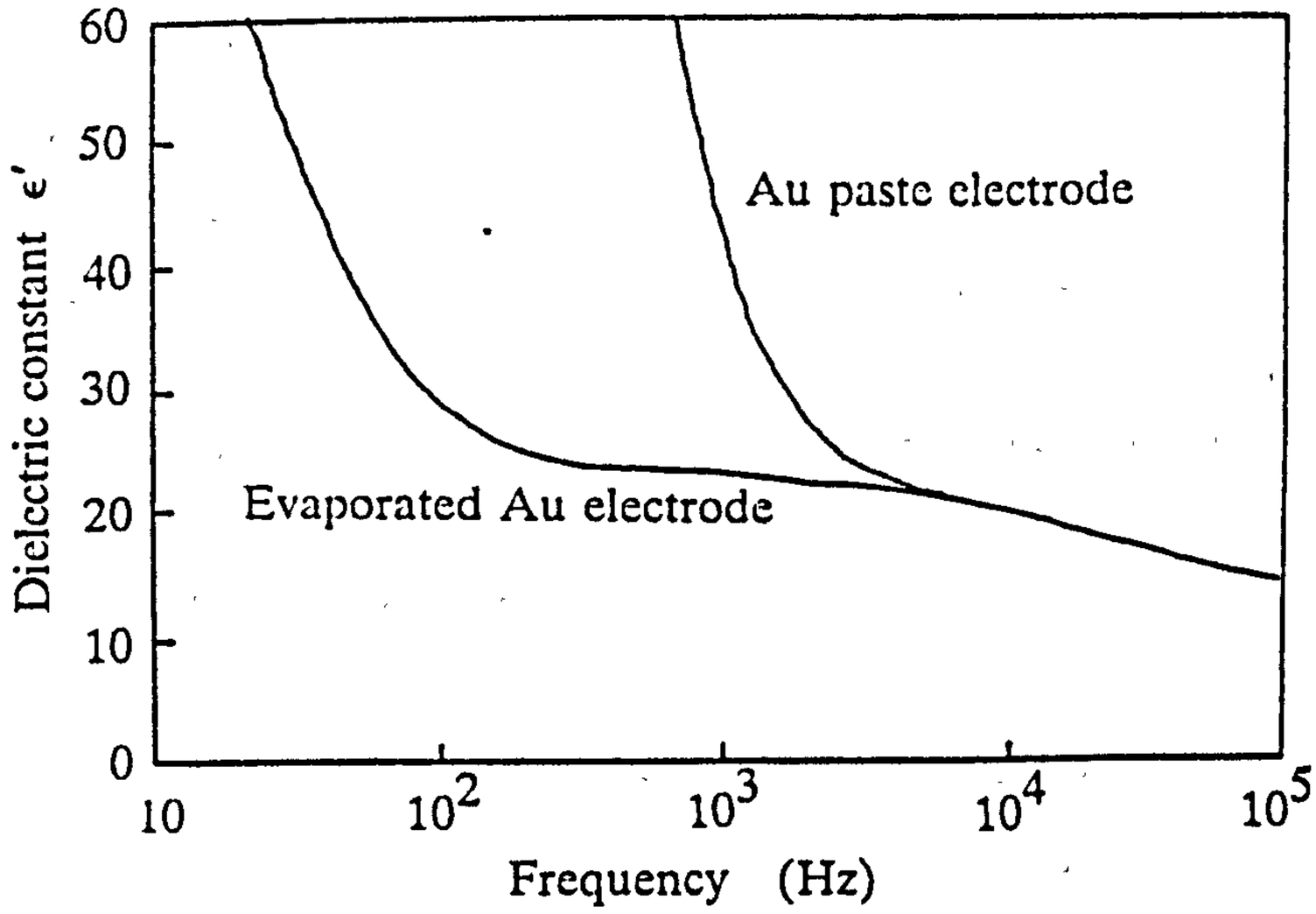

Fig 4.1 AC results obtained by Kim and Tomozawa [14] for gold/glass cells.

where ϵ is the real part at high frequency, ϵ_o is the permittivity of free space, ρ is the Chang-Jaffe discharge parameter and L_D is the Debye length.

Kim and Tomozawa expected different electrode behaviour from the different preparations because of the way that the metal adhered to the glass. Evaporated electrodes were found to be only loosely attached to the surface, indicating that the soft alkali hydroxide layer, which is normally resident on a free glass surface, was present, and would therefore give rise to partially blocking behaviour. No details of the mechanism for a partial charge transfer was given by the authors. The much stronger adherence of the paste electrodes was taken as an indication that the alkali hydroxide layer had been eliminated, probably by the 260°C curing process. In the absence of an interphase layer, the electrode was expected to be blocking.

The ω^2 dependence of ϵ' is consistent with equation 4.7 for small ρ because the term involving ρ was much less than 1. The identification of nonblocking behaviour with the evaporated electrodes was based on the observation that ϵ' was smaller than that for the paste electrodes at all frequencies, consistent with a larger value of ρ.

The only discrepancy admitted by the authors was that the Debye length necessary for the results to fit was about 25 nm for the soda-silica glass, whereas that calculated by the formula for L_D, using the concentration of sodium as the figure for the carrier density, was less than 0.1 nm. The latter is not physically possible, since it is less than the diameter of the ions involved. Kim and Tomozawa suggested that the problem might be resolved if only a small fraction of the sodium was dissociated and therefore mobile. Another possible explanation may lie in the limitation on the number of available ionic sites, which was not taken into account by Beaumont and Jacobs when they developed the theory [18]. The effect of this would be to reduce the maximum excess charge density and hence the interface capacitance. This phenomenon has been taken into account in some theoretical situations by Macdonald [19] where it is mathematically formalised as the lattice-gas model, with similar results, although they are not directly applicable to Kim and Tomozawa's data, since the necessary density of sites is not available.

The use of a detailed theoretical expression for the space-charge polarisation to discuss these results is not necessary, however, and the identification with this particular theory was not justified. This is clear if a series RC circuit rather than the dielectric dispersion, which is equivalent to the capacitive branch of a parallel one, was used. The capacitance is then constant over the same frequency range, a fact which is

illustrated in figure 4.2, where the component values of a series circuit are calculated so that its impedance is equal to that of a parallel circuit whose capacitance is proportional to ω^{-2}. This constant capacitance in series with a resistance may simply be interpreted as the approach of the ions to a certain distance from the electrode, with the resistance being that of the bulk. Nothing more can be said about the nature of the space between this point and the electrode on the basis of Kim and Tomozawa's data. In particular, it cannot be said that the steady state around which the AC signal was applied corresponded to the point of zero charge condition required for the validity of Beaumont and Jacobs' theory. Sufficient explanation for the other piece of evidence, ie the lower ϵ' of the evaporated contacts, would be provided by the presence of a resistive surface layer increasing the distance between the metal and the region where the excess charge accumulates.

A similar piece of work, but one with strikingly different results, was carried out by Mitoff and Charles [5]. The glass in this case had the composition 73% SiO_2, 13.5% Na_{2O}, 9% CaO, 3% MgO, and 1% Al_2O_3, and platinum contacts were used. AC measurements were made in air between 371 and 560°C. Instead of the ω^{-2} response Mitoff and Charles found that a plot of C_p vs ω had a slope of $\omega^{-3/2}$, fitting the equivalent circuit of figure 4.3, where the critical element is the Warburg impedance. Mitoff and Charles identified this behaviour with that of a standard electrochemical cell, with a charge-transfer reaction occurring across a constant-width double layer, and movement of ions by diffusion in a layer near the surface. The Warburg impedance element was claimed to provide evidence of diffusion-controlled transport, since this response is observed in liquid electrolytes where there is other evidence of diffusion. Evidence for a charge-transfer process had also been found from DC charging and discharging data (see section 4.5). The double layer, in the absence of supporting electrolyte, must have corresponded to the space-charge region where the concentration of sodium ions deviated from the bulk level, so that the electric field would have had a significant influence on the transport. However it was assumed in this instance that transport of sodium was by diffusion only, giving rise to the Warburg response.

Additional evidence of charge transfer was provided by the absolute magnitude of the capacitance, which was very large, implying that if no charge transfer took place, the ions would have to accumulate within 0.1 nm of the electrode, which is not physically possible.

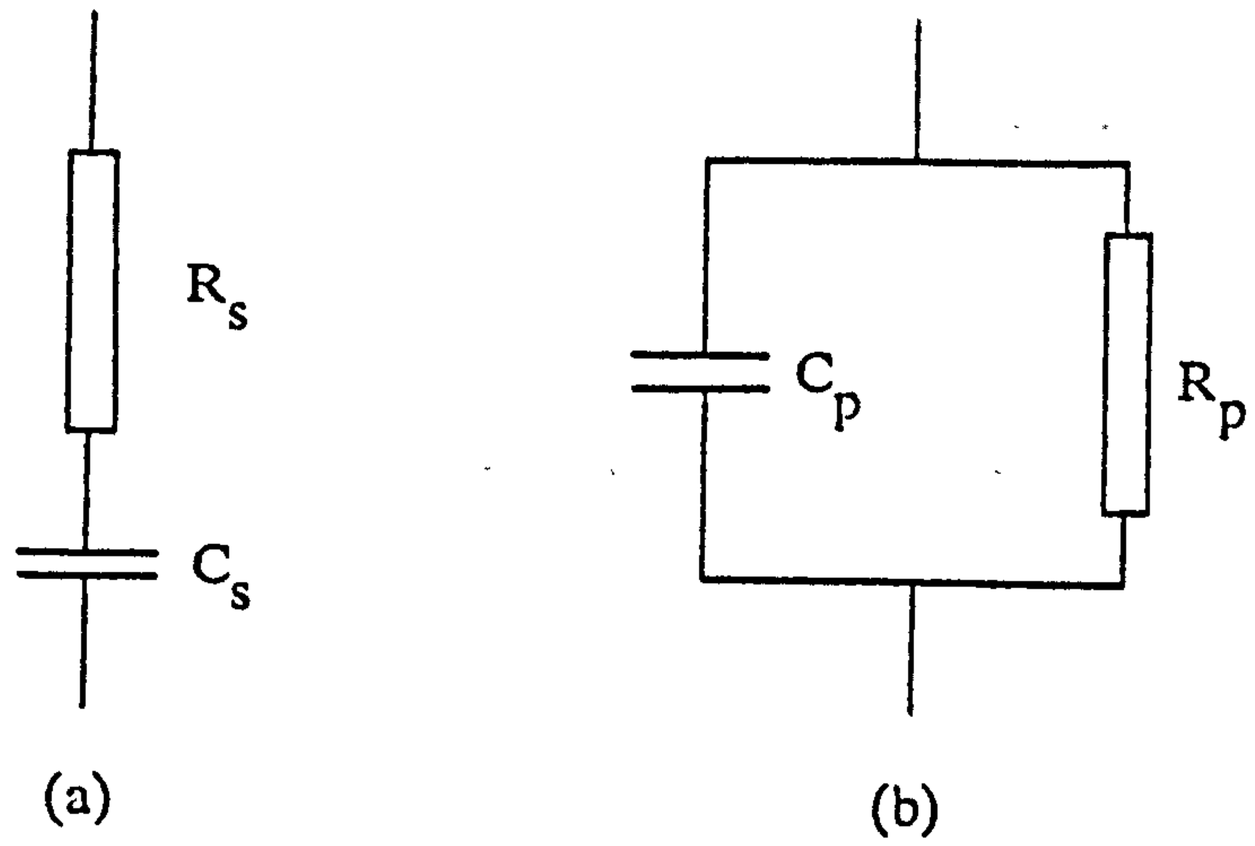

If the impedance of (a) is equal to that of (b) then

$$C_p = \frac{C_s}{\omega^2 R_s^2 C_s^2 + 1}$$

$$= constant.\ \omega^{-2} \quad \text{if} \quad \omega^2 R_s^2 C_s^2 > 1$$

Fig 4.2 Circuits demonstrating the equivalence of a series RC circuit with constant component values to a parallel circuit with C varying as ω^{-2}.

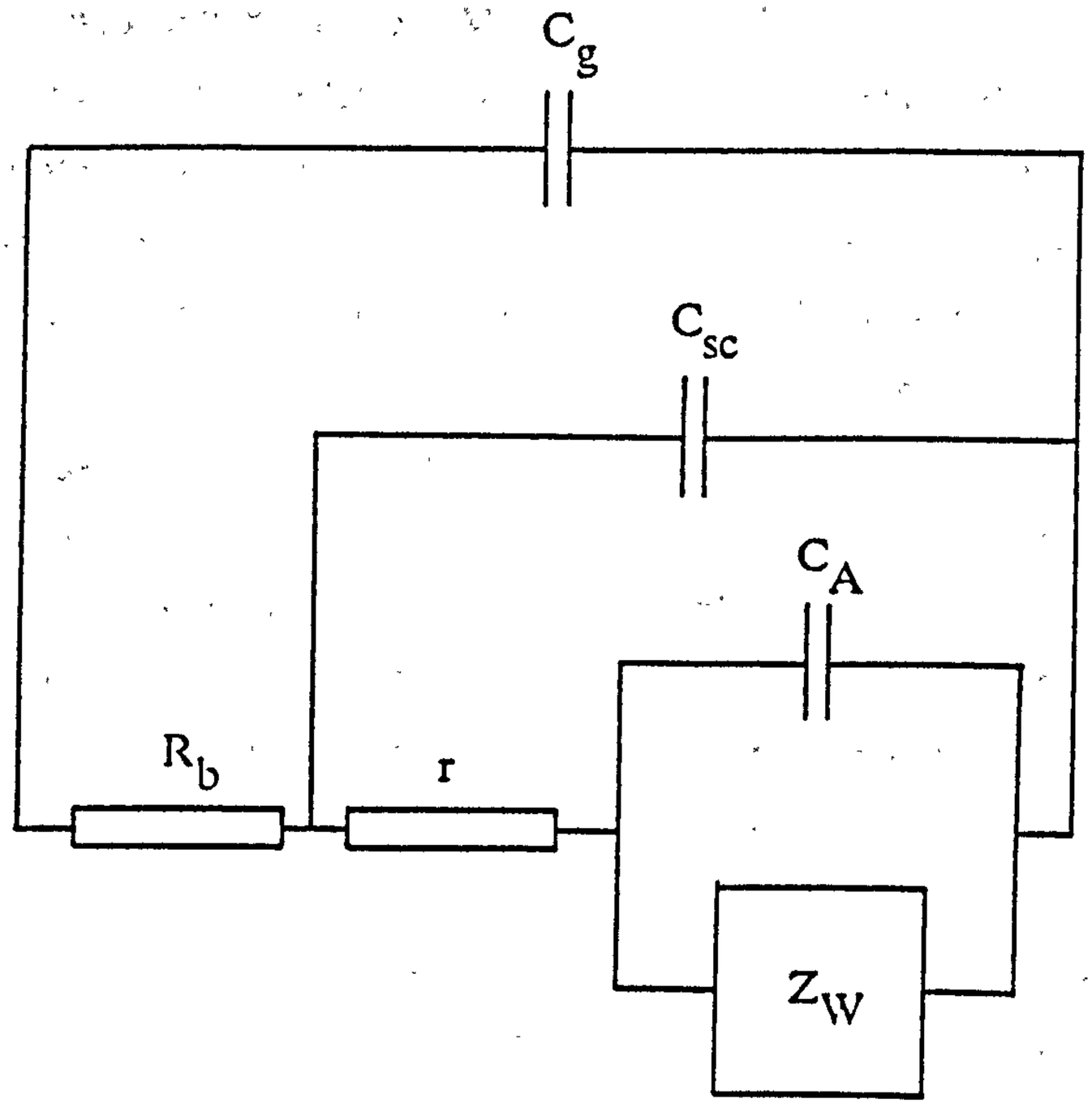

Fig 4.3 Equivalent circuit used by Mitoff and Charles [5] to model the response of their platinum/glass/platinum cell.

The diffusion model, however, does not take into account the lack of supporting electrolyte. This point was taken up by Macdonald [6,7] who, by applying his analysed the data of Mitoff and Charles [5], using a more sophisticated space-charge theory involving two mobile ions with recombination/generation and arbitrary mobilities (see chapter 2). He showed that the diffusion mechanism is not necessary, since the Warburg response can be generated by a system where the interface potential is governed by space charge produced by two carriers. In order to apply his theory, he assumed that the discharge processes were not symmetrical. At the electrode which is made cathodic first, sodium ions would be expected to discharge, and on reversal during the next AC half-cycle the sodium metal so produced would be available for reionisation. At the original anode, however, there would initially be no sodium, and discharge would have to be of oxygen, either as gas or in production of platinum oxide. Assuming that a much greater impedance was associated with the anodic discharge, the overall response would be dominated by one electrode at which minority carriers were not blocked. The two-carrier theory was claimed to demonstrate the potential importance of minority carriers of very low mobility if they could be discharged at the electrodes.

The Chang-Jaffe boundary conditions, used by Macdonald to describe the ionic discharge, state that the current is proportional to the excess concentration C^* at the electrode:

$$i = (RT/F)\rho C^* \qquad 4.9$$

This may be interpreted as diffusion through a constant-width layer:

$$i = (RT/F)(D/w)C^* \qquad 4.10$$

where D is the diffusion constant and w is the width of the layer. Incorporation of the Chang-Jaffe conditions into the Nernst-Planck system might therefore be expected to give rise to a diffusion-like behaviour in the theoretical response anyway. Mitoff and Charles used the magnitude of the capacitance and the Warburg-type frequency dependence of the impedance to back up their theoretical explanations. Macdonald used the same features of the data to criticise their conclusions. Neither set of authors considered the likely effects of reaction overpotential associated with kinetic limitation of the reaction. Since one set of assumptions included a physically unlikely diffusion

mechanism, and the other a physically unlikely point of zero charge and concentration-dependent boundary condition, neither point of view could be said to be proven.

Another approach to a similar system was the AC measurements on soda-silica glass with platinum and gold electrodes on soda-silica glass by Ravaine et al [20]. Symmetrical cells with either evaporated platinum or gold, or powdered platinum were tested with different partial pressures of oxygen in an otherwise inert atmosphere (argon). Figure 4.4 (a) shows an example of complex admittance plot of their results. The values of the components of the approximate equivalent circuit of figure 4.4 (b), along with the angle of depression of the centre of the complex admittance arcs, β, were calculated at various partial pressures of oxygen.

In all cases C_{el} increased as the oxygen partial pressure decreased. In the case of gold, R_{el} was too large to measure. With the platinum electrodes R_{el} was found to increase as pO_2 decreased, and it was larger with evaporated than with powdered platinum contacts.

All of these observations were interpreted as the effects of a reaction involving oxygen gas, but the exact mechanism was not elucidated, nor any reason given why it should have been different in the cases of platinum and gold.

4.4. DC Experiments

The major limitation of AC experiments is that interpretation of the data assumes a small-signal perturbation of a steady or equilibrium state. The response to a simple DC stimulus such as a constant applied potential or current may be viewed as a change of state of the system if that is appropriate.

Proctor & Sutton [2-4] examined in detail the effect of a constant applied voltage in order to investigate space-charge-dominated potential-development in glass. They derived their own solution to the Nernst-Planck equation for a single carrier with a finite rate of generation and recombination and ideally blocking contacts, but concerned themselves with the space distribution of the potential in a steady state instead of the time response of the current. Their approach was based on that taken by Macdonald in 1954 [21], with the difference that Macdonald's was for one carrier of each sign and did not allow for generation and recombination.

The concentration and voltage variation throughout the sample were calculated numerically for different values of the dissociation parameter R. A high value of R

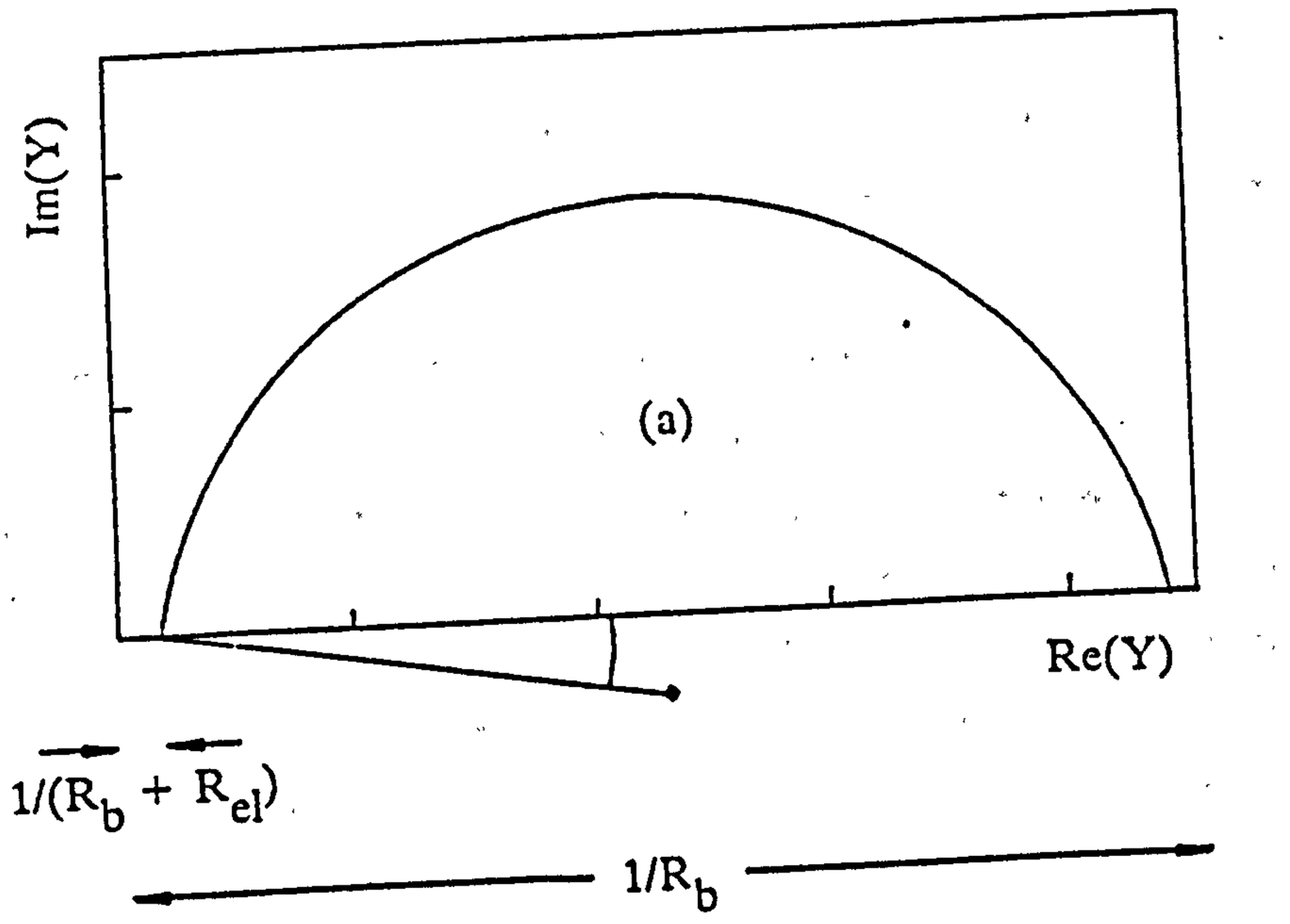

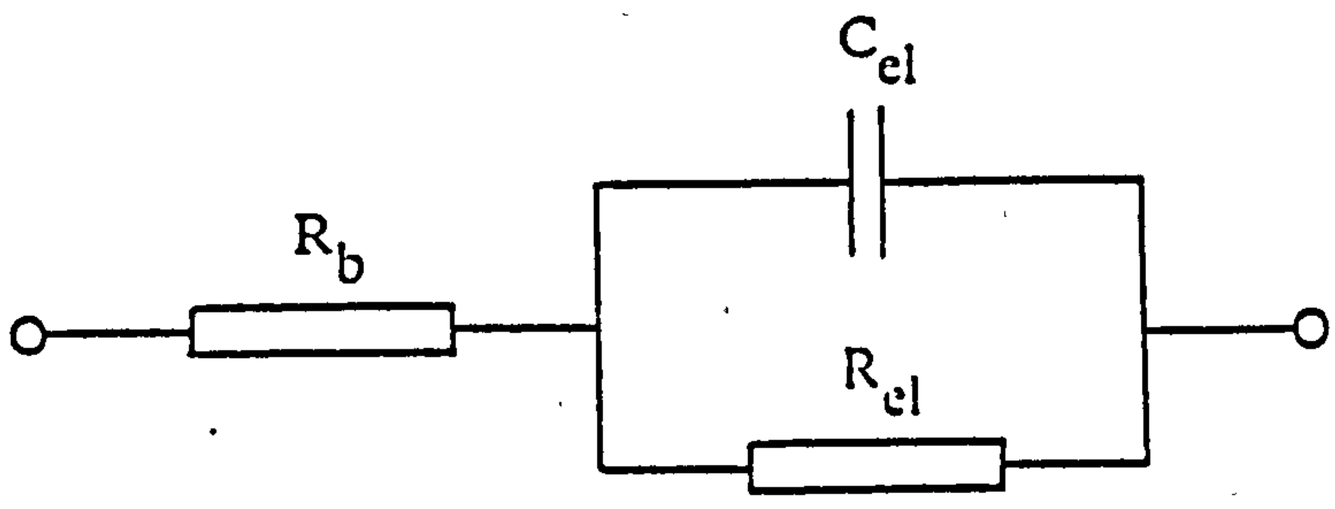

(b)

Fig 4.4 (a) Complex admittance plot of results of Ravaine et al [20] for platinum/glass cell.
(b) Approximate equivalent circuit used to model (a).

corresponds to a relatively high generation rate, ie to a high bulk equilibrium concentration of mobile charge. The theoretical results of Proctor and Sutton are reproduced in figure 4.5 (a). In the steady-state, the major part of the potential is dropped across a region at the anode whose thickness is a few Debye lengths, with the remainder across a similar region at the cathode.

Experimental evidence to support this picture was obtained using aluminium electrodes in the arrangement of figure 4.5 (b). A cell was made out of several thin layers of glass with aluminium foil probes between each layer, so that the potential at each internal point could be monitored [4]. Aluminium was used because it was believed not to be mobile in glass, and the assembly was "sealed" at an unspecified temperature to allow free movement of ions between the plates. The thickness of the layers (about 50 μm) was much greater than the Debye length (about 10 nm) and so only one internal potential could be measured in the steady state, as can be seen in figure 4.5 (c). The results for only one applied potential (9.2 V) were published.

Proctor and Sutton fitted their results to their one-carrier space-charge model, by varying R until the distributions of potential between the anode and cathode agreed. They found that the level of dissociation implied by the calculated R-value is about 1%. This is the same result obtained by Kim and Tomozawa [14] on fitting a similar space-charge theory to AC data.

The problem of reconciling the theoretical capacitance with the experimental value analogous with that encountered in AC experiments was avoided by the simple expedient of not measuring the capacitance or the current at all.

Despite this meagre level of evidence, their results are often quoted in the literature as being a valid description of the polarisation behaviour in glass [eg 22]. But there are several reasons to doubt their conclusions. If the 7 V is dropped across such a small anode region as that shown in figure 4.5 (a) (about 100 nm), then oxidation of the anode might be expected. Proctor and Sutton do not consider this possibility. Even if the electrode metal does not itself react so as to allow charge transfer, the very high field near the anode could cause movement of some of the other constituents of the glass, such as negative oxygen ions which could then migrate to the anode. At the cathode, where the potential drop was much less, it was pointed out by Proctor and Sutton that the observed behaviour could equally well be explained by reduction of sodium metal.

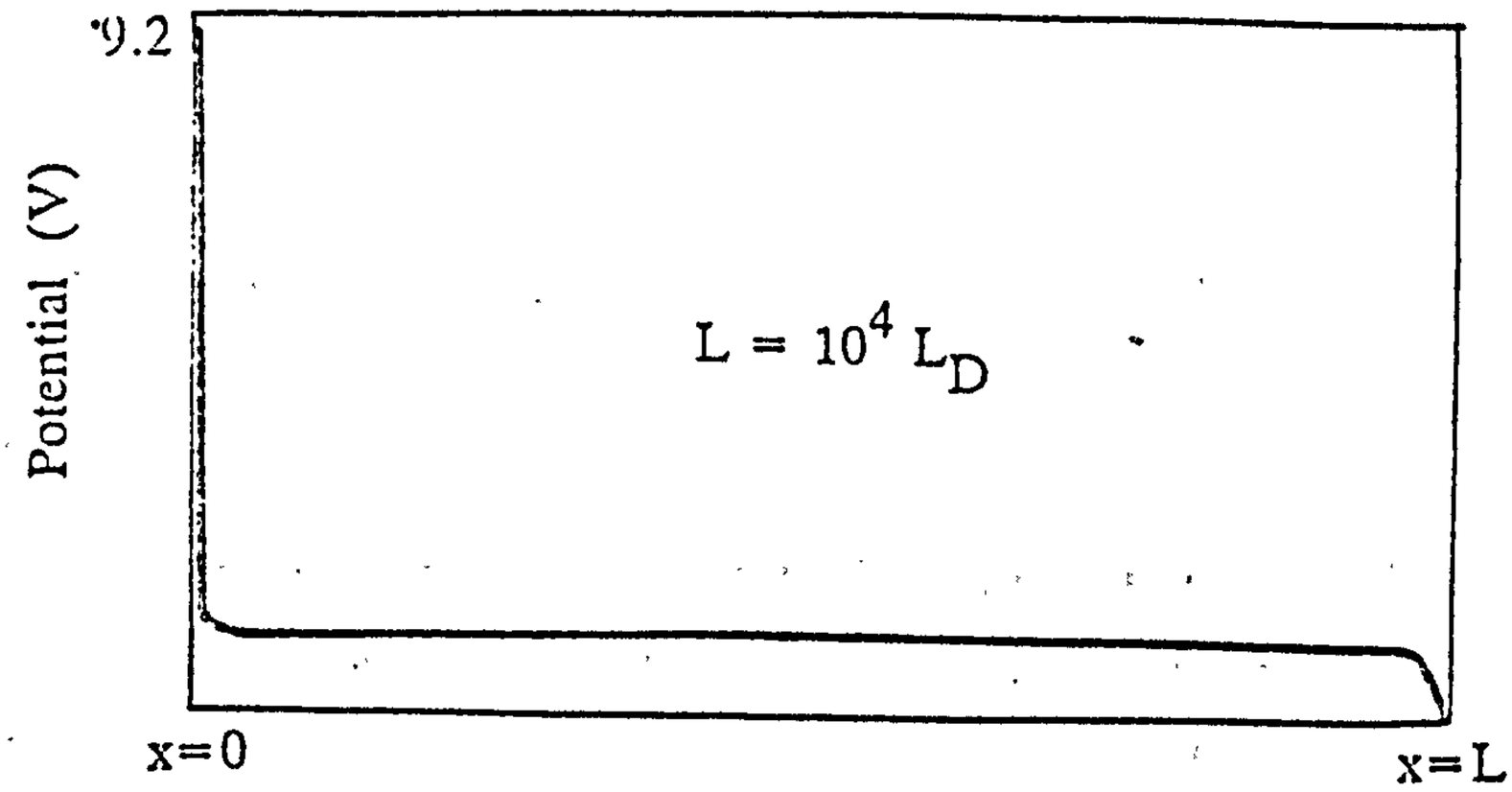

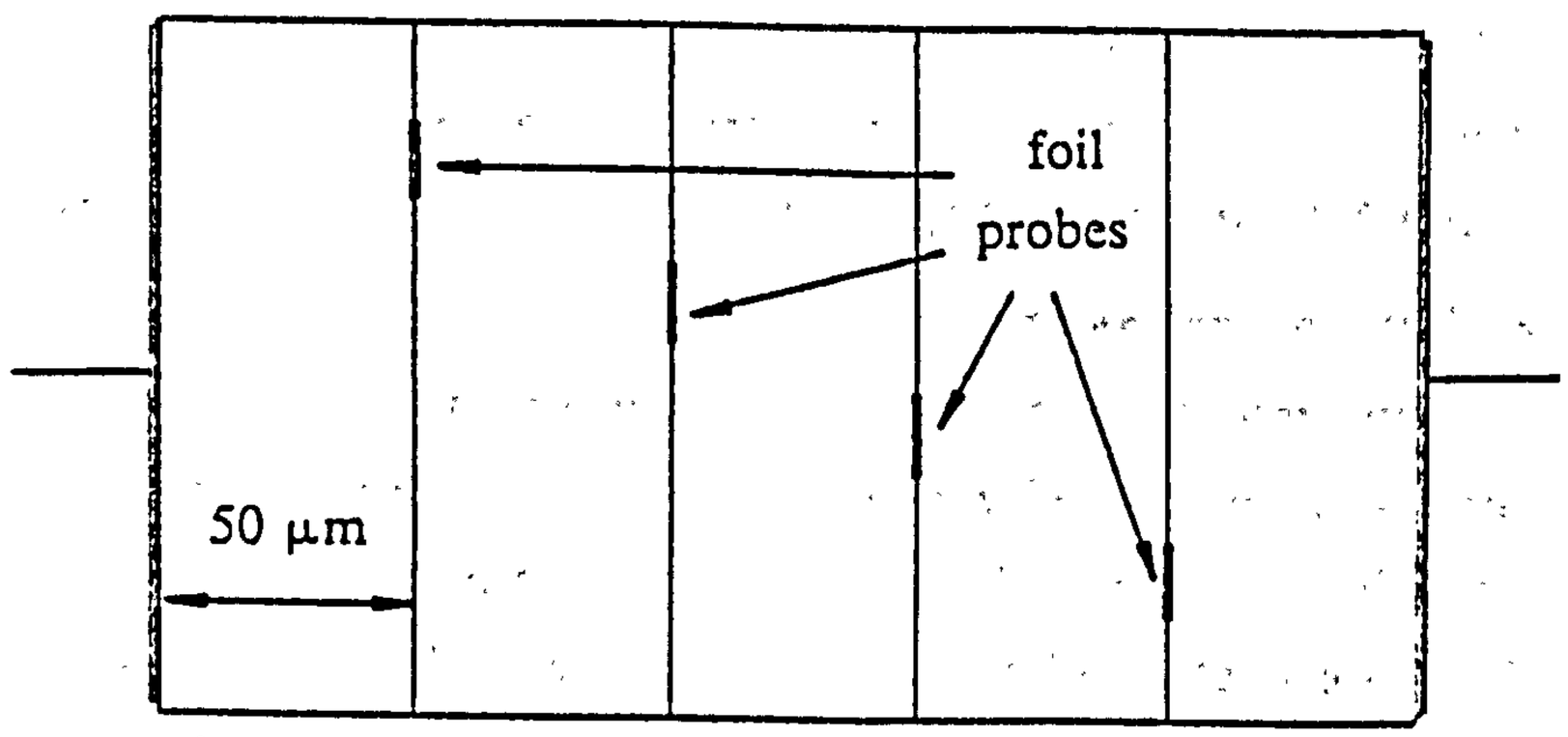

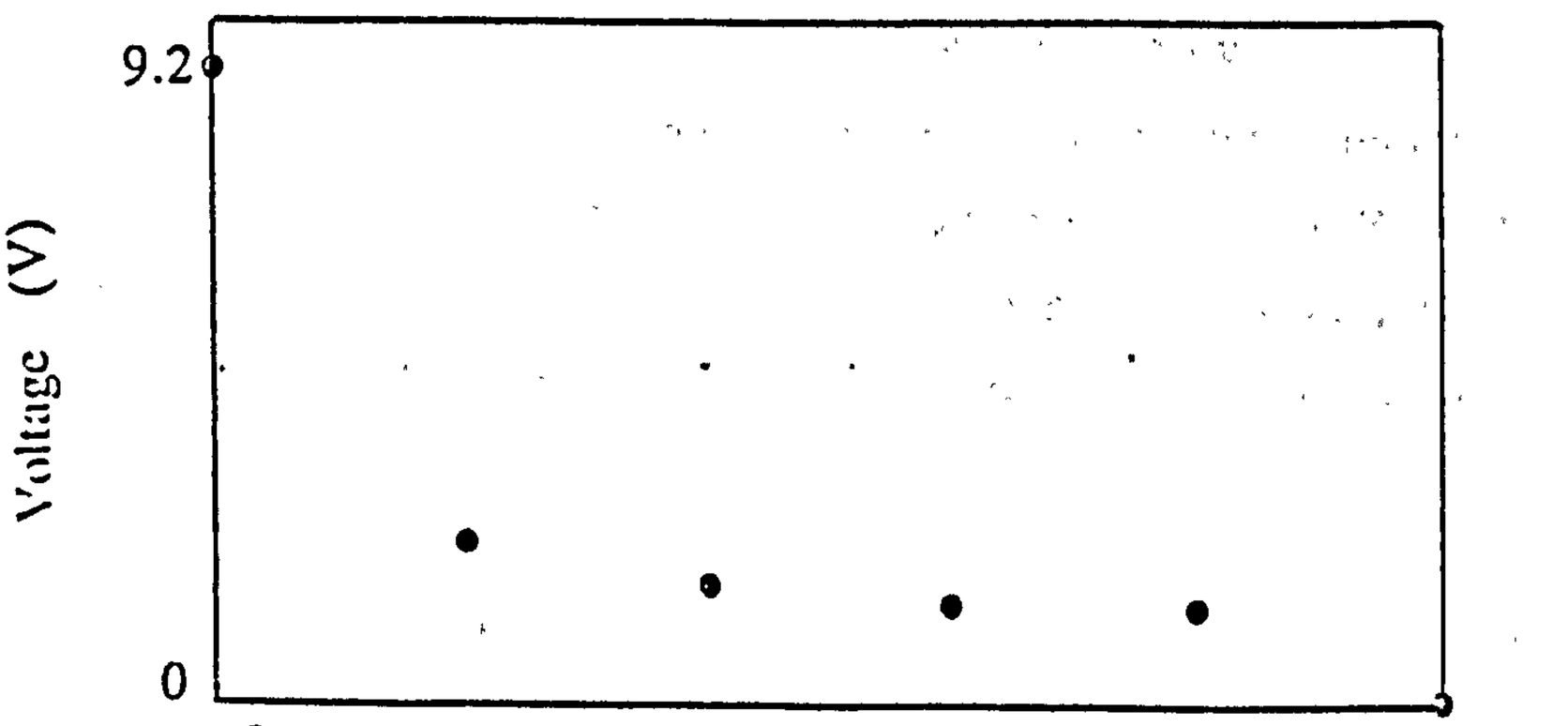

Fig 4.5 (a) Theoretical dependence of potential on x in case of static space charge with a single carrier (after [2]).
(b) Experimental structure used to test theory.
(c) Potential distribution in sample after polarisation.

4.5. Electrochemical Effects at Solid-State Interfaces

4.5.1. Reversible Electrodes

A reversible reaction can only give rise to an equilibrium potential when there are species of both sides of the reaction present originally [1]. Any such reaction in the case of an electrode on soda-silica glass must therefore involve a sodium or oxygen reaction. Sodium metal is thus the ideal choice as a reference electrode, but its extreme reactivity and low melting point makes it impractical for most purposes. It was used by Mitoff and Charles to investigate the reaction characteristics at a sealed platinum electrode. They used the experimental arrangement of figure 4.6 (a) which was constructed so that measurements could be made at a high temperature (415°C).

Sodium amalgam electrodes could also be used for this purpose, and electrolysis experiments have shown [23] that a reversible reaction occurs. Sodium tungsten bronze is a metallic crystalline material in which sodium may be present in varying amounts [24]. The possibility thus presents itself of an all-solid system which displays similar characteristics to the amalgam-glass system. Since such solid systems are much easier to handle, there would be considerable advantages to be gained, especially if high temperatures were to be used, as is frequently desirable in electrical measurements on glass in order to reduce the bulk resistance. The advantages that such an arrangement would have for handling and experimental design are obvious. However no electrochemical studies using this as a reference electrode seem to have been attempted. Electrodes supporting a reaction involving atmospheric oxygen were used by Ravaine and Souquet for contacts to the concentration cells they used for measuring the activity of sodium in Na_2O-SiO_2 glass [25]. In that case an equilibrium potential was assumed to be established via the reaction:

$$O_2 + 2e^- \rightleftharpoons 4O^{2-} \qquad 4.11$$

4.5.2. Inert Electrodes

Many electrodes are used under the assumption that they are inert, ie do not themselves react with the glass. Gold and platinum are in this category, although Proctor and Sutton also made the same assumption for aluminium. Inert electrodes are used either where blocking is required, as in the investigation of space-charge effects

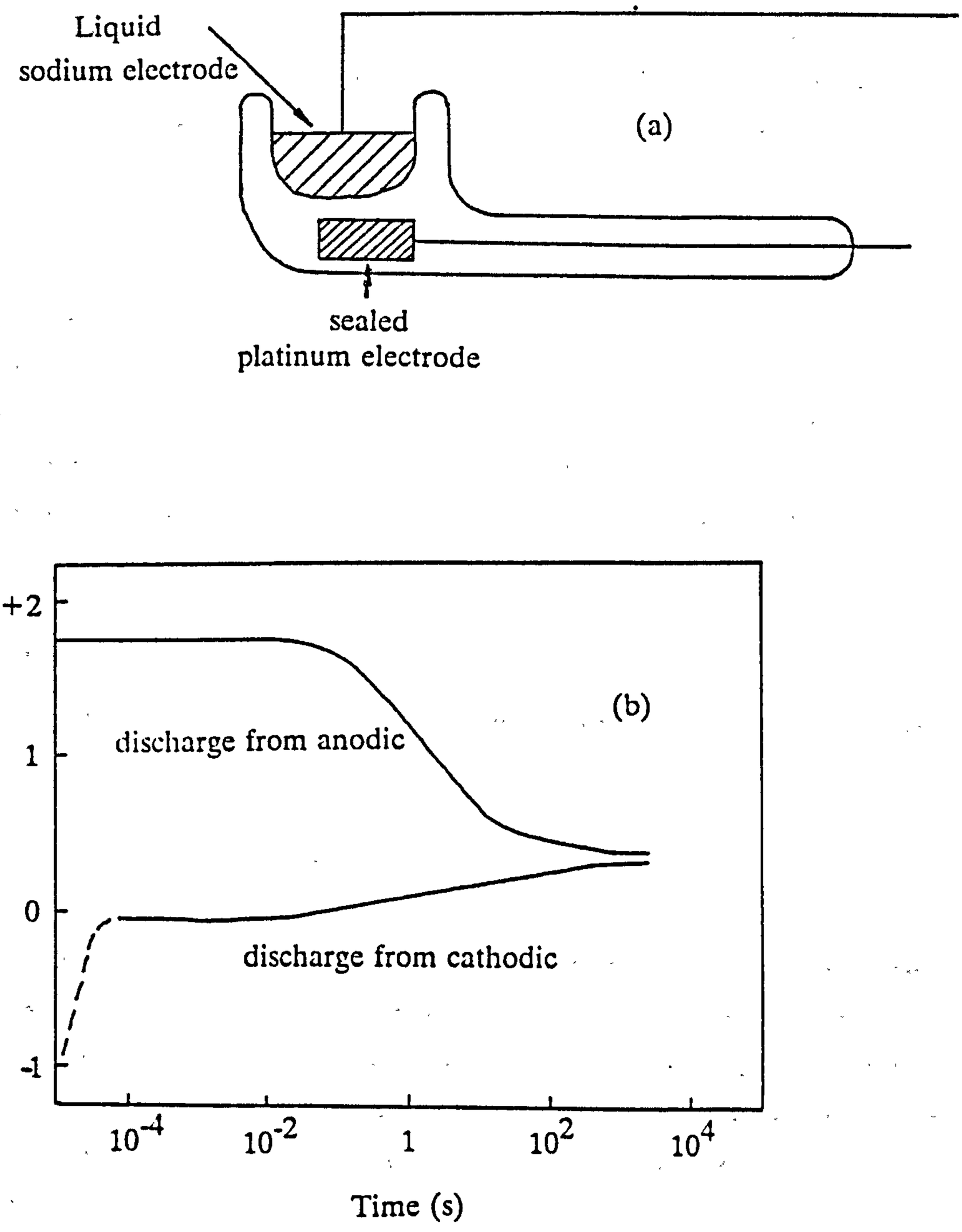

Fig 4.6 (a) Apparatus used by Mitoff and Charles to determine effects of reaction products at a platinum electrode [5].
(b) Results of discharging platinum electrode through 15 kΩ after 2 V polarisations in either direction.

[14,3], or to study the decomposition behaviour [5]. The cell illustrated in figure 4.6 (a) was used to find the energy storage properties of discharge products at the cathode and anode by holding the sealed platinum electrode at a steady potential relative to the sodium reference for a certain time and then measuring how much charge could be recovered by discharging the cell through a resistor. The results are shown in figure 4.6 (b). Oxygen produced during a 2 V anodic polarisation appeared to undergo a reverse reaction on removal of the applied voltage so that about 100μC had to flow to discharge the cell. By comparison, sodium reduced during the cathodic polarisation did not appear to reoxidise appreciably on connection to the discharging resistor. The cathodic response is consistent with the observed colouration of the cathode after a long polarisation attributed to reduction of the sodium while still inside the glass, rather than plating out at the surface.

4.5.3. Reactive Electrodes

The potential difference between the metal and the glass can also depend on a reaction between the electrode metal and the glass:

$$M_{(metal)} \rightarrow M^{+}_{(glass)} + e^{-}_{(metal)} \qquad 4.12$$

Because there is no bulk equilibrium concentration of the M^+ ions, the potential is not fixed, since the surface concentration will depend on the rate of the reaction and the rate of diffusion of M^+ in the glass. Silver electrodes have been used [26] to find the diffusivity of Ag^+ in glass. Silver has also been used [27] as a solid contact to a glass electrode, but the measured potential was found to be unstable.

4.6. High Field Effects

Applied potentials of hundreds of volts were used by Carlson et al [28] in experiments on soda-lime glass using platinum electrodes, with a single piece of glass incorporating a platinum internal probe. They found that, in the steady state, most of the applied voltage of up to 200 V fell across the anode region. Irreversible breakdown of the silicate structure following total alkali-ion depletion in the anode region was demonstrated by subsequent surface analysis of the samples. Oxygen gas evolution from the anode during the passage of current was detected by a mass spectrometer incorporated into the experimental arrangement. This was identified as the liberation of oxygen ions from the silica network which had previously been the sites of the

sodium ions. After sodium depletion, .these oxygen ions had drifted to the anode under the very high field which had been set up. The magnitude of the field which was required to set off the movement of the non-bridging oxygen atoms was not established.

The cathode potential drop remained at about 1 to 5 volts for applied voltages of up to 200 V. Subsequent examination found a layer of Na_2O at the surface. At higher applied voltages the cathode drop rose considerably, an effect which was attributed to reduction of the sodium while it is still inside the glass, inhibiting the reaction so that the electrode effectively becomes partially blocking.

An application of the high-voltage polarisation properties of glass is electrostatic metal-glass sealing [22]. The metal to be sealed is made 200 V anodic at about 200°C below the softening point of the glass for a few minutes. If the surfaces are sufficiently flat, a very strong permanent seal is obtained. Although the forces pulling the surfaces together were explained in general terms using the space-charge model, the actual sealing was claimed to be due to chemical bonds. It seems likely that these bonds were due to a reaction between the metal and the oxygen ions brought to the surface by the field.

Reactions between glass and both solid and liquid metal contacts were observed during high-field electromigration experiments by Regnier et al [29]. They applied 5000 V across a 1.2 mm sample of soda-lime silica glass at 80°C for several days. Subsequent depth profiling using Rutherford backscattering found sodium depletion at the anode to a depth of up to 6 μm. This was associated with the penetration of metal ions to varying depths depending on the metal and whether the contact was in the solid or liquid state. Mercury, and the components of liquid Woods alloy (Bi, Pb, Sn and Cd) penetrated up to about 4 μm into the glass. Solid iron, nickel chromium and copper only reached a few tens of nanometres. However zinc was found at a considerable depth from both solid and zinc-amalgam electrodes, although about three times as deep in the amalgam case. All this indicated that these metals are electrochemically active at the glass surface, although the authors were primarily concerned with the migration of the metal within the glass.

4.7. Summary

The range of factors affecting the development of electric potential at glass-metal interfaces has been reviewed. Glass surfaces themselves are capable of great variety according to the method of their fabrication and their subsequent treatment. The accompanying variety of electrochemical processes has complicated the task of finding the potential which is generated at interfaces with other substances but studies of the reactions themselves, such as those involved in leaching and corrosion, can provide clues to the problem. The detailed development of the theory of operation of the glass electrode has demonstrated the importance of diffusion potentials when electrochemical reactions are taking place at the surface of the glass. The ion-exchange element of the operation of the glass electrode is probably less relevant to the situation at solid contacts, however, since the reaction there seems to be fixed by the special conditions created by the hydration of the glass.

AC measurements are the most widely used method of investigating all kinds of electrical phenomena in glass. However most of the concepts available for the interpretation of the results are based on the bulk properties of glass and are of dubious relevance to studies of the interface. The only clear information that AC studies can provide about particular processes are of the form found by Ravaine et al [20] where evidence of nonzero conductance at very low frequency was clear indication of a charge-transfer process at the interface. Attempts to fit detailed theories, like those of Kim and Tomozawa [14], are invariably based on data which is too ambiguous to allow definite conclusions.

Since the existence of electrochemical reactions implies the generation of potentials, it seems more likely that DC measurements, or at least measurements which allow for variation of DC potential across the interface, would be more appropriate for investigating them. However careful experiments taking all the relevant factors into account, of the kind done by Raleigh on silver bromide cells do not seem to have been done for glass. The DC experiment of Proctor and Sutton [3] does not take the possibility of interfacial reactions into account. That of Mitoff and Charles [5] only considers conditions under which the glass decomposes and gaseous reaction products are not allowed to escape. For his work on silver bromide crystals, Raleigh used an electrode which was known to be reversible, and it is the provision of such an electrode for glass which might allow useful electrochemical measurements to be made. The liquid sodium electrode provides a reversible electrode for glass but it is very inconvenient to

use. The same can be said of sodium amalgam electrodes. A solid metallic material which can accommodate varying concentrations of sodium, such as sodium tungsten bronze, is required. Preliminary electrical experiments involving sodium tungsten bronze electrodes are described in chapter 6.

REFERENCES

1. Raleigh DO, Electroanal Chem **6,** (ed AH Bard) p87-186, Dekker, New York (1973).
2. Proctor TM and Sutton PM, J Chem Phys **30,** 212-220 (1959).
3. Proctor TM and Sutton PM, J Amer Ceram Soc **43,** 173-179 (1960).
4. Sutton PM, J Amer Ceram Soc **47,** 188-194 and 219-230 (1964).
5. Mitoff SP and Charles RJ, J App Phys **43,** 927-934 (1972).
6. Macdonald JR, J App Phys **45,** 2343-2345 (1974).
7. Macdonald JR, J App Phys **44,** 3455-3458 (1973).
8. Macedo PB, Moynihan CT and Bose R, Phys Chem Glass **13,** 171-179 (1972).
9. Dunken HH, in *Treatise on Materials Science and Technology,* **22,** (ed H Herman) p1-73, Academic Press, (1982). 10. Pescatore C and Machiels AJ, J Non-Cryst Solids **49,** 379-388 (1982).
11. Melling PJ and Allnatt AR, J Non-Cryst Solids **42,** 553-560 (1980).
12. Wikby A, Phys Chem Glass **15,** 37-41 (1974).
13. Wikby A, Talanta **22,** 663-7 (1975).
14. Kim C and Tomozawa M, J Amer Ceram Soc **59,** 127-130 (1976).
15. Eisenman G, in *Glass Electrodes for Hydrogen and Other Cations,* (ed G Eisenman) p133-135, Dekker, New York (1967).
16. Doremus RH, ibid, p101-132.
17. van der Ziel A, *Solid-State Physical Electronics* p483, Prentice-Hall, New Jersey (1957).
18. Beaumont JH and Jacobs PWM, J Phys Chem Solids **28,** 657-667 (1967).
19. Macdonald JR, J Chem Phys, **75,** 3155-3157 (1981).
20. Ravaine D, Audier M and Souquet J-L, J de Chim Phys **73,** 75-81 (1976).

21. Macdonald JR, J Chem Phys **22**, 1317-1322 (1954).

22. Wallis G and Pomerantz DI, J App Phys **40**, 3946-3949 (1969).

23. Owen AE *Progress in Ceramic Science* **2**, (ed JE Burke) p77-196, Pergamon, London (1963).

24. Cotton FA and Wilkinson G, *Advanced Inorganic Chemistry* p849-850, Wiley, New York (1980).

25. Ravaine D and Souquet JL, Phys Chem Glasses **18**, 27 (1977) and *ibid* **19**, 115 (1978).

26. Kraus CA and Darby EH, J Amer Chem Soc **44**, 2783-97 (1922).

27. Portnoy H, in *Glass Electrodes for Hydrogen and Other Cations*, (ed G Eisenman) p259-266, Dekker, New York (1967).

28. Carlson, Hang and Stockdale, J Amer Ceram Soc **55**, 337-341 (1972).

29. Regnier P, Serruys Y and Zemskoff A, Phys Chem Glasses, **27**, 185-189 (1986).

CHAPTER 5

EXPERIMENTAL

5.1. Introduction

The principal requirement of a solid-state connection to a glass electrode is that its potential be stable over a long period. Whether this is achieved via a reversible electrode reaction with precisely defined activities of ions on each side of the interface or otherwise is of secondary importance. The experiments described below were therefore designed to find out how potential was developed at the interface between various different metals and pH-sensitive glass. For this purpose, cells were made with various electronically conducting materials as electrodes. Aluminium, copper and silver contacts were made by vacuum evaporation. For sodium metal, tungsten trioxide and sodium tungsten bronze contacts, evaporation was not possible, and the electrodes were formed by applying the solid electrode material directly to the surface of the glass.

5.2. Experimental Techniques

The small-signal regime, ie with applied voltages of not much more than RT/F (25 mV), was studied at zero bias using AC voltammetry. DC biasing was not considered appropriate because of the the difficulty in achieving a steady state in a metal-glass system; even at high temperature, application of a steady voltage leads to a current which decays over long periods [1]. Larger potentials were measured using a constant applied current.

5.2.1. AC Voltammetry

The application of a small AC potential and the measurement of the amplitude and phase of the resulting current is the most common method for studying the electrical response of solid ionic conductors, whether the bulk or the interface properties are of interest. The results, in the form of a frequency dependent impedance, can be

interpreted by terms of an equivalent circuit with components which themselves may be frequency-dependent, as was described in previous chapters.

5.2.2. Transient-DC Voltammetry

AC techniques are restricted to small perturbations about a fixed point which is at some point of equilibrium or steady state, since above this region harmonics appear in the response which are difficult to interpret and the convenience of the technique is lost. In order to investigate deviations from that steady state, a simpler waveform is required. If the system can be accurately modelled, such as in the case of liquid electrochemistry, it is possible to calculate the response to a signal which runs through the entire range of potential of interest, such as a voltage ramp. This is not the case with the glass-metal system under consideration here, and so the most appropriate waveform for the applied signal is the simplest, so that the results can be interpreted as directly as possible. This implies a constant applied voltage or current. In principle there is no distinction between the information which the two techniques are capable of providing. Since the overall problem was being approached in terms of the effect on interface potential of the passage of charge then a constant rate of charge flow, ie a constant current, was chosen, with the potential being measured as a function of time. It is also easier to visualise the processes involved in the time development of potential, because the current is uniform throughout a series circuit, and the possibility exists of identifying changes of potential with resistances and capacitances of various points of the system. The experimental procedure is identical to that of the electrochemical technique of chronopotentiometry, but since few of the electrochemical assumptions are used to interpret the results, the technique will be referred to as "galvanostatic" measurement.

5.3. Fabrication of Samples

5.3.1. General Considerations

Test samples were fabricated out of glass plates with various contacts. One basic problem was the very low room-temperature conductivity of the glass, which tended to cause the contribution of interface effects to the overall impedance of the cell to be very low. The plates were therefore made as thin as possible, to keep the bulk resistance low, while retaining sufficient mechanical strength for handling. The thickness was typically 300μm, for which the room temperature conductance is typically 10^{-10} S, too low for measurements on a convenient timescale - for an interface capacitance of 1

μF, the time for significant polarisation would have been several hours - and so all measurements were made at elevated temperatures, between 150° and 400°C.

Another problem was the identification of processes at a single interface, which was the aim of two experiments. Any electric circuit involving an ionic conductor involves at least two contacts, and if the current carried by one is anodic then that carried by the other at the same time will be cathodic. The usefulness of a simple symmetrical two-electrode test structure as shown in figure 5.1 (a) is therefore very limited, since the contribution to the response of each side is not distinguishable.

One way of overcoming the problem would be to use a reversible electrode on one side, as shown in figure 5.1 (b), which has a fixed potential with respect to the glass. However only sodium metal or sodium amalgam are known to form reversible contacts with well-defined potentials, and the problems of migration of and contamination from liquid electrodes on a planar structure of the sort being used at the high temperature involved are such that these were not considered practical in the present case.

For two-electrode measurements, the potential drop across one of the contacts was minimised by making its area as large as possible, so that most of the observed interface impedance was due to the other contact. The resulting asymmetrical structure is shown in figure 5.1 (c) and will be referred to as the "type 1" structure.

A different approach is to use a three-electrode structure, analogous to that used in electrochemical experiments. One form of this, type 2, is shown in figure 5.2 (a). It consists of two identical current-carrying electrodes which are interchangeable as the working and counter electrodes, and a third, reference electrode. Because this third contact carries no current, it is reasonable to assume that its potential does not change with respect to the glass beneath it. If the current and temperature are such that the potential drop within the glass is small compared to that at the working electrode, then it is possible to measure *changes* in the working electrode drop by comparing its potential with that of the reference electrode. Figure 5.2 (b) shows an alternative but similar configuration, type 3, which allows several identical electrodes to be made on one piece of glass. Only the top contacts were used as working electrodes in type 3 samples.

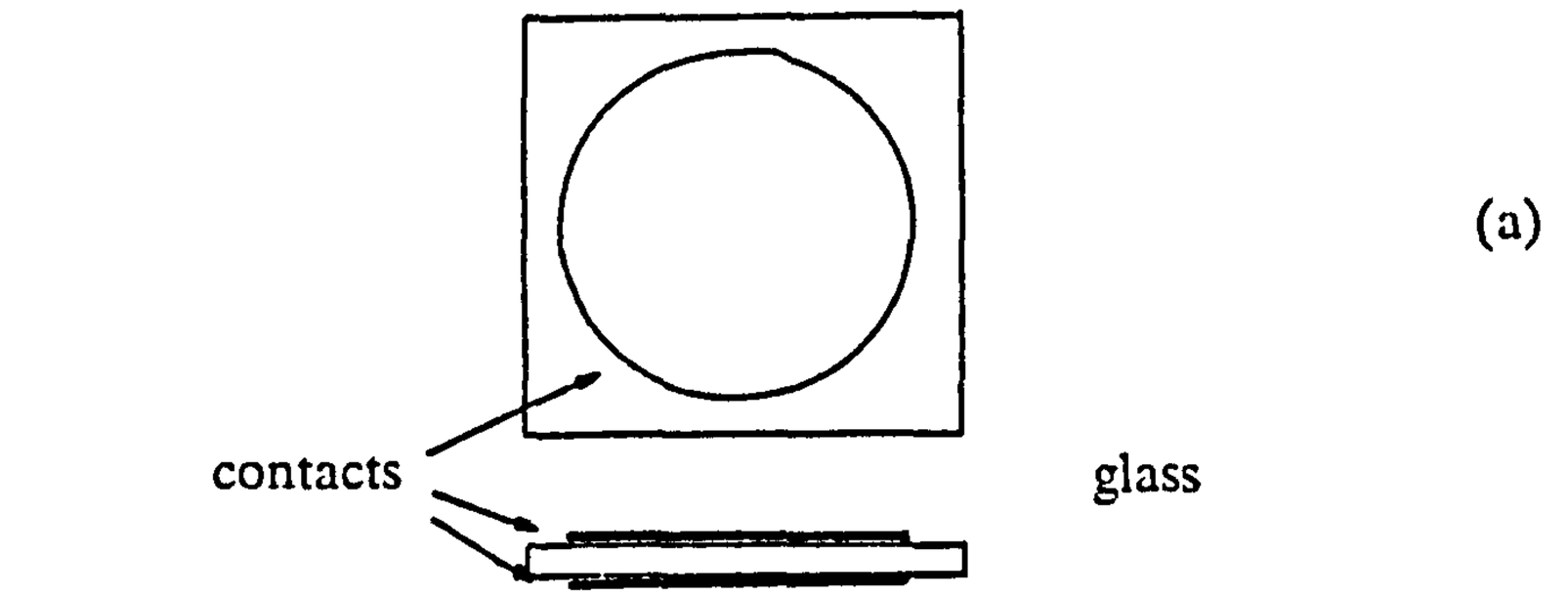

(a)

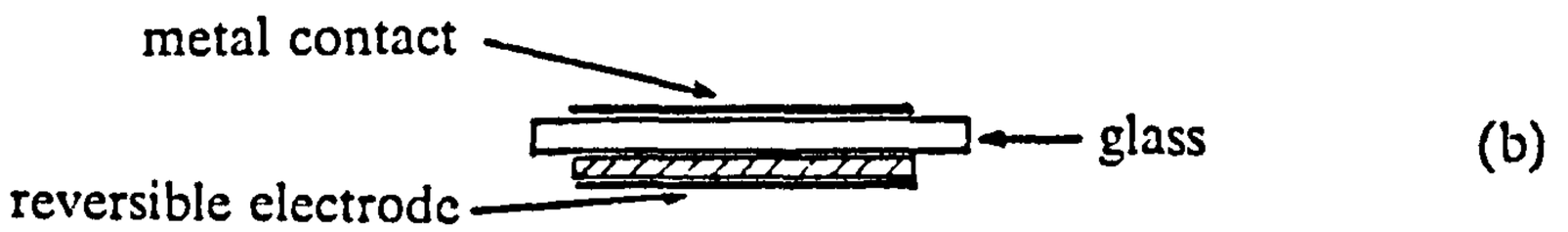

(b)

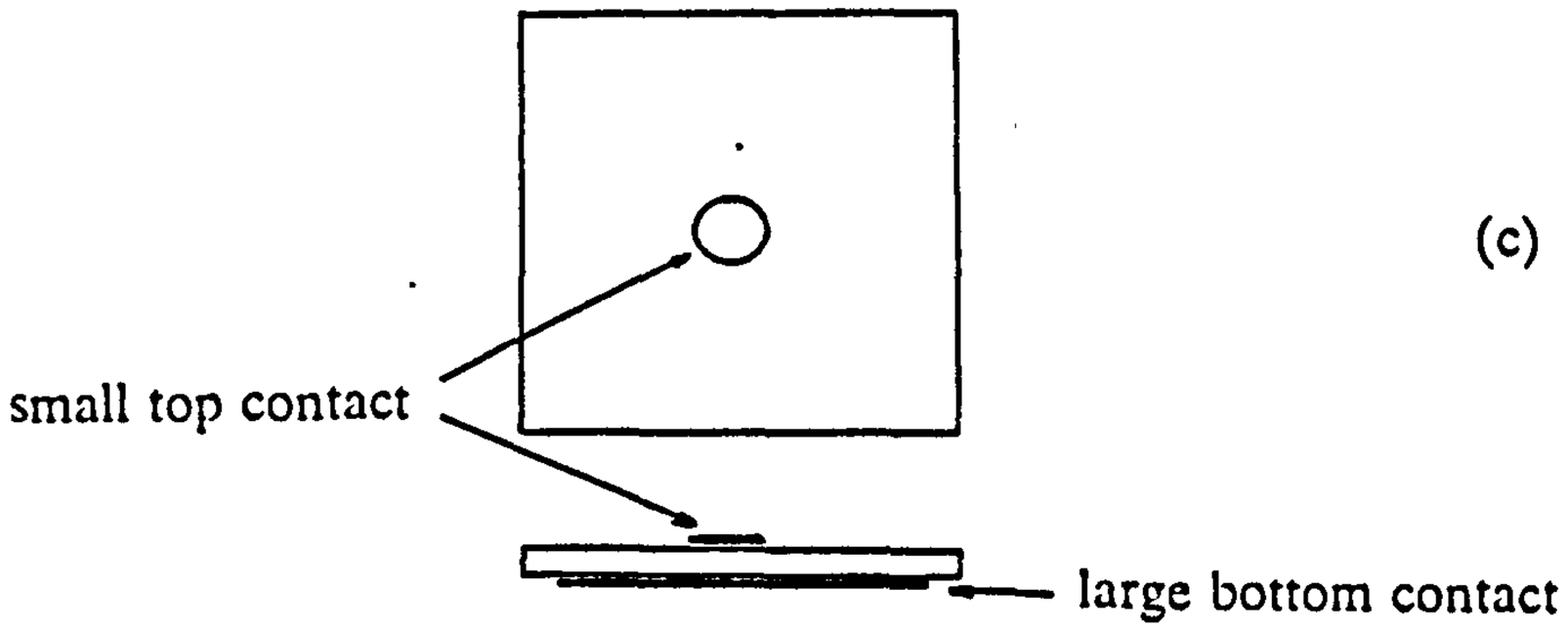

(c)

Fig 5.1 Two Electrode Cell Structures.

(a) Simple symmetrical cell

(b) Hypothetical cell with reversible electrode.

(c) Asymmetrical type 1 structure-used in two electrode measurements.

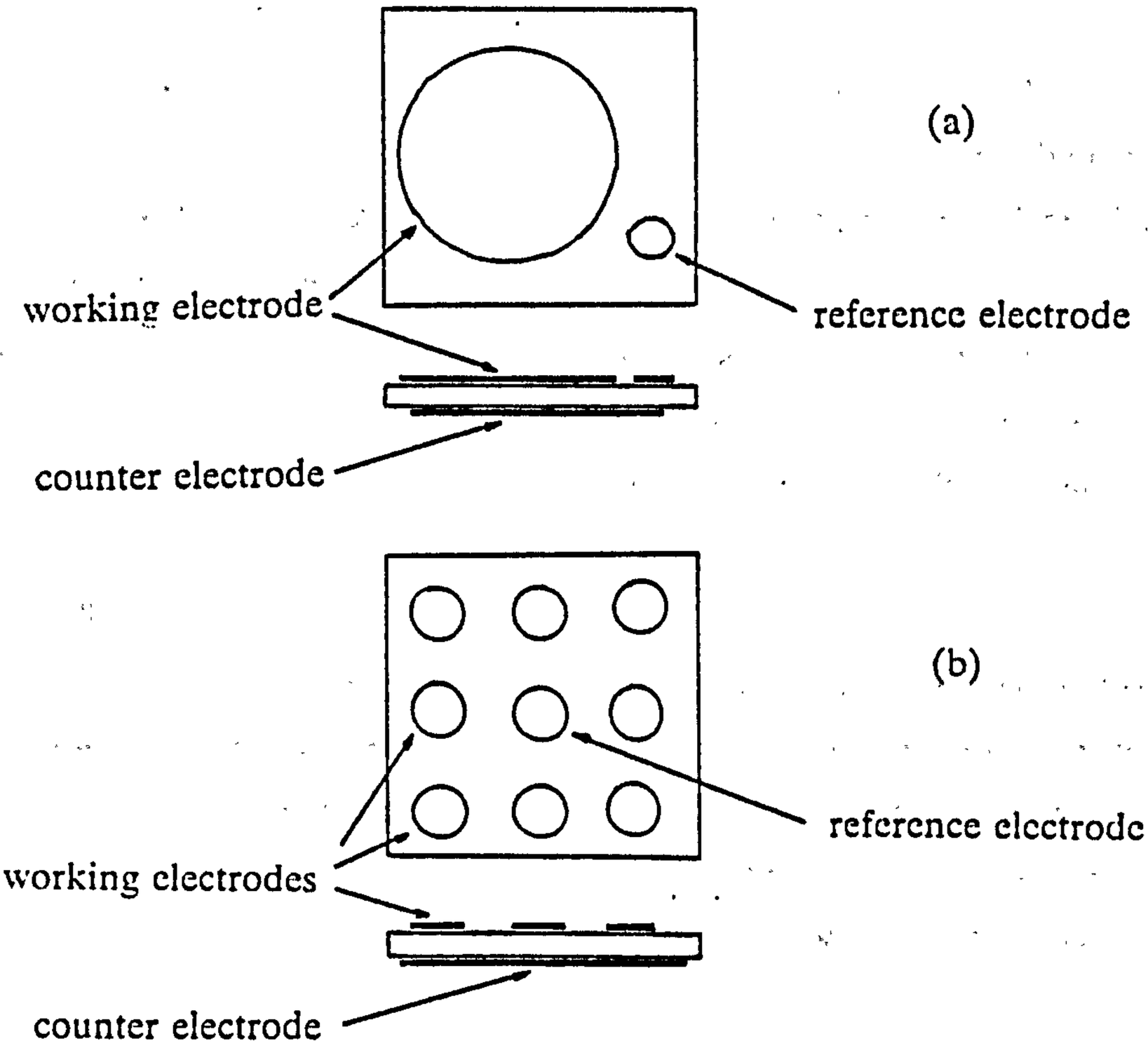

Fig 5.2 Three-electrode Structures.

(a) Type 2

(b) Type 3

5.3.2. Preparation of Glass

The pH-sensitive soda-lime-silica glass known as Corning 015 was used for all of the samples. This has the nominal composition by weight of 72% SiO_2, 22% Na_{20} and 6% CaO, and was obtained in the form of cast ingots from the Department of Ceramics, Glasses and Polymers, Sheffield University.

Plates were cut from the ingots using a diamond-bladed saw, with the ingot held in place with wax. The plates were cut in batches and stored in air before the next stage. Immediately before application of the electrodes, they were cleaned ultrasonically in acetone for a short period.

The variety of surface conditions which can obtain in glasses has already been discussed. In the absence of proper means of surface analysis or characterisation, the approach which was taken was to prepare the surfaces as identically as possible.

5.3.3. Evaporated Contacts

The aluminium, silver and copper contacts were applied by evaporation from a tungsten filament under vacuum, using a Nanotech vacuum-evaporation system. In most cases the thickness was neither controlled nor measured precisely, but was usually about 200 nm. This technique of application was chosen so that the contacts, made of different materials, were physically as identical as possible, and any differences between them would be solely due to the material.

5.3.4. Sodium Contacts

The facilities for preparing and testing the sodium-contacted samples were provided by Dr PG Bruce at Heriot-Watt University, Department of Chemistry. Sodium metal contacts were made in an argon-filled glove-box by cutting a small piece, about 10 mm in diameter and 1 mm thick, of dry sodium with a knife and laying it on the glass plate. The procedure was repeated for the contact on the opposite side. While still in the glove-box, this assembly was then placed in the holder shown in figure 5.3, which was then placed inside a glass tube and sealed with an O-ring and clamp. Only AC measurements were carried out on these samples, and all of these were done using this test cell without exposing the sample to the atmosphere.

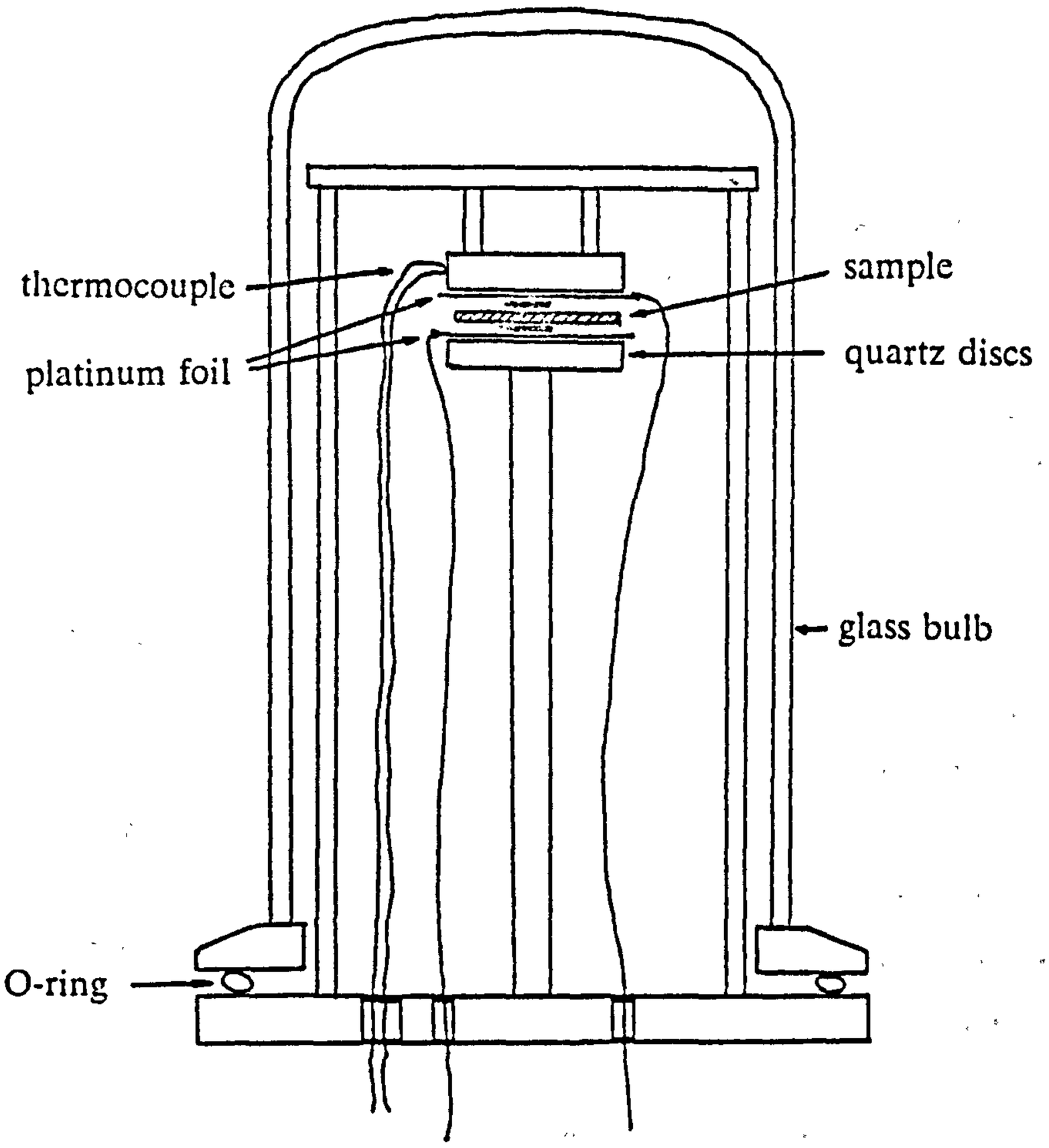

Fig 5.3 Sample holder and tube for sodium contacts.

5.3.5. Tungsten Trioxide

Contacts were prepared by pressing tungsten trioxide powder in a die to which a force of 4 tonnes was applied for 2 minutes so that a pellet 11 mm in diameter and about 2 mm thick was obtained. Two of these discs were attached to a glass plate to make the cell shown in figure 5.4. An attempt was made to achieve a good contact by placing the sandwich assembly in a furnace at 700°C for 10 minutes so that the glass softened briefly.

5.3.6. Sodium Tungsten Bronze

This material was not available commercially and so it was made using a published synthesis technique [2] by electrolysis of a mixture of molten WO_3 and Na_2WO_4. Analar-grade reagents were prepared for electrolysis by grinding each to a fine powder and intimately mixing in an agate mortar. 100g of Na_2WO_4 and 50g of WO_3 were used. The mixture was then put into the electrolysis cell shown in figure 5.5. This consisted of a cylindrical alumina crucible with a platinum lid and electrodes. The rectangular anode protruded through the lid, and connection was made to the disc cathode by a platinum wire in a ceramic tube. The platinum parts were held together and fixed to the crucible by a refractory cement.

The assembly was placed in a muffle furnace and heated to 780°C, whereupon the voltage was applied to the electrodes, and the current adjusted to 45 mA as recommended in reference 2, which required about 2 V. After ten hours, the resistance began to increase gradually until after 24 hours 50 V was required to maintain the current. Thereafter, the voltage was held at this level and the current eventually levelled at about 20 mA. After a total electrolysis time of 5 days, the furnace was allowed to cool with the voltage still applied. The contents of the crucible were recovered by breaking it with a hammer and the metallic bronze was separated from the flux (a white powder) by placing it in boiling water until the flux had dissolved. After grinding to a fine powder in an agate mortar, the bronze was ready for use as a contact material.

Contacts were made to glass by two methods. In one, a disc of bronze powder was made by pressing in a die under a force of 4 tonnes for two minutes. The cell shown in figure 5.6 (a) was constructed by laying the disc on a glass plate with an aluminium back contact (counterelectrode) and reference electrode. Aluminium was used because it was found in the other experiments not to deteriorate after subjection

Fig 5.4 Sample with tungsten trioxide contacts.

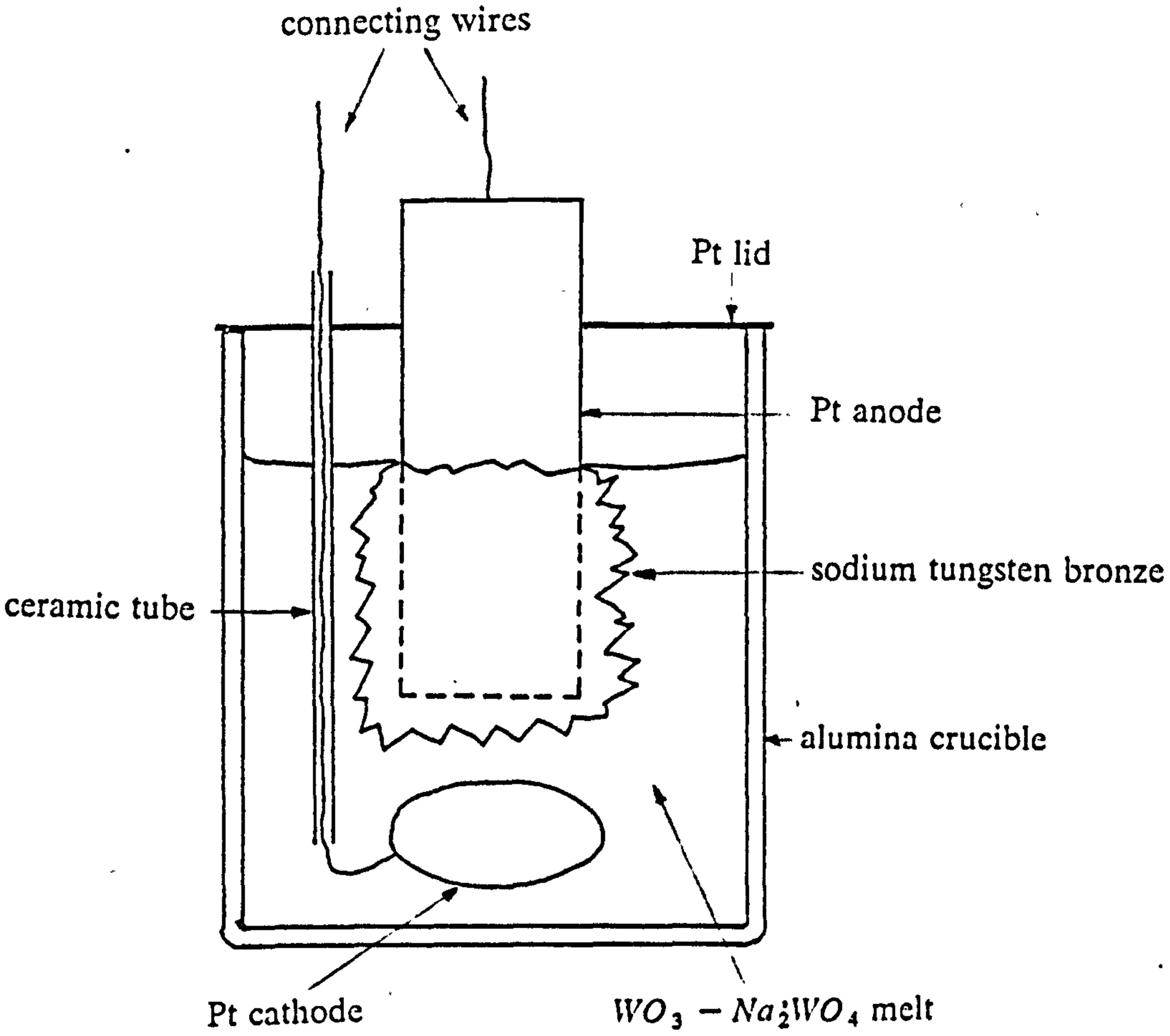

Fig 5.5 Electrolysis of sodium tungsten bronze.

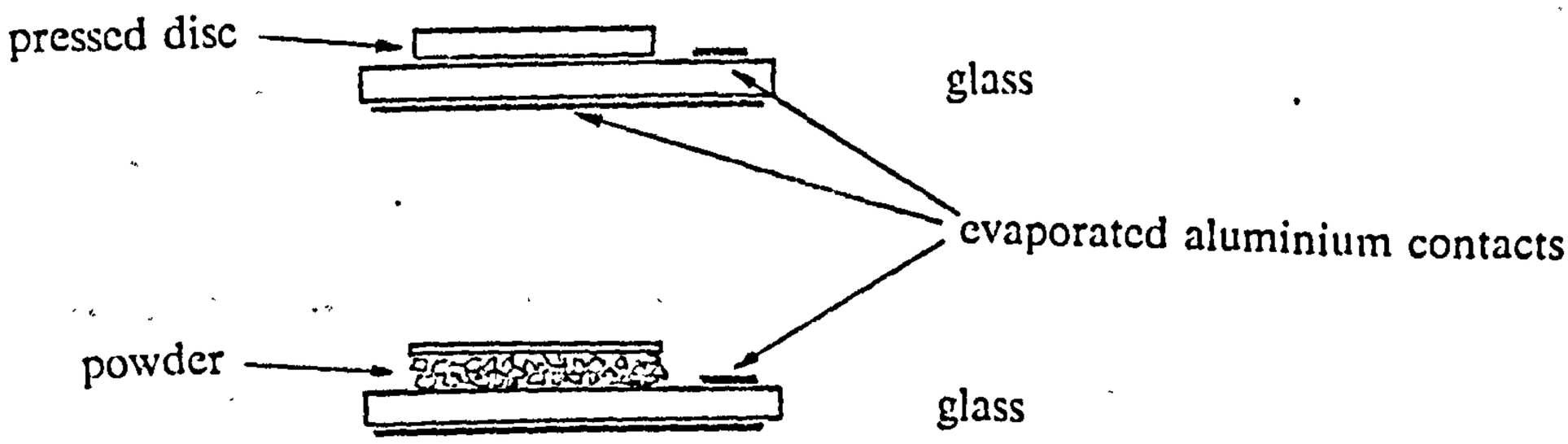

Fig 5.6 Sodium tungsten bronze samples:

(a) Pressed disc contact.

(b) Powder contact.

to the high temperature in the chamber. The other method of making the contact was by laying the powder directly on the glass surface, resulting in the cell of figure 5.6 (b). A metal plate on was placed on top to prevent disturbance of the powder by the probe contact.

5.4. Sample-holder and Vacuum Chamber

The sample-holder and contact arrangement is shown in figure 5.7. The aluminium block is heated by an internal heater, and its temperature measured by a platinum-film resistance sensor which is contacted via two spring-loaded probes. Two-electrode samples are electrically insulated from the block by a thin layer of mica, and contact made on one side through a tungsten wire. This wire was chosen because it maintains its resilience even at high temperature, ensuring a good electrical contact. On the other side the contact was via a combination of a similar wire and aluminium foil. The bottom (counterelectrode) contact of three-electrode samples made direct contact with the platform, the probes being used to contact the working and reference electrodes. The assembly was enclosed by an aluminium casing which was pumped down to less than 10^{-4} torr by a sorption pump cooled by liquid nitrogen.

5.5. AC Impedance Measurements

A Solartron 1170 Frequency Response Analyser was used for all the AC work. Its principle of operation may be summarised as follows. The output of a generator capable of a sinusoidal signal of 10 mV to 9.99 V RMS at frequencies between 0.1 mHz and 1 MHz is applied to the system under test, and the response of the system can be measured at two points by the two-input analyser which detected the magnitude of the voltage, and its phase relative to that of the generator signal. A correlation process is used to achieve this, which ensures that only voltages of the same frequency as that which was applied are measured.

The impedance of the sample is found by measuring the response of a test circuit consisting of the sample and known components. The circuit used for the two-electrode samples is shown in figure 5.8. The voltage appearing at the y-input of the analyser is given by:

$$V_a = V_s \left(\frac{Y}{Y_a + Y} \right) \qquad 5.1$$

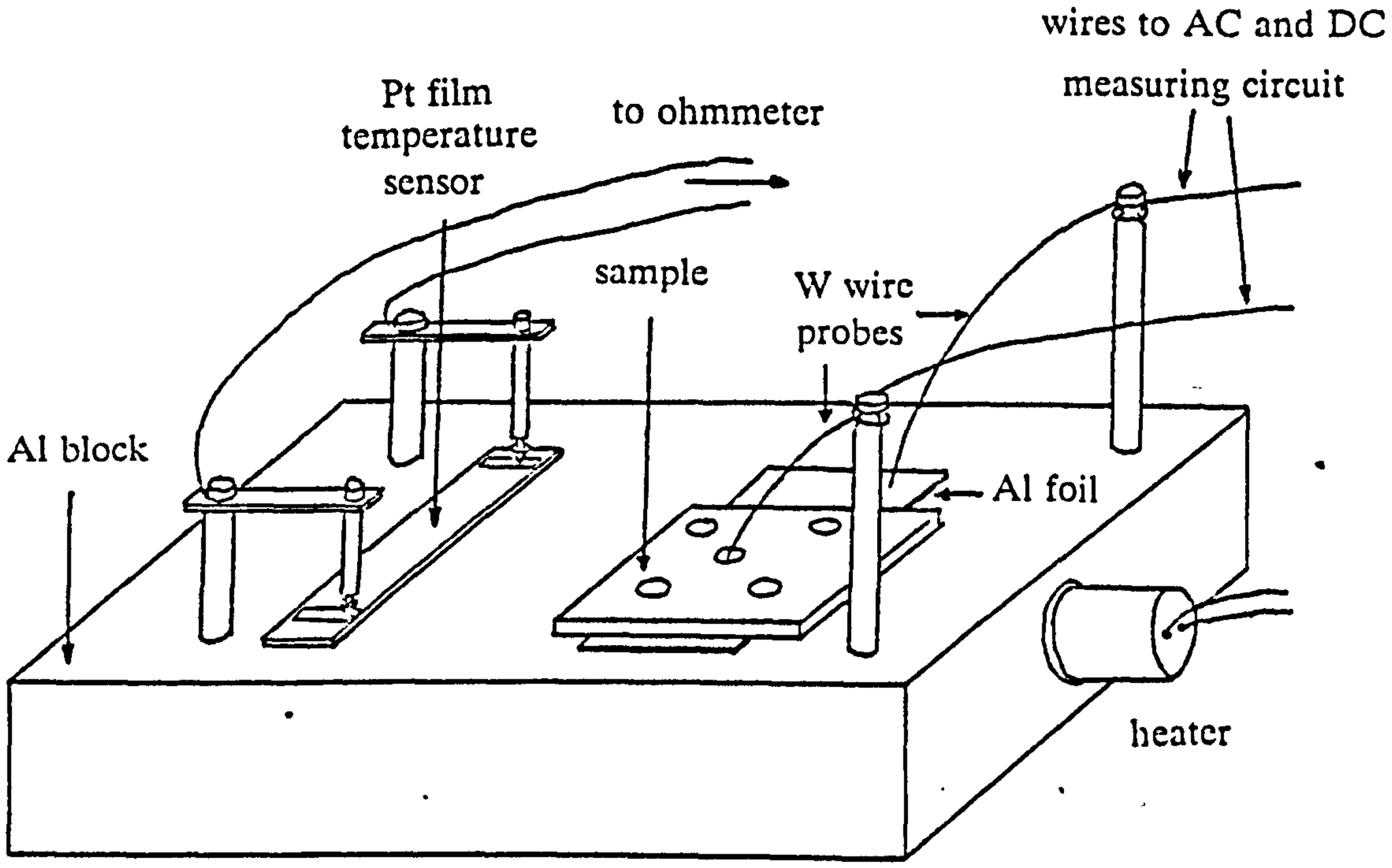

Fig 5.7 Sample holder and contact arrangement.

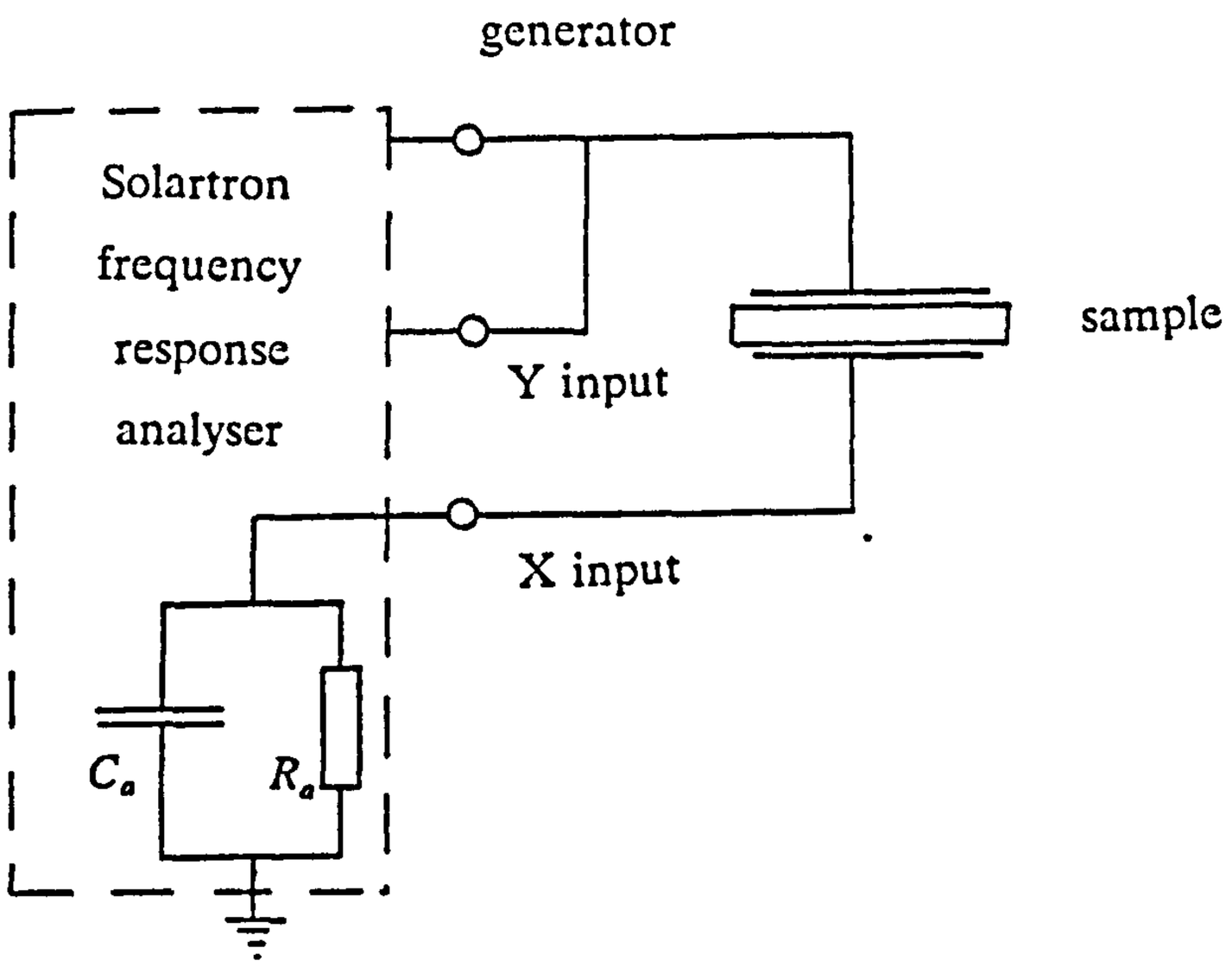

Fig 5.8 AC measuring circuit for two electrode samples.

where Y is the admittance of the sample and Y_a that of the analyser the admittance which appears between the y-input and ground. The analyser measures the ratio of the voltage at y to that of the generator and gives the result as a complex number r such that

$$r = a + jb. \qquad 5.2$$

From equation 5.1, the admittance of the sample can be expressed in terms of r and Y_a:

$$Y = \frac{rY_a}{1 - r} \qquad 5.3$$

from which the real and imaginary parts may be calculated as:

$$Re(Y) = \frac{(1-a)(aG_a - b\omega C_a) - b^2 G_a - ab\omega C_a}{(1-a)^2 + b^2} \qquad 5.4$$

and

$$Im(Y) = \frac{(1-a)bG_a + (1-a)a\omega C_a + abG_a - b^2\omega C_a}{(1-a)^2 + b^2} \qquad 5.5$$

The "other components", conductance G_a and capacitance C_a, should ideally be chosen to present an impedance similar to that of the sample for maximum accuracy of readings, so that the voltage at the y-input is half that of the generator. However the smallest value that Y_a can have is presented by the input resistance and capacitance of the analyser itself, in parallel with the impedance of the connecting leads, and any stray coupling to earth. This effectively sets a lower limit to the admittance which can be measured by the analyser for a given applied voltage. The lowest conductance which can be measured reliably with $V_g = 200\,mV$ was found experimentally to be about 10^{-8} S. Since the samples in the temperature range which was used had dc conductances of about 5×10^{-5} S maximum and down to 10^{-11} S at room temperature, the magnitude of Y_a did not have to be increased by extra shunting components across this input impedance. Because the values of R_a and C_a were dependent on the connections and geometry of the system, they had to be measured using a precisely-known resistor,

R_d, in place of the sample. The input admittance is then given by:

$$G_a = \frac{a(1-a) - b^2}{R(a^2 + b^2)} \qquad 5.6$$

and

$$C_a = \frac{b}{\omega R_d (a^2 + b^2)} . \qquad 5.7$$

The test circuit for the three-electrode samples is shown in figure 5.9, and is rather more complicated than that for the two-electrode samples. The voltages at the working and reference electrodes are measured separately by the two inputs of the analyser. The important difference between this setup and the two-electrode arrangement is that the sample is in parallel with the analyser instead of being in series with it. The data from the analyser is nowin the form of two complex numbers, r_1 and r_2. From the x-input,

$$r_1 = a_1 + b_1 = \frac{G}{G + Y_s + Y_{ax}} \qquad 5.8$$

where G is the conductance of the resistor in figure 5.9 and Y_1 is the admittance of the whole system between x and ground. And from the y-input,

$$r_2 = a_2 + b_2 = \frac{Y}{Y_s} \qquad 5.9$$

Eliminating Y_s between the equations 5.8 and 5.9 gives:

$$Y = (a_2)\left\{G\left(\frac{1 - a_1 - jb_1}{a_1 + jb_1}\right) - G_{ax} - j\omega C_x\right\} \qquad 5.10$$

Taking the real and imaginary parts of this expression gives:

$$Re(Y) = G\left(\frac{a_1a_2(1-a_1) + a_1b_1b_2 + b_1b_2 - a_1b_1b_2 - a_2b_1^2}{a_1^2 + b_1^2}\right) - a_2G_{ax} + b_2\omega C_{ax}$$

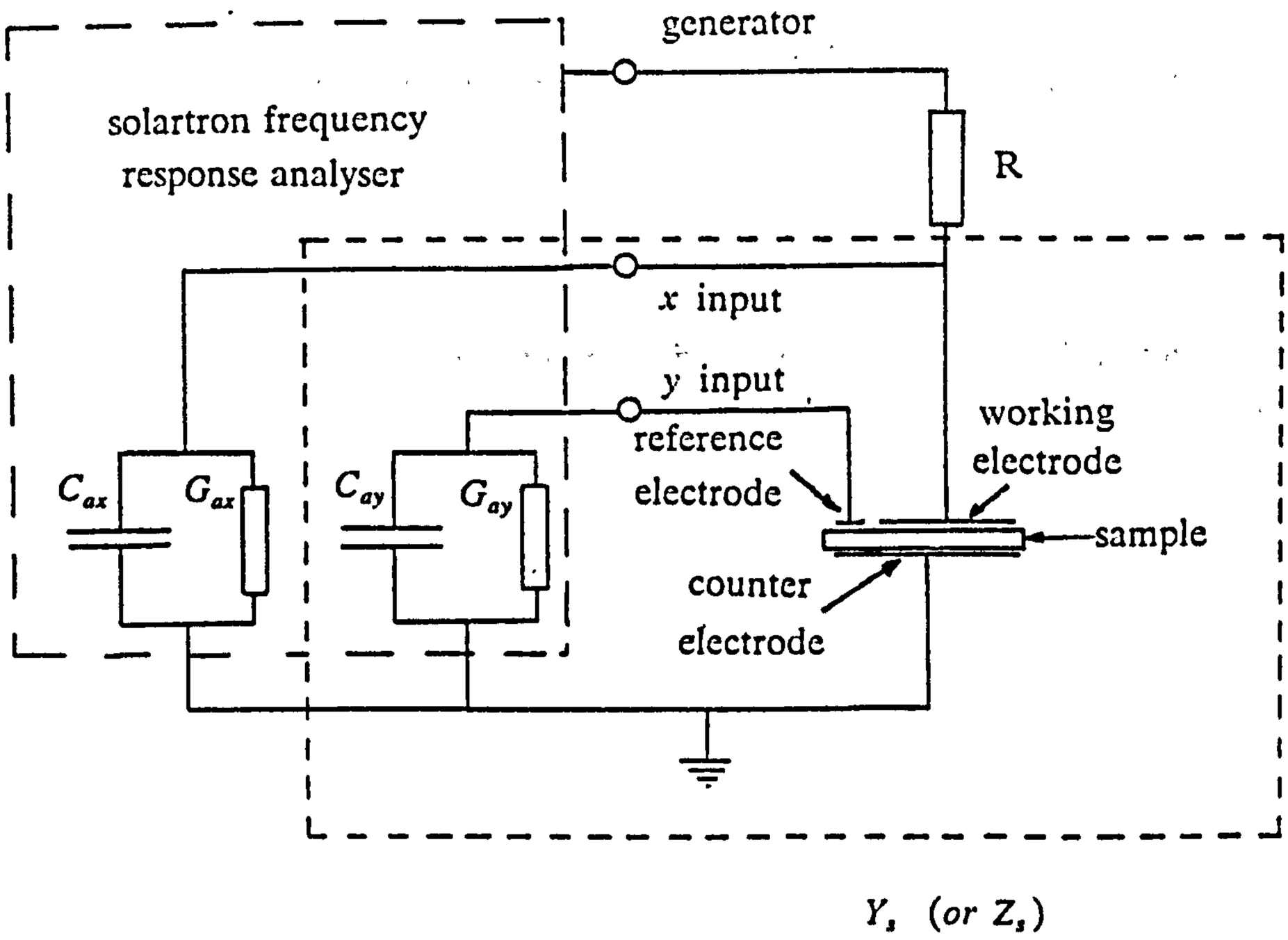

Fig 5.9 Three electrode circuit for AC work

5.11

and

$$Im(Y) = G\left(\frac{a_2b_1(a_1-1) - b_1^2b_2 + a_1b_2(1-a_1) - a_1a_2b_1}{a_1^2 + b_1^2}\right) - b_2G_{ex} - a_2\omega C_{ex}\ .$$

5.12

As in the case of two-electrode measurements, the values of G_{ex} and C_{ex} had to be measured. This was done using the circuit of figure 5.10. The component values are:

$$G_{ex} = \frac{1}{R}\left(\frac{a}{a^2 + b^2} - 1\right) - \frac{1}{R_t} \qquad 5.13$$

and

$$C_{ex} = \frac{b}{\omega R\,(a^2 + b^2)}\ . \qquad 5.14$$

The presence of the test resistor R_t is not necessary, but since it represents the sample, all of the connections to it must be in place.

The frequency-response analyser is controlled and the data collected by a Hewlett-Packard HP-86 computer via an HP-IB (IEEE 488) interface bus. The computer also performs the calculations of the sample parameters using the appropriate equivalent circuit and plots the results, in the form of real part of admittance versus frequency and complex admittance for the two-electrode samples, and interface capacitance versus frequency for the three-electrode samples.

5.6. Galvanostatic Measurements

The circuit diagram for the current source which was used for all of the galvanostatic measurements is shown in figure 5.11. It is continuously variable either from -500 to +500 nA or -50 to +50 μA, depending on the choice of feedback components in the current-controlling circuit.

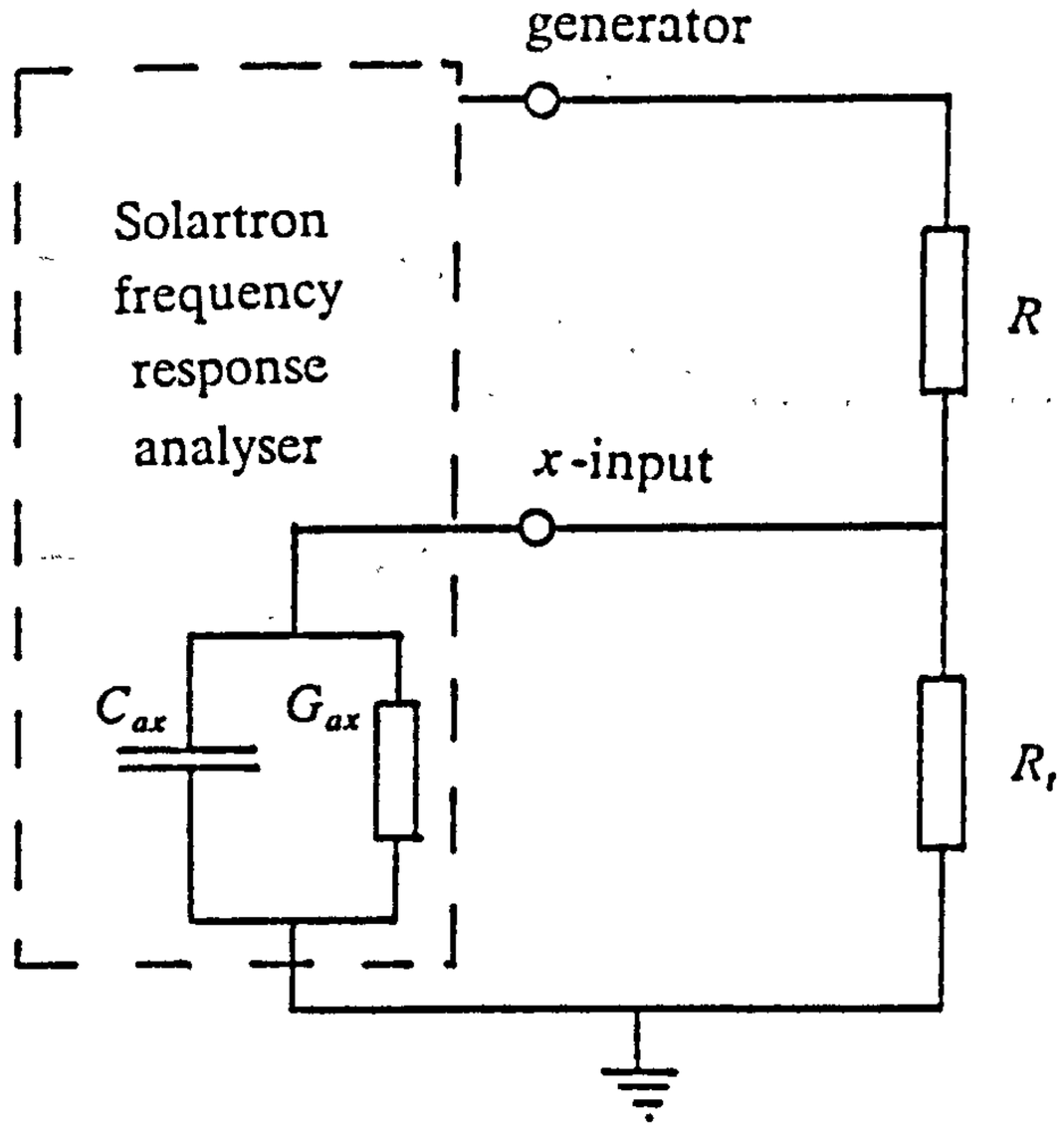

Fig 5.10 Circuit used to find input admittance of the x input

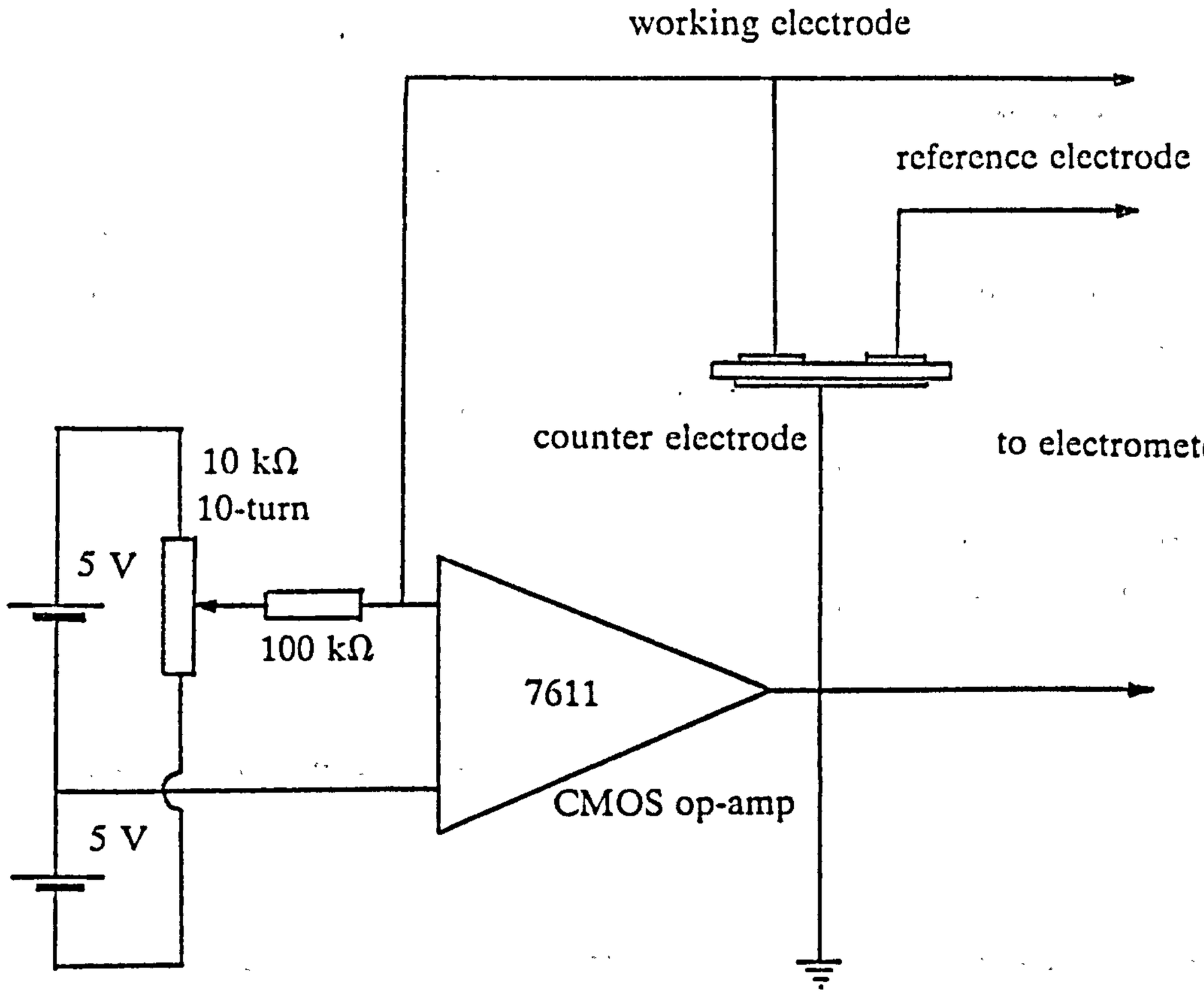

Fig 5.11 Circuit diagram of current source used for galvanostatic measurements

The voltage is measured by a Keithley 610C electrometer coupled to a microprocessor-based data interface which supplies the voltage-time data to the computer in a digital form via the same IEEE bus as used for the AC data. The input to the interface has a single range of +/-5 V and the analogue to digital converter has a resolution of 12 bits, so that the theoretical voltage resolution is 2.5 mV. The minimum time between measurements is 80 ms, limited by the speed of the computer, since readings are taken and passed along the data bus one at a time.

A galvanostatic measurement consisted of applying the current between the working electrode and the counterelectrode, and measuring the potential of the working and reference electrodes.

5.7. Experimental Procedure and Form of Results

5.7.1. AC Impedance

The simplest equivalent circuit which can be used to represent the real system is shown in figure 5.12. C_i and G_i represent the interface capacitance and conductance, and C_b and G_b represent those of the bulk. In the case illustrated, $G_i << G_b$ and $C_i >> C_b$. The high-frequency response is determined by C_b, and so is of less interest here. To evaluate the other component values, the complex admittance representation is most appropriate, and the form of this for the ideal circuit is shown as the solid curve in figure 5.13 (a). The dotted curve is the schematic plot of an actual system: it differs from the ideal in that the centre of the circular arc is depressed from the real axis. This depression is quantified by the angle β. G_b is the length along the real axis between the intercepts of the complex-admittance curve. If the interface is completely blocking, so that G_i is zero, then the arc goes through the origin. The variation with frequency of the real and imaginary parts of the admittance of the ideal circuit is shown on the logarithmic axes in figure 5.13 (b). The real-part plateau is due to the bulk conductance. At lower frequency, where the reactance of C_i is comparable to G_b, the magnitude of the admittance is less and the real part falls off as frequency decreases. The imaginary part reached a peak when ωC_i is equal to G_b. This relation was used to calculate C_{ac}. The angle of depression, α, of the centre of the arc from the real axis is also found from the complex-admittance data.

In some cases, a sufficient range of temperature was used for the activation energy of conduction to be calculated from the slope of the G_b vs $1/T$ graph. Because

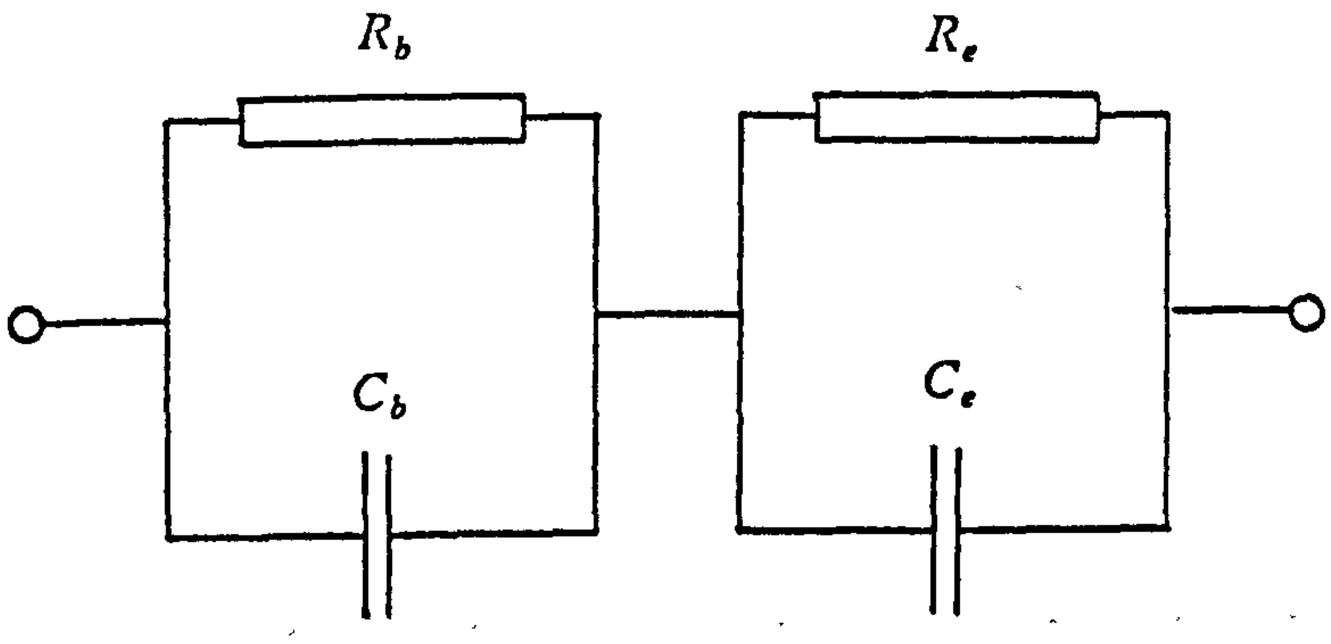

Fig 5.12 Equivalent circuit of sample for interpretation of AC results on two-electrode samples.

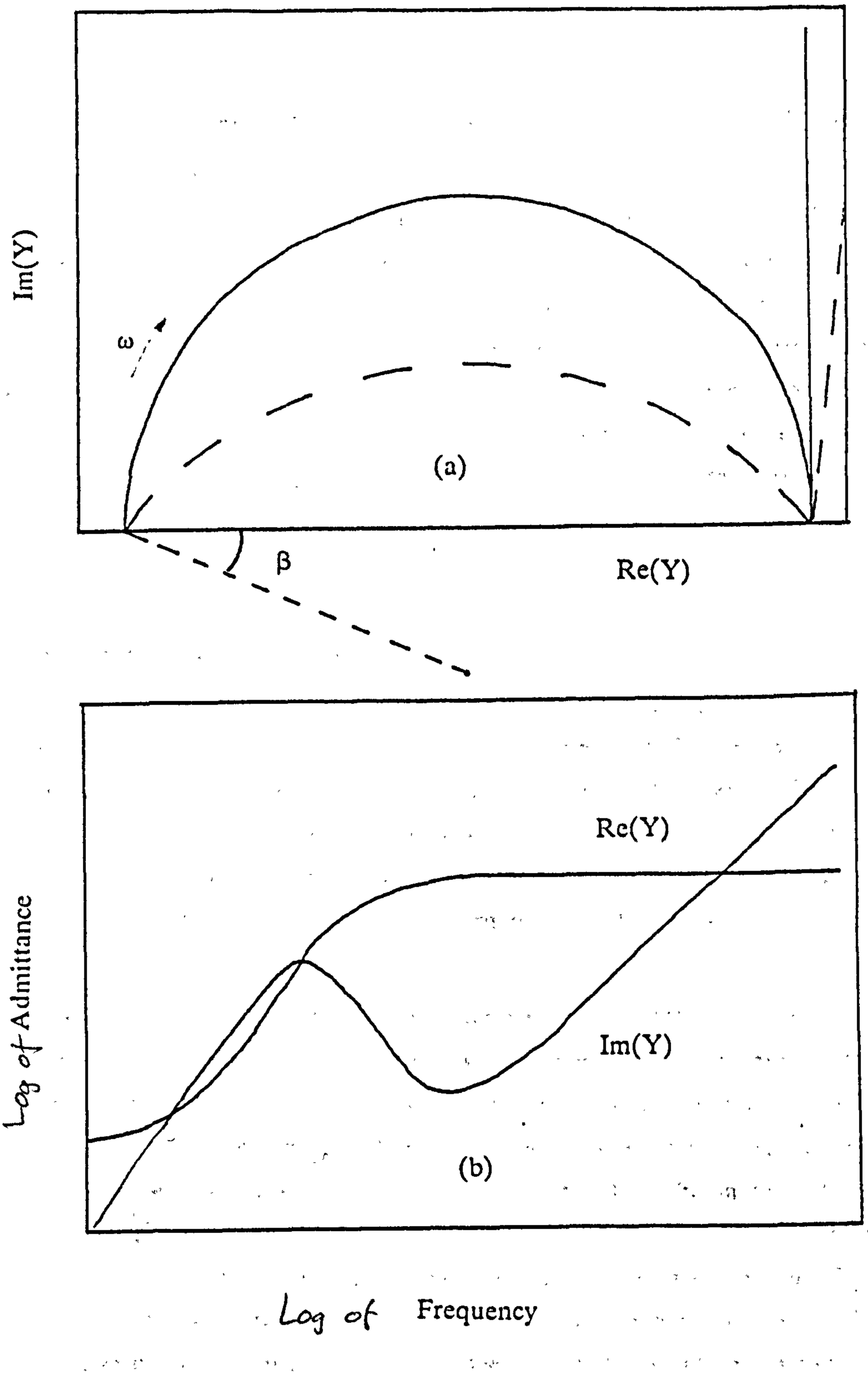

Fig 5.13 (a) Complex admittance curve for circuit of figure 5.12
(b) Real and imaginary parts of admittance for figure 5.12

of the asymmetry of the samples, the absolute conductivity could not be calculated accurately from the conductance.

. The extraction of the parameters of a single interface form the overall AC response was made easier by using a three-electrode configuration of the testing circuit. For this, the bulk conductance had to be sufficiently high that its contribution to the measured impedance was negligible. In practice this was only true below a certain frequency. If this could be assumed, the equivalent circuit which would be appropriate is that of figure 5.14, and if the interface was completely blocking, the response should have been that of a capacitor alone. Results of these measurements were presented in terms of capacitance, defined as $C = Im(Y)/\omega$, vs frequency. This gave a different value from C_{ac} because of the depression of the arc.

5.7.2. Constant-Current Measurements

The aim of galvanostatic experiments was to measure the change of potential difference between the electrode and the electrolyte as charge passed through the system. The potential drop due to the resistance of the bulk, as for AC, was an impediment to this and it was minimised by using a sufficiently high temperature for all measurements. In practice the temperature was kept between 370° and 380°C, at which G_b was typically 10^{-4} S. At significantly higher temperature, the glass would have softened.

Before each galvanostatic measurement, the sample was brought to a state where its voltage and temperature were steady, or at least not changing significantly on the time scale of the experiment. The current was then switched on and the voltage measured as a function of time. The highest voltage which was reached was 5 V, but such a high voltage usually led to irreversible effects, in the sense that the same response could not be obtained from the same contact, no matter what further treatment it received. If repeatability was required, a lower voltage range was chosen. The currents which were employed were varied over as wide a range as possible. The upper limit was determined in some cases by the speed of response of the measuring system and in others by the effects of the bulk resistance. The highest current was such that the voltage rose over the whole range within about 3 s. The lowest current was that for which the voltage range was covered in about 30 minutes. Measurements at longer times were unreliable because of voltage drifts due to effects other than the applied current.

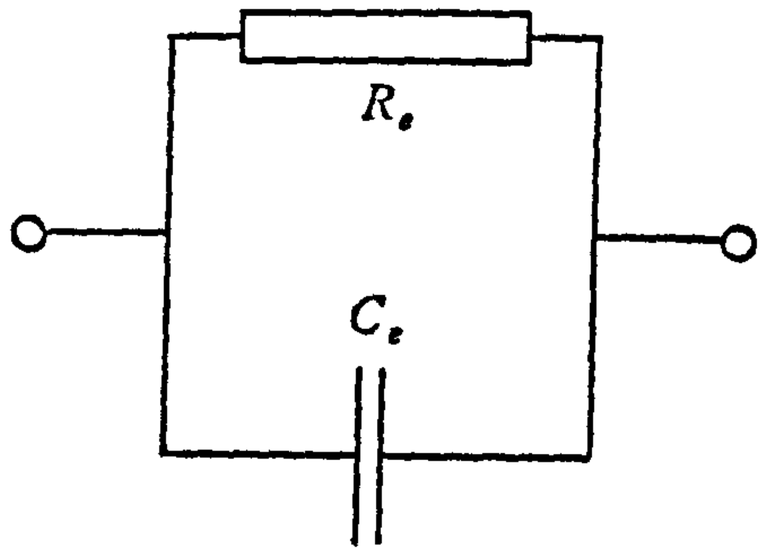

Fig 5.14 Equivalent circuit for interpretation of three-electrode measurements.

A voltage curve for an ideal capacitor subjected to a constant current is shown as curve (a) in figure 5.15. It is a straight line which goes through the origin, and when the current is switched off the voltage stays at a constant value. In fact, a typical galvanostatic response of a real sample was curve (b), showing an apparent decrease in capacitance as the voltage increases, and a falling voltage after the current has been switched off. The shape of the curves were usually different in the anodic (positive current from the electrode to the electrolyte) and cathodic directions. Since the reaction between the metal and the glass was of primary interest, anodic current was used more often than cathodic, since the former was expected to promote oxidation of the metal while sodium accumulation was the more likely outcome of the latter.

Repeatability of the curves was checked using a galvanostatic run where the current was periodically reversed in the way illustrated in figure 5.16, ie applying a square current wave, and comparing the shape and size of the voltage curves of each phase.

When it was required to do several runs on the same electrode, but at different currents, it was necessary not only to use a voltage range where the response was repeatable, but also to bring the interface back to the same steady state after each run. In practice, this was only attempted for anodic runs, and it was achieved by passing an equivalent charge in the cathodic direction after each run and then waiting until the voltage was changing at a rate negligibly slow on the time scale of the experiment. This procedure was arrived at empirically, and was evidently imperfect, because the starting voltage at each run was never exactly the same, varying across a range of a few tens of millivolts, and the rate of change of voltage at each start, although very small, also varied. Precise control of the interface conditions would have required complete knowledge of the surface processes beforehand.

An alternative form of presentation of the data to that of figure 5.15 is as a differential capacitance C_d. This is calculated by the computer through numerical differentiation of the voltage with respect to time. For this the voltage curve over a certain range is fitted to the nearest straight line by the least squares fit formula:

$$Slope = \frac{\Sigma t_i V_i - \frac{1}{N}\Sigma t_i \Sigma V_i}{\Sigma t^2 - \frac{1}{N}(\Sigma t_i)^2} \qquad 5.15$$

where N is the total number of points in the range, and t_i and V_i are the time and

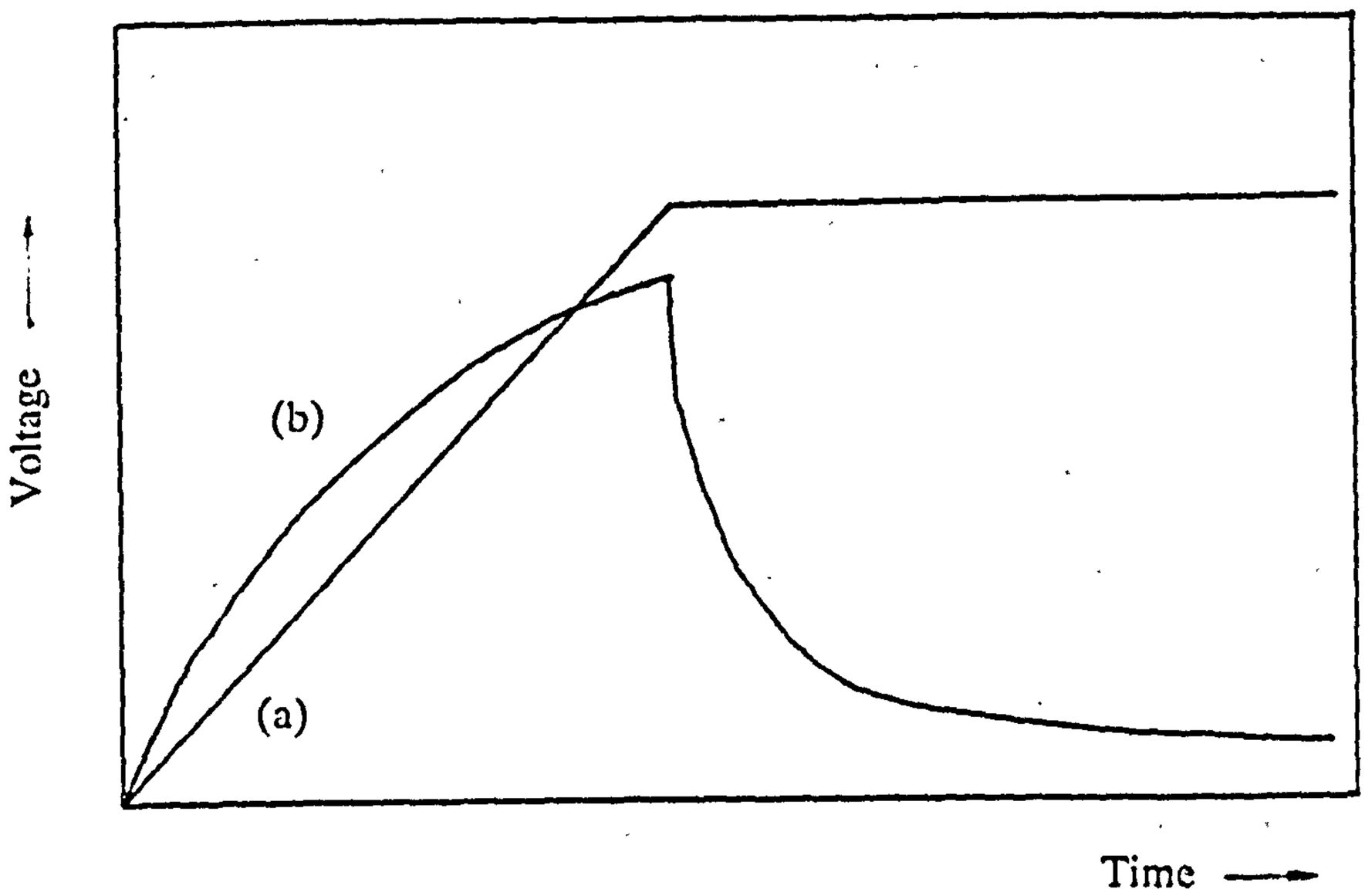

Fig 5.15 Anodic galvanostatic curves

(a) an ideal capacitor

(b) a typical aluminium-contact sample.

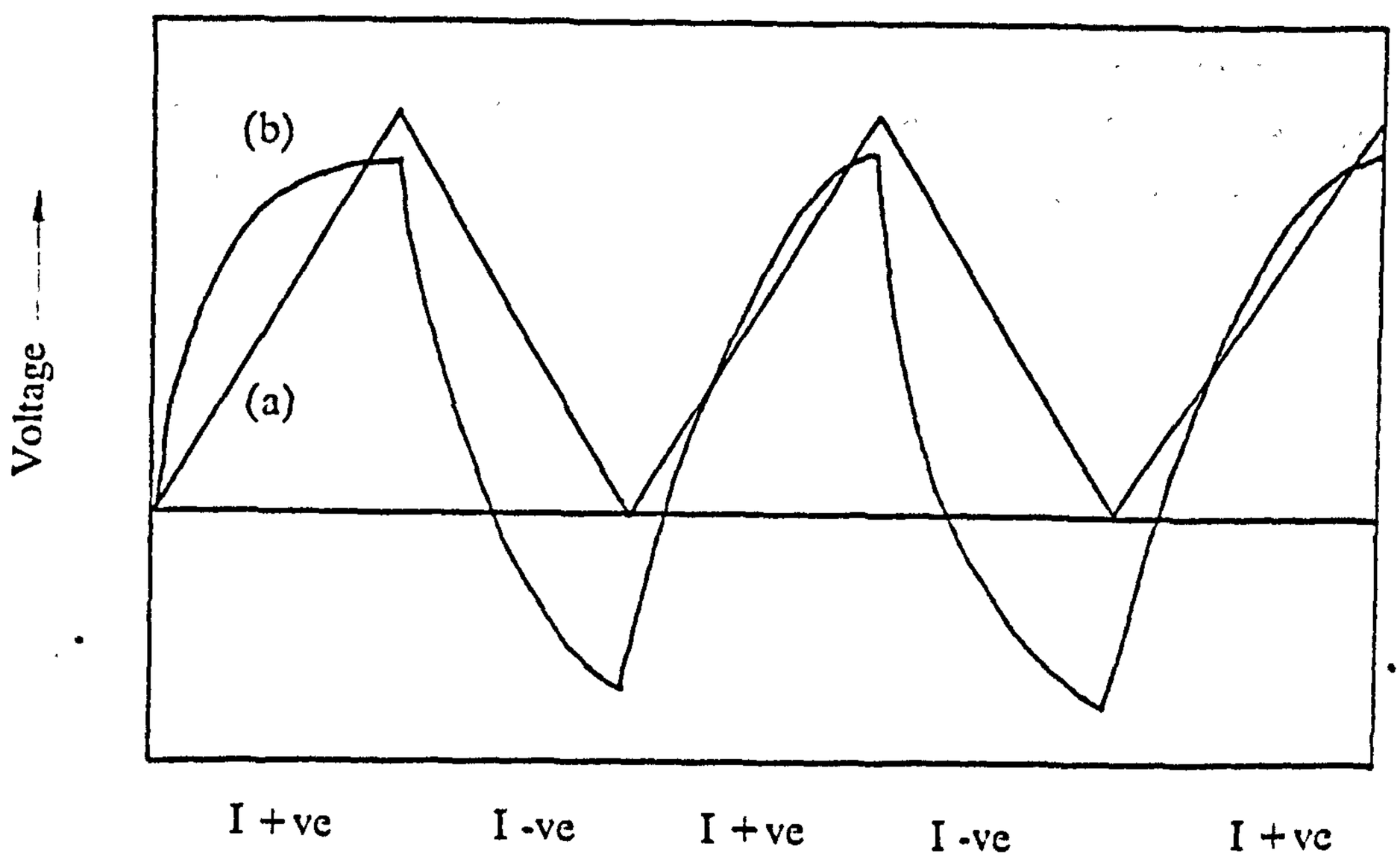

Fig 5.16 Result of alternating direction of current for examples of figure 5.15.

voltage, respectively, at the i^{th} point. The capacitance in the centre of the range is then:

$$C_d = \frac{I}{Slope} \qquad 5.16$$

In general, the voltage interval between points at which the capacitance was calculated was less than the range over which they were calculated. The log of C_d for the data of figure 5.15 is shown in figure 5.17.

In order to compare the effects of different currents, an "equal-charge" plot was used so that different curves could be drawn on the same axes. The voltage was plotted with charge passed as the ordinate, instead of time. The form of this is shown in figure 5.18.

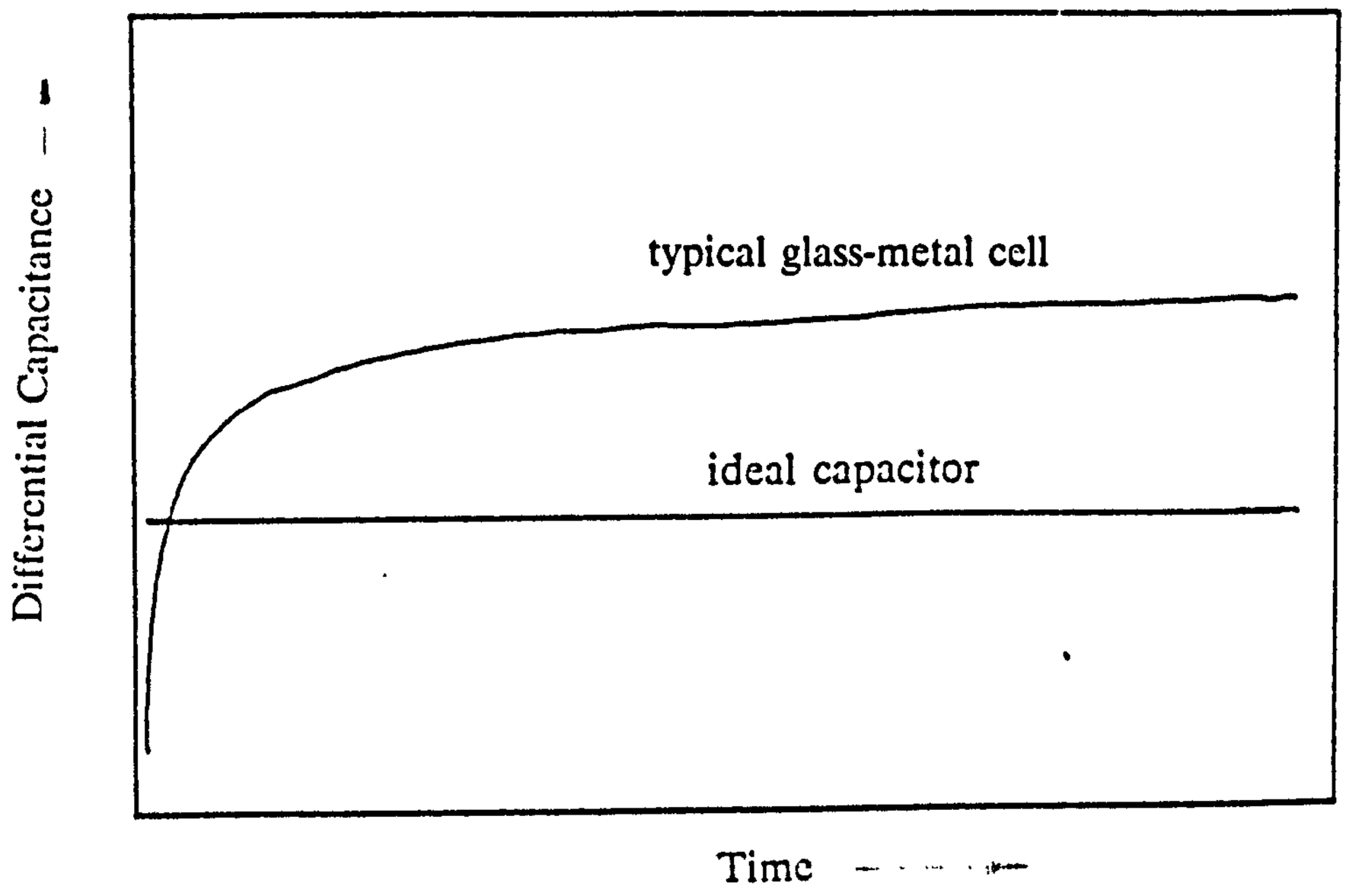

Fig 5.17 Differential capacitance of ideal capacitor and typical sample.

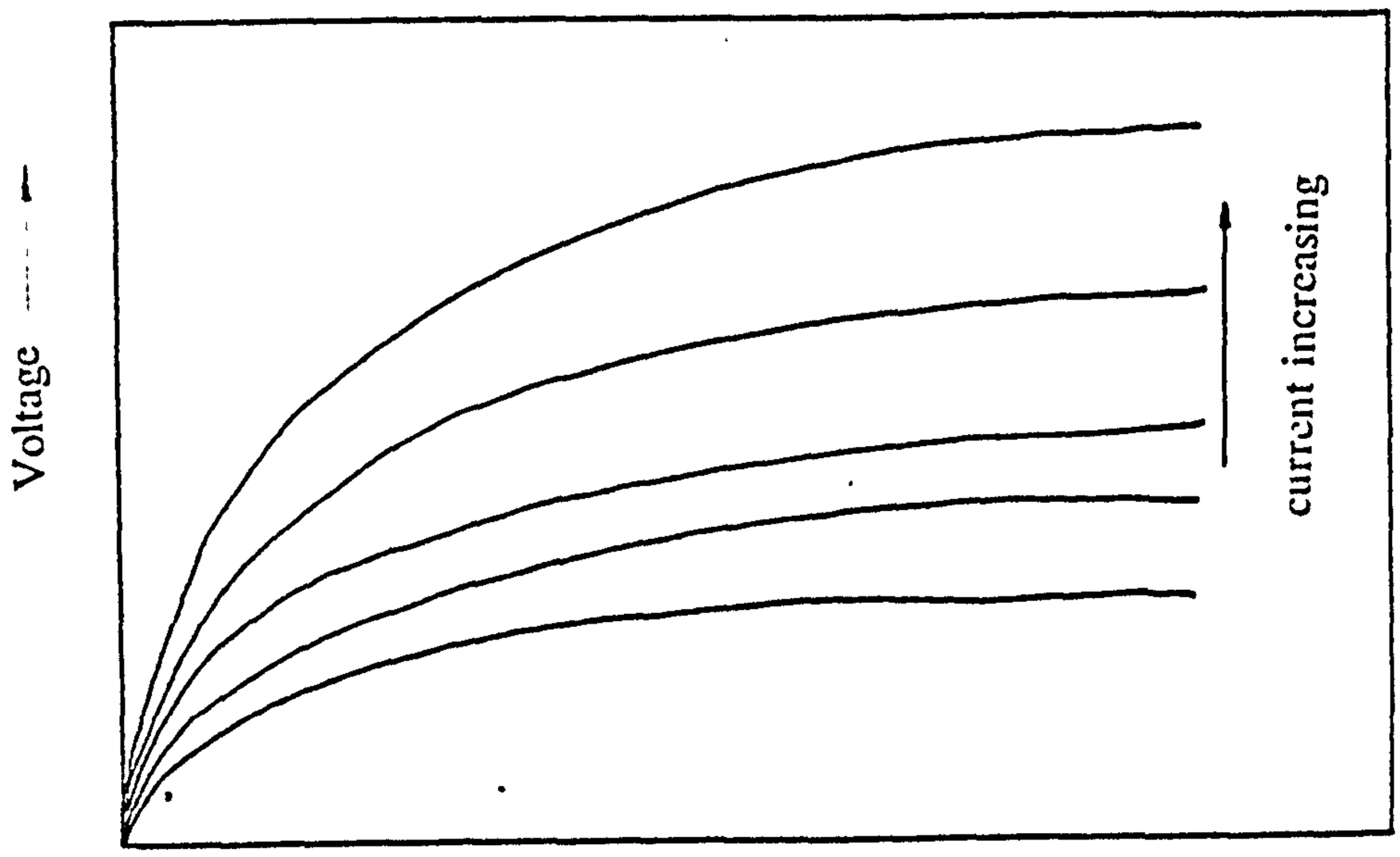

Fig 5.18 Equal charge plot for typical sample (aluminium contacts) at various currents.

REFERENCES

1. Doi A and Day DE, J App Phys **52,** 338-343 (1981).

2. Hauck CT, Wold A and Banks E, Inorganic Syntheses **12,** (ed RW Parry) 153-158 (1970).

CHAPTER 6

RESULTS AND DISCUSSION

6.1. Introduction

The procedures described in chapter 5 were applied systematically to the samples listed in Table 6.1. As far as was appropriate, the same experiments were carried out under the same conditions for each type of sample, but there were some exceptions. For example, the variation of the bulk conductance with temperature, since it was not expected to be sensitive to the electrode type, was only measured using one sample, which had aluminium contacts. These required two-electrode connections, but all the other measurements involved the three-electrode circuit.

In the following sections, the results for samples of different electrode types are described separately. The important features are compared in section 6.8, and the possible reaction mechanisms responsible for the observed behaviour of the different systems are discussed in sections 6.8 and 6.9.

6.2. Sodium Metal

Since sodium provides a formally reversible electrode with glass through the reaction:

$$Na_{(metal)} \rightleftharpoons Na^{+}_{(glass)} + e^{-} , \qquad 6.1$$

the response of the sodium metal-glass system was of interest as a point of comparison with that of other metal contacts.

The AC response of the sodium-connected glass sample was measured at a temperature of 86°C. The real part of the analyser reading is shown in figure 6.1. At low frequency this corresponds to the real part of the admittance. This is the flat part of the curve, and it is evident that there is no fall-off of the real part at low frequency. It

Table 6.1

Experiments Conducted on Different Samples

Contact Material	Type	Measurements Made
Sodium	Na	AC only, low temperature
Aluminium	1,3	AC: temperature dependence of G_b ; high temperature frequency dependence of admittance; Galvanostatic.
Copper	3	AC: 380°C low-frequency admittance; Galvanostatic.
Silver		As for copper
Tungsten Trioxide disc		AC only: attempt to find bulk conductance
" " cell		AC only: attempt to establish good contact
Sodium tungsten bronze		As for copper and silver

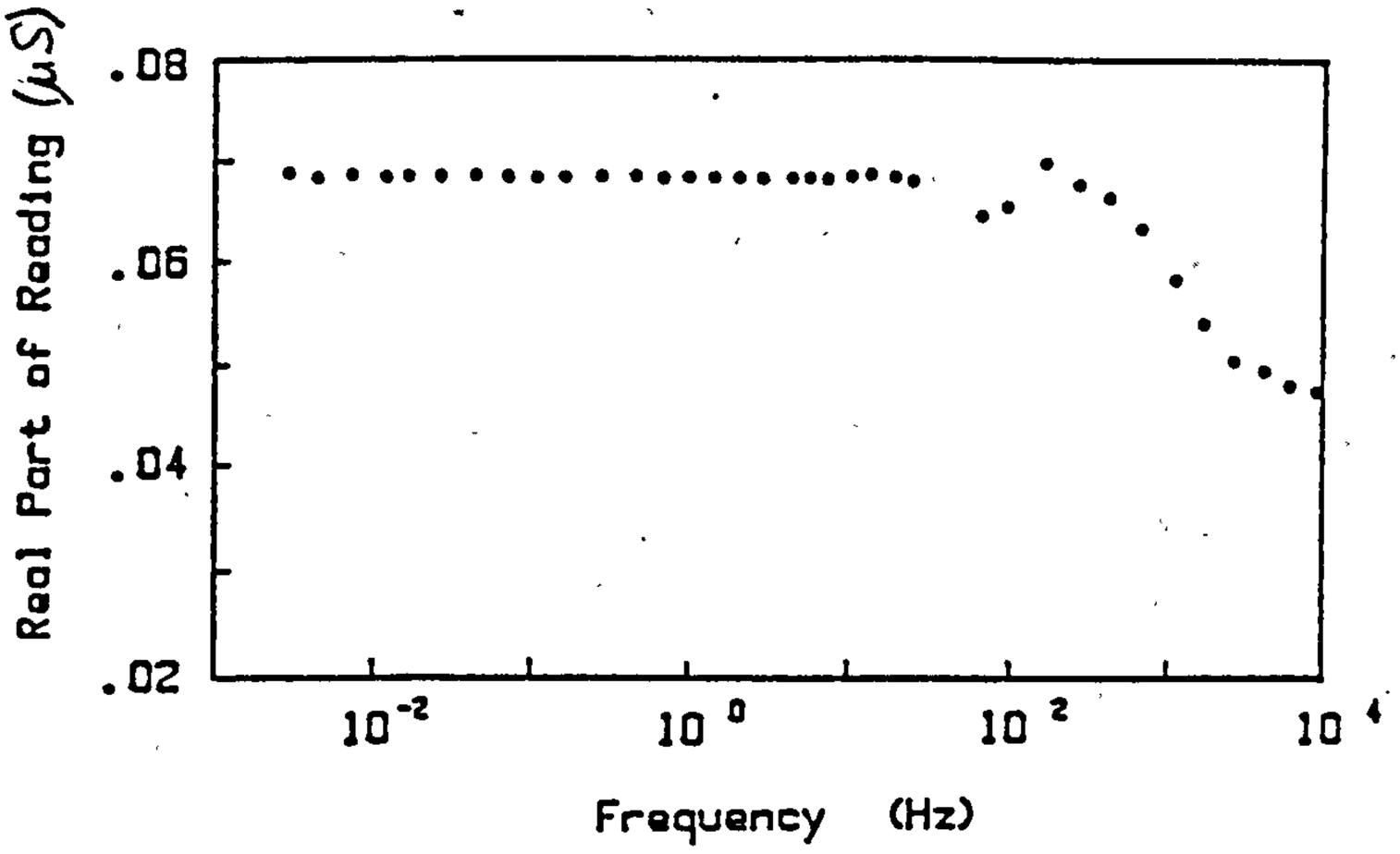

Fig 6.1 Real part of admittance of cell with sodium contacts.

may therefore be concluded that the interface allows charge to pass freely between the electrode and the glass with no appreciable charge storage at the interface, which would have introduced a series reactance. This is probably because the rate of sodium exchange is sufficiently fast that any significant excess or deficiency of ion concentration is avoided.

The only other possible explanation is that charge transfer via the above reaction is not significant, but the bulk resistance and the interface capacitance are so large that insufficient current flows to polarise the interface. Since the bulk resistance was 13.7 MΩ, then, if the resolution of the impedance measurement is 1%, the capacitive reactance must have been less than about 0.2 MΩ. At 2.5 mHz, this implies a capacitance of more than 600 μF on each side. This compares with values of no more than about 25 μF for any of the evaporated contacts, after allowing for different contact area. Measurements were taken very close to the melting point of sodium, when it was very soft, and so it was possible that it made as good a contact as those applied from the vapour phase, but such a large difference in capacitance seems unlikely to arise from the geometry alone.

The shape of the curve at high frequency is affected by the capacitance and conductance of the measuring circuit and so the fall-off in the real part does not reflect the behaviour of the cell.

6.3. Aluminium

6.3.1. AC Data

Figure 6.2 (a) shows the real and imaginary parts of the admittance of an aluminium top-contact, silver bottom-contact sample of type 1. This response may be described with reference to the simple approximate equivalent circuit of figure 5.14. The extent of the plateau region of the real-part curve, where the response is dominated by the bulk resistance, indicates that the capacitance in parallel with the bulk, C_b, was very much less than that of the interface, C_{ac}. The high-frequency part of the imaginary-part curve gives a value of C_b of about 0.1 pF. Thus, when measuring the interface parameters, the bulk capacitance could be neglected. The bulk conductance and a value of capacitance for the interface were found from the complex admittance plot, which is shown in figure 6.2 (b). In this case they were 122 μS and 0.2 μF respectively. At the low-frequency (left-hand) end the complex admittance curve goes

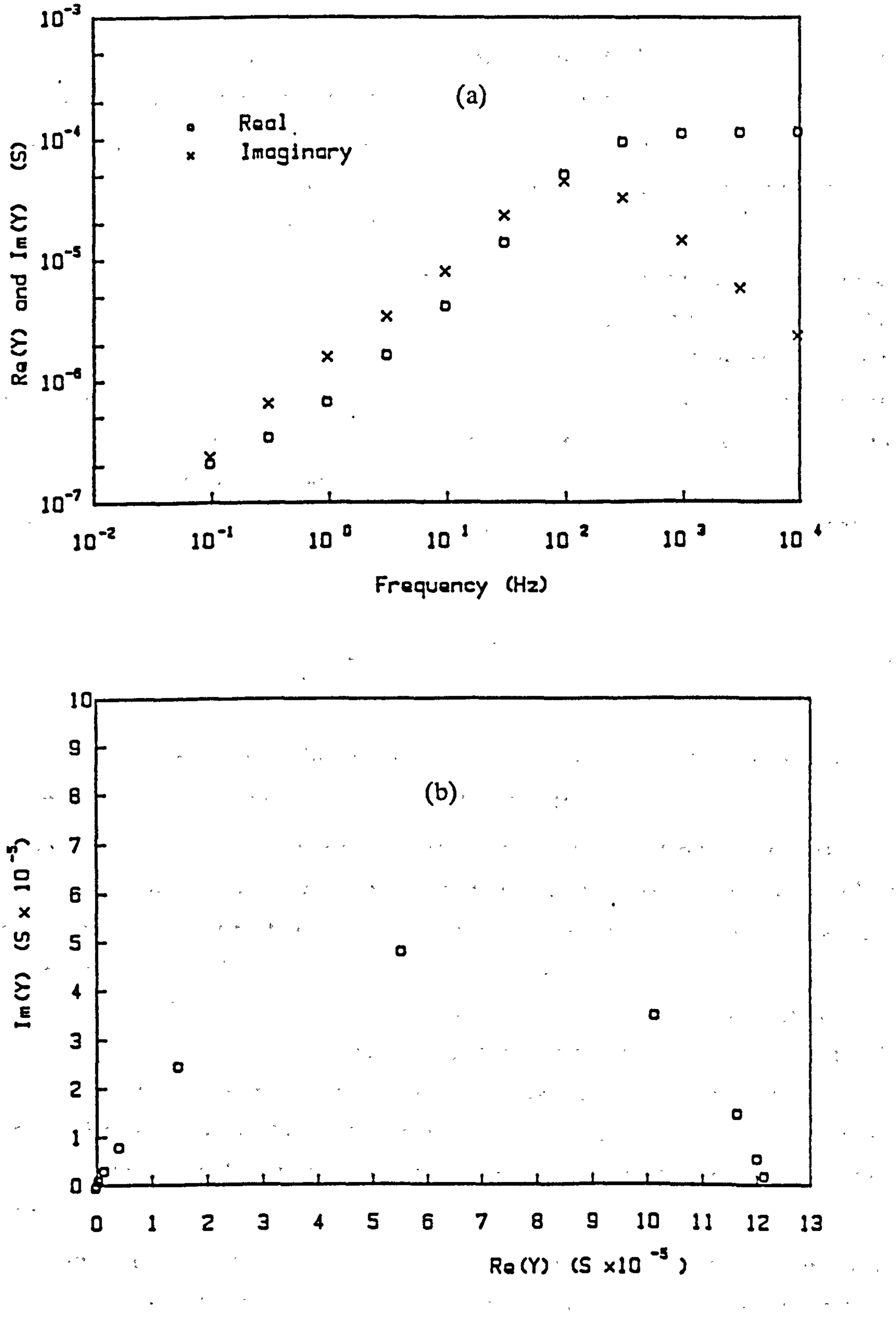

Fig 6.2 AC data of two electrode cell with aluminium contacts:

(a) Real part of admittance vs frequency.

(b) Complex admittance.

through the origin, indicating zero dc conductance through the interface. A charge transfer process under conditions of zero bias was thus clearly absent.

On this sample, AC measurements were made at temperatures between 100° and 329°C. Figure 6.3 is a plot of the variation of conductance with temperature It exhibits the Arrhenius law as expected, with an activation energy of 0.8 eV.

Figure 6.4 (a) is the complex-admittance curve for a three-electrode sample of type 3, which exhibits the same depressed arc going through the origin, giving a value of C_{ac} of 1 μF. It is clear that the equivalent circuit of figure 5.14, which represents the interface as a simple RC parallel combination, does not apply precisely, because the complex admittance plot is not an exact semicircle. The depression of the arc below the real axis may be described in terms of the angle β in figure 5.13. As described in chapters 3 and 4, the frequency dependence of the admittance, Y, may be related to β through the equation [1]:

$$Y = Y_o + \frac{(Y_x - Y_o)(j\omega\tau_o)^{1-\beta}}{1 + (j\omega\tau_o)^{1-\beta}} . \qquad 6.2$$

Both the real and imaginary parts of this expression vary as $\omega^{1-\beta}$ For this reason the phenomenon is known as "fractional power frequency dependence".

Figure 6.4 (b) shows the interface capacitance of the same sample as was used for (a). The capacitance graph allows the relationship of equation 6.2 to be tested at lower frequency: if the equation is valid the slope of the log capacitance vs log time should be equal to β. The data confirm this; the angle of depression of the complex admittance arc is 13° and the slope of the capacitance curve, when converted from radians to degrees, is 14°. The variety of physical interpretations of equation 6.2, reviewed in chapter 3, are such that no firm conclusion may be drawn from these data concerning the behaviour of the mobile charged species near the interface. Table 6.1 shows that β varied with temperature, in general becoming smaller as temperature increased.

The absence of a high-frequency spike in the complex admittance plot of figure 6.4 (a) was due to the limitations of the measuring system, since the sample was in parallel with the analyser which has an internal capacitance of 103 pF, and so was unable to resolve the small bulk capacitance of the sample.

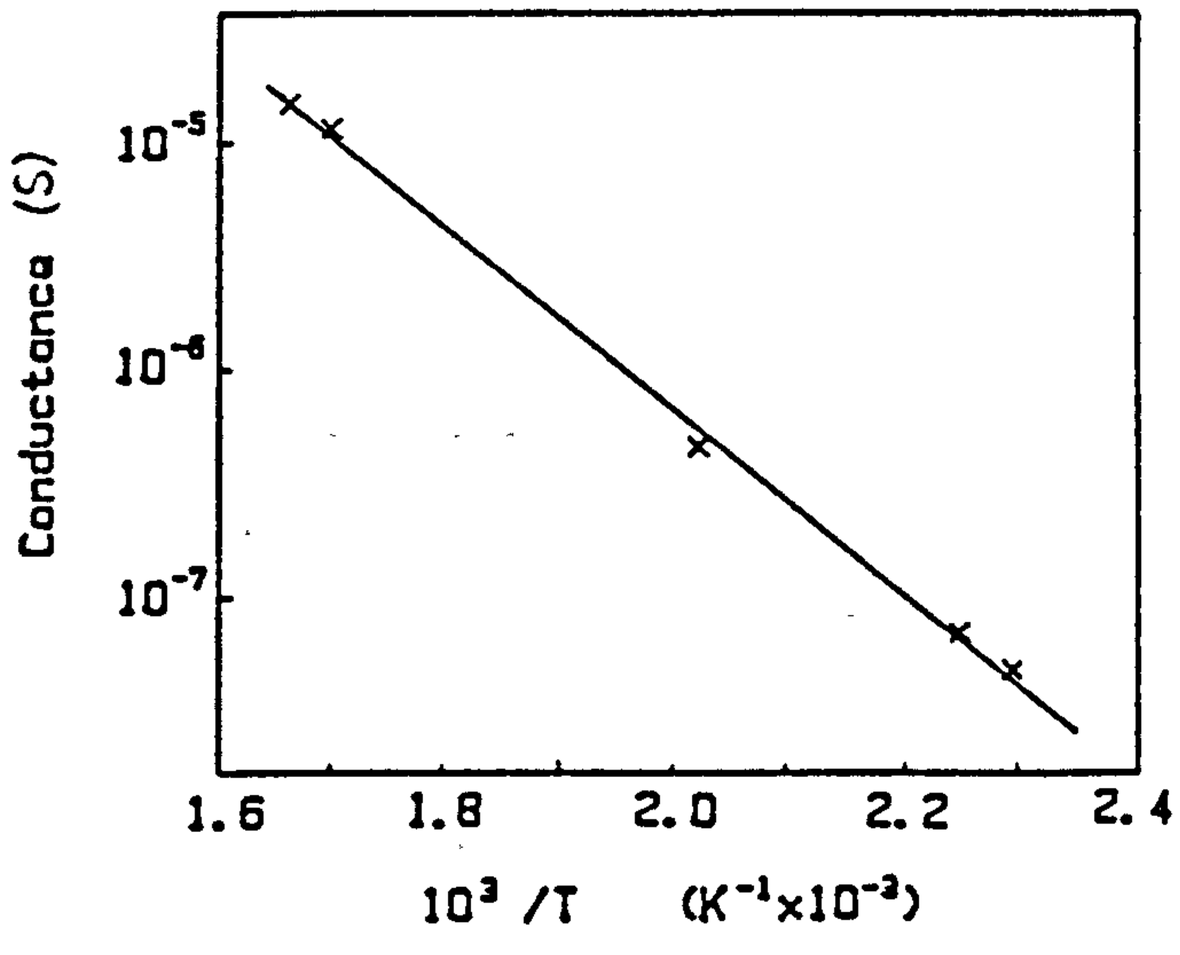

Fig 6.3 Arrhenius plot of conductance of glass with aluminium contacts.

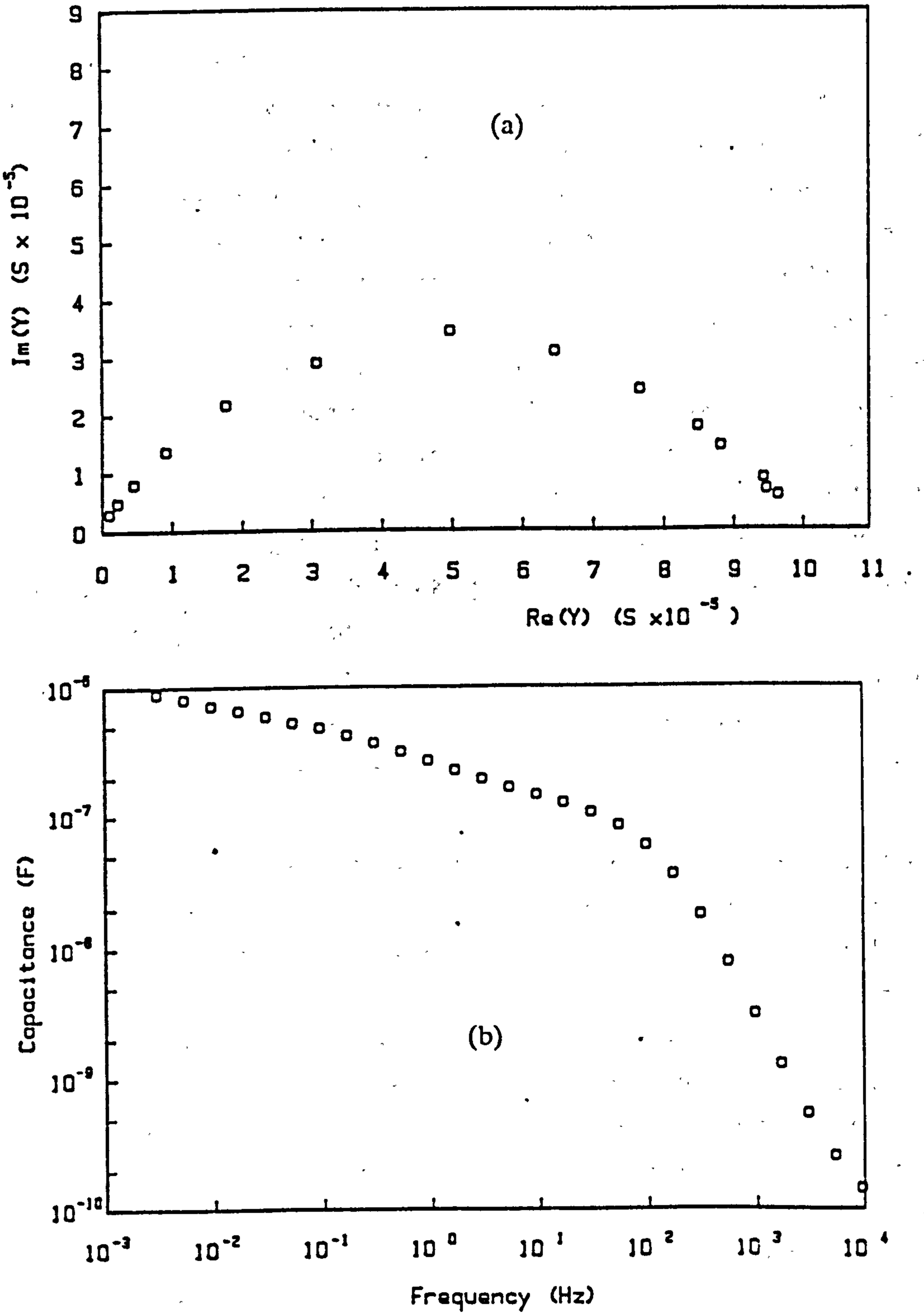

Fig 6.4. (a) Complex admittance of three-electrode aluminium cell.
(b) Log capacitance of the aluminium-glass interface versus frequency.

6.3.2. Galvanostatic Data

The response of the working electrode of an aluminium three-electrode cell of type 3, on application of a constant current of 0.1 μA, is shown in figure 6.5 (a). The general features of this curve, comprising a sharp initial rise and a shoulder followed by a convex curve of lower and more slowly-varying slope, are typical of the anodic response of aluminium contacts. The voltage initially rose relatively quickly, with the slope reducing above 1 V. The slope then settled to a roughly constant value between 1.7 and 4 V. Before the current was switched off, at just over 4 V, the slope reduced slightly. The total charge passed was 27 μC. The final voltage was high in electrochemical terms, since any charge-transfer processes are expected to occur within an overall interface voltage range of two or three volts. Since the potential of the reference electrode hardly changed throughout, it was clear that in this case nearly all of the potential developed between the working and the counter-electrodes was dropped between the working electrode and the glass.

Figure 6.5 (b) shows the differential capacitance versus time, which also has high and low slope sections. From about 1 μF, which was the same as C_{ac} for this sample, C_d rises to about 10 μF. It then approximately levels out, suggesting a constant rate of charge storage at the interface.

Figure 6.6 (a) shows the results of applying a periodically reversing current of 0.1 μA for 10 s each way. Previous to this measurement, only small charges had been passed in either direction, and the system had been allowed to settle for long enough for the voltage to level out. The first phase was anodic, and so the voltage curve was similar to that of figure 6.5 (a). The next anodic phase was markedly different from the first, but all following anodic phases were then identical to the second, indicating that the response was repeatable under these circumstances. This was demonstrated more clearly by superimposing the successive curves, as in figure 6.6 (b). The close similarity between these curves suggested that if there was an irreversible process involved, its effect on the development of potential was not significant. The contrast between the first anodic phase and the others indicated that charge was stored during the cathodic phase and had to be discharged before the "true" anodic response took over. Since sodium ions approach the electrode during the cathodic phase, it is clear that the stored charge consists of sodium ions, either building up in the vicinity of the interface or taking part in some partially reversible reaction there.

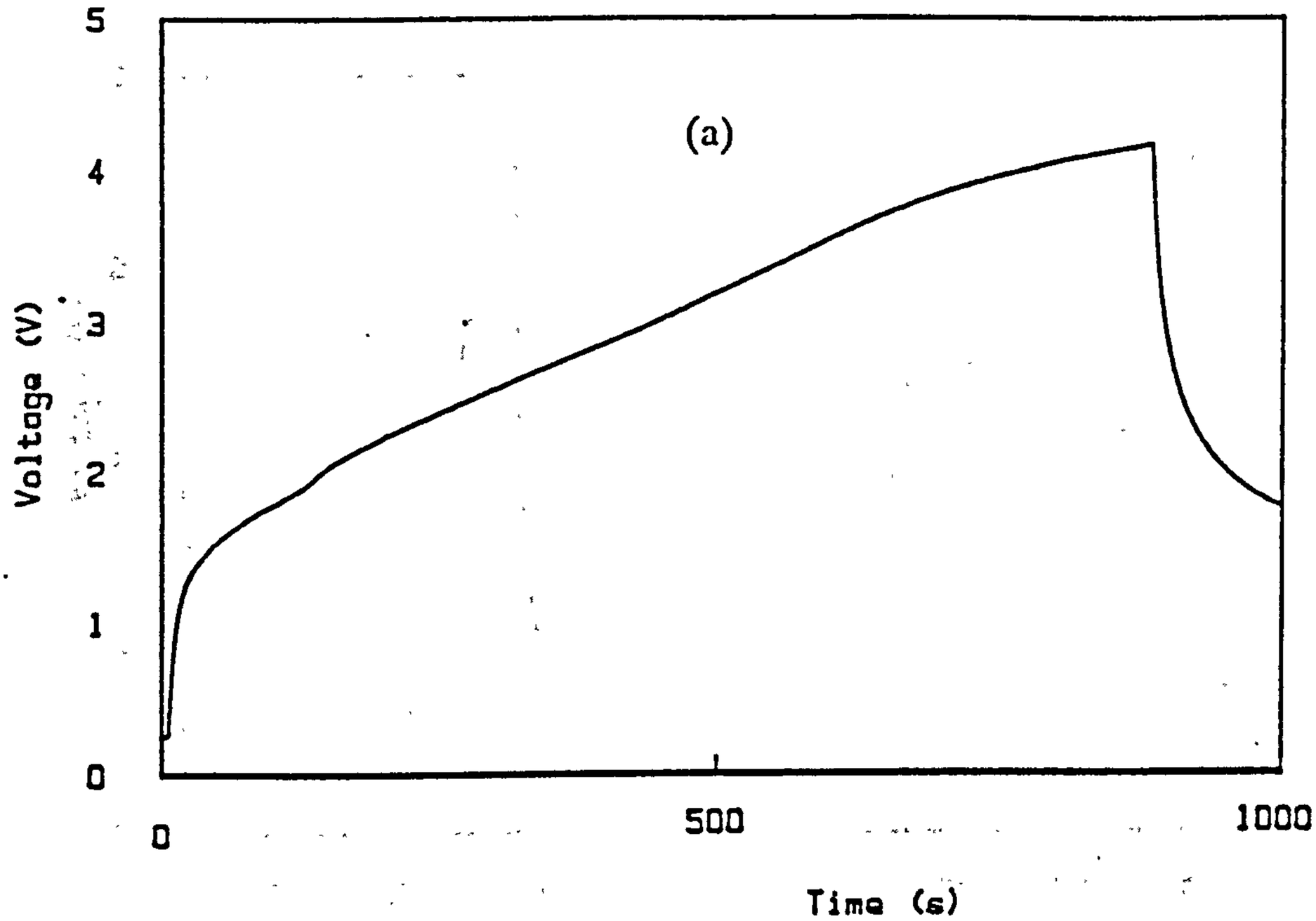

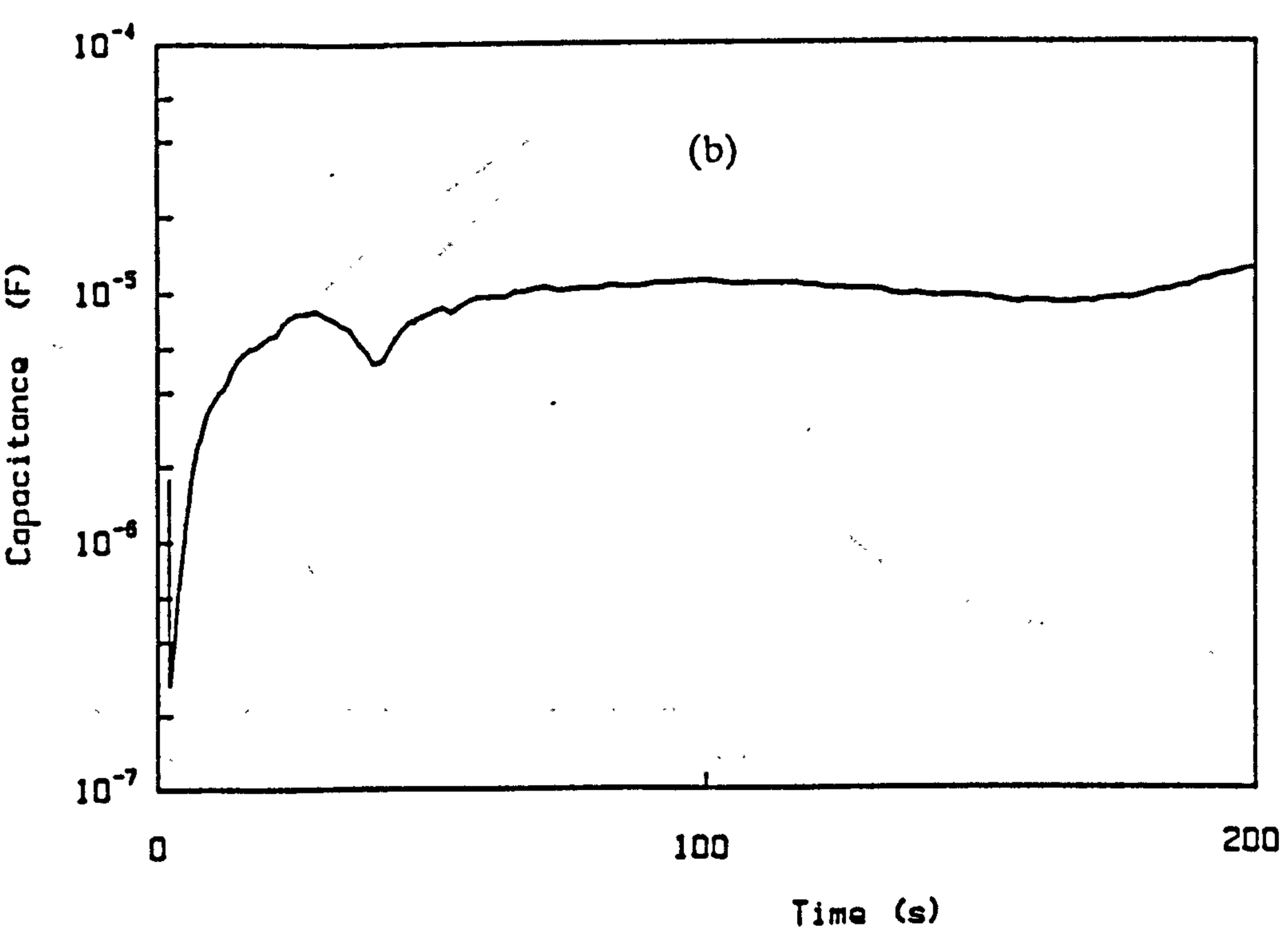

Fig 6.5 (a) Anode curve of aluminium curve.
(b) Differential capacitance of (a).

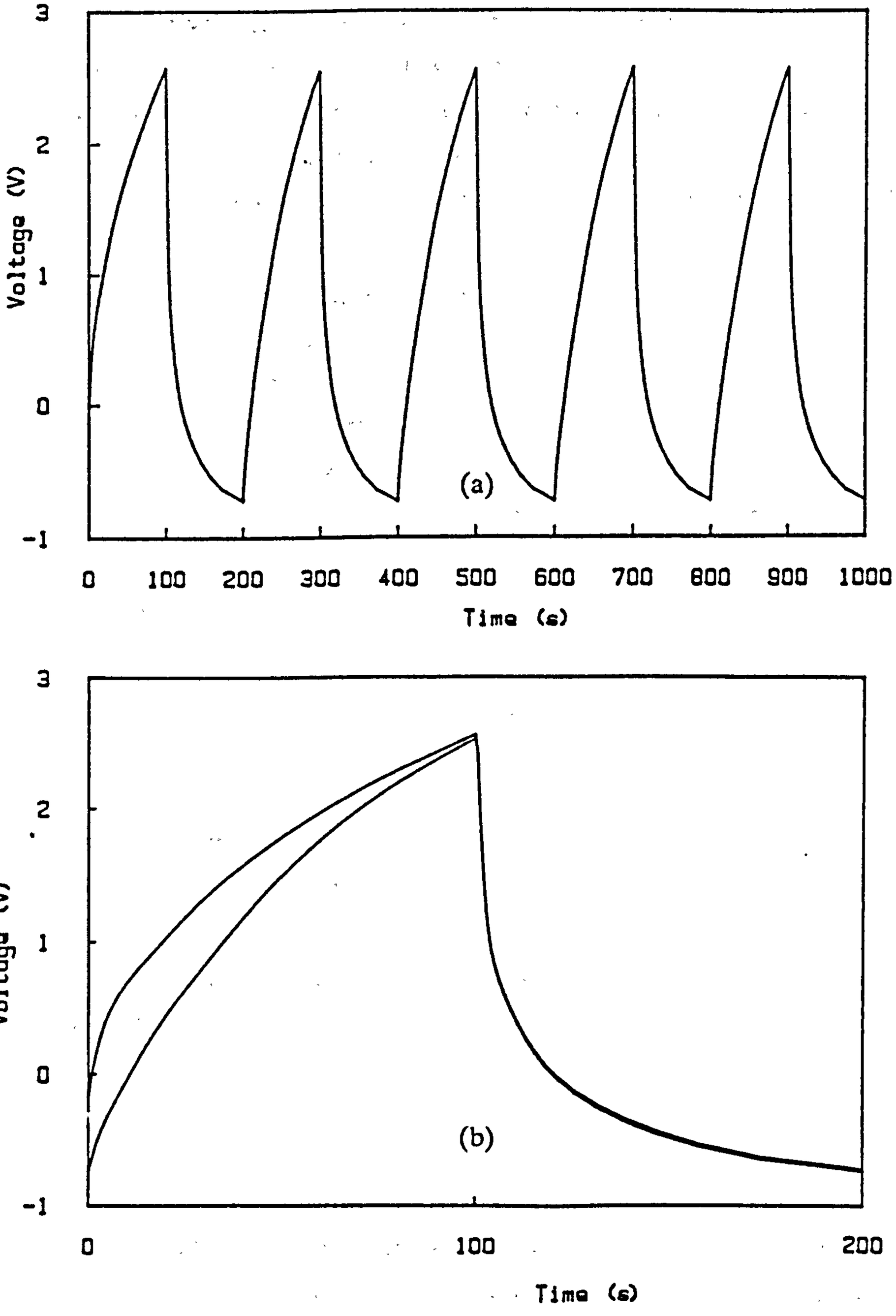

Fig 6.6 (a) Reversed current results of aluminium cell.
(b) Superimposition of cycles of (a).

The voltage-charge plot of a set of equal-charge runs within the range where the response was repeatable is shown in figure 6.7 (a). The charge in each case was 10 μC, and they were done in order of decreasing current. Between each run a cathodic charge of 10 μC was passed using 0.33 μA and the system was allowed to "rest" for about five minutes, which was long enough for the voltage to level out.

After about 1.5 μC had passed, the curves are almost parallel. Such behaviour suggested that the voltage across the interface was the sum of two effects: one was proportional to the accumulated charge which had passed, and the other was a function of the current flowing at the time. A similar set of curves was obtained for 1 μC,shown in figure 6.7 (b). The relationship between the final voltage and the current is demonstrated in figure 6.8, where the logarithm of the current is plotted against the voltage at the end of the curve. The straight line relationship obtained is identical to that of the Tafel law for a kinetically limited electrode charge transfer reaction relating the current, i_o, to the overvoltage, η:

$$i = i_o \left(1 - \exp\left(\frac{-\alpha z F \eta}{RT}\right)\right) \qquad 6.3$$

where z is the charge transferred to each ion in the reaction. The curves for both the 10 and 100 μC sets of data fit this equation with the parameter α having the value 0.16.

The dependence of the voltage on the charge may have been consistent with the equation

$$V = V^o + (RT/F) \log a_{Na} + \eta \qquad 6.4$$

which was derived for supported electrolytes, since the electroactive species in this case were the aluminium ions, and so the sodium may behave as a supporting electrolyte.

The actual electrochemical process responsible for charge transfer must have been either oxidation of the metal followed by migration of metal ions into the glass, or the migration of oxygen ions from the sodium-depleted region of the glass to the surface followed either by evolution of oxygen gas or by formation of an oxide layer.

Figure 6.9 (a) shows the data for figure 6.5 (a) continued to show the voltage after the current had been switched off. The rapid decay followed by a slow decrease

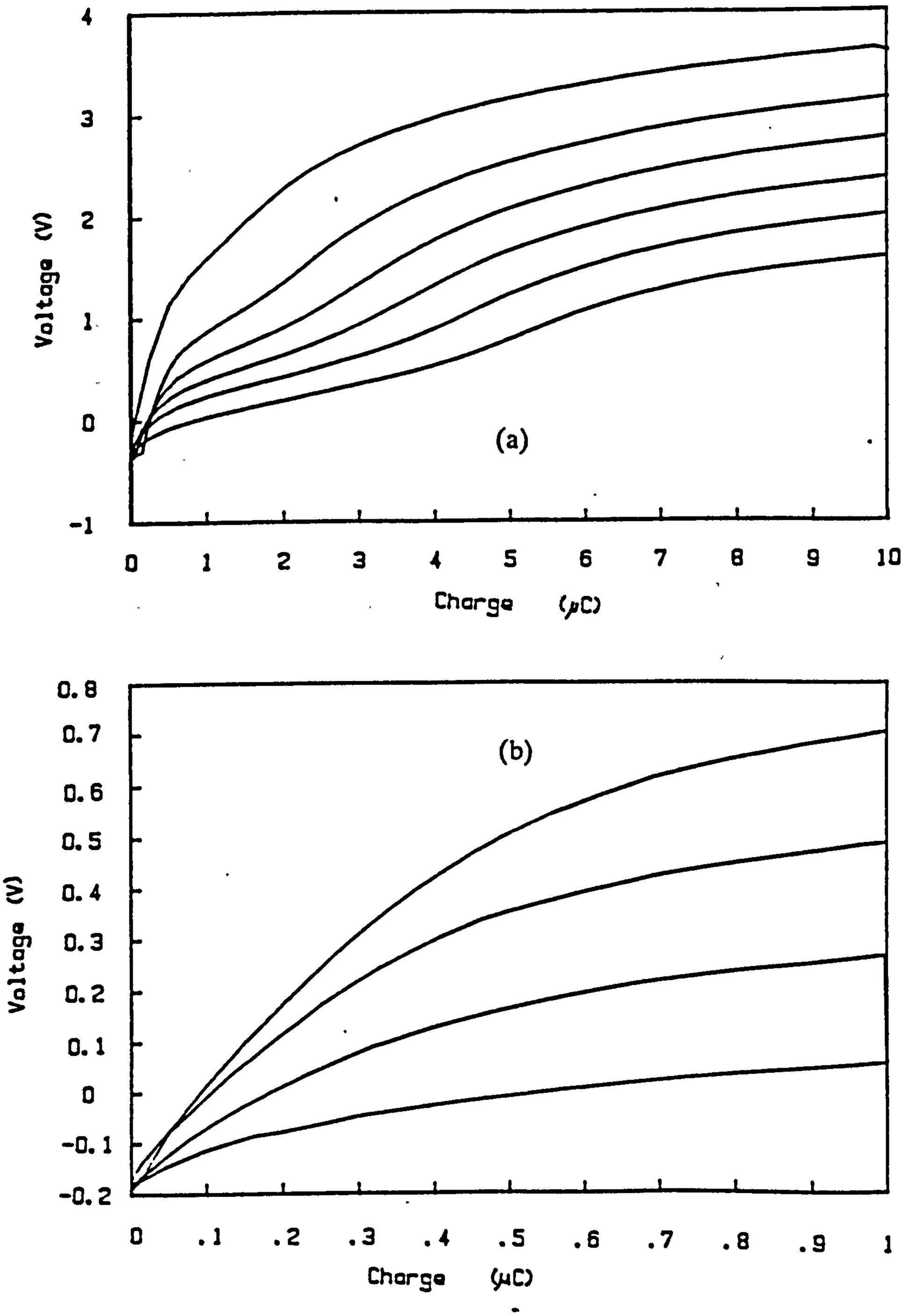

Fig 6.7 (a) 10 μC equal-charge plot of aluminium cell.
(b) 1 μC equal-charge plot of aluminium cell.

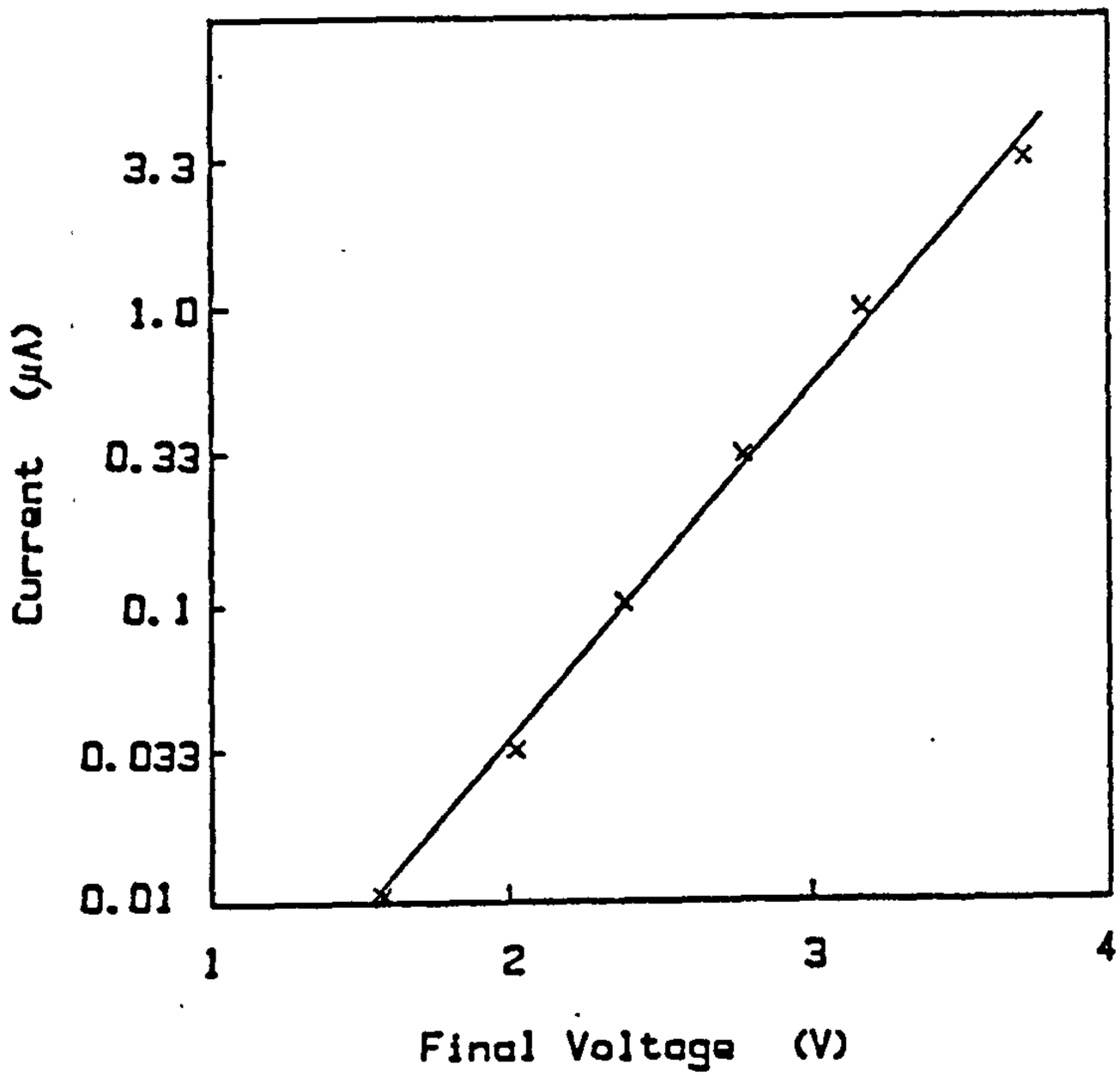

Fig 6.8 Tafel plot of 10 μC final voltages.

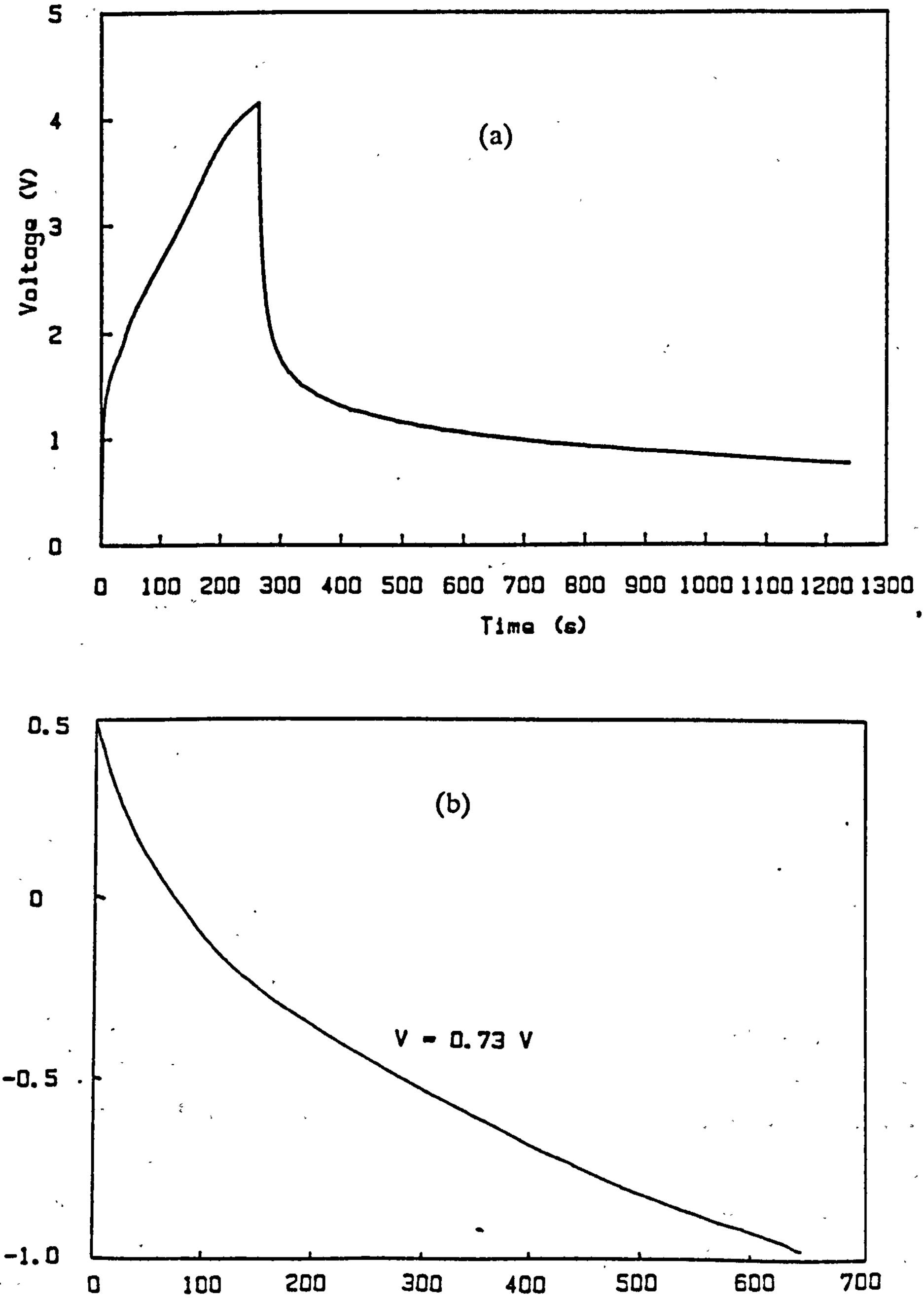

Fig 6.9 (a) Zero current voltage decay after run of figure 6.5 (a).
(b) Logarithmic plot of data of (a) showing non-exponential nature of decay.

over a long time is a characteristic which was shown by other aluminium contacts. Here the decay was recorded for 700s, but the voltage was still decreasing. It was not exponential, as is apparent from the graph of log voltage versus time, figure 6.9 (b), which was plotted assuming an eventual voltage (V_o) of 0.9 V. This curve suggests the presence of two processes: one was fast, causing the rapid initial decline, and the second caused a gradual change at a steady rate.

The passage of a larger quantity of charge led to the introduction of irreversible effects, as is shown in figure 6.10. In this case, 3 μA was applied and the curve was similar to (a) up to 3 V, but at the high-voltage end the slope of the curve increased. Comparison of the two was complicated by the lower starting voltage, 0.3 V, and the different total charge which passed before the working electrode potential was raised by 4 V, in this case 40 μC.

The voltage curve for a cathodic run is shown in figure 6.11. These started from different non-steady state voltages after an anodic charge of 10 μC had been passed at different currents. After the starting-point of the voltage had been passed, the development of potential in the cathodic direction had the same general form to the anodic equivalent, but the magnitude of the voltage rise after any given time was much less. Cathodic runs after a variety of other anodic runs followed almost identical curves, which suggests that the cathodic response was not strongly affected by the anodic reaction.

6.4. Copper

6.4.1. AC Data

The real and imaginary parts of the admittance of a copper contacted sample of type 3 is shown in figure 6.12 (a). The low-frequency features of these are similar to those of the equivalent graphs for aluminium. Figure 6.12 (b) is the complex admittance plot which is clearly not a simple arc of a circle as was found for aluminium. It is skewed, with the high-frequency side approximating a circular arc but the low frequency side being closer to a straight line. This is similar to the Warburg admittance, which is encountered in diffusive systems, such as liquid electrochemical cells where excess supporting electrolyte is present. Such behaviour may be possible in the present case if there is a second cation present, which could move diffusively if the field is screened by the sodium ions. Copper ions are the obvious candidates, but their

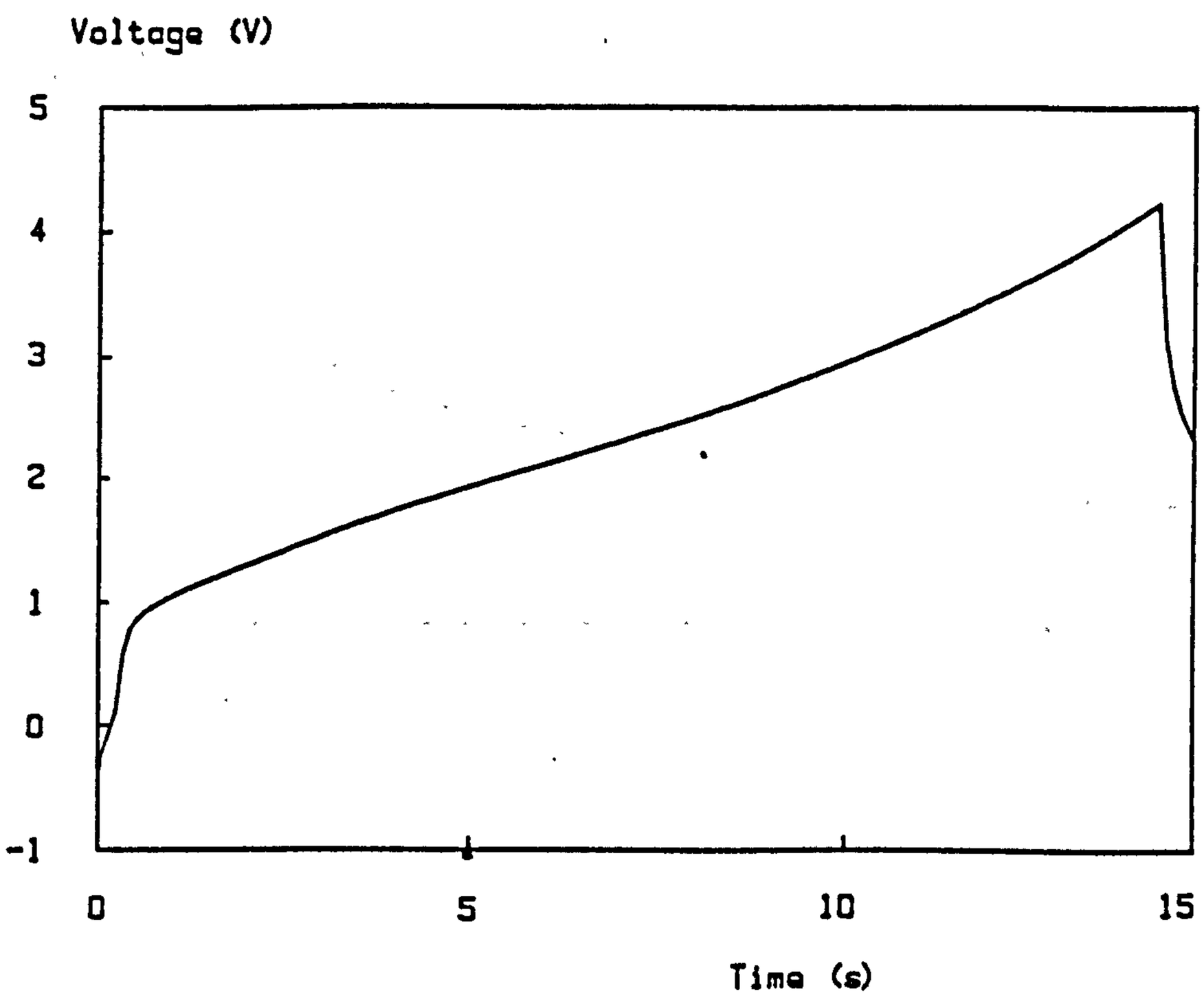

Fig 6.10 Anodic run for 15s with 3 μA.

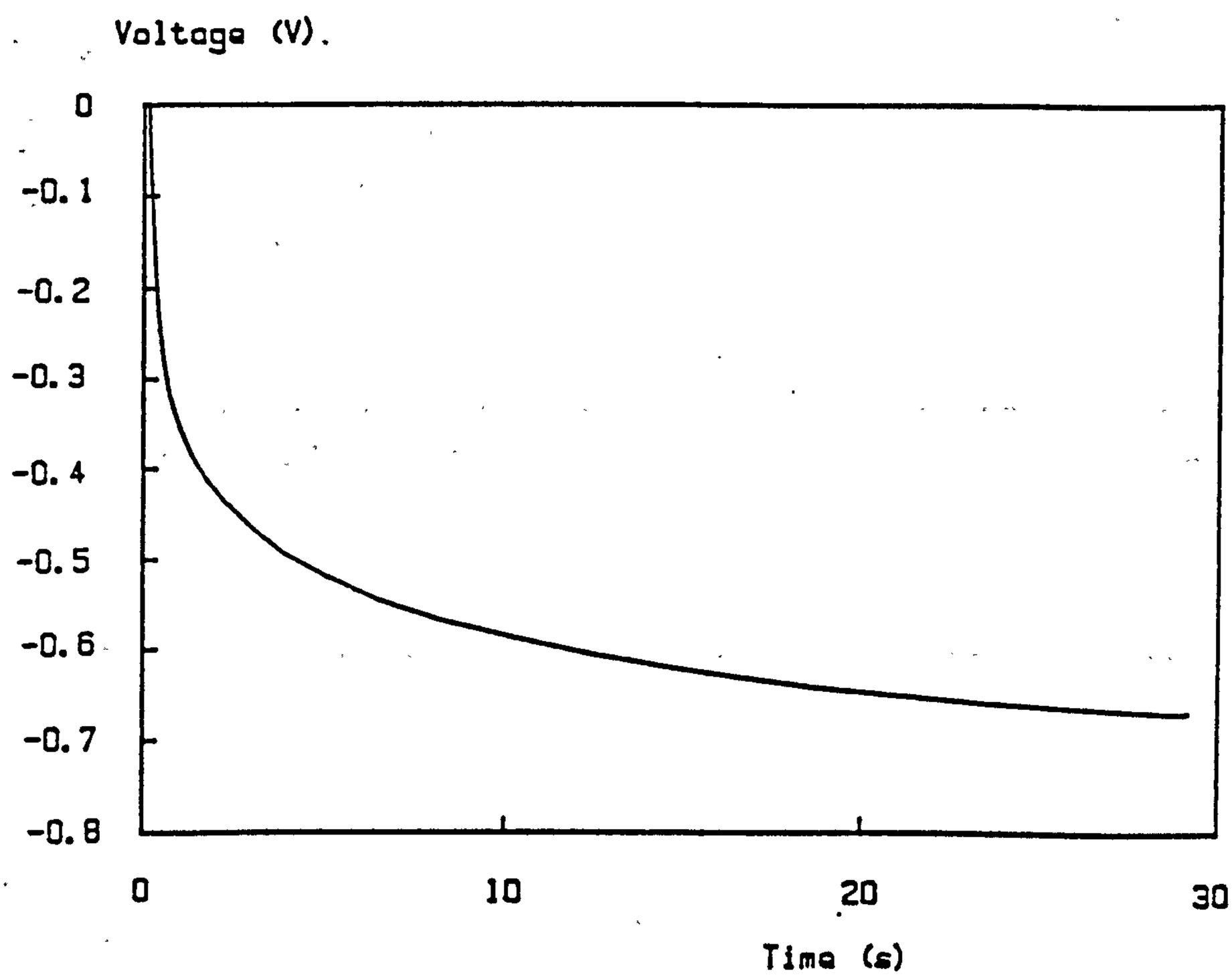

Fig 6.11 Cathodic run on aluminium sample.

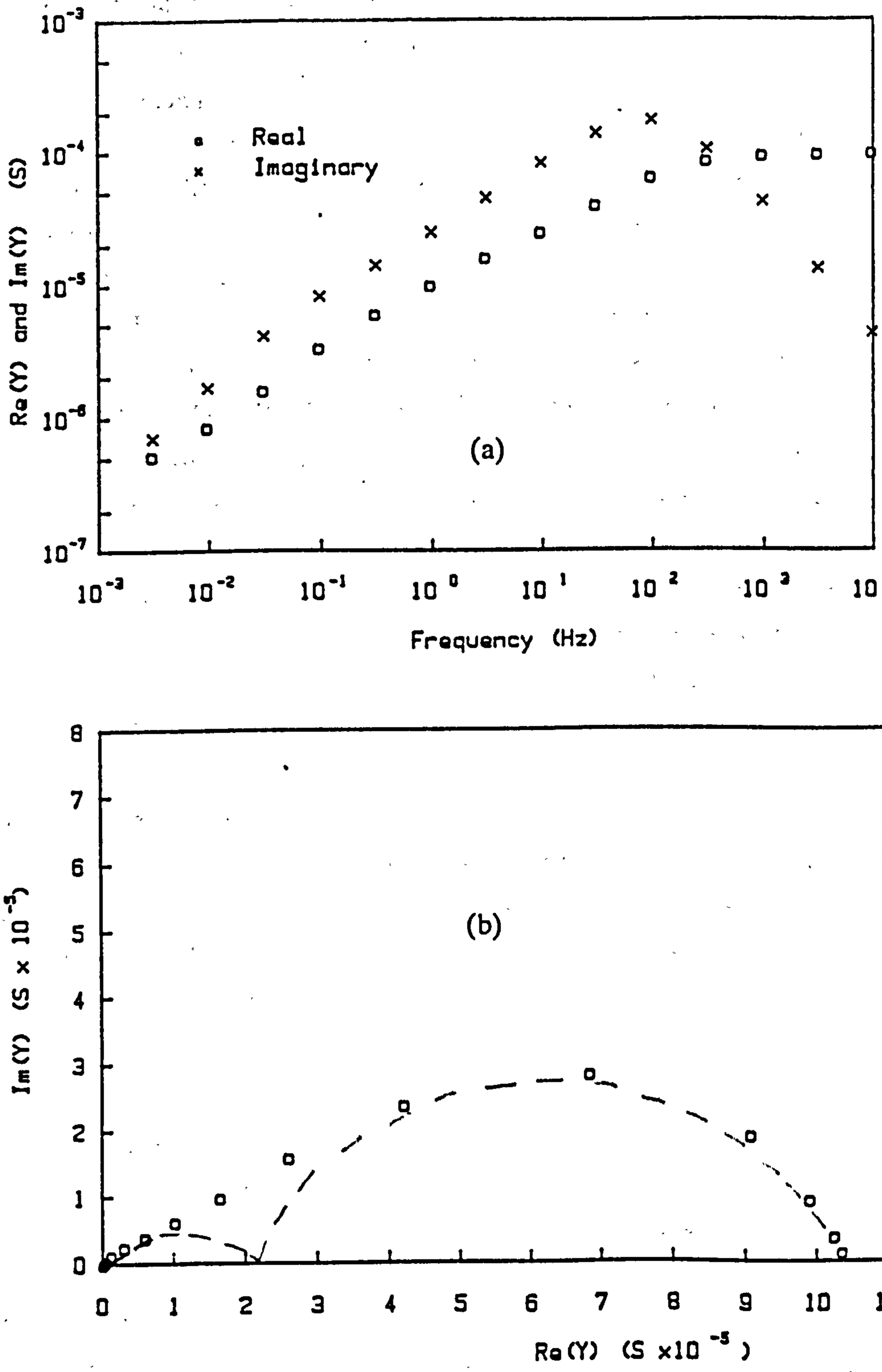

Fig 6.12 AC data of two-electrode sample with copper contacts:

(a) Real and imaginary parts of admittance.

(b) Complex admittance.

influence is unlikely because of the absence of conduction at low frequency, indicating that no reaction capable of supplying copper ions, such as the oxidation of the copper electrode, takes place under zero-bias conditions.

Another explanation for the shape of the curve is that it is the result of two impedances in series, which would individually give rise to the dotted circular arcs. These would have different angles of depression, and so the effect should show up in the frequency dependence of the capacitance, which is plotted in figure 6.13. The low frequency part of this curve is approximately a straight line, with a slope which gives a value of β of 34°. The value of G_b which corresponds to this angle is 1.0×10^{-4} S, which is the width of the whole complex admittance curve. From this it may be concluded that there is only one impedance and therefore one process involved.

A further possibility is that the electrochemical reaction responsible for the galvanostatic results (see below) introduces a nonlinearity at low frequency which to some extent invalidates the interpretation of the AC data as an admittance at all. The effect of this would be to cause an asymmetry between the positive and negative phases of the generator cycle. The results are not predictable without a precise knowledge of the nature of the reaction, but some distortion of the AC response, relative to the response of a linear system, could be expected.

6.4.2. Galvanostatic Data

A typical anodic curve is shown in figure 6.14 (a), displaying a sharp initial rise followed by an almost linear section. The sample in this case had not previously had any current passed through it. Its associated differential capacitance, figure 6.14 (b), rises continuously as charge passes. The absolute magnitude of the capacitance is an order of magnitude greater than that of aluminium, strongly suggesting from the outset that some electrochemical reaction is present.

For the current-reversal experiment, a current of 10 μA was applied for 10 s each way. The results, shown in figure 6.15 (a), show that as for aluminium, the first anodic curve reaches a plateau faster than the subsequent anodic phases, but the same plateau level is reached by all anodic curves eventually, as is shown more clearly on the superimposed plot of figure 6.15 (b). The difference between the first and subsequent anodic phases is probably due to a discharging process associated with charge storage during the cathodic phase.

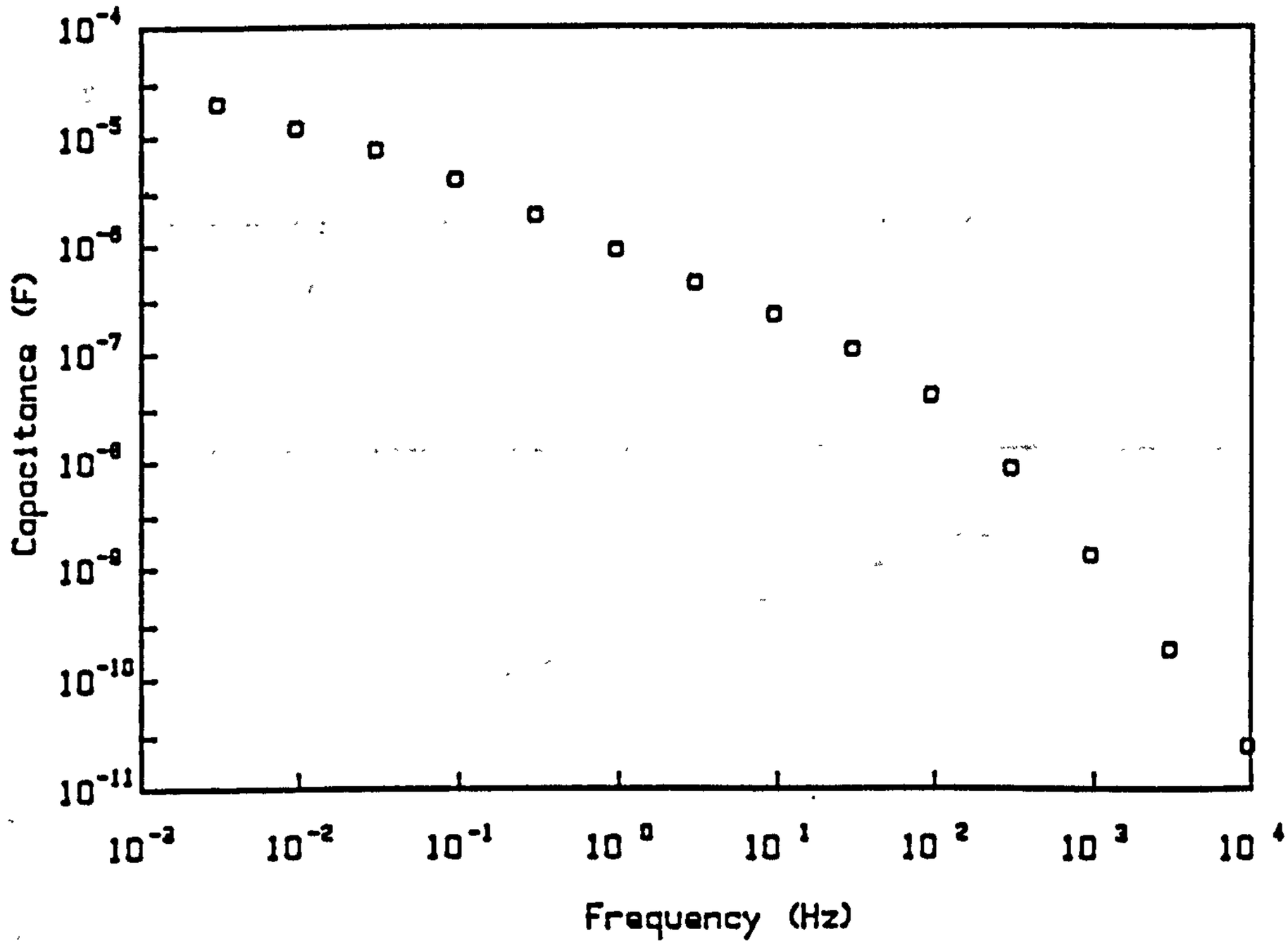

Fig 6.13 Interface capacitance versus frequency of copper sample.

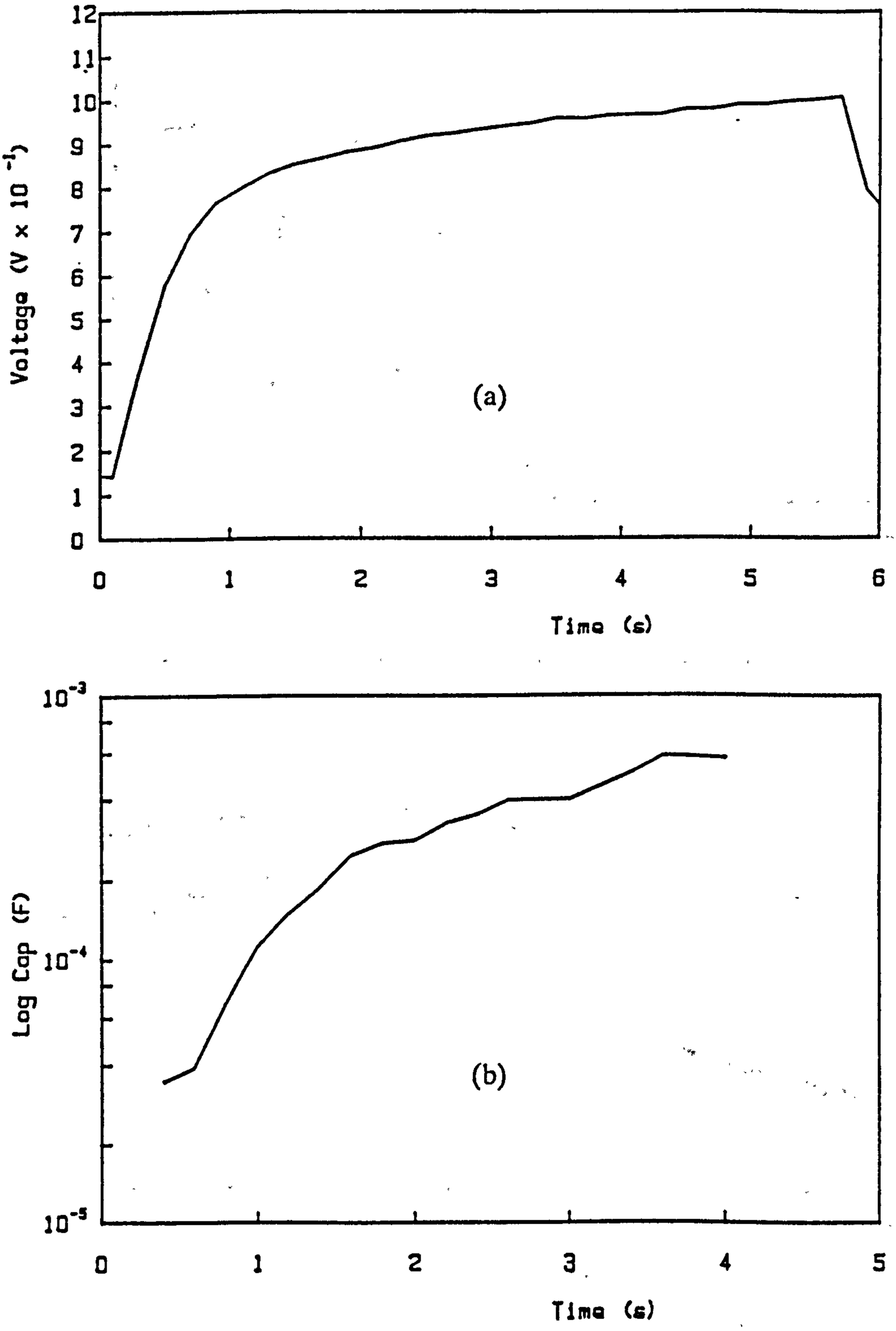

Fig 6.14 (a) Anodic curve for I= 10 μA, copper sample.

(b) Differential capacitance of data of (a).

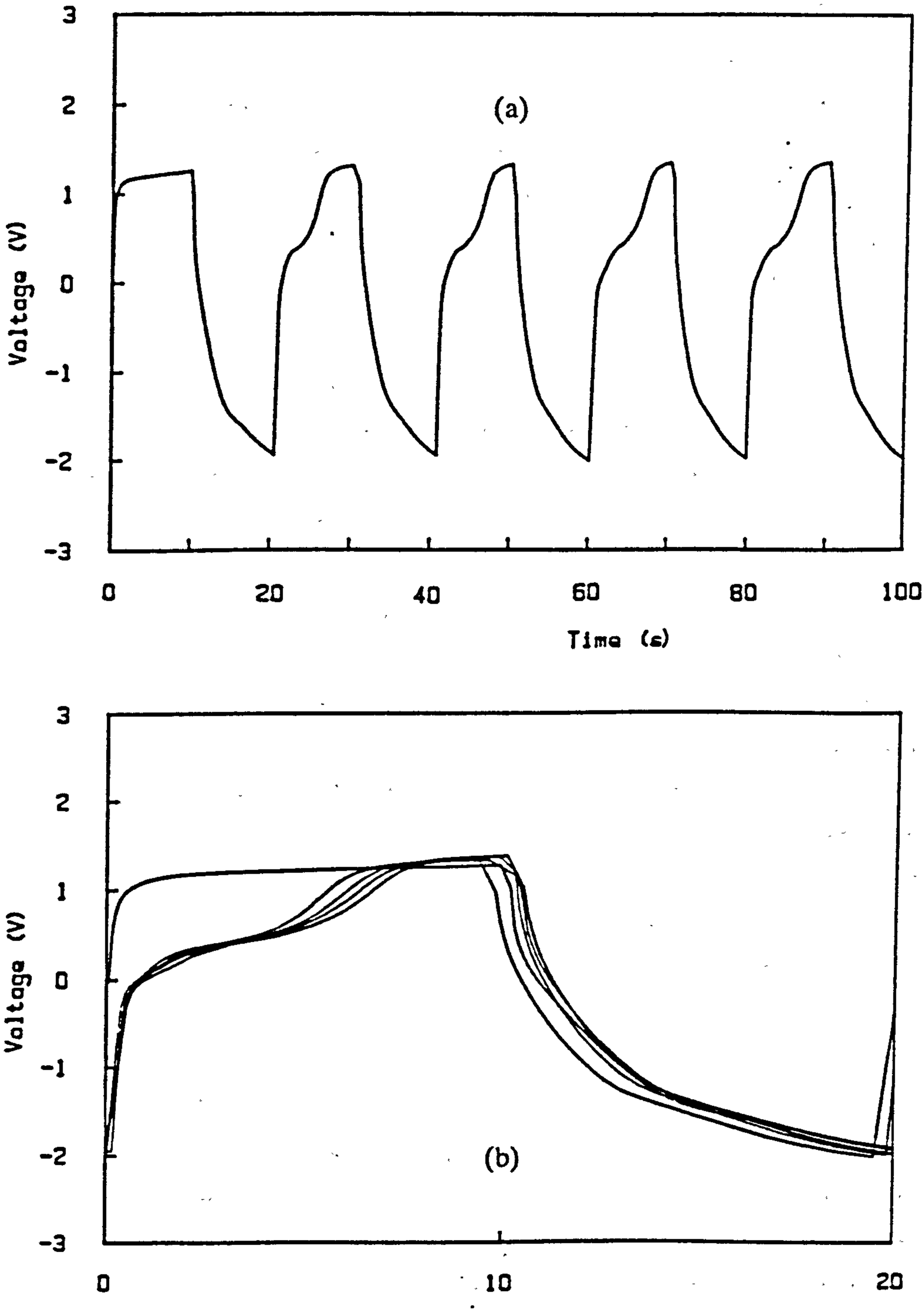

Fig 6.15 (a) Reversed-current results of copper cell.

(b) Superimposed cycles of (a).

Figures 6.16 (a) and (b) are equal-charge runs using 10 μC and 100 μC respectively. They are parallel curves, but in this case, when the voltage differences are plotted versus the logarithm of the current, as in figure 6.17, the straight-line Tafel behaviour is not followed over the full range. If it is assumed that kinetic limitation occurs at the low-voltage end then the parameters α and i_o in equation 6.3 have the values 0.74 and 3 nA respectively, but clear evidence that the potential is dominated by a kinetically-limited charge-transfer reaction is not provided by these data, in contrast to the case of aluminium.

The presence of some charge transfer reaction is strongly suggested by other observations. The shape of the zero-current voltage-decay curve, figure 6.18, which follows the anodic run of figure 6.14 (a), is very similar to that for aluminium, where there was clear evidence of a reaction.

The effect of passing a comparatively large quantity of charge through the electrode also suggests the presence of charge transfer. Figure 6.19 (a) is a high-current (50 μA) anodic galvanostatic curve for a copper sample of type 3, and shows that up to about 3 V, the voltage rose in the same manner as for the lower current, with a sharp initial rise followed by a slow linear region. As more charge passes, the voltage rises comparatively steeply to 5 V, at the end of the run. This latter rapid rise is associated with some irreversible process, because after it has occurred it is not possible to reproduce the response on the same sample no matter how it is treated; any further anodic current causes a rise to a high voltage without passing through a comparable plateau region. The differential capacitance, figure 6.19 (b), undergoes a very sharp initial rise from just greater than the value given by AC measurements (25 μF) to about 2000 μF at the shoulder. Thereafter it rises smoothly until the point where the voltage curve shows an upturn.

The cathodic plot for a contact which had been subjected to a small anodic voltage is shown in figure 6.20. The anodic charge passed was only sufficient to reach the plateau. The result is a smooth curve which levels out at about the same time as the voltage curve. The high value of the differential capacitance on the plateau strongly suggests the presence of some charge-transfer reaction during the cathodic phase. The amount of charge which passes before this plateau is reached is also very high. From visible changes to the electrode after a high anodic charge had passed, it was apparent that the reaction involved the oxidation of copper. When the sample was removed from the chamber after a run such as that of figure 6.19, the metallic working

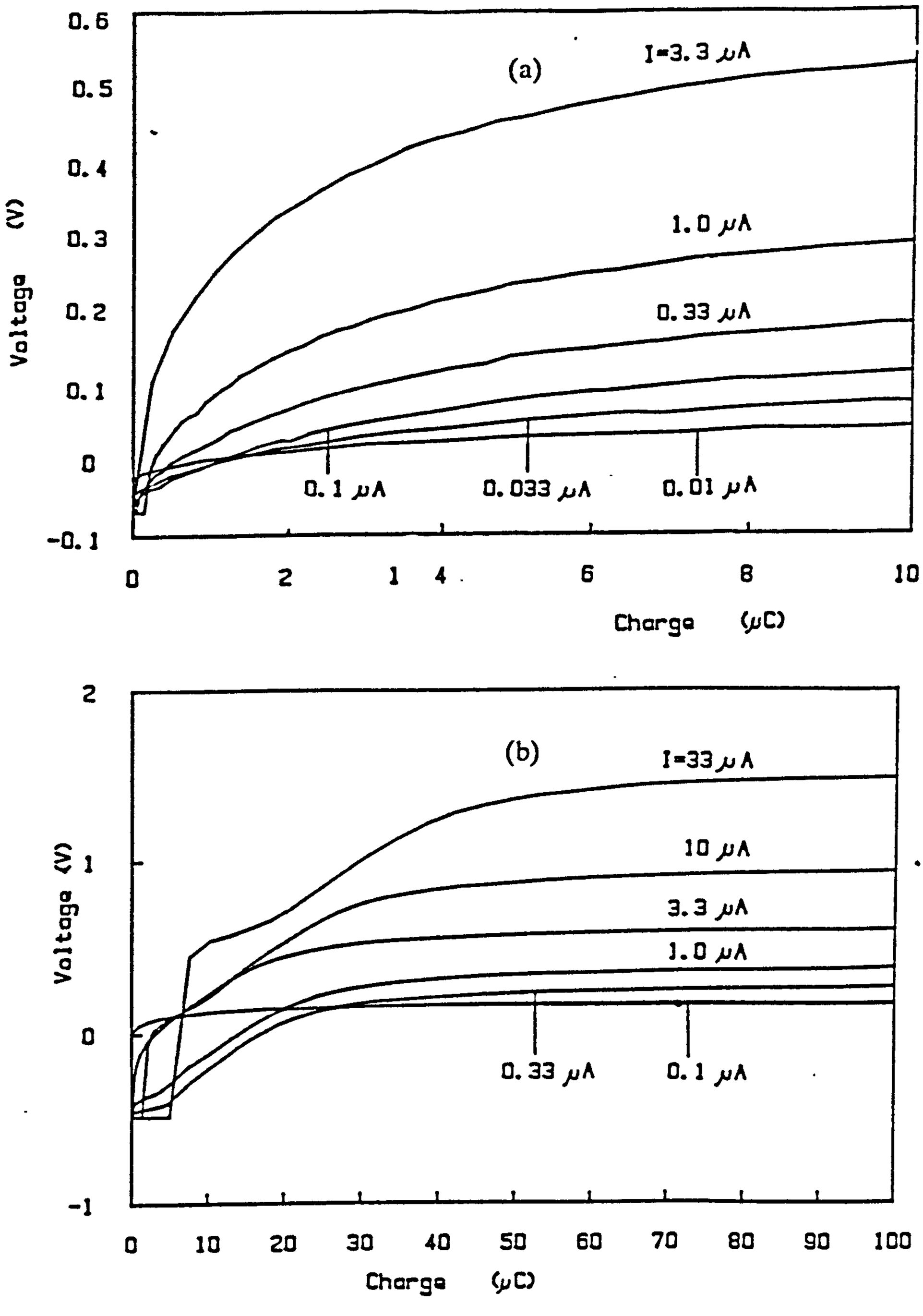

Fig 6.16 (a) 10 μC equal charge curves for copper sample.
(b) 100 μC equal charge curves for copper sample.

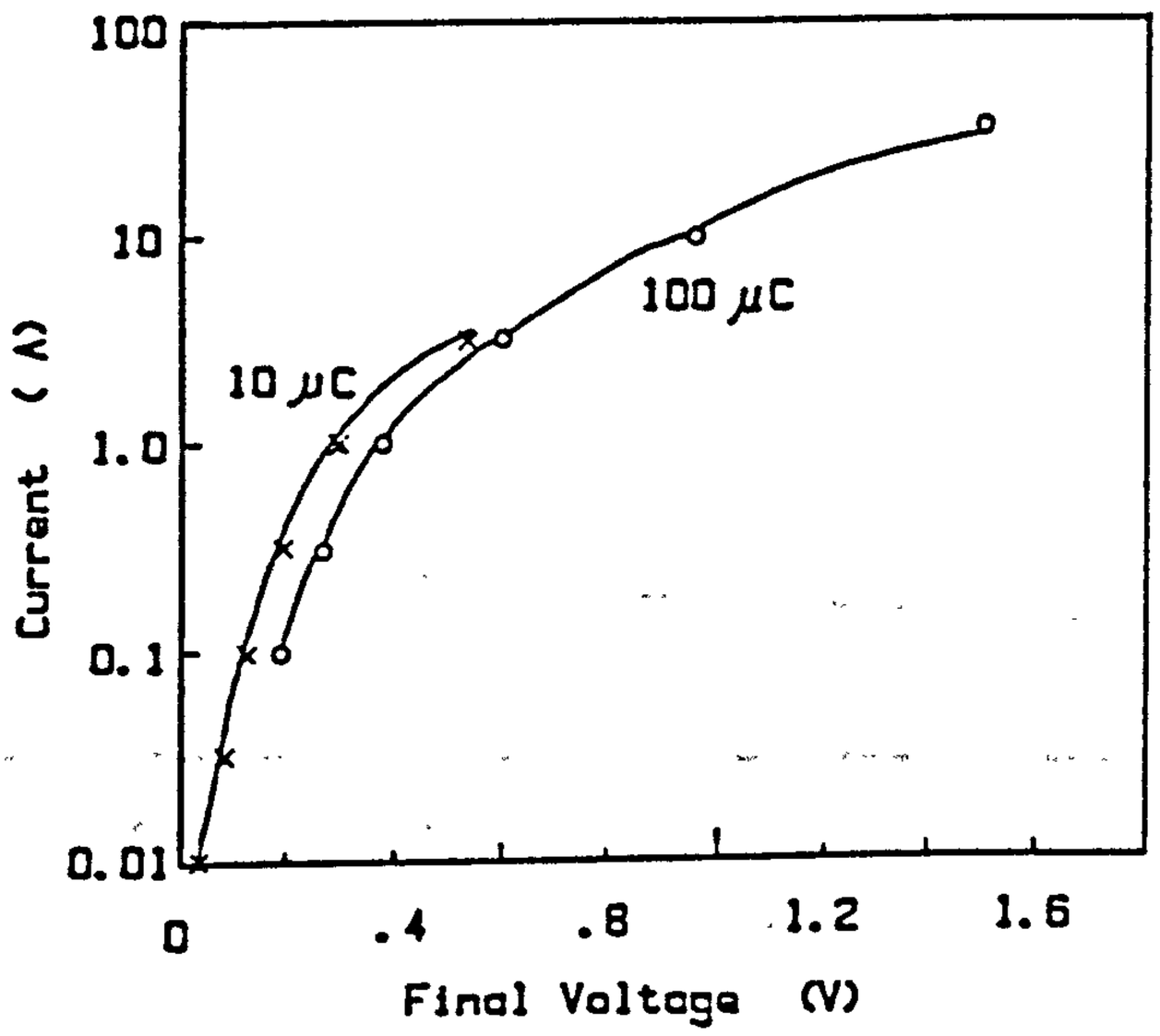

Fig 6.17 Tafel plot of data of figure 6.16.

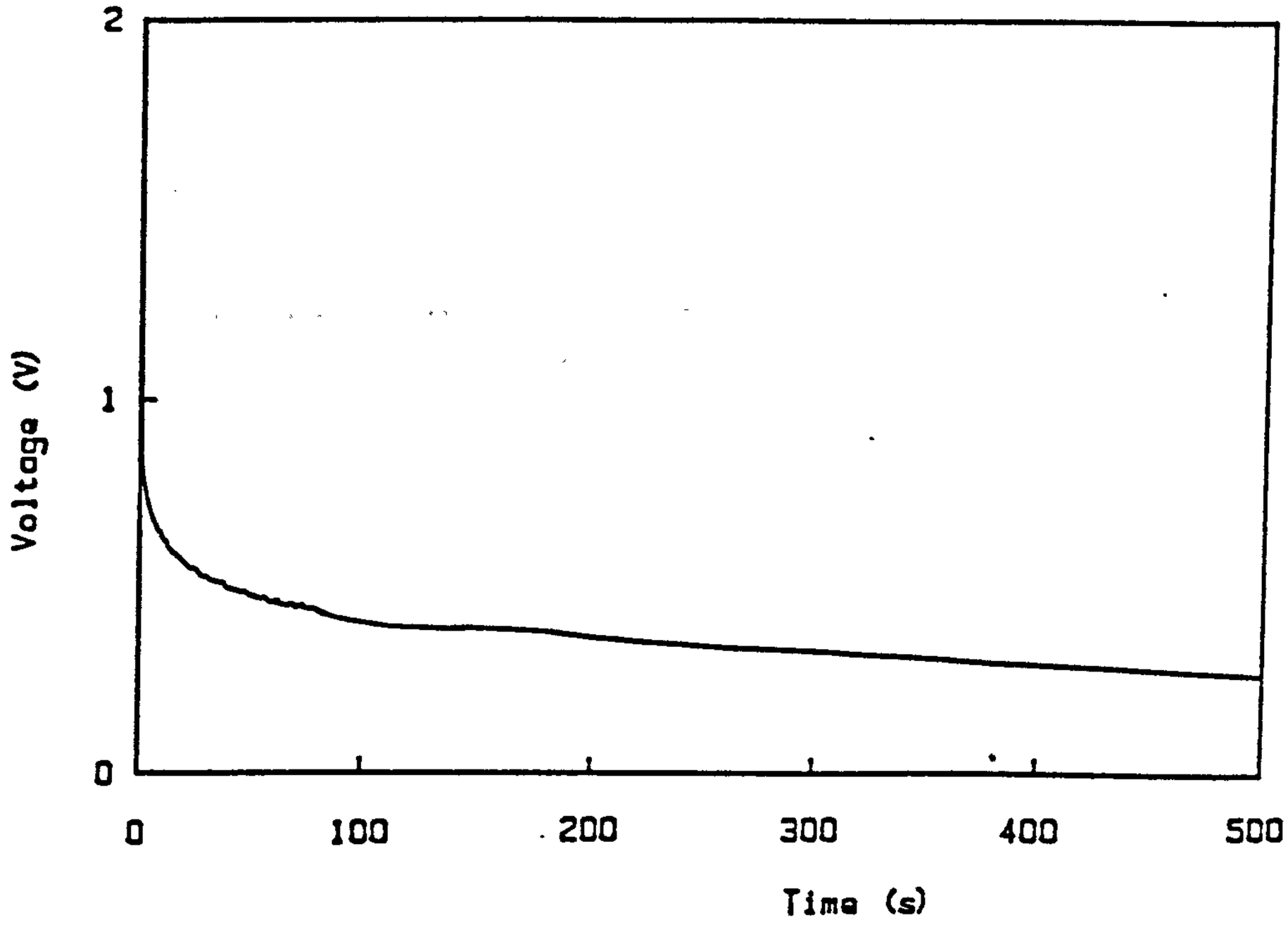

Fig 6.18 Zero-current decay data after the anodic run of figure 6.14.

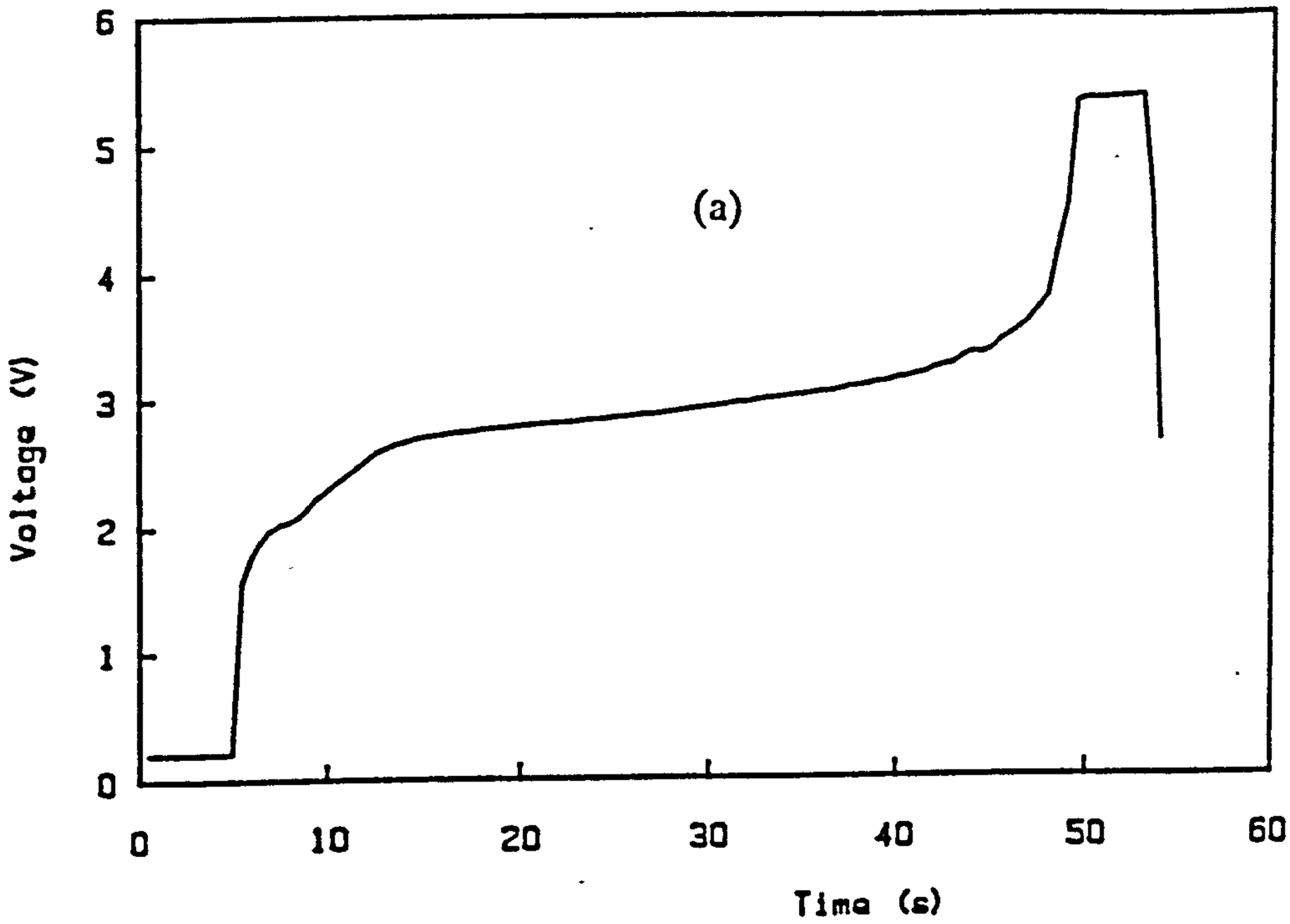

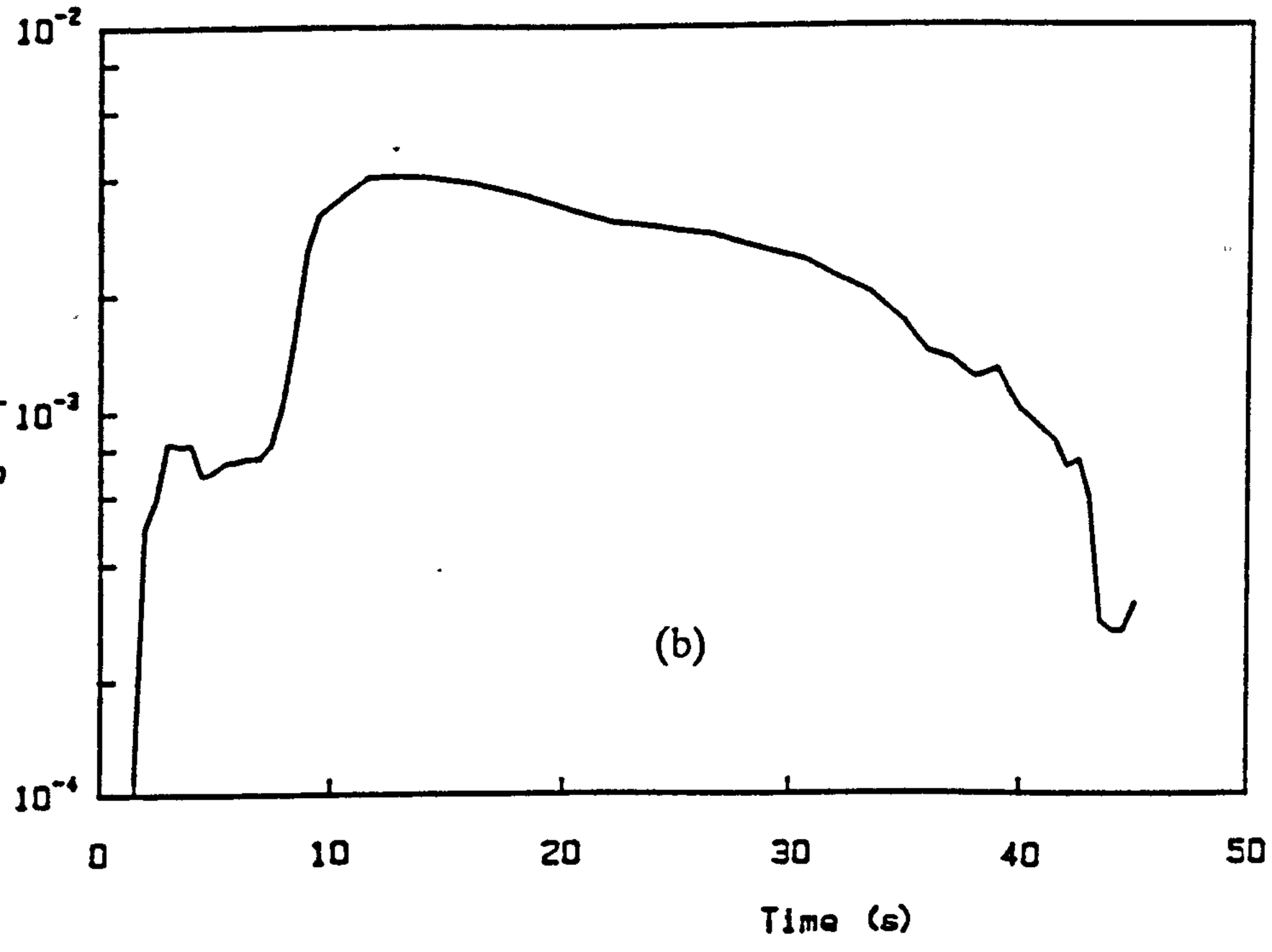

Fig 6.19 (a) 5 μA anodic run on copper sample.
(b) Differential capacitance of data of (a).

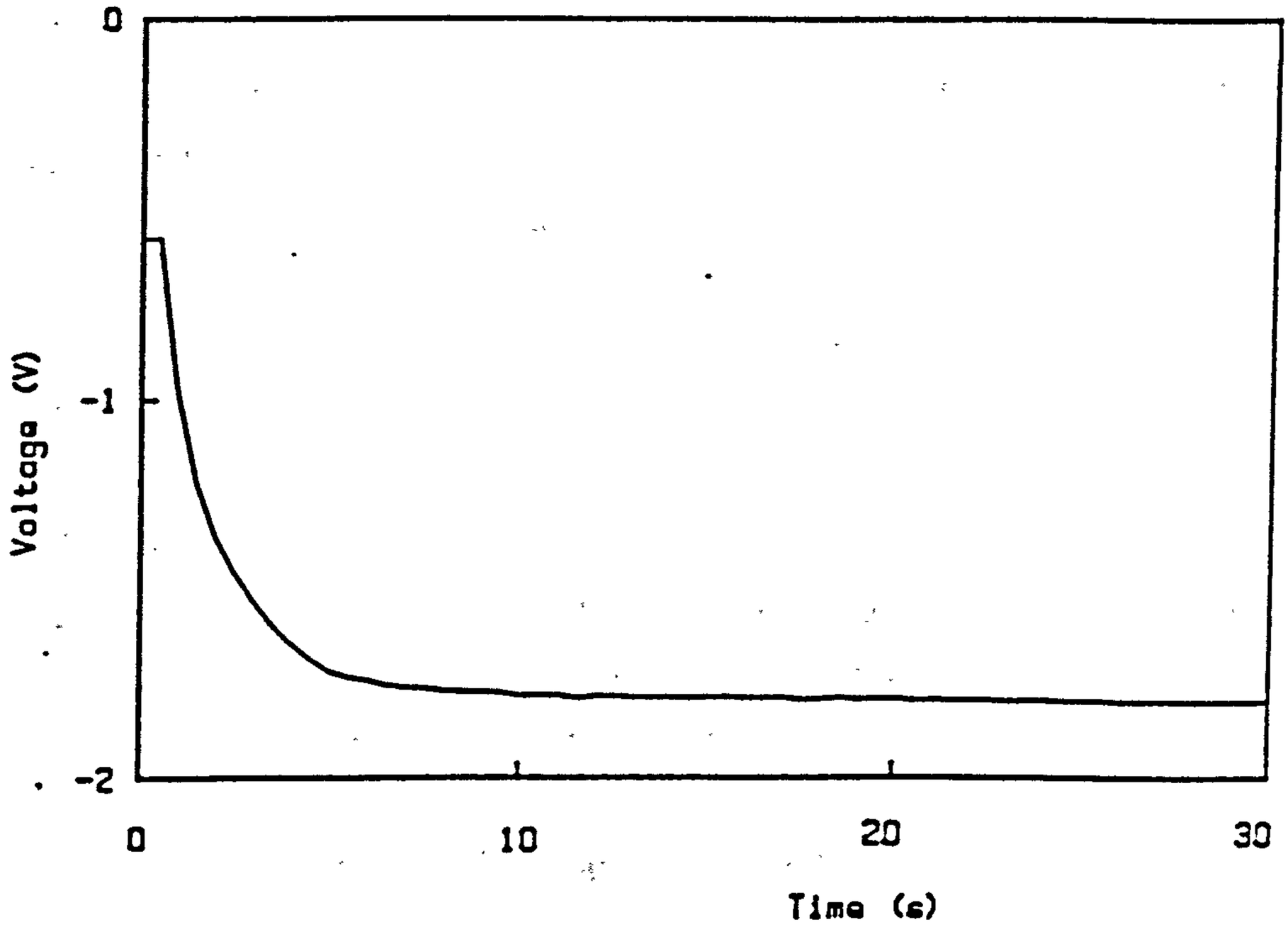

Fig 6.20 Cathodic run on copper sample.

electrode had been replaced by a greenish-brown colouration on the surface of the glass, indicating that all the metal had been consumed by the reaction. If the colouring was due to a faradaic reaction involving all of the metal in the electrode, then the quantity of metal should be related to the total charge passed via Faraday's law. The thickness could only be estimated as 1 μm by calculating the amount deposited during evaporation. This is only expected to be accurate to within an order of magnitude. The total number of atoms in this amount of metal is about 3×10^{14}. The total charge passed was 500 μC, which corresponds to 10^{15} electrons, which is in reasonable agreement, bearing in mind the uncertainty in the estimation of the thickness.

Simple inspection of the substance left behind after such an anodic run was not sufficient to establish whether it was an oxide layer which had developed on the surface or whether the copper ions had migrated into the glass itself. This question will be returned to in section 6.9.

6.5. Silver

6.5.1. AC Data

Figures 6.21 (a) and (b) and 6.22 show the response of a silver sample of type 3 at 385°C, obtained using the parallel analyser configuration. They follow the same form as those for copper. The complex admittance curve gives an interface capacitance of 2.9 μF. There is a distortion of the arc at the low frequency end, similar to, but much less marked than that for copper. The effect is too small for any calculation of a series capacitance as was done in the case of copper, and it does not appear to have any effect on the variation of interface capacitance with frequency, as measured by the three-electrode method. The value of β found from the capacitance graph, 23°, agrees to within the uncertainty of measurement to the angle of depression of the complex admittance arc, 27°.

6.5.2. Galvanostatic Data

An anodic voltage curve for a "new" contact measured up to 0.2 V with 1μA flowing, and its associated differential capacitance, is shown in figure 6.23. Both of these show the gradual nature of the potential development with the differential capacitance continuously increasing with charge from 20 to 100 μC. Silver differed from other electrode materials in that there was no single overall curve shape which could be

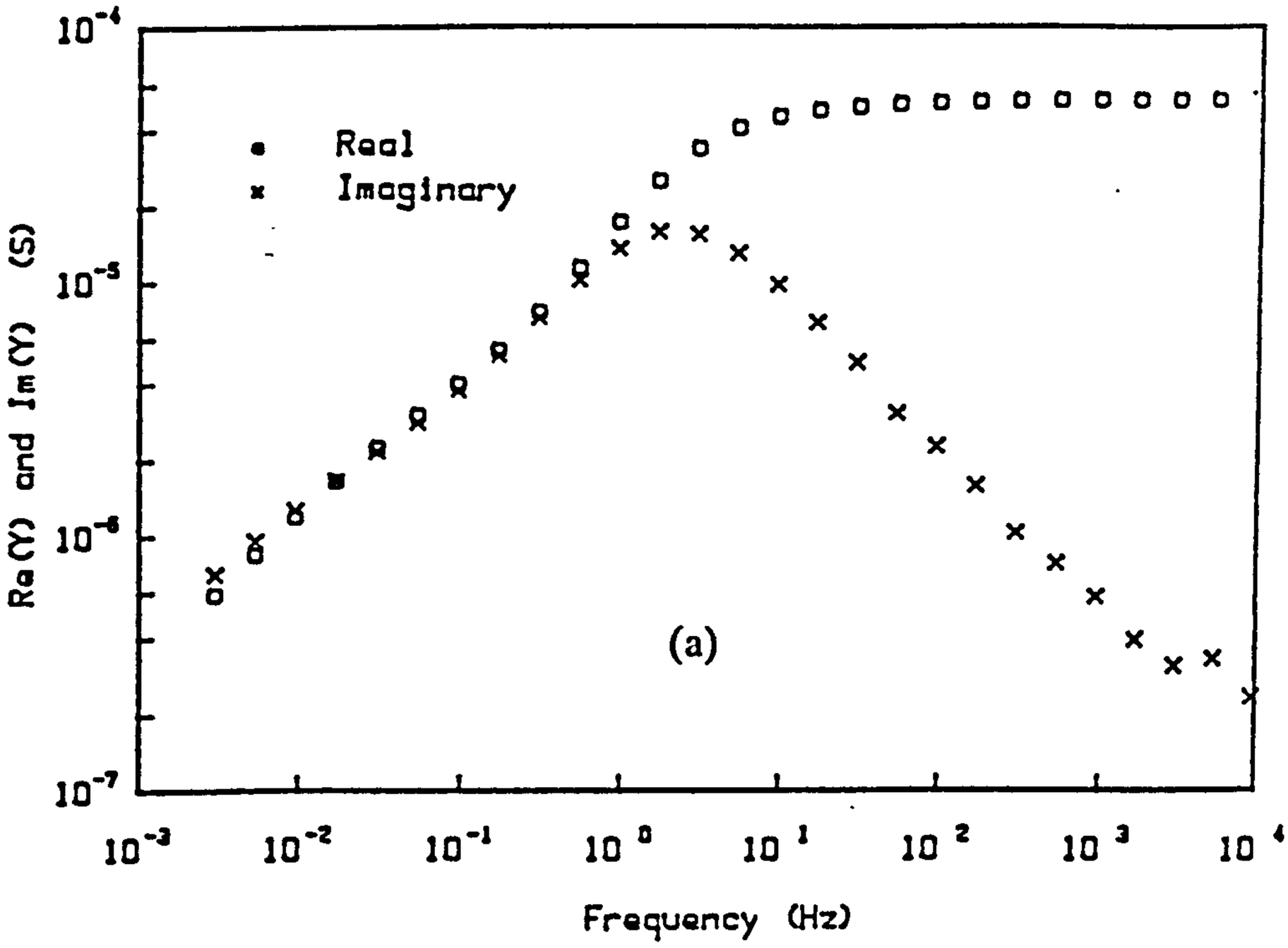

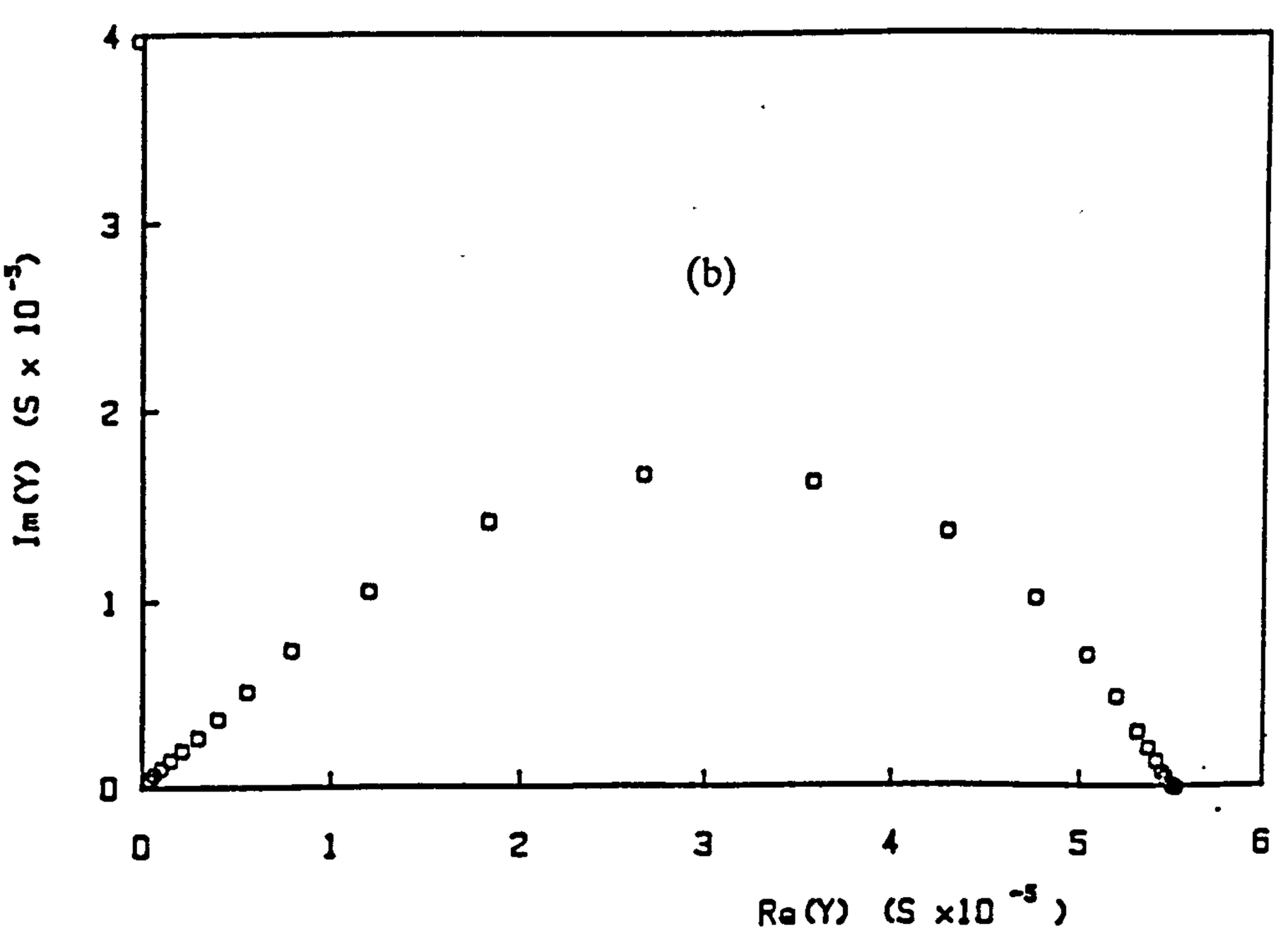

Fig 6.21 AC data of three electrode silver sample:

(a) Real and imaginary parts of admittance.

(b) Complex admittance.

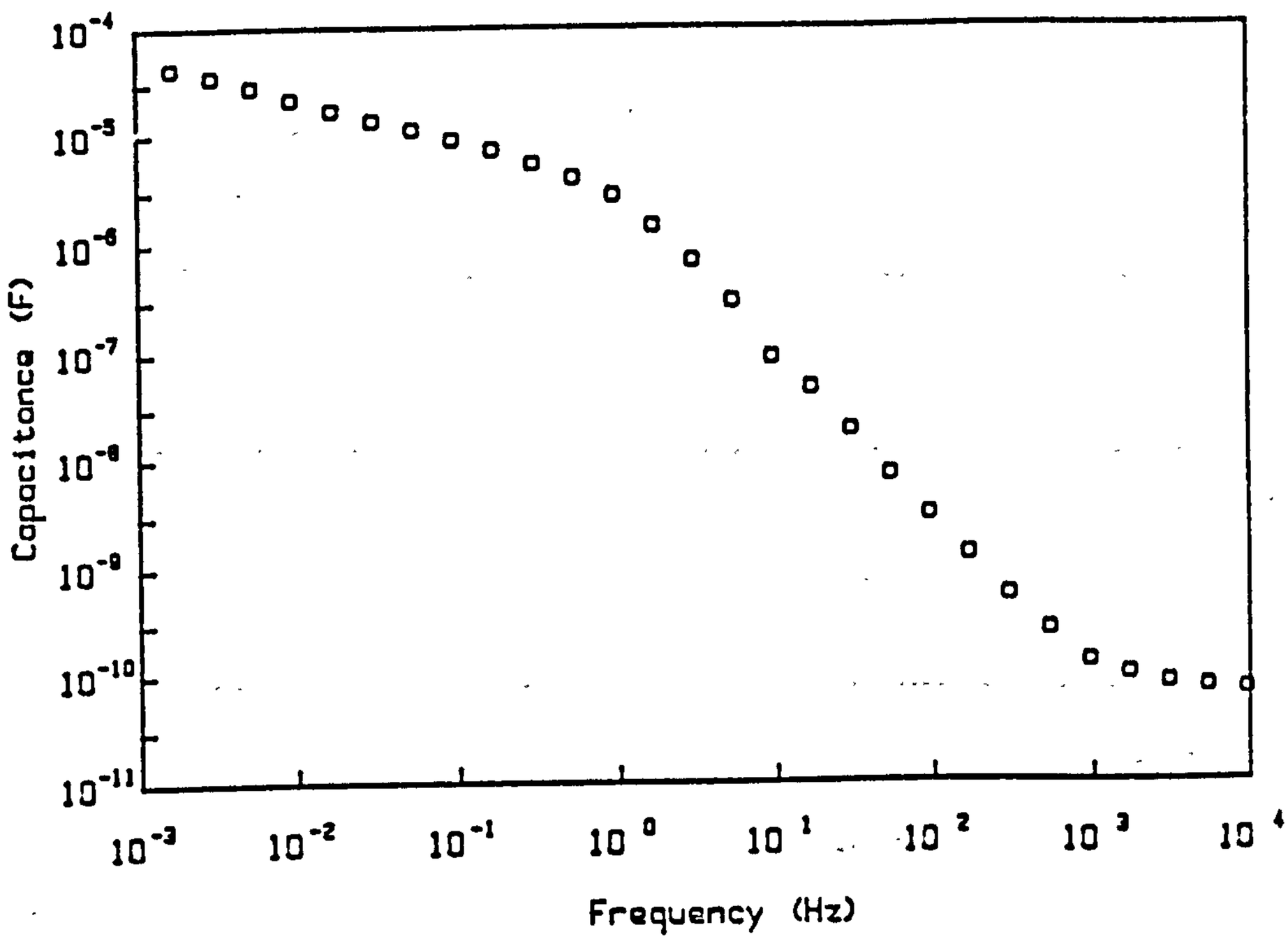

Fig 6.22 Interface capacitance versus frequency of silver sample.

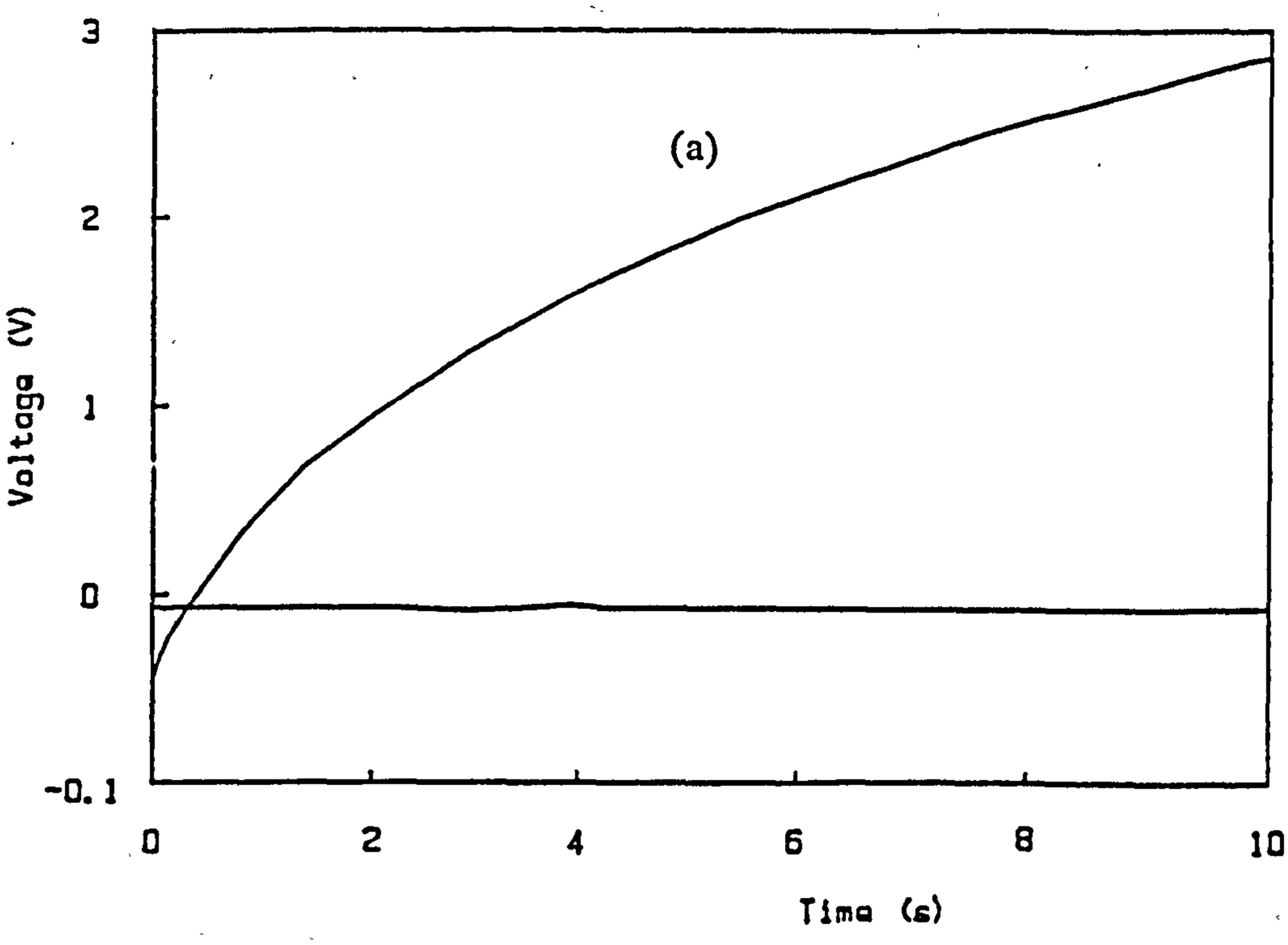

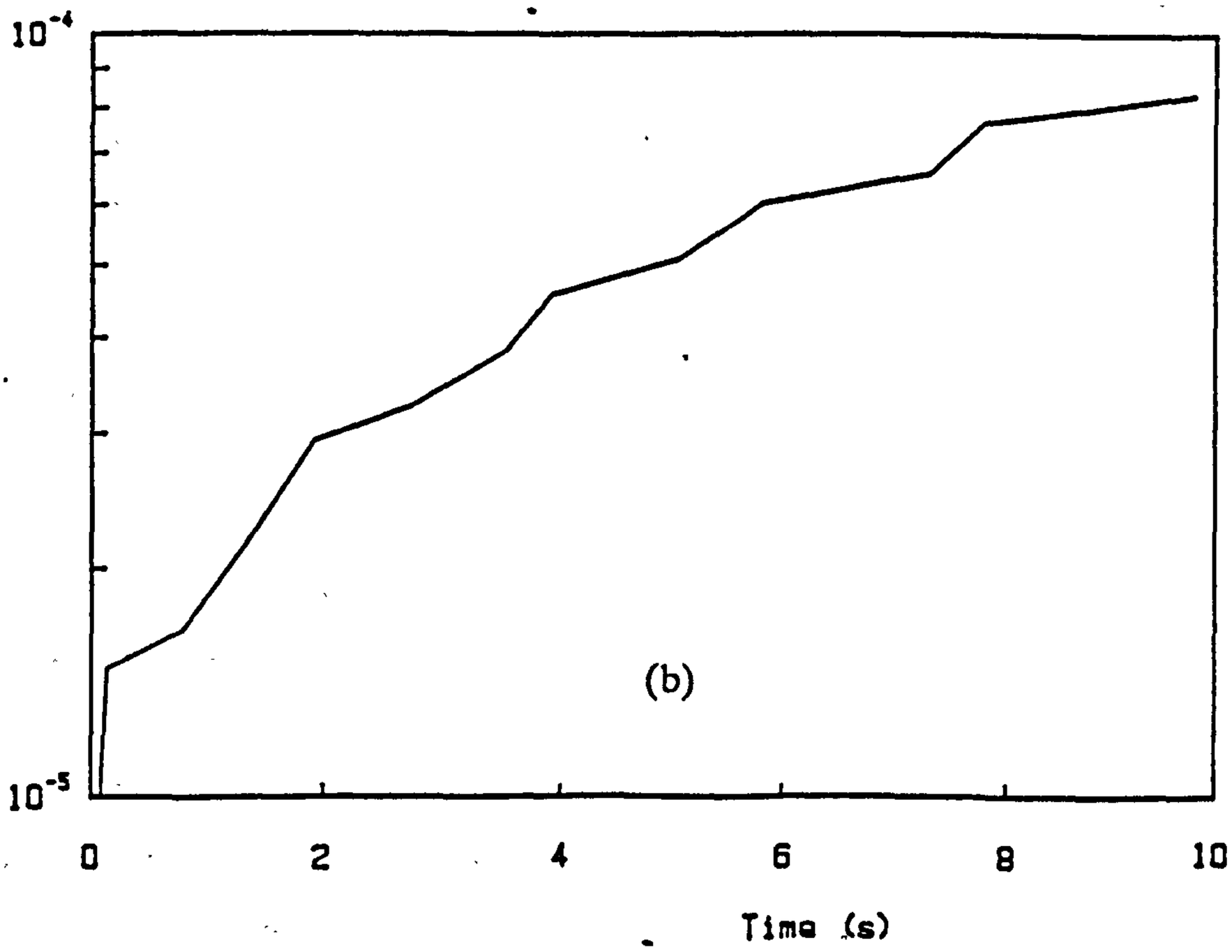

Fig 6.23 (a) Anodic response of silver sample

(b) Differential capacitance of data of (a).

said to be typical of a wide variety of applied currents. It shared with copper the very high measured capacitance but unlike that metal, the voltage curve was never straight.

Figure 6.24 (a) is the voltage response to successive reversals of 10 μA for 10s each way. The voltage in this case reaches the same level in the negative direction as it does in the positive, with the cathodic cycle clearly affecting the subsequent anodic ones, as is shown in the superimposed plot of figure 6.24 (b).

The set of voltage curves in figure 6.25 is the response of a silver contact to 10 μC anodic charge at different currents. The curves are approximately parallel for currents up to about 0.33 μA but diverge at currents greater than this. Figure 6.26 is the logarithmic plot of final voltage versus current. It is approximately linear at the low-voltage end, which, if it is interpreted as the Tafel relationship relationship of equation 6.3, then the values of the kinetic parameters are 3.5 nA for i_o and 0.52 for α.

Figure 6.27, the voltage decay from 0.7 V after 100 μA anodic current had flowed for 100s, follows almost exactly the same curve as that of the other evaporated contacts, with a rapid decline followed by long-term drift.

Figure 6.28 (a) is the anodic response of a silver sample of type 3 up to 5 V. It has a continuously decreasing slope up to the highest voltage, with no abrupt upturn associated with exhaustion of reactive metal, such as that found with copper contacts. The slope does not change smoothly, however, with several quite clearly defined sections being present. This irregular rise of voltage with charge shows up clearly in the variation of C_d, figure 6.28 (b). The passage of such a large charge (360 μC) has an irreversible effect, as is demonstrated by figure 6.29, which is the result of using 1 μA on the same contact after the voltage has been allowed to decay to a steady level. The voltage rises to about 4 V after only 10 μC.

The response to a cathodic current of 1 μA in this case, shown in figure 6.30, is almost a mirror image of that to an equivalent anodic current. It is also very close to the cathodic response of a copper contact.

6.6. Tungsten Trioxide

Figure 6.31 shows the bulk conductance, as a function of frequency, of a pressed disc of tungsten trioxide, measured using stainless steel contacts with the two-electrode configuration of the Solartron frequency-response analyser. It is comparable to that of a glass plate of similar dimensions and so had to be taken into account when tungsten

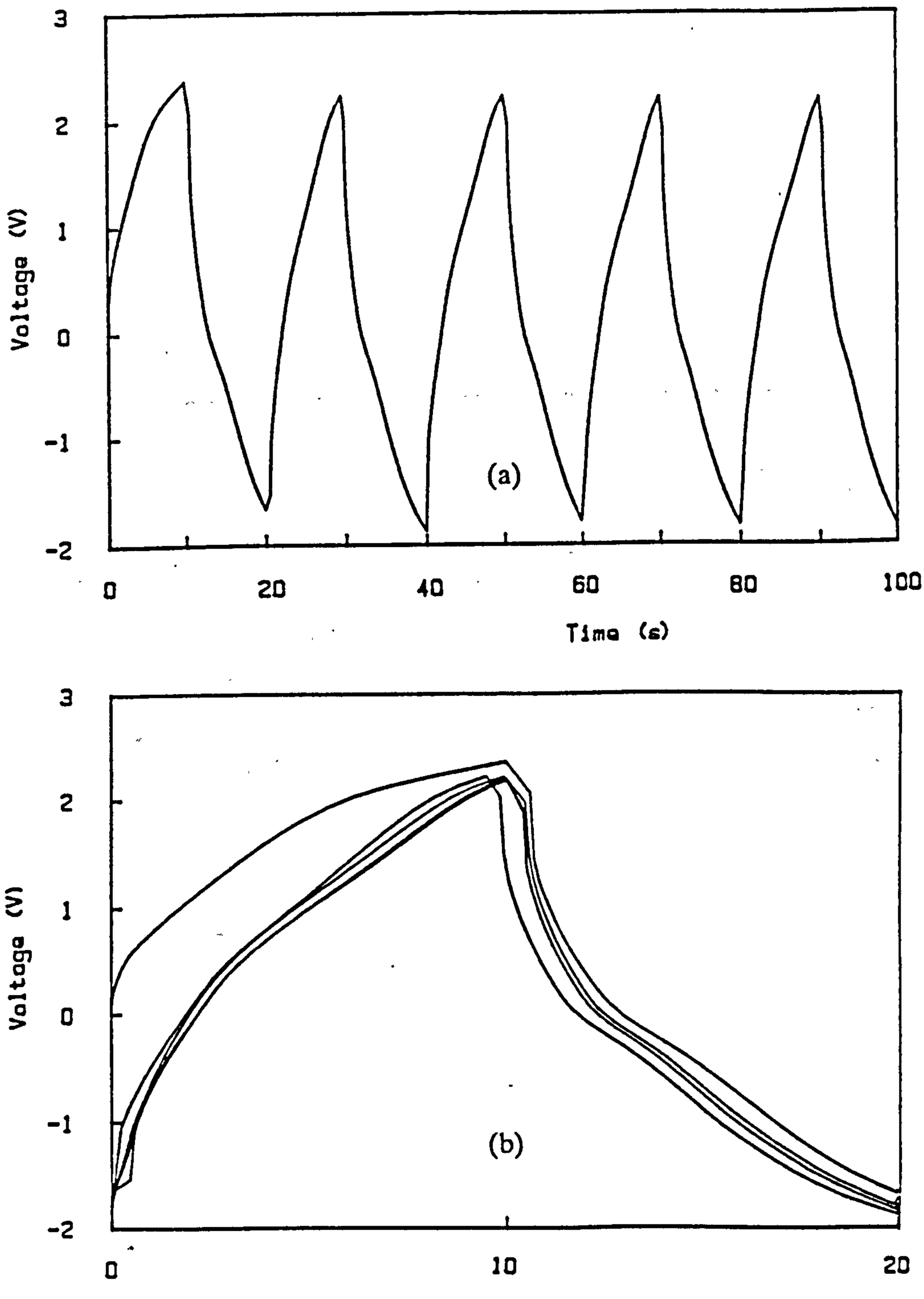

Fig 6.24 (a) Reversed-current results on silver sample.
(b) Superimposed plot of data of (a).

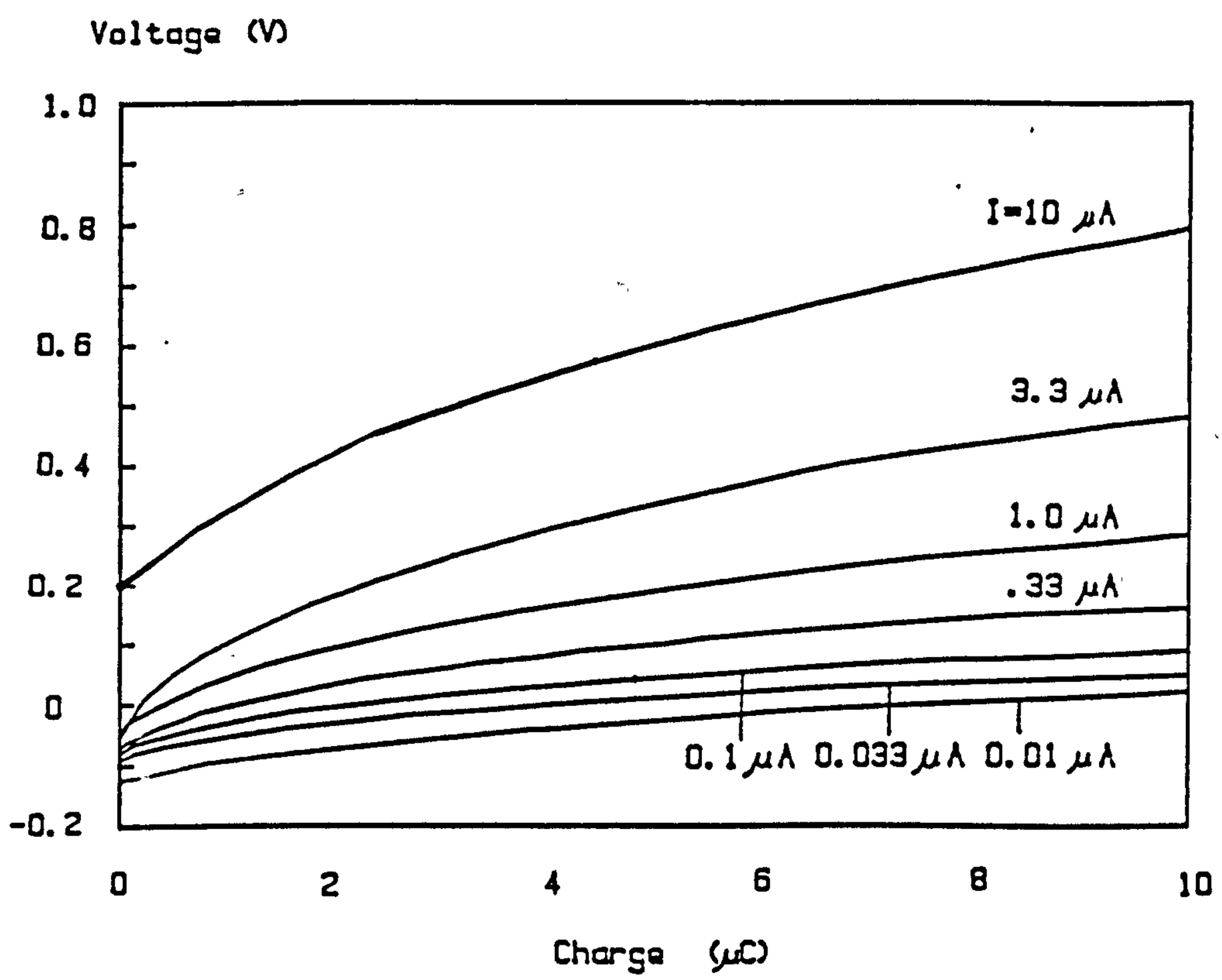

Fig 6.25 10 μC equal charge plot of silver sample.

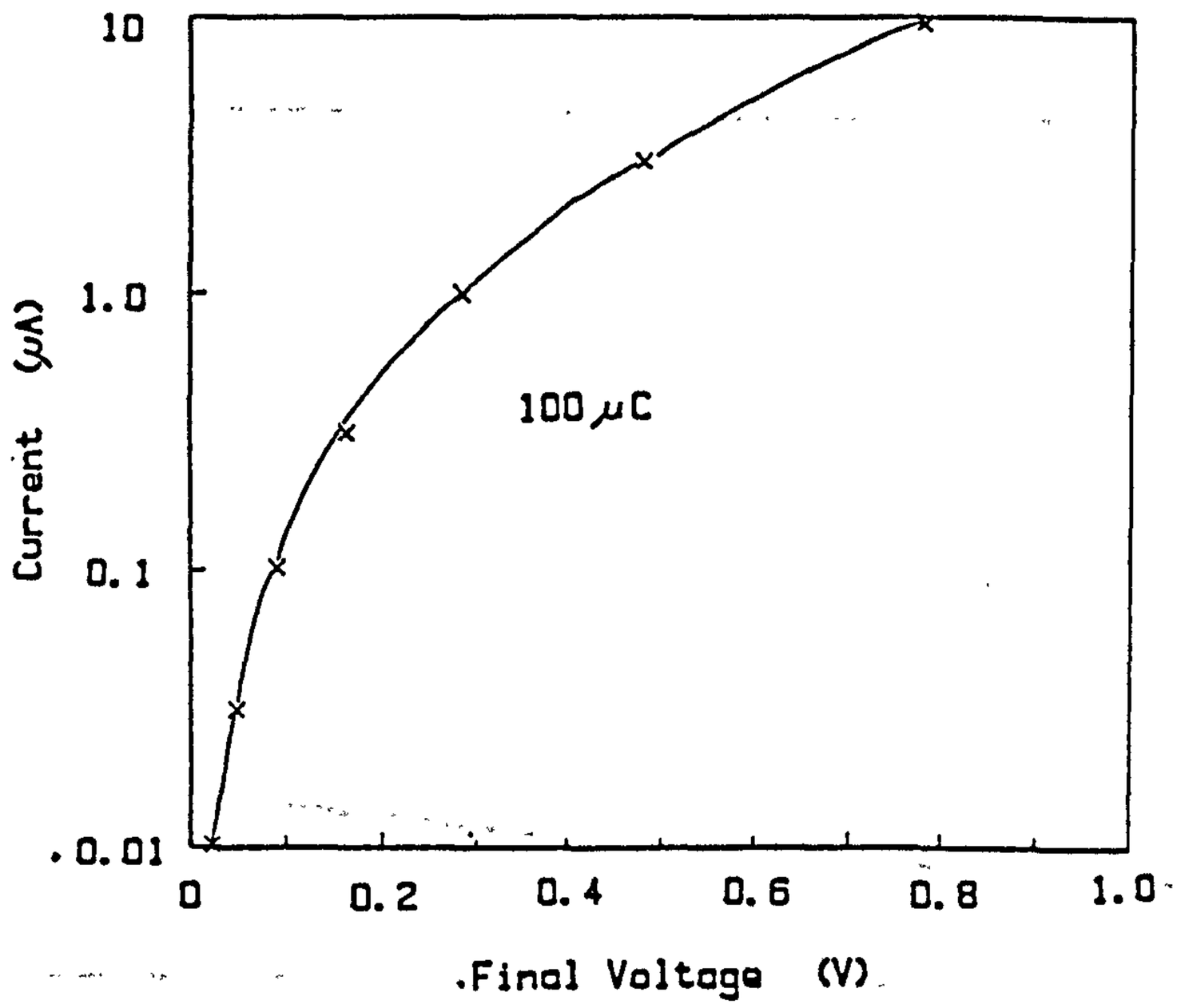

Fig 6.26 Tafel plot of final voltages of 10 μC equal charge runs.

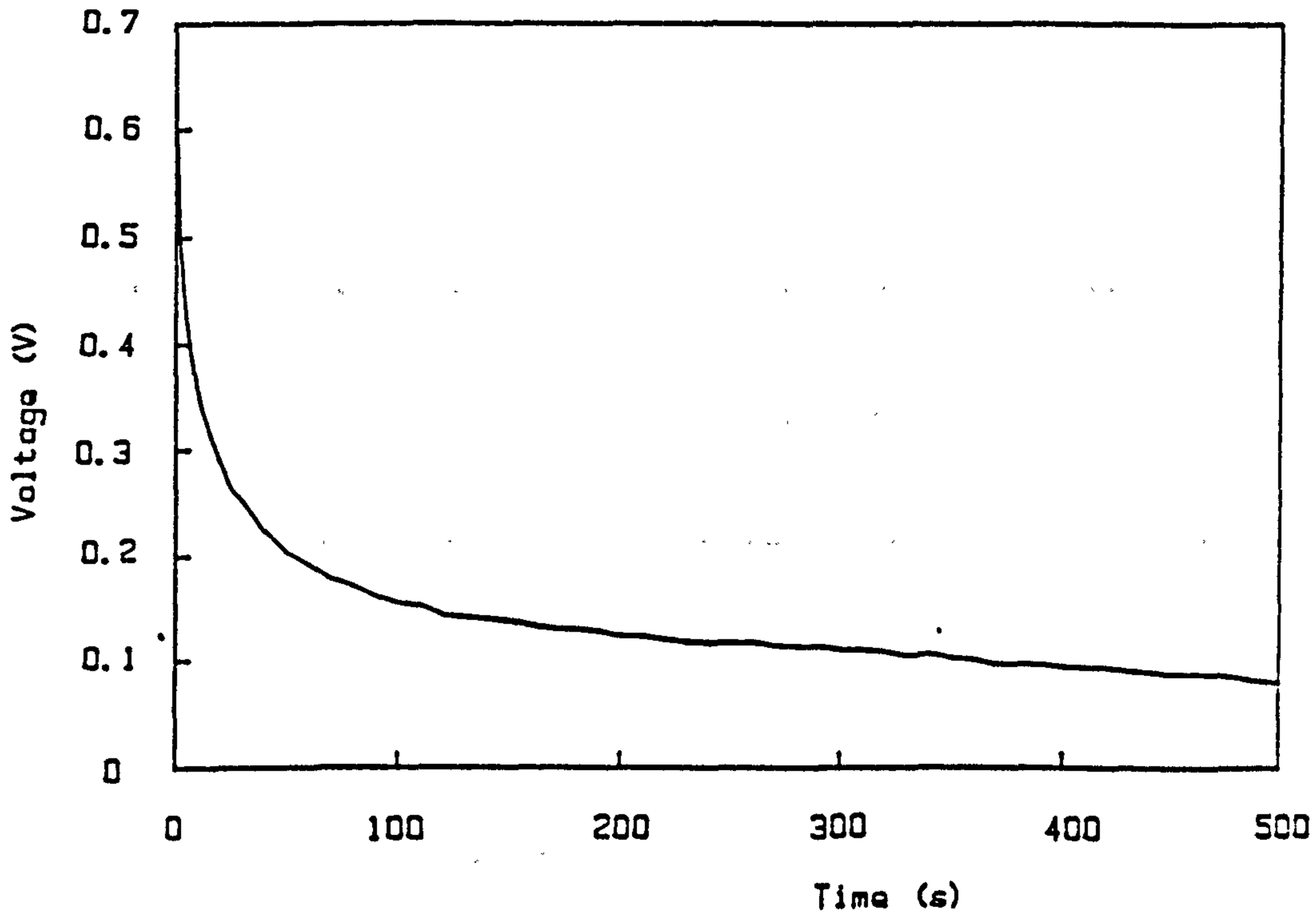

Fig 6.27 Zero-current decay after anodic run of figure 6.23.

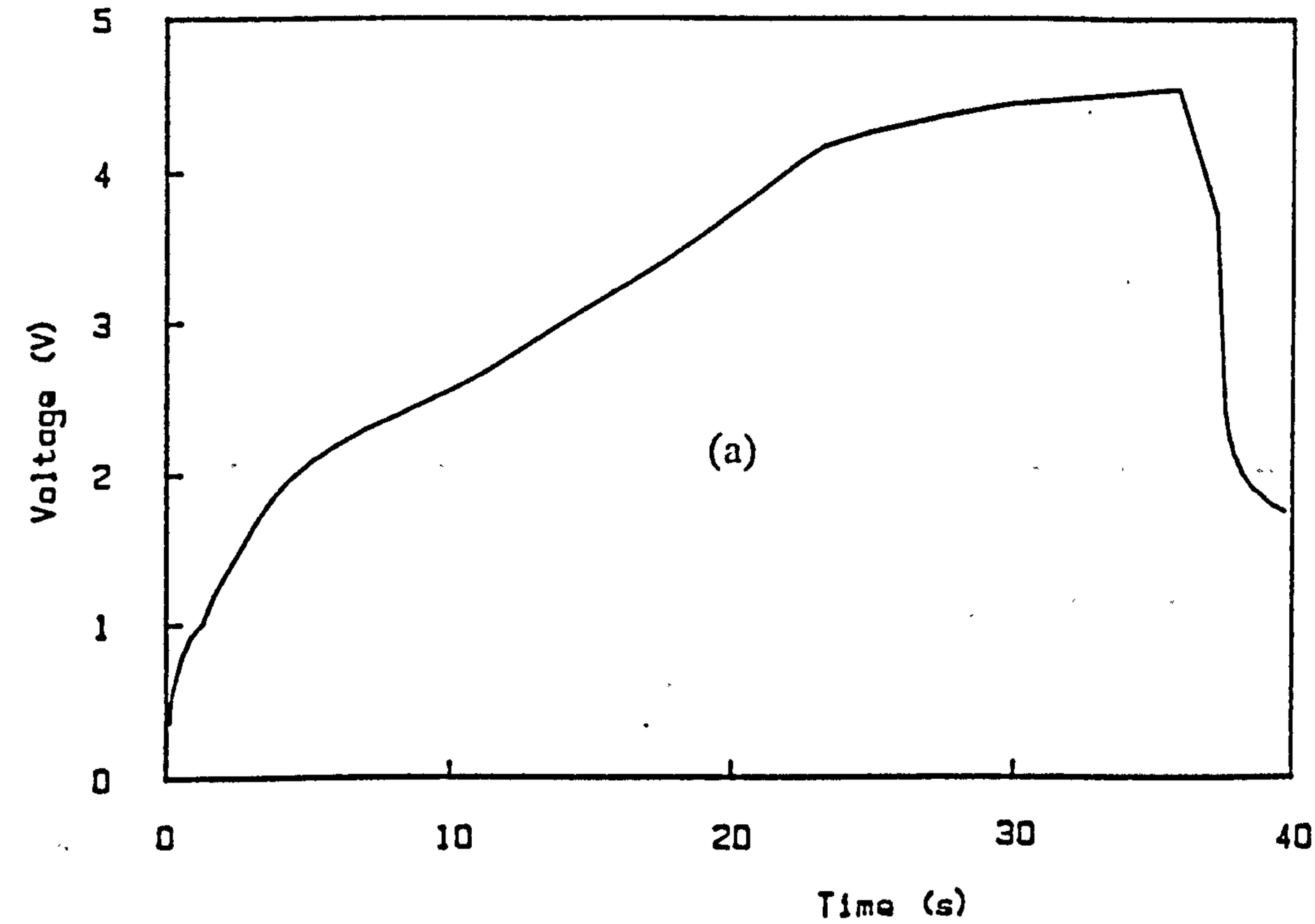

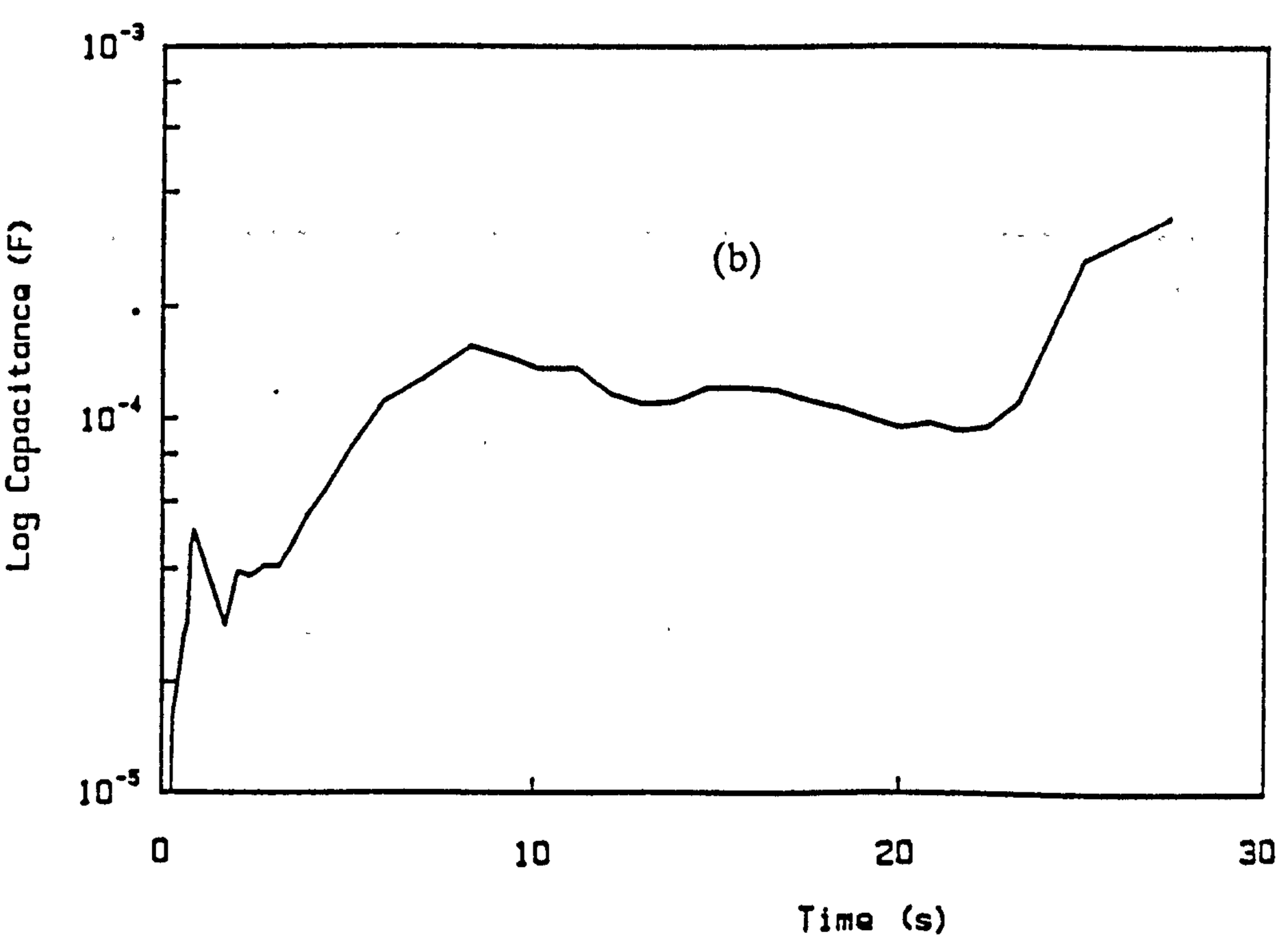

Fig 6.28 (a) 10 μA anodic run on silver sample.
(b) Differential capacitance of (a).

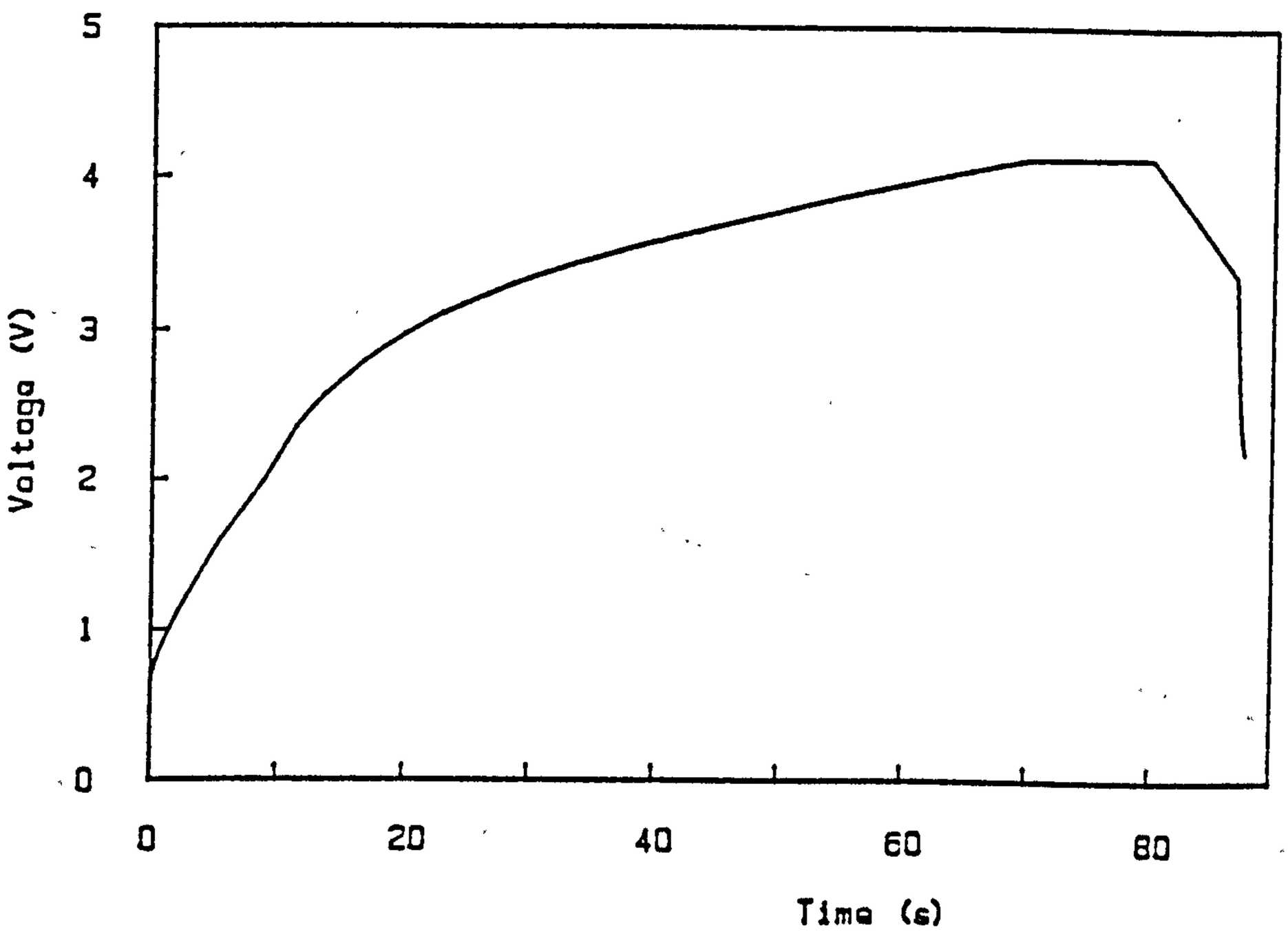

Fig 6.29 1 μA anodic run after 10 μA run of figure 6.28.

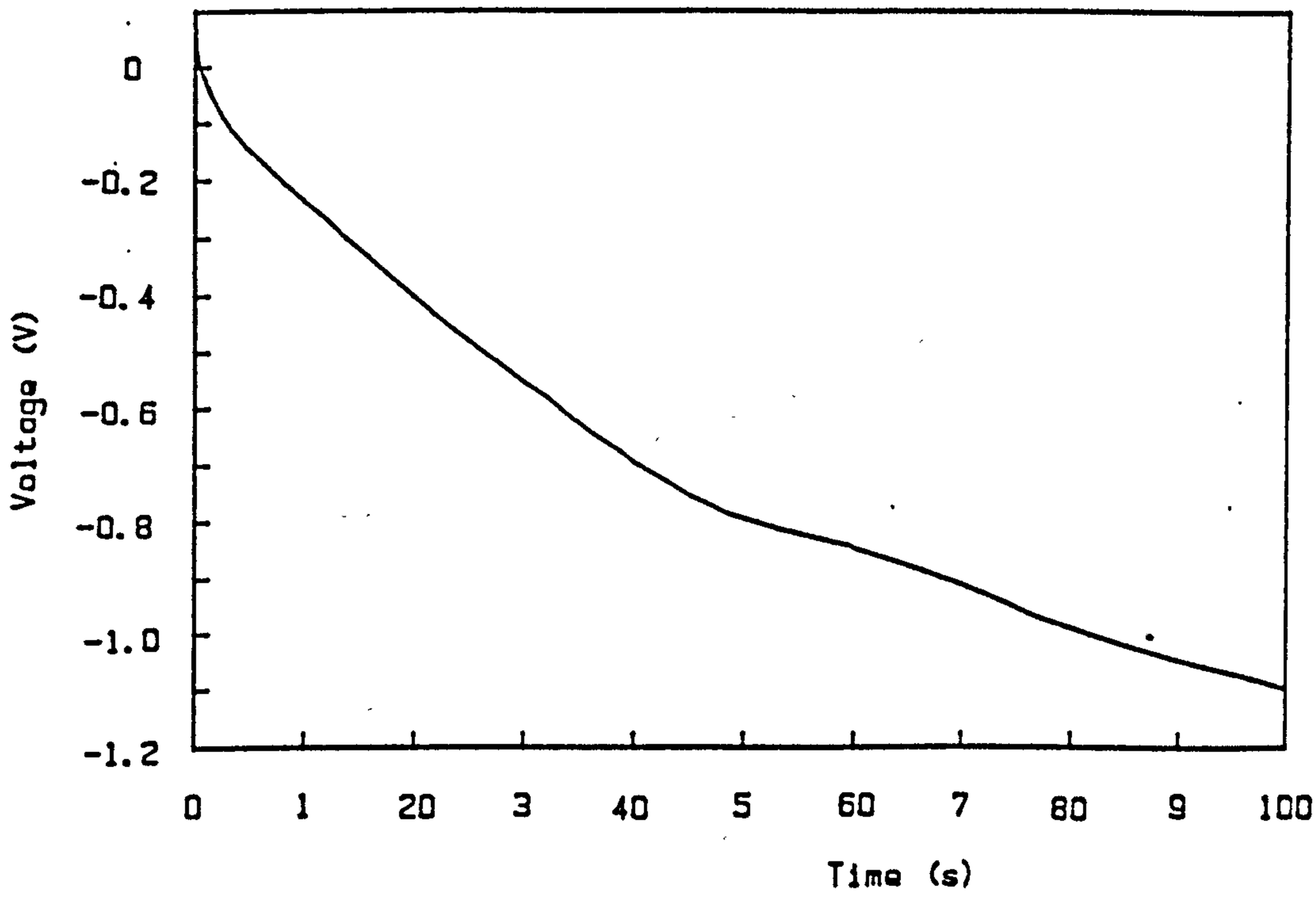

Fig 6.30 Cathodic run on silver electrodes.

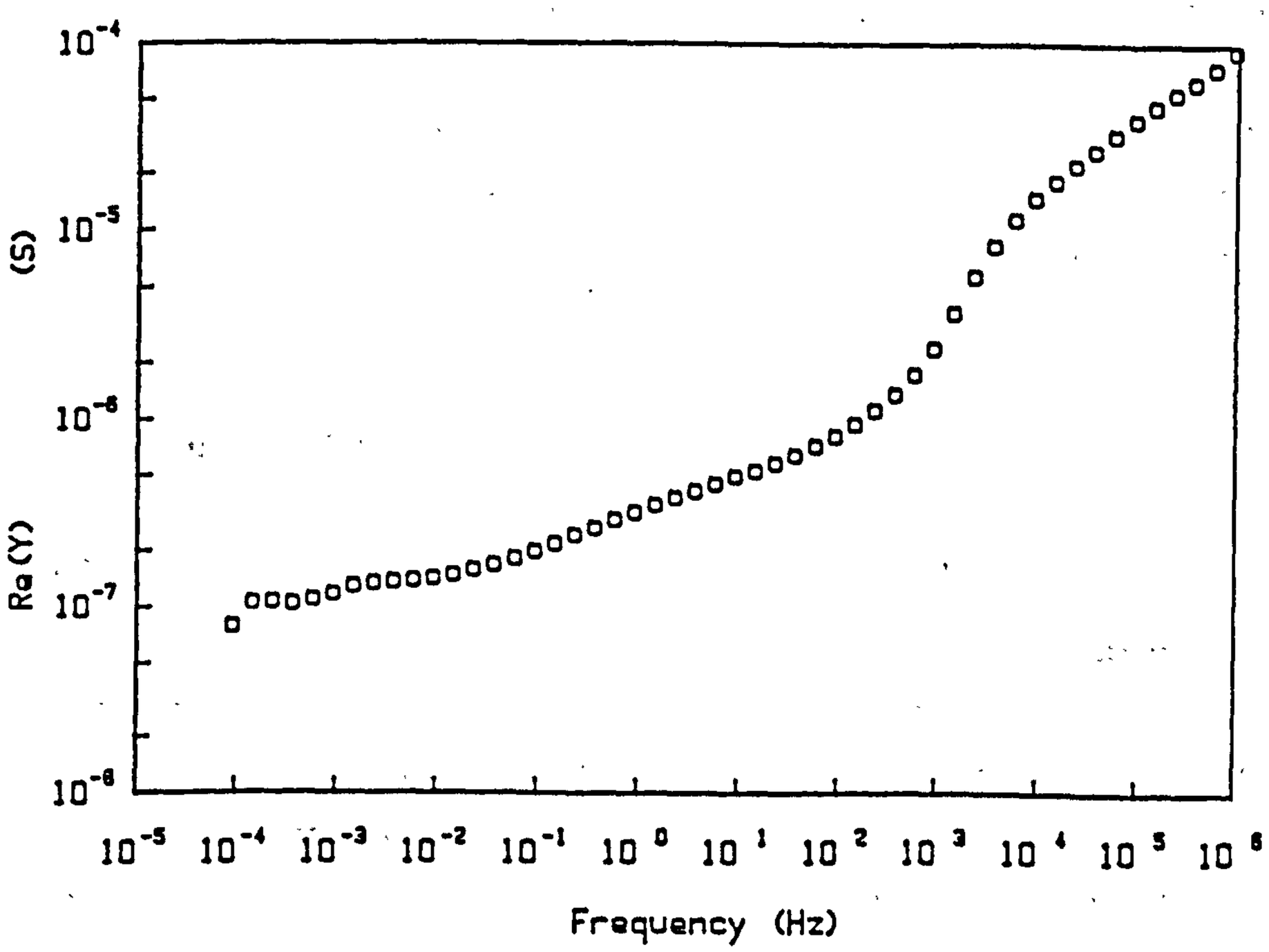

Fig 6.31 Real part of AC response of tungsten trioxide disc.

trioxide was used as a contact to the glass.

A two-electrode cell composed of an 015 plate between two of these discs was then tested. The real part of its admittance, shown in figure 6.32, does not display the usual plateau despite the wide range of frequency used. Instead there is only a slight kink in the middle of the curve indicating the region over which the bulk resistance has most influence on the response. Such behaviour was a good indication that the contact between the two materials was unsatisfactory, despite the achievement of adhesion by softening the glass during fabrication of the sample. As a result no useful information was gathered about the likelihood of sodium ions passing between the glass and the electrode. In the form used here, tungsten trioxide is clearly unsuitable as a contact material and for this reason no galvanostatic measurements were attempted on this sample.

6.7. Sodium Tungsten Bronze

6.7.1. AC Data

Unlike tungsten trioxide, sodium tungsten bronze is a metallic conductor and so no problems arose with bulk resistance. However the contact problem was expected to be similar, since application of the contact was by directly laying the solid material on the glass, either as a pressed disc or as powder. In fact the contact between the disc and the glass was so poor that no recognisable plateau appears in the real part of the response and so only the powdered contact was usable. Figure 6.33 (a) is the real part of the response for the powdered contact, showing a well-defined contact.

The AC results are different in form from those of the evaporated contacts, however, as is illustrated by the complex-admittance plot of figure 6.33 (b). The angle of depression of the arc is 46°, which is very much higher than that for any of the evaporated contacts. A similar value, 42°, is obtained from the slope of the low-frequency part of the capacitance versus frequency graph, shown in figure 6.34.

The rise of the imaginary part of the admittance with frequency (fig 6.33 (a)) at intermediate frequency indicates a capacitance of about 200 pF in parallel with most of the series resistance. This capacitance is not that of the bulk, which from two-electrode measurements on other samples is found to be about 0.1 pF. Figure 6.35 is a schematic diagram of the possible contact pattern of the glass and the bronze powder. It is possible that the large low-frequency capacitance (0.37 μF) is associated with

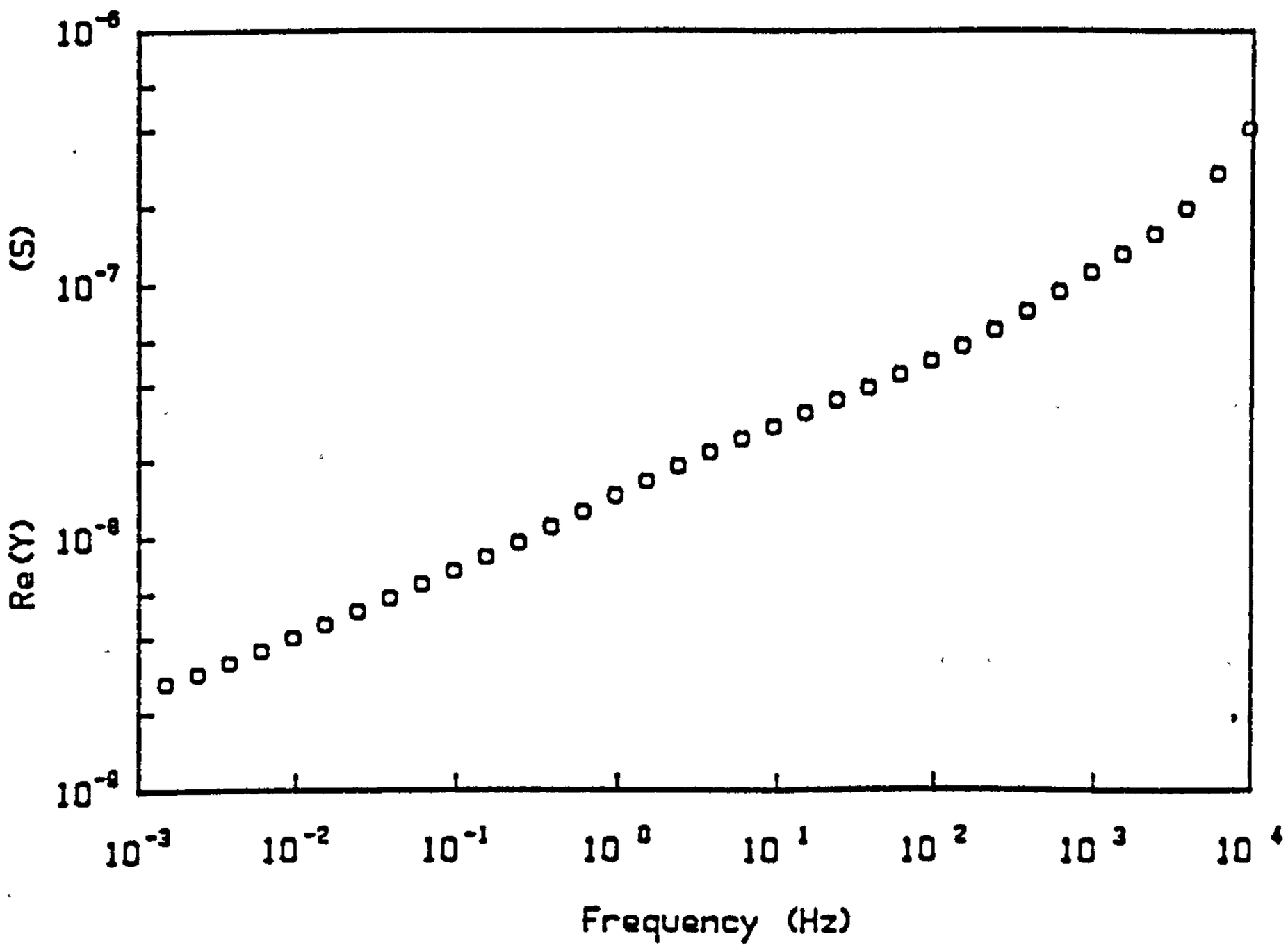

Fig 6.32 Real part of AC response of cell with tungsten trioxide contacts.

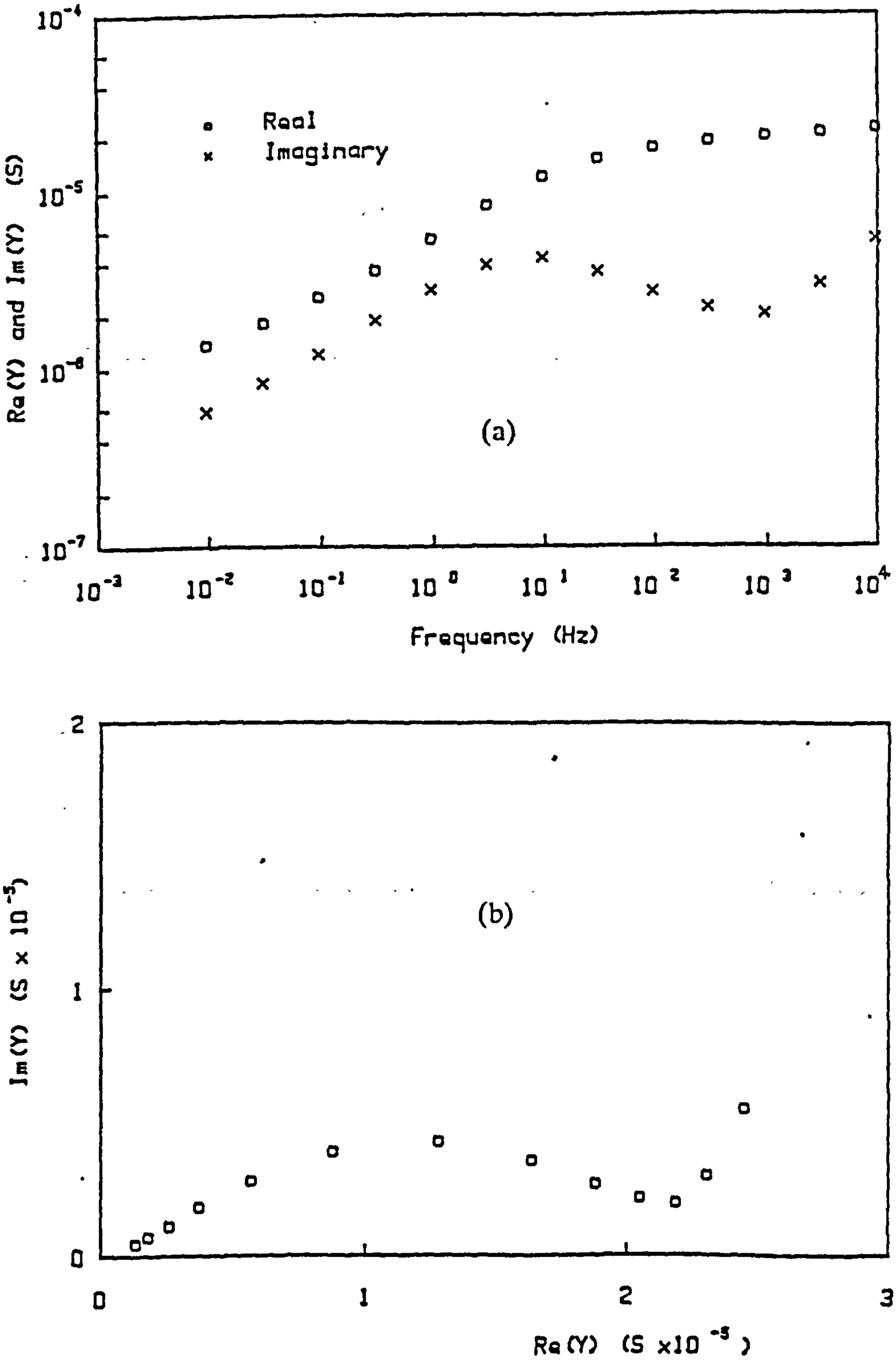

Fig 6.33 (a) Real part of sodium tungsten bronze cell.
(b) Complex admittance.

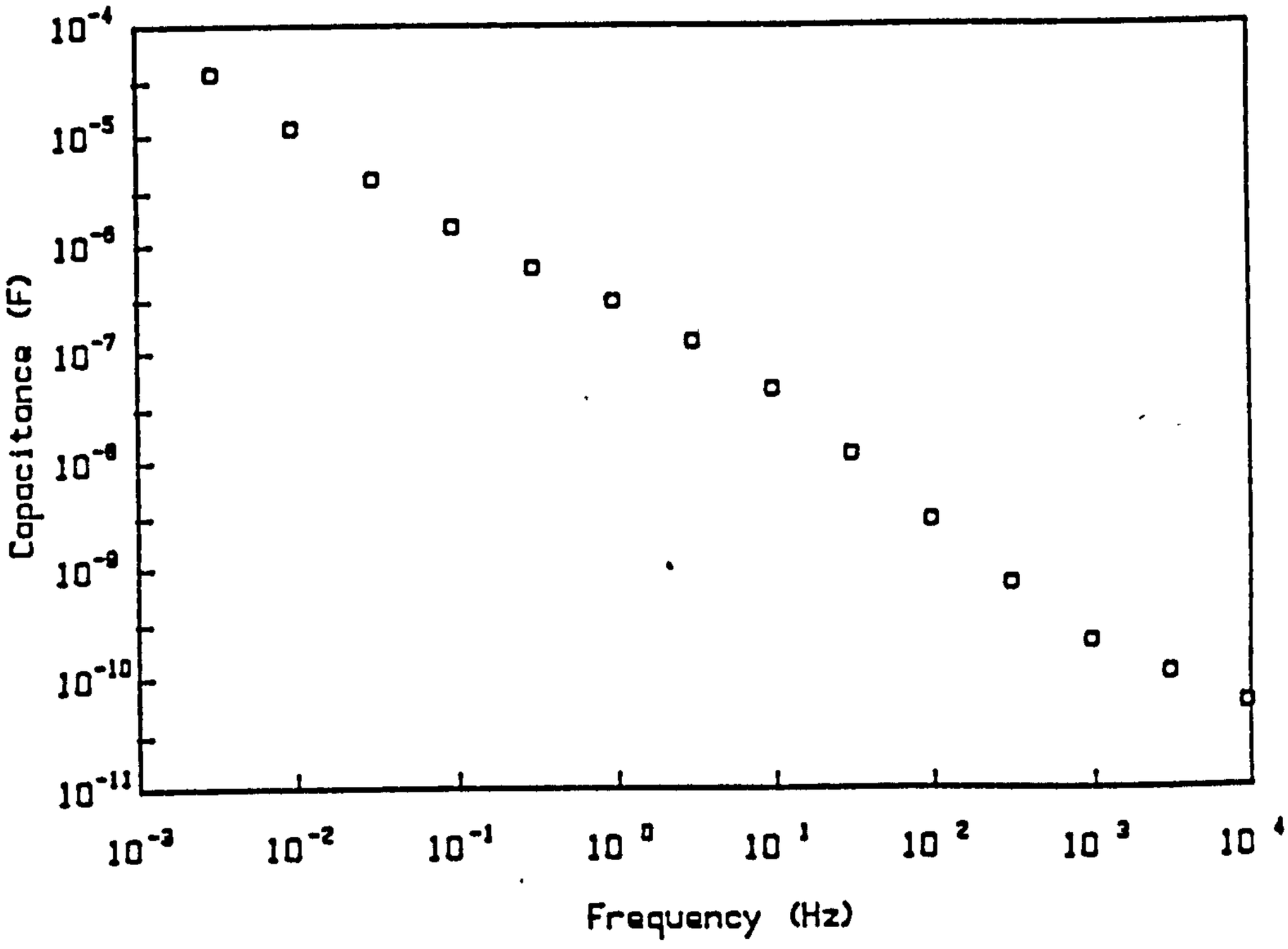

Fig 6.34 Interface capacitance versus frequency of sodium tungsten bronze cell.

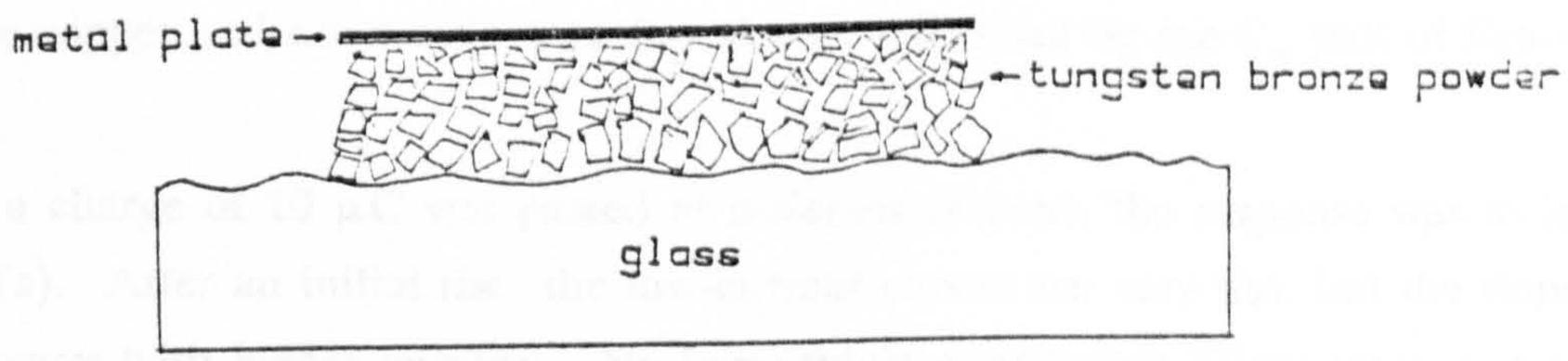

Fig 6.35 Contact pattern of sodium tungsten bronze powder on surface of glass.

those points where the bronze powder makes good contact with the glass. A comparatively large contact resistance could be expected here, with which the 200 pF capacitance would appear in parallel. The air-gap between the rest of the glass surface and the bronze may have been responsible for creating this intermediate capacitance. It is not possible to be more precise because of insufficient knowledge of the effective contact area produced by the powder.

6.7.2. Galvanostatic Data

Only the powder-connected sample was used for galvanostatic measurements. The voltage difference between the working and reference electrodes started out at 0.7 V, as can be seen in figure 6.36 (a). This must be due to the different reactions with glass of the two electrode materials: the bronze powder of the working electrode and the evaporated aluminium of the reference electrode. Figure 6.36 (a) is the result of applying a current of 10 μA to the working electrode, producing a smooth voltage response up to 2 V. No complicating features as were seen in galvanostatic measurements on the copper and silver cells were found, as emphasised by the C_d plot of figure 6.36 (b).

When a charge of 10 μC was passed at different currents the response was as in figure 6.37 (a). After an initial rise, the low-current curves are very flat, but the slope steadily increases with higher currents. No logarithmic relationship is apparent, but at low current a linear relation appears to hold, and a set of currents more suited to demonstrating this was used to generate the date of figure 6.37 (b). This linear relationship suggests a constant resistance at the interface and could be explained on the basis of point contact as the AC data were, but the value of the resistance, about 0.7 MΩ, was considerably greater than that estimated from the AC data, which was 52 kΩ.

A striking feature of the galvanostatic results for the bronze-electrode cell was the readiness with which the starting voltage of 0.7 V was returned to after each run. This is clearly demonstrated by the zero-current decay curves of figure 6.38, which show a very rapid return to 0.7 V after anodic charging.

Evidence for a fast charge-transfer reaction with a well-defined potential in this case was provided by the flatness of the anodic response, the fast zero-current voltage decay, and the tendency of the voltage to settle to the same value no matter what charge has passed through it. Since sodium tungsten bronze is chemically inactive [2]

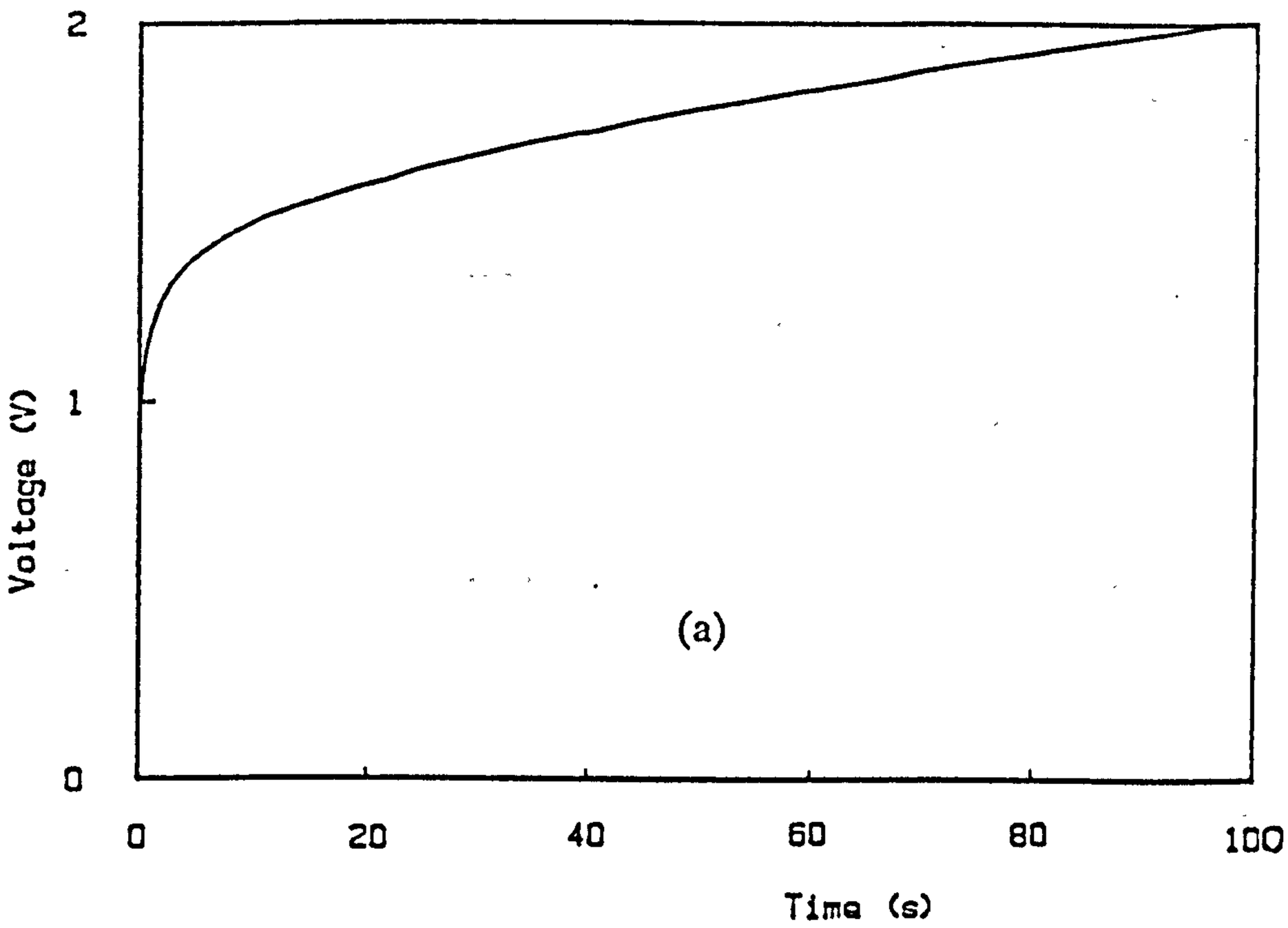

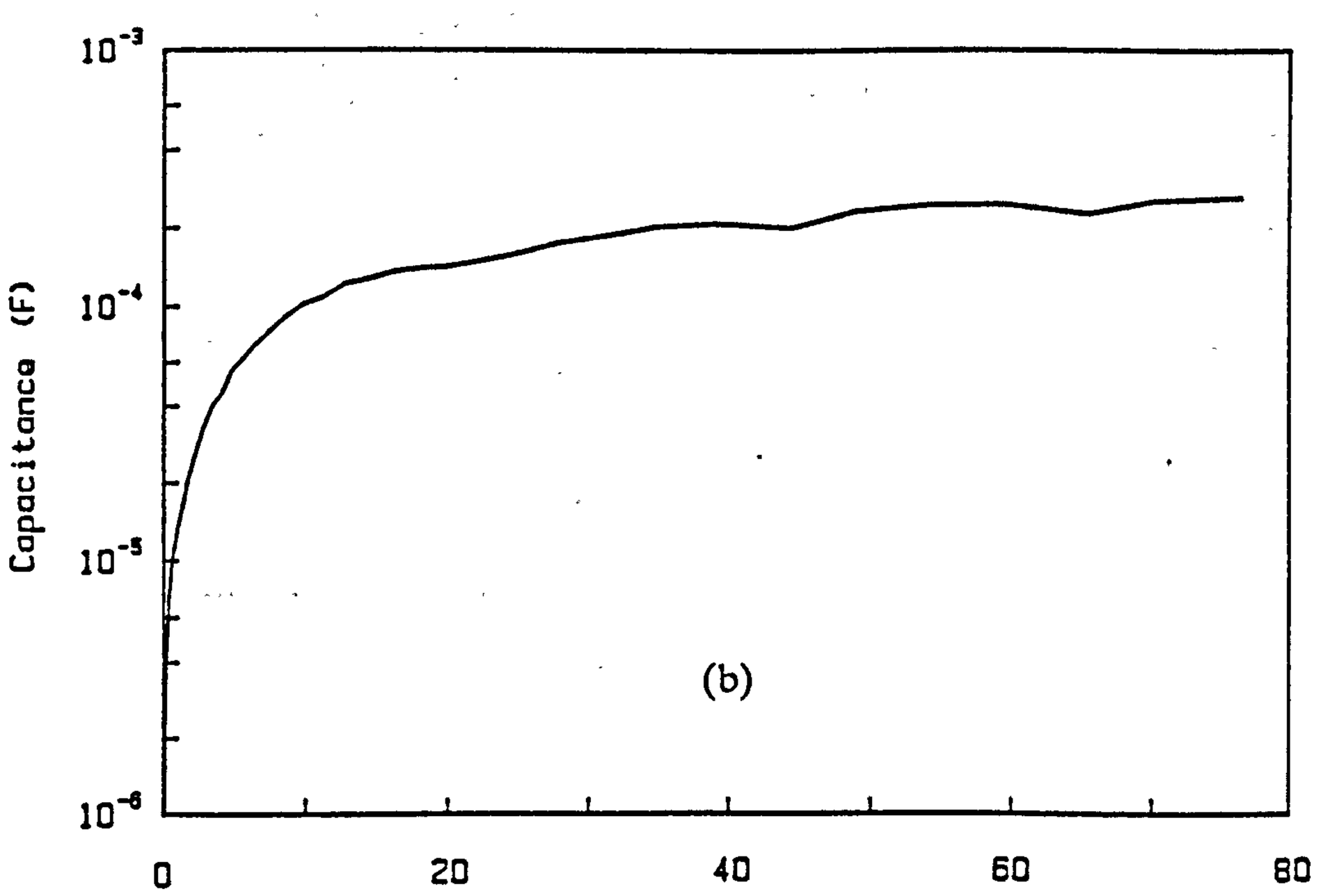

Fig 6.36 (a) 1 μA anodic run on bronze cell.
(b) Differential capacitance of (a).

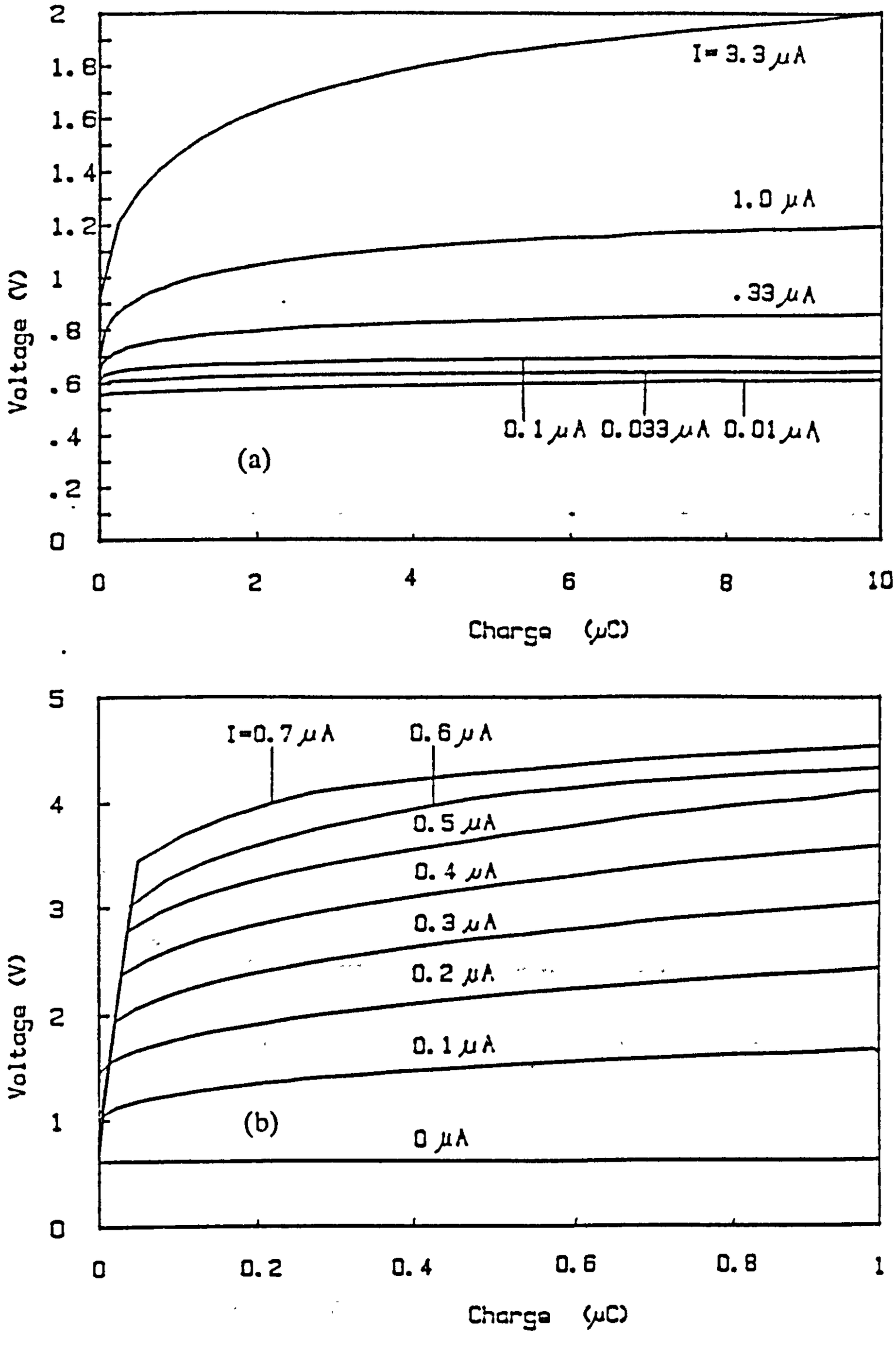

Fig 6.37 (a) 10 μC equal-charge data for sodium tungsten bronze powder contacts.

(b) As (a) but with equal spacing of the current.

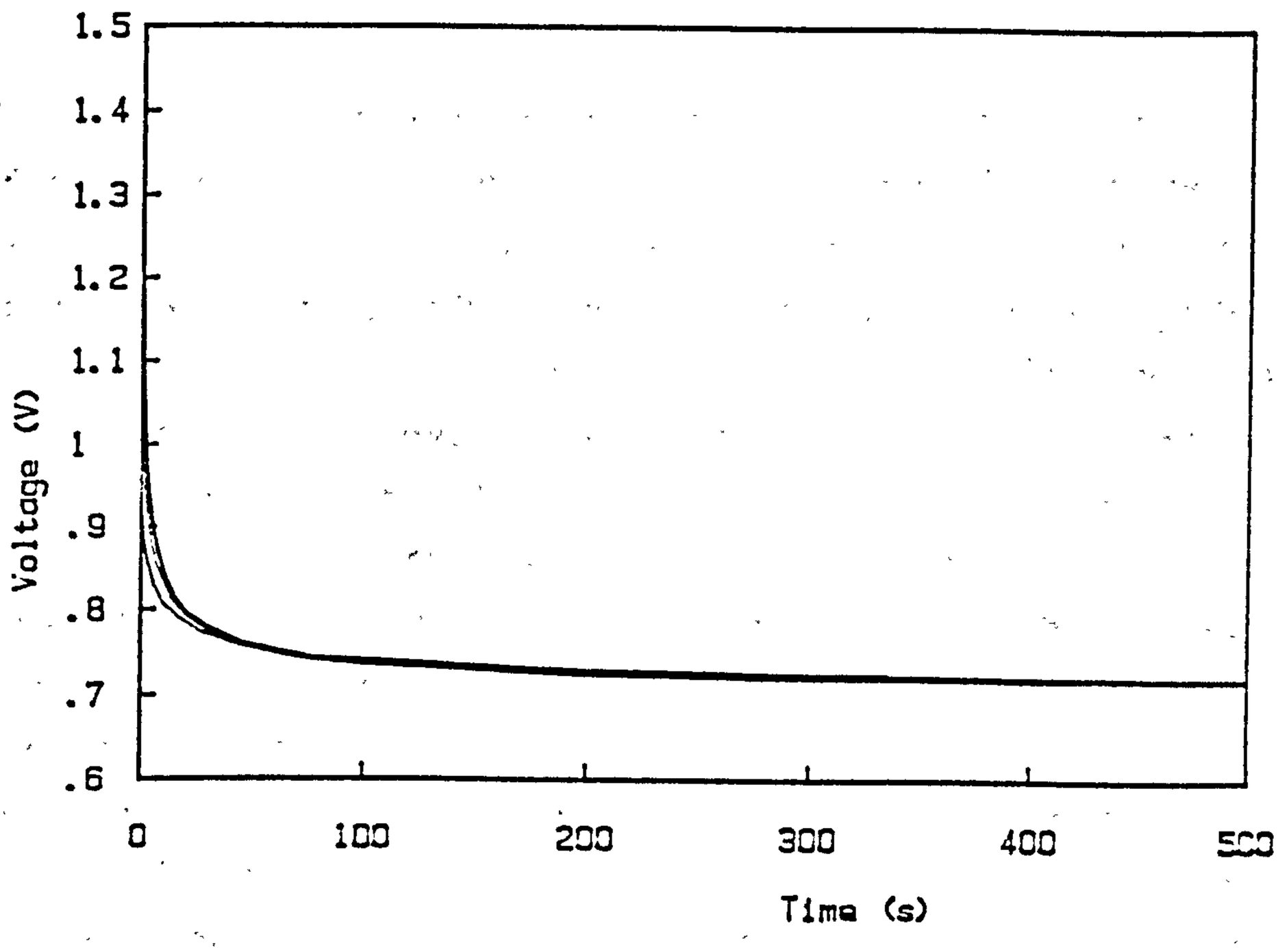

Fig 6.38 Zero-current decay after run of figure 6.36.

and an oxidation reaction is thus very improbable, exchange of sodium ions across the boundary is the most likely candidate for the charge-transfer mechanism.

6.8. Comparison of Responses of Different Electrodes

Most of the parameters measured by both the AC and galvanostatic techniques scale with contact area, and so strict quantitative comparisons can only be made among contacts whose method of preparation was identical, ie the evaporated aluminium, copper and silver contacts, since the effective contact area is affected by the method of preparation. Qualitative comparisons are possible among all the results.

6.8.1. AC Results

In all cases except sodium tungsten bronze the complex-admittance curves go through the origin. This is the only aspect of the results from which a clear-cut conclusion can be drawn, ie that there was no measurable dc conduction through the interface at zero bias. The tungsten bronze arc does not pass through the origin but, since it does not reach the real axis at all, the existence or otherwise of DC conduction could not be inferred from this curve. Some of the parameters for the different contact materials are shown together in Table 6.2. As expected, the variation of conductances is no greater than can be accounted for by the differences in sample thicknesses and temperatures. More significant variation was found among the interface capacitances and α's. Since the method of application was alike, the surface morphologies of the evaporated contacts should have been very similar. The capacitance at a blocking interface is solely a function of the geometry, and since there was no apparent evidence of charge transfer from the AC data, the capacitances at the different electrodes were expected to be similar. In fact the capacitance of the copper electrode was over seven times as high as that of the aluminium one, and that of silver 24 times as high. No obvious explanation for this presents itself, but oxidation of the metal by reaction with the glass or with ambient air giving rise to an intermediate oxide region, may be responsible for reducing the capacitance. The different characteristics of the oxides of different metals would account for the variations among the results. Alternatively, a reaction with the adsorbed moisture at the glass surface as proposed by Kim and Tomozawa [3] could allow some metals to take up a position closer to the glass surface than others, thus increasing the observed AC capacitance even in the absence of a charge-transfer reaction. The same considerations apply to the depression of the complex-admittance arcs below the origin, as measured by β.

Table 6.2

AC Parameters

Contact Metal	Type	Temperature	β	G_b
Aluminium	1	99	39°	2.6×10^{-9}
"	1	163	34°	4.5×10^{-8}
"	1	173	19°	6.7×10^{-8}
"	1	329	11°	1.5×10^{-5}
"	1	380	13°	1.2×10^{-4}
Copper	3	380	14°	6.8×10^{-5}
Silver	3	385	27°	5.5×10^{-5}
Sodium Tungsten Bronze		387	46°	2.3×10^{-5}

6.8.2. Galvanostatic Results

The anodic curves of the same four electrodes, with currents of 1 μA for 10 s, are plotted on the same axes in figure 6.39. All the samples had reference electrodes of the same metal as the working electrodes except for tungsten bronze, which had an aluminium reference. The non-zero starting point of the aluminium contact of about 0.7 V was due to a previous cathodic run, as was the slight distortion of the curve in the first three seconds. However, these effects are small and the shapes of all of the curves may be compared. After the initial rises, all voltage curves with this current are smooth and rise monotonically. However the slope of the aluminium curve is considerably higher at all times than those for the other electrodes. The contrast between aluminium and the other three implies that the rate of polarisation was much faster than at the other electrodes.

The differential capacitances for these curves, figure 6.40, also show up the differences between the metals. The differential capacitance of the tungsten bronze contact at the high voltage end was surprising in view of the low capacitance observed in the AC results. A very fast reaction relative to the others was suggested by this, so that considerable charge transfer occurs through the small points of contact of figure 6.35.

It is useful at this point to compare the shapes of these curves with a typical chronopotentiogram of the type encountered in liquid electrochemistry, which consists of a rapid rise associated with charging of the double layer followed by a plateau region when the reaction takes place. The closest resemblance is to the anodic behaviour of copper electrodes, where the same three regions can be identified. However the shape is not similar, which is not surprising because the chronopotentiogram represents the response of a system where products and reactants are in solution and moving solely under the influence of diffusion, with the surface concentration of the reactant species decreasing as the reaction proceeds, whereas the copper at the metal-glass interface is itself reacting, and presumably maintaining its activity until it is completely used up, as is evidenced by the observed colour change.

The anodic curves of aluminium and silver do not really resemble the chronopotentiogram at all. The voltage range of the aluminium curve in its comparatively slowly-varying region is much greater than that expected for an electrochemical reaction, and suggests the development of some series resistance, perhaps due to the same intermediate layer of oxide which accounts for the variety of capacitances observed at

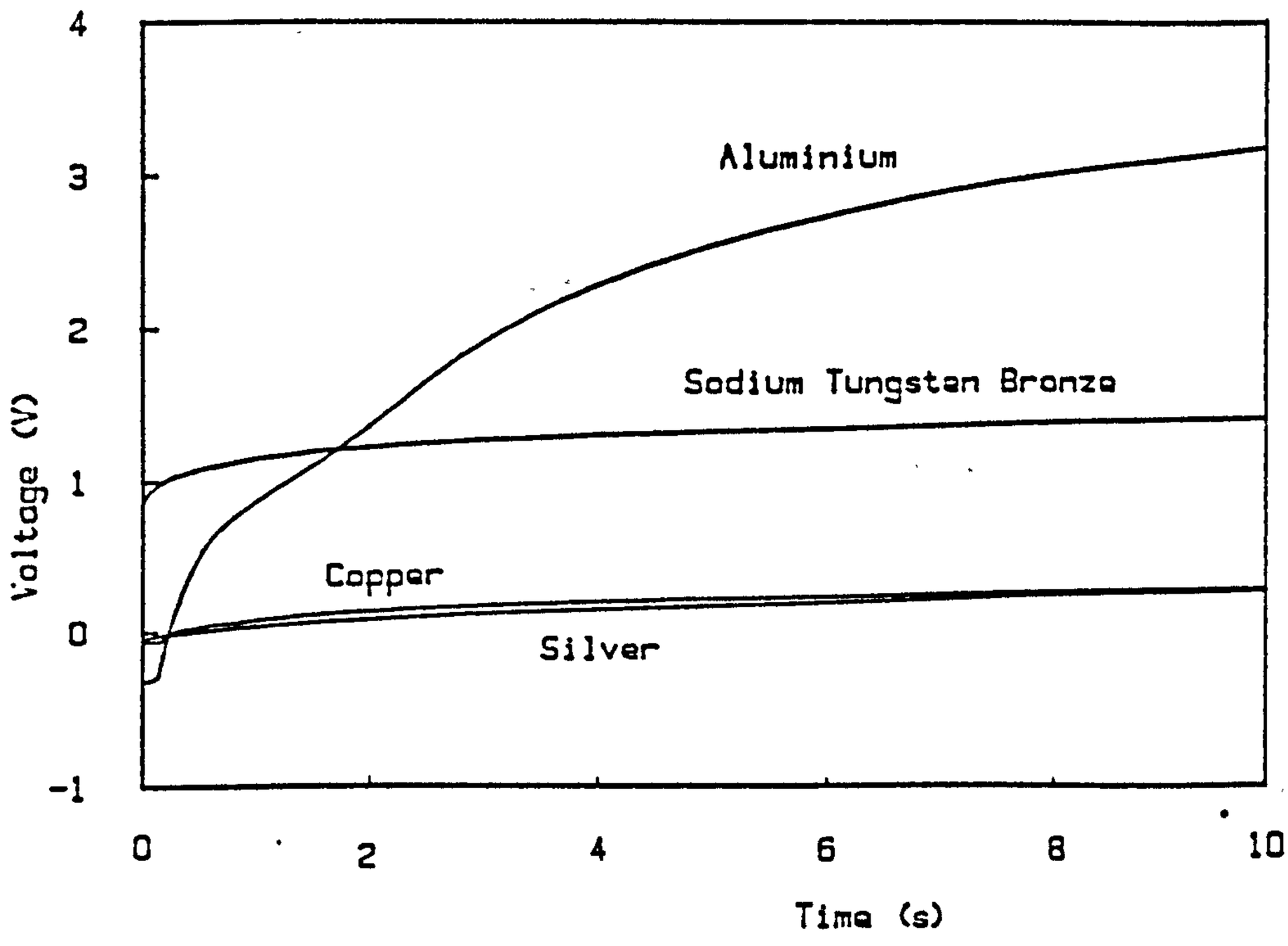

Fig 6.39 10 μA anodic runs on aluminium, copper, silver and sodium tungsten bronze cells.

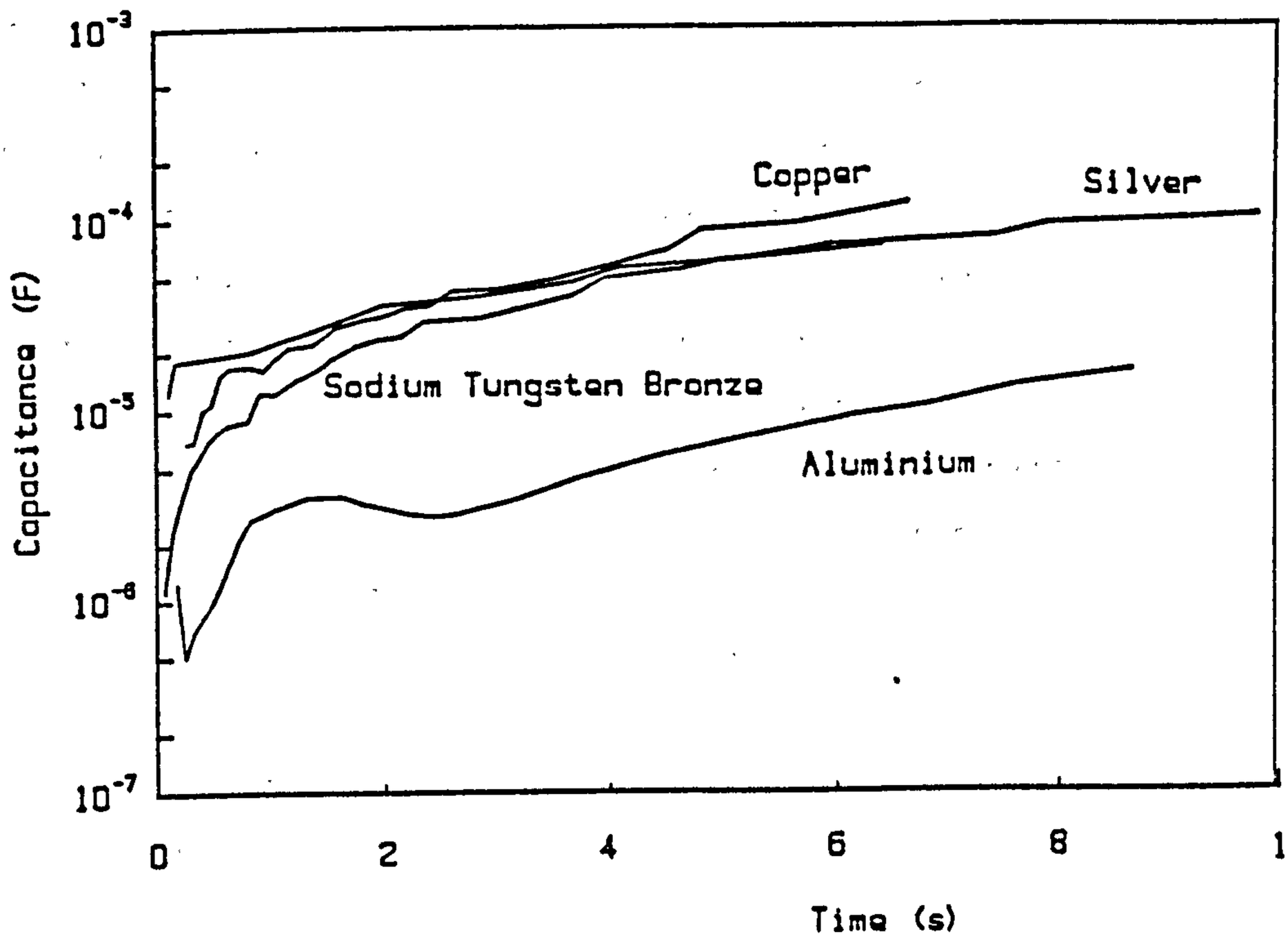

Fig 6.40 Differential capacitances of figure 6.40.

evaporated contacts. The same explanation may be proposed for the irregular anodic voltage development at the silver electrode, but with a lower-resistance layer or perhaps incomplete coverage. The zero-current decay curve, which is shown plotted on the same axes as those for the others in figure 6.41, also supports this view. A fast reaction would cause charge stored near the interface to be transferred across it and restore the interface to its previous potential difference.

Further evidence for the differing nature of the potential-determining phenomena at the different contacts was provided by comparing the equal-charge data. These are summarised in figure 6.42, where the final voltages of 10 μC runs are plotted against the log of the current. The aluminium curve was straight, indicating Tafel behaviour throughout the range. However the voltage range is very high in electrochemical terms, so that if kinetic limitation is indeed responsible then the energy barrier involved in the reaction is very high. Tafel curves for copper and silver are straight at low current and deviate further up. If the straight region is indicative of kinetic limitation, then the barrier height is very much lower than that of aluminium, because the voltage is also small. The deviation from linearity at larger current does not contradict the kinetically-limited picture of the lower voltage, but indicates that some other factor has come into play, and the obvious candidate is the oxide layer, although why the aluminium oxide layer, which was invoked to explain the shape of the curve, does not cause a deviation from Tafel behaviour is not clear. The tungsten bronze curve does not display a logarithmic dependence at any point, suggesting that the reaction was so fast that a resistive layer is dominant from the lowest current.

6.9. Reaction Mechanism at Evaporated Contacts

There are three possible overall reactions which may account for the observed behaviour of the aluminium, copper and silver contacts.

$$2O^{2-}_{(glass)} \rightleftharpoons O_{2(glass)} + 4e^{-}_{(electrode)} \qquad 6.5$$

$$2M_{(metal)} + O^{2-}_{(glass)} \rightleftharpoons M_2O + 2e^{-}_{(electrode)} \qquad 6.6$$

$$M_{(metal)} \rightleftharpoons M^{+}_{(glass)} + e^{-}_{(electrode)} \qquad 6.7$$

The visible oxidation of copper rules out reaction 6.5 for that metal. Since this reaction is the same for all metals, a similar response would be expected wherever it occurs.

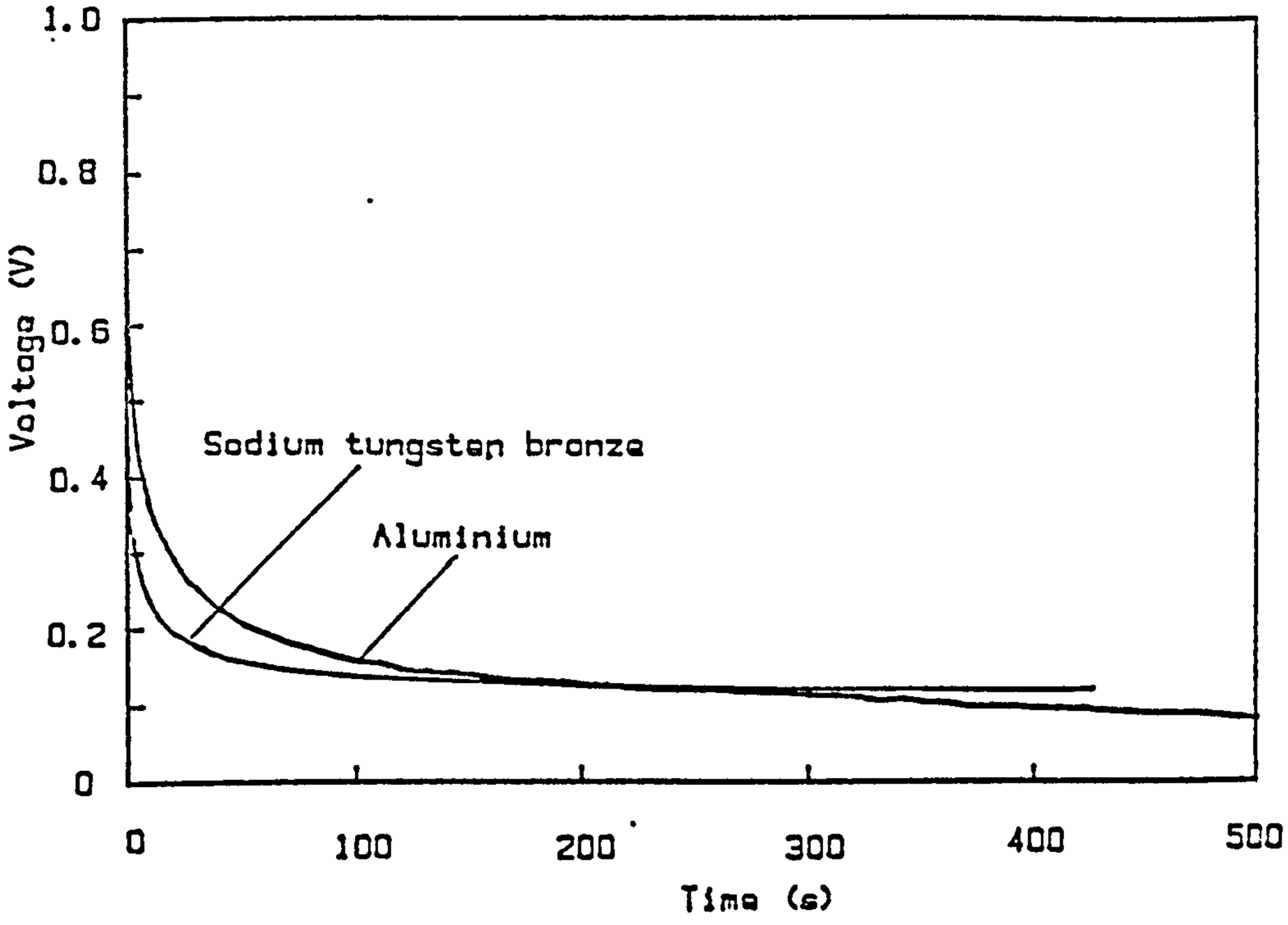

Fig 6.41 Zero-current voltage decays after anodic runs on aluminium and sodium tungsten bronze cells.

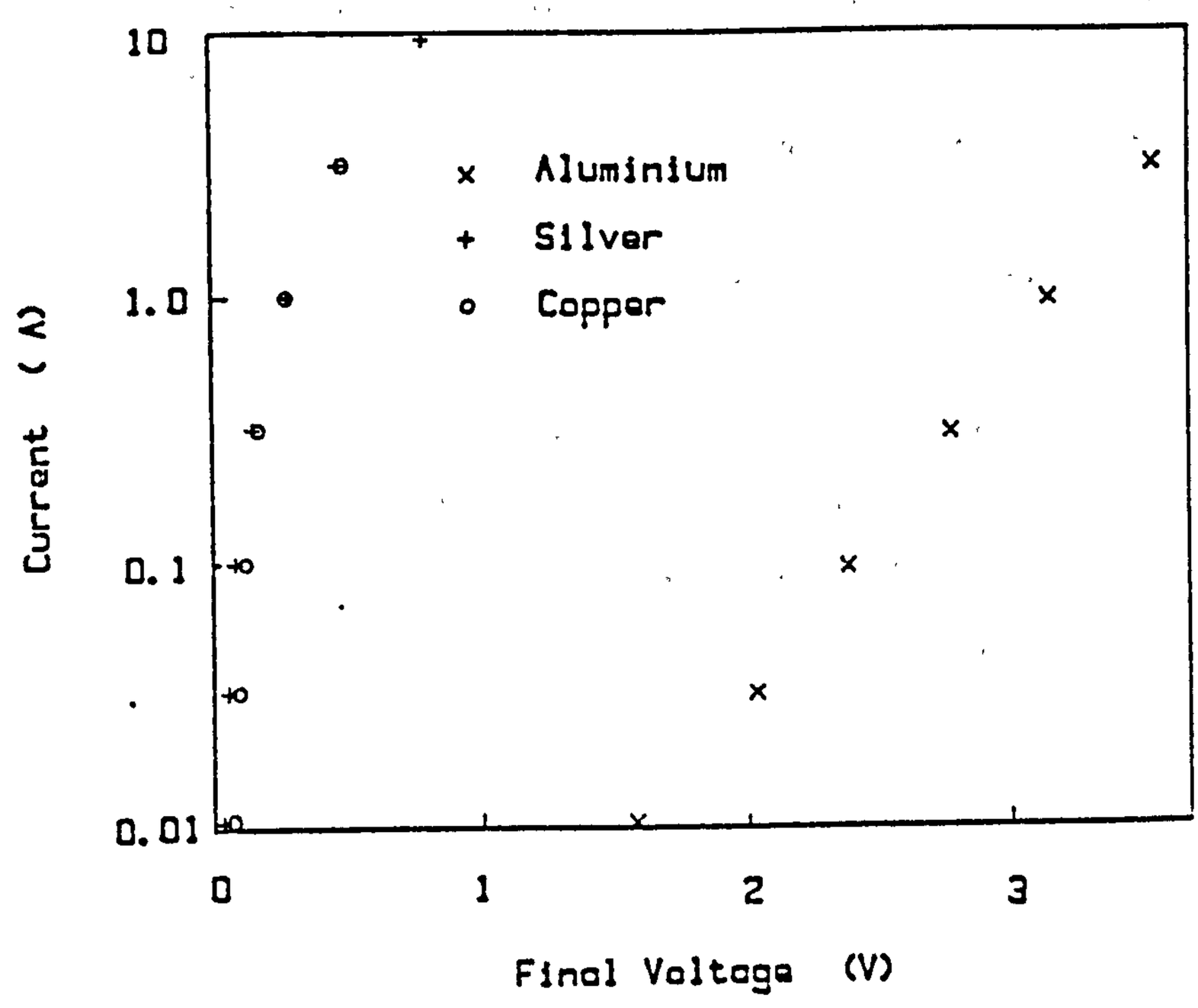

Fig 6.42 Tafel plots of final voltages of 10 μC equal-charge runs on different cells.

The dissimilarity of the responses of the other two metals therefore makes it unlikely for those either. Reactions 6.6 and 6.7 each require a step involving movement within glass of O^{2-} and M^{+} respectively. Such a movement would also involve a field and therefore a potential difference. Thus there would be three contributions to the overall electrode potential:

1. Charge transfer.
2. Diffusion/migration of active ions.
3. Space-charge development due to depletion of sodium.

If 6.6 was the appropriate mechanism, the potential due to steps 2 and 3 would depend on the mobility of the non-bridging oxygen atoms in a sodium-depleted network. The potential difference would rise to a level where the oxygen flux equalled the electron flux at the electrode. Without independent data for the mobility of oxygen in such alkali-depleted regions, it is not possible even to estimate this potential or how it develops with time.

If mechanism 6.7 is responsible, however, then it is likely that step 3 is insignificant, since any sodium ions vacating their sites would be replaced by metal ions from the electrode. Transport of metal ions would therefore be predominantly by diffusion, since the net charge density would be zero. The Nernst-Planck equation for this situation is:

$$\Phi = D_M \frac{\partial C_M}{\partial x} + D_{Na} \frac{\partial C_{Na}}{\partial x} + E(\mu_M C_M + \mu_{Na} C_{Na}) \qquad 6.8$$

where Φ is the net flux, D_M and D_{Na} are the diffusion coefficients, and μ_M and μ_{Na} are the mobilities. This is the equation solved by Doremus [4] as described in chapter 4, but with the addition of a nonzero constant flux, which produces the same result but with an extra term:

$$V = V_D + \frac{RT}{F} \int \frac{\Phi}{\mu_M C_M + \mu_{Na} C_{Na}} dx \qquad 6.9$$

Evaluation of the integral requires knowledge of the actual values of the ionic concentrations throughout the electrolyte. This is a static equation, and the time-variation of potential would require a full solution of equation 6.8 with time-dependent boundary conditions. However the overall form may be inferred from the observation that C_M and therefore V_D would rise as the surface reaction proceeded. The flux-dependent

term would increase as the distance of penetration of M^+ increased, if $\mu_M < \mu_{Na}$. This qualitatively accounts for the observed increase of potential with time, and implies that the mobility of the aluminium ions is much less than those of copper and silver.

The shapes of the decay curves also fit this picture. When the current is switched off, the flux term immediately becomes equal to zero. The continuing charge transfer causes the voltage to decline very rapidly until the overpotential has reduced to a level where the reaction stops. At this point the measured voltage will be solely the diffusion potential which decays slowly as the surface concentration of M^+ reduces.

6.10. Reaction Mechanism at Sodium Tungsten Bronze Contact

The most obvious reaction mechanism for sodium tungsten bronze is the reversible exchange of sodium ions between the electrode and the glass. For this to be true, there must be a steady equilibrium electrode potential which is a function of the sodium activity in the glass and the bronze. The strongest piece of evidence for this is the rapid decay of the voltage after each anodic run to the same voltage with respect to the reference electrode. Since sodium is mobile in both media, a large barrier hindering the rate of transfer is not expected, and indeed no evidence of Tafel or Butler-Volmer dependence of the transfer current on the electrode voltage has been observed. The apparently linear overvoltage-current relationship was most likely due to restricted movement of the ions in the glass near the points of contact with the powdered electrode.

CHAPTER 7

CONCLUSIONS

7.1. Equilibrium Electrode Potential

Evidence for a stable potential due to a reversible electrochemical reaction was only found in the sample with the sodium tungsten bronze contact. The tendency to return to the same potential after current of either direction had passed was the most direct indication. The flatness of the constant-current voltage development with time, in contrast to that of other contacts, indicated that the concentrations of the reactants did not change significantly as charge was passed.

The only other cell to show signs of reversible behaviour was the sodium metal two-electrode cell. However equilibrium potential measurements and response to the passage of direct current were not possible because of the high bulk resistance.

7.2. Oxidation of Electrode Metal

The potential development at electrodes which did not contain sodium, ie aluminium, copper and silver, was such that a straightforward space-charge picture is untenable. The charge density implied by the amount of charge passed would not be physically realisable by depletion of sodium ions. All of the voltage-time curves at all currents for all the evaporated contacts featured a low slope region following one of lower slope. The most plausible explanation is that the initial rise involves the establishment of a double layer across which a charge-transfer reaction occurs when the potential difference reaches the required level. Clearly all of these phenomena involve a reaction of the form:

$$M \rightleftharpoons M^{n+} + ne^{-} \qquad 7.1$$

However the subsequent movement and reactions involving these ions is not

immediately obvious.

7.3. Reaction Kinetics

The nonlinear dependence of the electrode potential on the current at evaporated contacts is clear evidence that the metal oxidation occurs at a rate which varies with the potential difference between the electrode and the electrolyte. In the case of aluminium, the voltage after the passage of equivalent charges is proportional to the logarithm of the current, in direct conformity with the Butler-Volmer law of electrode kinetics, with an exchange current of about 1 nA.

A Butler-Volmer relationship involving both the forward and reverse reactions appears to hold for the silver and copper electrode reactions at low overpotential, but the relation breaks down at higher voltages and currents, probably due to the effect of a resistive interphase layer which acts in series with the reaction. In both of these cases the exchange current was about 10 nA.

7.4. Potential Drop due to Hindered Electrode Ion Motion

The calculation of the potential drop due to the motion of the oxidised ions in the glass would involve a knowledge of the mobilities of the ions under the specific surface conditions of the glass. There are several possible processes which may be responsible for the charge-dependent part of the potential development.

One possibility is the drift and diffusion of the metal ions within the glass. The slow part of the decay curve is suggestive of a steadily decreasing surface concentration of ions as they move into the bulk. In addition, the relatively steep rise of the potential at aluminium contacts, compared with that at copper and silver contacts, may indicate the slower diffusion of aluminium ions into the glass, causing a higher surface concentration and hence a higher diffusion potential.

The explanation, using this picture, of the relative rates of decay in the long-time regions, is less obvious. Comparisons are difficult, because in no case can a simple exponential decay with an identifiable end-point and time constant be established. This is especially true of the data of figure 6.41 which, although plotted on the same axes, involve different overvoltages and initial voltages. However it can be said that the decay-rates do not appear to be spread over as wide a range as that of the rate of growth of the potential. A qualitative explanation for this can be arrived at by assuming that the potential, other than that due to reaction kinetics, is a result of metal-ion

motion. The diffusion potential is a function both of the concentration difference between the surface and interior regions, and the diffusion coefficient. The rate of change of potential is also a function of these two quantities, and so if the potential at switch-off is the same at two electrodes, then the decay of voltage is likely to be at least approximately equal.

Another possible explanation involves the assumption that no appreciable diffusion of the metal ions takes place but instead oxygen ions from the glass combine with the oxidising metal to form an oxide interphase layer. The shape of the voltage-time curves would then depend on the thickness and electrical properties of this oxide. Conduction through such thin films is a very complicated area, and the experiments are insufficient to distinguish conclusively between the effects of tunnelling, space-charge limited current, and ohmic conduction all of which have been recorded [1].

7.5. Effects of Surface Irregularities

The observed depression of the complex-admittance arcs is best explained as being due to the effects of the variation of effective contact area as a result of the deviation from smoothness of the interface. These results do not add any substantial new knowledge to this phenomenon.

The discrepancy between the small-signal and DC differential capacitances of the sodium tungsten bronze contact has a less obvious explanation but is probably also due to surface morphology. The sodium tungsten bronze powder could only have made contact at a few points which together accounted for only a small fraction of the contact area. At the very low voltages applied during the AC measurements, the measured capacitance would only have been due to charging at these points. But at higher voltages, the possibility of charge transfer across small gaps near the contact points would give rise to a higher measured capacitance. This point contact probably also accounts for the linear relationship between the voltage and the current at the sodium tungsten bronze contact. Even if the charge-transfer itself is fast, the sodium ions involved have to move through narrow regions in the glass and the bronze where the concentration and potential gradients are likely to give rise to ohmic behaviour.

7.6. Suggestions for Further Work

Evidence for the presence of a kinetically-limited charge transfer reaction has been found at some interfaces between evaporated metal electrodes and soda-lime-silica glass. The next stage of the investigation must identify the conditions which support this reaction by varying the surface conditions. For example, the application of electrodes to surfaces which have been freshly cleaved, or subjected to different cleaning procedures, such as chemical etching and sputter etching, may give rise to cells with different electrical characteristics.

The influence of the glass composition should also be investigated by varying it systematically and carrying out the same experiments.

Information about the distribution of metal ions within the glass near the interface could be usefully obtained from depth-profiling surface analysis. There are a number of techniques which might be suitable; the primary requirement is that the process of removing the surface layers should not seriously affect the distribution of the ions as it proceeds. From this information, insight could be gained into the mechanism of transport of charged species in the interface region.

Since the work was originally connected with the development of a solid state pH sensor, continuation of the work should bear in mind the possible application of the electrode metal as the back electrode of a chemically sensing device. The most promising candidate in this respect is sodium tungsten bronze. It is thus proposed that some solid-state sensors incorporating this material be constructed and tested.

REFERENCE

1. Seraphim DP, in *Thin Films* p135-172, Amer Soc for Metals (1963).